National Technical University of Athens
School of Naval Architecture & Marine Engineering
Division of Marine Engineering

Diploma Thesis

Software Development for Dynamic Behavior Assessment of the Propulsion System with Parametric Design

Oikonomou Zacharias-Panagiotis

Thesis Committee:
Supervisor: C.I. Papadopoulos, Associate Professor NTUA
Members: L. Kaiktsis, Professor NTUA
K. Anyfantis, Assistant Professor NTUA

Athens, November 2023

Εθνικό Μετσόβιο Πολυτεχνείο
Σχολή Ναυπηγών Μηχανολόγων Μηχανικών
Τομέας Ναυτικής Μηχανολογίας

Διπλωματική Εργασία

Ανάπτυξη λογισμικού για την Αξιολόγηση Δυναμικής Συμπεριφοράς του Αξονικού Συστήματος Πλοίου με Παραμετρική Σχεδίαση

Οικονόμου Ζαχαρίας-Παναγιώτης

Εξεταστική επιτροπή:
Επιβλέπων: Χ.Ι. Παπαδόπουλος, Αναπληρωτής Καθηγητής ΕΜΠ
Μέλη: Λ. Καϊκτσής, , Καθηγητής ΕΜΠ
Κ. Ανυφαντής, Αναπληρωτής Καθηγητής ΕΜΠ

Αθήνα, Νοέμβριος 2023

Contents

List of Figures

[1] "Guide for Enhanced Shaft Alignment 2022", ABS.
[2] "Guide for Enhanced Shaft Alignment 2022", ABS.
[3] *Elastohydrodynamic Lubrication (EHL)*, Vlachos O.
[4] *Elastohydrodynamic Lubrication (EHL)*, Vlachos O.
[5] "Guide for Enhanced Shaft Alignment 2022", ABS.
[6] "Guide for Enhanced Shaft Alignment 2022", ABS.
[7] "The Finite Element Method for the Analysis of Non-Linear and Dynamic Systems", D. E. Chatzi.

List of Tables

Acknowledgements

This work marks the end of my undergraduate studies in the School of Naval Architecture and Marine Engineering of the NTUA, concluding with the best way this cycle of my life. In my years in the National Technical University of Athens I gained knowledge, friends, skills and a way of thinking and work ethic that will follow me onto my future career.

First of all, I would like to thank from the bottom of my heart my supervisor, Dr. Christos Papadopoulos, for being an excellent mentor, listener and tutor simultaneously. His assistance was of great importance for the completion of the present thesis and my shaping as an engineer.

Furthermore, I would like to thank PhD Candidate George Rossopoulos, for his significant assistance and excellent communication , as well as the interesting criticisms.

I would also like to thank Mr. Nikolaos Bouzalas for taking me under his wing and exposing me to my first dry docking and teaching me as much as I could learn.

Also, I would like to thank my family for their continued support and trust in my entire student life. Their faith drove me to succeed and their encouragement to seek new learning experiences.

Last, but definitely not least, I would like to thank my friends for their assistance and motivation all of our years in the NTUA. Their friendship and encouragement sustained me through the any obstacle. All of our experiences, memories, jokes and moments of pure comedy will be will me for life. Thank you for sailing in this journey with me.

Abstract

The present Diploma Thesis aims to develop a parametric simulation software for analyzing the dynamic behavior of complex shafting systems. Leveraging Finite Element Analysis theory, an extensible framework is established to simulate shafting systems comprehensively, serving as a foundational component for potential Digital Twin implementations of entire propulsion systems. The motivation stems from the ongoing revolution in the shipping industry, necessitating a precise understanding of the entire ship as well as the performance and interactions of her subsystems.

The shafting system, a complex and intriguing subsystem, is traditionally simulated using simplistic models, such as representing rotational dynamics with rotating masses and torsional springs. The software development process followed a iterative refinement approach to ensure early operational accuracy. Special attention was given to High-Performance Computing Elements (HPC) to enable workload parallelization and maximize parametric flexibility. The resulting software is fully parallelized, capable of accommodating various shafting systems, incorporating cylinder torque as a function of crank angle, and providing accurate output for stress and displacement analysis. Model validation has included testing with simple cases and comparison to results of a real-world shafting system, particularly focusing on eigenmodes for lateral vibrations.

This diploma thesis serves as a foundational platform, facilitating the seamless integration of additional elements of the propulsion system, as well as multiphysics simulations. Future extensions may include incorporating the full Reynolds equation for bearing analysis, integrating a combustion model for cylinder torque, and exploring alternative propulsion system simulations.

Σύνοψη

Η παρούσα διπλωματική εργασία στοχεύει στην ανάπτυξη λογισμικού παραμετρικής προσομοίωσης για την ανάλυση της δυναμικής συμπεριφοράς σύνθετων αξονικών συστημάτων πρόωσης. Αξιοποιώντας τη θεωρία της ανάλυσης πεπερασμένων στοιχείων, αναπτύχθηκε ένα επεκτάσιμο πλαίσιο για την ολοκληρωμένη προσομοίωση των αξονικών συστημάτων, το οποίο μπορεί να χρησιμοποιηθεί ως θεμελιώδες στοιχείο για πιθανές εφαρμογές Ψηφιακού Διδύμου (Digital Twin) του συνόλου των στοιψείων που συνθέτουν ένα σύστημα πρόωσης ενός πλοίου. Το κίνητρο για την εκπόνηση της παρούσας εργασίας πηγάζει από την σύγχρονη απαίτηση της ναυτιλιακής βιομηχανίας, για ακριβή κατανόηση ολόκληρου του πλοίου, καθώς και των επιδόσεων και των αλληλεπιδράσεων των διαφόρων υποσυστημάτων του.

Το αξονικό σύστημα του πλοίου, ένα περίπλοκο και ενδιαφέρον υποσύστημα, προσομοιώνεται παραδοσιακά με τη χρήση απλοποιημένων μοντέλων, όπως η αναπαράσταση με σημειακές περιστρεφόμενες μάζες και στρεπτικά ελατήρια. Η διαδικασία ανάπτυξης λογισμικού ακολούθησε μια προσέγγιση σταδιακής εξέλιξης, ώστε να εξασφαλιστεί η ακρίβεια και επαναληψιμότητα των προσομοιώσεων. Ιδιαίτερη προσοχή δόθηκε στα στοιχεία παραλληλισμού για υψηλή απόδοση (High-Performance Computing Elements, HPC) για να καταστεί δυνατός ο παραλληλοσμός του φόρτου εργασίας και η μεγιστοποίηση της παραμετρικής ευελιξίας. Το λογισμικό που αναπτύχθηκε υποστηρίζει πλήρως τον παραλληλισμό, είναι ικανό να μοντελοποιεί διάφορα συστήματα άξονων, να ενσωματώνει τη ροπή του κυλίνδρου ως συνάρτηση της γωνίας του στρόφαλου και να παρέχει ακριβείς υπολογισμούς των τάσεων και μετατοπίσεων του συστήματος. Η επικύρωση του μοντέλου περιλαμβάνει δοκιμές με απλές περιπτώσεις αξόνων, καθώς και σύγκριση με τα αποτελέσματα ενός πραγματικού συστήματος άξονα πλοίου, εστιάζοντας ιδιαίτερα στον υπολογισμό ιδιοσυχνοτήτων και ιδιομορφών σε καμπτικές ταλαντώσεις.

Η παρούσα διπλωματική εργασία φιλοδοξεί να χρησιμεύσει ως θεμελιώδης πλατφόρμα, διευκολύνοντας την απρόσκοπτη ενσωμάτωση πρόσθετων στοιχείων του συστήματος πρόωσης, καθώς και προσομοιώσεις πολυφυσικής (multiphysics simulations). Οι μελλοντικές επεκτάσεις μπορεί να περιλαμβάνουν την ενσωμάτωση της πλήρους εξίσωσης Reynolds για ανάλυση των ακτινικών εδράνων ολίσθησης την ενσωμάτωση ενός μοντέλου καύσης για τον ακριβή υπολογισμό της ροπής των κυλίνδρων καθώς και την προσομοίωση εναλλακτικών σχεδιάσεων συστημάτων πρόωσης πλοίων.

1 Introduction

1.1 Goals of the Present Study

The main goal of this research project is to create an easily customisable framework utilises HPC elements and simulates the shafting system, including the shaft, the bearings and the engine and propeller at a rudimentary level.

Specifically the goals set are:

- Static FEA simulation of the Shaft with the engine side applying torque and the propeller side applying torque and axial force
- Implementation of High Performance Computing (HPC) elements that distribute the problem over all available processors and RAM
- Dynamic FEA simulation utilising Newmark-Beta's integration algorithm
- Implement the Bearings as area forces onto the shaft
- Generate a Parametric Tool that converges for any shafting system given as an input and can be run as a batch run to create a Data Set for Machine Learning applications

To carry out this research, it's essential to outline the methods used and the basic assumptions made. A key goal of this thesis is to ensure scalability and parametric functionality. In line with this, all calculations will be done using Message Parssing Intefarce (MPI) processes, specifically through Portable, Extensible Toolkit for Scientific Computing (PETSc) wrappers. The **deal.II** library is utilized to integrate the mathematical computations with the hardware, giving the programmer complete control over each process and parameter.

The basic assumptions for this research involve the balance of forces on the shaft and the hydrodynamic lubrication of the bearings. It's assumed that the engine produces a constant torque, and transient rpm conditions are not considered in this study. The bearings are idealized as perfect cylinders without any slopes. Also, it's assumed that the shaft material only undergoes small deformations, staying within the elastic region, meaning there's no hardening of the material considered.

The simulation process begins with defining the parameters, which include engine and ship velocity data, bearing data, shaft geometry data, and solver inputs like tolerances and mathematical constants. Meshing and distribution of the Degrees of Freedom (DoFs) are managed for the shaft's cylindrical body, and boundary regions are set. The bearings are simulated by two springs and they are incorporated into the System Stiffness Matrix. The solution employs the Newton Raphson Method, with time stepping managed by the HHT-α algorithm.

Following every advancement in the mathematical core of the software, the validity of the results are evaluated with simple test cases where the analytical solutions are available. These test cases evaluate the maximum stress and deformation a cantilever cylindrical beam is subjected to in compression, bending and torsion, in order to ensure that the software can provide sufficiently accurate solutions.

Lastly, a case study will be conducted in order to observe and assess the dynamic behavior of the shafting system under combined torsion, bending and compression loading conditions, focusing on the Maximum Continuous Rating of the Diesel Engine. Following this, the eigenvalues of the system will be calculated and the resulting eigenvalues and eigenmodes will be compared to the reports provided by the shipyard for the test case ship.

1.2 Historical Background

In a Maritime Industry, with a constant need for high efficiency and with a Decarbonization trend enforced by a plethora of newly established rules, the shafting system of the average merchant vessel undergoes fundamental changes. The current trajectory calls is shaped by the following:

- Upward trajectory of the Oil and LNG prices
- The limited supply of spare parts due to the geopolitical landscape
- Guidelines and laws that require the minimising of GHG emissions, as described below

Specifically, the maritime industry is taking significant steps towards decarbonization, as reflected in various laws and regulations, among them the Energy Efficiency Existing Ship Index (EEXI), Energy Efficiency Design Index (EEDI), Carbon Intensity Indicator (CII), and Ship Energy Efficiency Management Plan (SEEMP). The EEXI, mandated from 1 January 2023, requires all ships to calculate their energy efficiency, which is a stride towards reducing greenhouse gas (GHG) emissions from ships[8]. Similarly, the EEDI, initiated in phases since 2015, mandates ships to incrementally reduce their carbon intensity, aiming for at least a 30% reduction in some cases[9].

On the other hand, the CII is a measure of a ship's energy efficiency, represented in grams of CO_2 emitted per cargo-carrying capacity and nautical mile, with the first verification of attained annual operational CII set for 2024 concerning operations in 2023[10]. Moreover, the SEEMP is a structured approach to enhancing the energy efficiency of ships, consisting of a ship management plan to improve energy efficiency and a ship fuel oil consumption data collection plan[11]. Additionally, 2023 will see the introduction of SEEMP III alongside EEXI and CII to further curb carbon emissions from ships[12]. The maritime decarbonization regulations, including EEXI, EEDI, CII, and SEEMP, affect the shafting system, particularly when the Maximum Continuous Rating (MCR) of engines falls below the 70% threshold, challenging the bearings' normal function[13]. Concerns arise, especially during turning conditions at MCR speed, where exaggerated propeller bending moments reduce the shaft-bearing contact area, leading to potential operational failures[14]. Moreover, a surge in stern tube bearing failures has been reported, with several studies by DNV GL attributing these to the use of Environmentally Acceptable Lubricants (EALs) instead of traditional mineral oils, indicating a notable operational challenge amidst the industry's move towards decarbonization[15].

[8] *EEXI and CII - ship carbon intensity and rating system.*
[9] *IMO sustainable shipping amendments for EEDI, EEX, CII and BWM.*
[10] *CII - Carbon Intensity Indicator.*
[11] *EEXI and CII requirements taking effect from 1 January 2023.*
[12] *SEEMP III, EEXI & CII - 2023.*
[13] *Shaft alignment and propeller shaft aft bearing performance – recent trends call for action.*
[14] *Ensuring satisfactory aft stern tube bearing lubrication performance - DNV.*
[15] *Environmentally acceptable lubricants show reduced capabilities under certain conditions*, *DNV GL Study Ties Stern Tube Bearing Failures To The Use Of Synthetic EALs*, W. Journal, *Lagersmit | The effect of Environmentally Acceptable Lubricants on stern tube bearings*, *DNV GL completes study on the properties of EALs for stern tube applications.*

1.3 Literature Review

The propulsion system of a ship is crucial for its reliable navigation. In the past few decades, research aimed at optimizing propulsion systems has been conducted to ensure operational reliability under all service conditions. Notably, an important aspect of propulsion system research involves the development of oscillations during engine operation, specifically the development of torsional oscillations that can impose significant stresses on the system. The investigation of the oscillations is performed through dynamic system analysis. This vibrations analysis has been extensively utilized in the study of reciprocating engines, especially four-stroke engines. Although the literature on modeling two-stroke marine engines is more scarce, there have been studies conducted some studies in this area, with the main focus being the torsional vibrations.

Regarding the theoretical background of this thesis, an in depth understanding of the theories of FEM, ICE, vibration analysis, numerical integration as well as High Performance Computing Theory is required.

For the realisation of this thesis, the theoretical background for the geometrical parameters and function of the two-stroke marine diesel engines, further presented in **Section.** 2.2 and 2.3, was provided by the following the[16][17][18],[19][20]. These references delve into the theory of dynamic phenomena encountered in the two-stroke diesel engines, the propeller law required to estimate the torque the propeller demands from the engine, as well as the loading diagrams. For the friction in the engine, several models were investigated [14], [16], [17] Gas Pressure-Crank Angle diagrams. Finally, for the understanding of the thermodynamic phenomena for the diesel engine and for the production of the Gas Pressure-Crankshaft Angle diagrams, the following references were used [16], [18]

Regarding the theory behind the FEM integration and the Dynamic Simulation presented in **Section.** 4.1 and 4.2.1,the following references are of particular interest:[21][22][23][24][25][26][27][28][29][30][31]. These mathematical foundations explain in depth the theory behind FEM, numerical integration techniques and provide solutions to problems encountered in the definition of the system. Furthermore, the experimental procedure to evaluate the model using load cells is described in[32].

The above references, coupled with the bibliography references for the full dynamic simulation of the shafting system[33]

[16] *DNV GL completes study on the properties of EALs for stern tube applications*.
[17] "Basic principles of ship propulsion."
[18] "Torsional system dynamics of low speed diesel engines based on instantaneous torque," D. Palomo Guerrero *et al.*
[19] "Systematic Investigation of a Large Two-Stroke Engine Crankshaft Dynamics Model," K.-M. Tsitsilonis *et al.*
[20] *Transient Behavior-Function of Two-Stroke Marine Diesel Engine*, ΚΩΝΣΤΑΝΤΙΝΟΣ ΚΑΤΗΜΕΡΤΖΗΣ.
[21] "Improved numerical dissipation for time integration algorithms in structural dynamics," H. M. Hilber *et al.*
[22] *FEA Finite Element Procedures*, K.J. Bathe.
[23] "Hybrid physical and data driven modeling for dynamic operation characteristic simulation of wind turbine," J. Yan *et al.*
[24] *Damping in FEA Simulations | Materials*.
[25] "Method of Finite Elements I," N. Mojsilovic.
[26] *MATLAB codes for finite element analysis*, A. J. M. Ferreira.
[27] "Constitutive equations for elastic-plastic materials at finite strain," L. Freund.
[28] "The Finite Element Method for the Analysis of Non-Linear and Dynamic Systems," D. E. Chatzi.
[29] *ANSYS mechanical APDL for finite element analysis*, M. K. Thompson *et al.*
[30] "Problems encountered from the use (or misuse) of Rayleigh damping," J. F. Hall.
[31] *Numerical methods for partial differential equations*, S. Mazumder.
[32] **chatzi_finite_nodate-2**.
[33] "Experimental and numerical investigation on dynamic characteristics of ship propulsion shafting under uncertainty based on displacement response," X. He *et al.*

2 Marine Propulsion System

2.1 Reciprocating Internal Combustion Engines

Production of work using a thermal engine is based on the supply of heat to the working medium, resulting in a change in its energy state. This process is carried out through combustion, utilizing the chemical energy stored in the fuels. Part of this energy is converted into mechanical work, while the remainder is discharged back into the environment as heat.

The supply of heat can either take place within the main part of the engine or in a separate section. Internal Combustion Engines (ICE) are distinguished from external combustion engines by this exact feature, that is, the combustion for producing the necessary heat takes place within the engine. The main types of Internal Combustion Engines are piston engines, gas turbines, turbojets, static thermoreactors, and rocket engines. In ICEs, the working medium is air (with the fuel).

One of the most widespread motive thermal engines is the reciprocating internal combustion engine (ICE). Due to its simple construction and the ability to use the working medium at high temperatures, it is characterized by a high power density, good efficiency, and is extensively used in cars and ships. In all reciprocating ICEs, the working medium, whether it is air with fuel or just air, is drawn into the engine and compressed to a certain pressure. This increases its temperature and then the thermal energy from the combustion of the fuel is added, resulting in a further increase in temperature and pressure. During the subsequent expansion, mechanical work is produced. A part of this work is consumed for the previous compression and friction, while the rest is the useful work of the engine. Compression, combustion, and expansion are the basic operational phases of a reciprocating ICE. In addition to the three basic phases of operation, the phases of gas exchange are also of great importance for the engine's operation. That is the evacuation of the cylinder from the exhaust gas at the end of the expansion and the refilling of it with a new charge (air-fuel mixture) for the execution of a new cycle.

A fundamental classification of Internal Combustion Engines (ICEs) is made according to how the fuel ignition occurs. There are two categories:

- Otto engines
- Diesel engines

In Otto engines (named after their inventor, Nicolas August Otto), there is always ignition by some external means, most commonly an electric spark. Conversely, in Diesel engines (named after their inventor, Rudolf Diesel), there is always self-ignition due to the appropriate introduction of the fuel into the cylinder at a moment when its contents have been heated to a sufficiently high temperature, due to the prior relatively strong compression.
The main fuel for Otto engines is gasoline. Usually, a gasoline engine draws in a homogeneous air-fuel mixture that is prepared in a special device. However, there are also arrangements where gasoline is mechanically injected with the help of a fuel pump-injector system, which are distinguished into continuous injection systems and intermittent injection systems. Intermittent injection systems are divided into indirect injection (injection just before the intake valve) and direct injection (injection inside the cylinder).

The Diesel engine, also known as a diesel engine, always draws in atmospheric air and uses either light or heavy diesel oils as fuel. For the formation of the fuel mixture, the diesel is introduced into the cylinder dispersed into the mass of the already compressed air with the help of mechanical injection, that is, under the influence of the strong pressure created by the fuel pump-injector system.

Other classifications of Reciprocating Internal Combustion Engines can be made as follows:

1. **Number of Piston Strokes to Complete the Operating Cycle:**
   - Two-stroke engines
   - Four-stroke engines
2. **Angular Speed of the Crankshaft:**
   - Slow-speed engines up to 350 rpm (main ship engines)
   - Medium-speed engines up to 1500 rpm (ship, train engines, and power generation units)
   - High-speed engines up to 5000 rpm (wheel-based vehicles)
   - Very high-speed engines with rotational speeds above 5000 rpm (new technology cars, racing cars, large displacement motorcycles)
3. **Arrangement of the Cylinders:**
   - Vertical or in-line
   - Types V, W, H, Flat, X
   - Horizontal (boxer)
   - Radial (mainly as propeller aircraft engines)
   - Opposed, polygonal, double-piston
4. **Method of Connecting Piston – Crosshead:**
   - With connecting rod and crosshead
   - Without connecting rod and crosshead
5. **Method, Pressure, and Quantity of Air Introduced into the Cylinder:**
   - Atmospheric engines or natural aspiration engines
   - Supercharged engines
6. **Power Output per Cylinder at Normal Operating Revolutions:**
   - Low power (up to 20 PS)
   - Medium power (up to 200 PS)
   - High power (more than 200 PS)

The main characteristic of Reciprocating Internal Combustion Engines is the conversion of the reciprocating motion of the pistons into the rotary motion of the crankshaft. The piston-crosshead-crankshaft mechanism constitutes the main kinetic mechanism that makes up the reciprocating ICE, as presented in the following image:

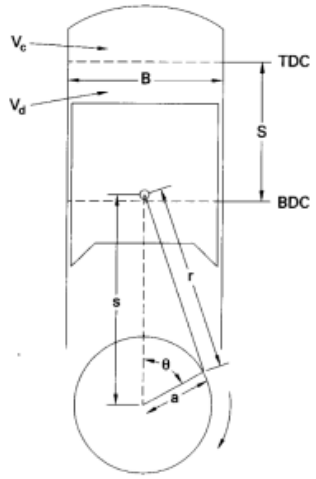

Figure 1: Kinematic Mechanism of Reciprocating ICE

With this mechanism, the reciprocating motion of the piston is converted through the crosshead into rotational motion at the crank. Due to this reciprocating motion, the piston operates between two extreme points called the Top Dead Center (TDC) and the Bottom Dead Center (BDC). The distance the piston travels from TDC to BDC is called the stroke of the piston and corresponds to a half rotation (180º) of the crankshaft.

The main geometric characteristics of the reciprocating engine are:

- The length of the connecting rod: r
- The length of the crank: a
- The stroke of the piston S, for which it holds: $S = 2a$
- The diameter of the piston D
- The displacement volume of the cylinder V_d, which is the volume swept by the piston during one stroke: $V_d = \frac{\pi D^2 S}{4}$
- The clearance volume V_c, which is the volume of the cylinder above the piston head when the piston is at TDC
- The compression ratio: $\epsilon = \frac{V_d + V_c}{V_c}$
- The rotational speed n in rpm
- The crank angle θ
- The mean piston speed: $c_s = \frac{2\pi n}{60}$

2.2 Two-Stroke Marine Engines

2.2.1 Basic Characteristics of Two-Stroke Marine Engines

In recent decades, the Diesel reciprocating engine has become the predominant main propulsion machinery for ships. The primary reasons are the superior thermodynamic efficiency of the Diesel reciprocating engine compared to steam turbines or gas turbines, and the ability of the Diesel reciprocating engine (similar to the steam turbine) to burn lower-quality, thus less expensive fuels, making it the most economical option. The marine engines used extensively in commercial or passenger vessels are categorized into:

- Two-stroke slow-speed
- Four-stroke medium-speed

This classification of engines is based on their basic operational phases (compression, combustion, expansion), the phases of gas exchange (intake of air into the cylinder, expulsion of exhaust gases from the cylinder), and the rotational speed of the crankshaft.

In two-stroke engines, the production of work is completed in two strokes (intake-compression, power-exhaust), as depicted in the image below.

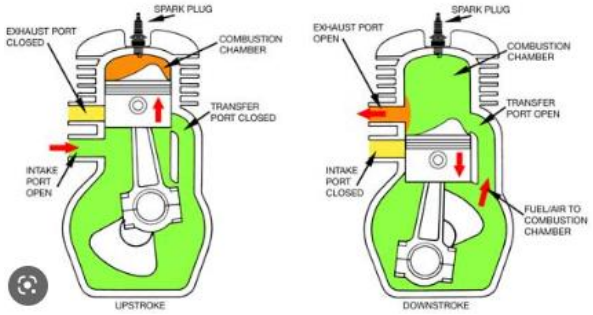

Figure 2: Two-Stroke ICE Function

Contrary to two-stroke engines, in four-stroke engines, the work production is completed in four strokes: intake, compression, power (expansion), and exhaust. This cycle allows for separate and distinct phases for each part of the engine cycle, which is presented in the image below.

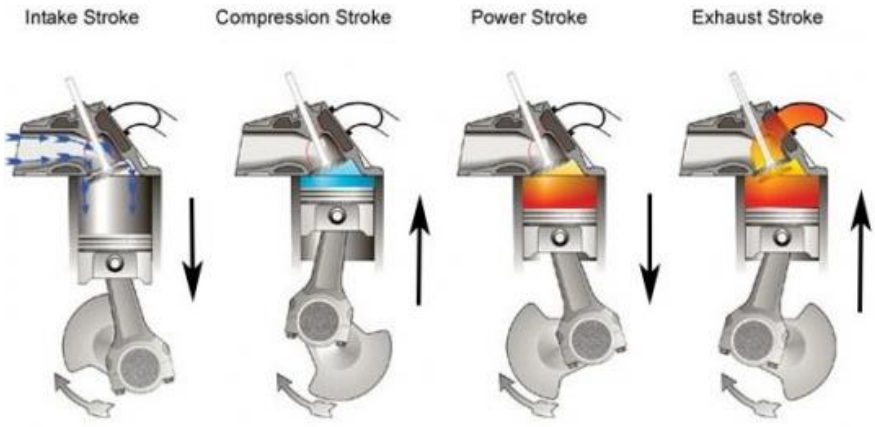

Figure 3: Four-Stroke ICE Function

On large commercial ships, large Diesel engines are used as the main propulsion system. TThe two-stroke engine has prevailed over the four-stroke because it has a more efficient power concentration for the same engine size and also has a higher efficiency. An key advantage of the two-stroke engine over the four-stroke is its ability to utilize lower-quality, hence less expensive fuels. This is feasible due to the slow rotational action of the two-stroke engine, which translates into a slow reciprocating motion of the piston, providing the necessary time for efficient combustion. A significant role in this process is also played by the large displacement volume of the cylinder, allowing for adequate air supply for complete combustion of the low-quality fuel used in commercial ships.
Another significant factor concerning the choice of the two-stroke slow-speed engine for the propulsion of a commercial ship is the rotational speed of the propeller. Large ships, with their large propellers, require low rotational speeds for a high degree of propeller efficiency. Generally, for a given ship

speed, lower revolutions, and therefore a larger propeller diameter within the constraints due to the geometry of the hull and the draft of the ship, lead to a higher degree of propulsion efficiency and thus to reduced fuel consumption of the propulsion installation. Therefore, slow-speed two-stroke engines have another advantage over medium-speed four-stroke engines since the latter require a reduction gear to connect with the propeller, increasing construction weight, moving parts, and mechanical losses of the system. Finally, due to the size of their cylinders, two-stroke engines can provide more power with fewer cylinders compared to four-strokes, thereby reducing moving parts and increasing their reliability.
A characteristic of engines is that the mean piston speed cannot fall below a certain value. For this reason, in two-stroke slow-speed engines, the reduction of revolutions, which is very important for the efficiency of the installation as previously described, is achieved by increasing the stroke of the piston. This leads to large stroke-to-bore ratios (Stroke/D), especially in large two-stroke marine engines.

However, four-stroke engines also have certain advantages over two-stroke engines, thus finding significant application in some commercial vessels such as Ro-Ro ships, passenger ships, and in smaller vessels like yachts. Their primary advantage is their size. In commercial ships such as Ro-Ro or passenger ships where the interior is configured with decks to serve their purpose, two-stroke engines are difficult to apply due to their considerable height. Furthermore, on such ships, the presence of two engines for safety reasons is necessary, thus the placement of two two-stroke engines becomes impossible due to spatial constraints and increased weight considerations.

Power Calculation

The dimensions of an engine are dependent upon multiple parameters, with a significant attribute being the generated power. The power output of an engine is contingent upon the quantity of cylinders it possesses, with each cylinder's power primarily influenced by the piston's diameter (bore) and the piston's travel distance (stroke).

The calculation of the power of a cylinder is given by the following formula:

$$P = P_e \cdot V_h \cdot \frac{n}{30 \cdot K} \tag{2.1}$$

where:

- P: Power per cylinder
- P_e: Mean effective pressure
- V_h: Displacement volume of the cylinder, $V_h = A \cdot Stroke$
- A: Piston area, $A = \frac{\pi \cdot D_p^2}{4}$
- D_p: Piston diameter
- $Stroke$: Stroke of the piston
- n: Operating revolutions of the engine
- K: Coefficient ($K = 2$ for two-stroke engines, $K = 4$ for four-stroke engines)

Finally, the power of the engine is calculated by multiplying the power of one cylinder by the number of cylinders of the engine.
For a two-stroke marine engine to be able to provide the power that is required, certain systems are necessary for its operation. All large two-stroke marine engines are supercharged and are equipped

with an intercooler for the supercharging air. This is done firstly to further increase the power concentration for a specific engine size and to achieve better cylinder scavenging, and secondly because it allows for the exploitation of the thermal energy of the exhaust gases, thus increasing the engine's efficiency. This process is carried out via the turbo-supercharger. The exhaust gases, with their high thermal energy, move a turbine that is connected by a shaft to another turbine that compresses air into the scavenging chamber. A two-stroke marine engine may have from 1 to 4 turbo-superchargers depending on the air supply requirements for a given fuel supply.

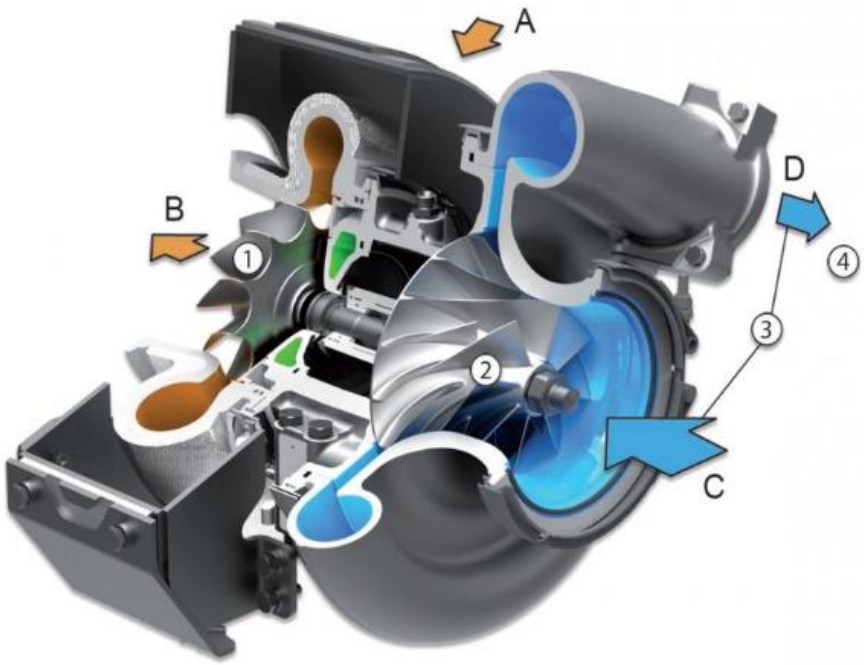

Figure 4: Section of Turbocharger

During engine operation at low load (starting, maneuvering), the temperature of the exhaust gases is low, resulting in the turbocharger alone not being able to provide the required scavenging pressure at low loads. Therefore, it must be assisted by some additional energy. This can be achieved with electrically driven blowers that provide the necessary amount of air so that the air pressure for scavenging is such that combustion occurs smoothly.

The starting system of two-stroke marine engines, which is done with compressed air, is also of interest. This is due to the large masses that need to be moved and require an initial impulse that cannot be provided by the fuel or through electrical energy (starter motor). Thus, there are air compressors that supply air to air reservoirs where the compressed air is stored. During starting, the compressed air is supplied to the cylinder that is in the appropriate position (slightly after Top Dead Center) so that the engine movement begins. In case the start is not possible by supplying air to only one cylinder, the compressed air is also provided to a second cylinder. The compressed air is usually supplied at a pressure of 30 bar.

A typical starting system of a two-stroke marine engine is presented in the image below.

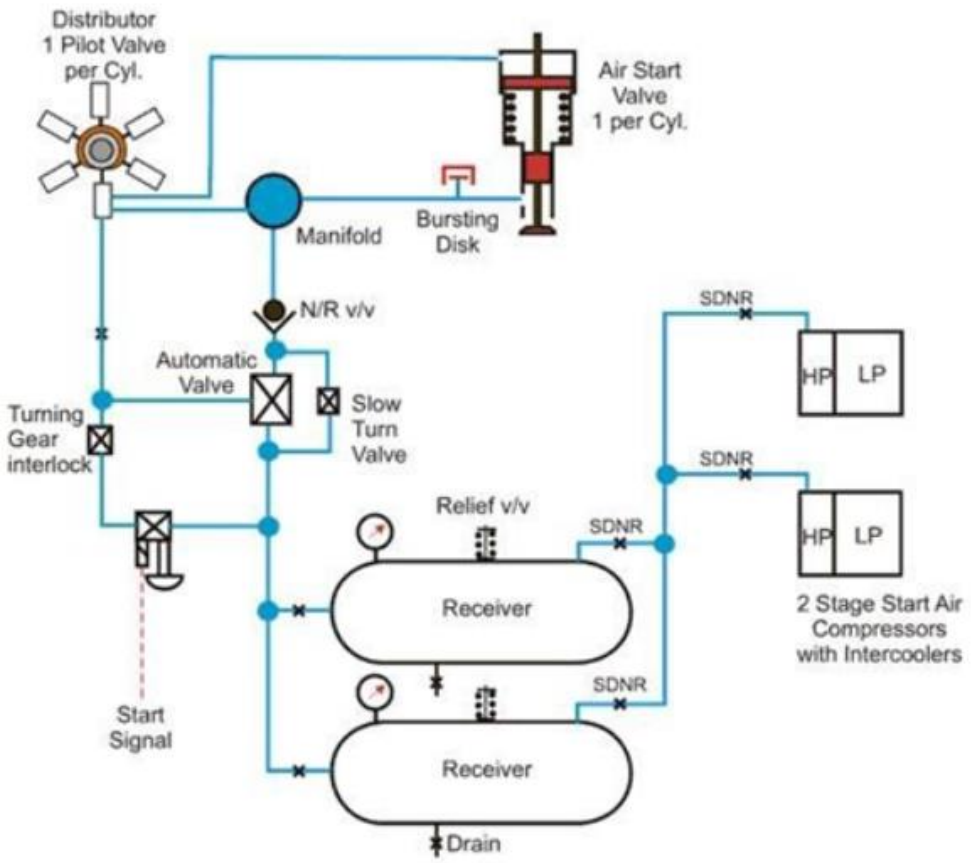

Figure 5: Starting System with Pressurised Air

The main configuration of a two-stroke marine engine consists of three distinct sections:

1. Base
2. Frame
3. Cylinder Cover

There are essentially three different sections in every two-stroke marine Diesel engine. The engine base is mounted on the ship's hull, supports the engine, and ensures the alignment of the shaft. The mounting of the base is carried out either with chocks (less commonly) or with liquid resins that solidify, filling any gaps between the engine base and the hull of the ship. Suitable materials are used for the construction of the engine base to make it as strong and rigid as possible while keeping its weight low.

The crankshaft is placed in the base of the engine and is one of the heaviest and most expensive components of the engine. It is manufactured in sections and is responsible for converting the reciprocating motion of the pistons into rotary motion. Each section consists of two arms (webs) that are connected to each other with the lower crosshead journal and make up the crank throw. The crank throws are interconnected with the main journals which are mounted on the base of the engine.

Figure 6: Crankshaft of a Two-Stroke Marine Engine

The frame of the engine connects the cylinder assembly with the engine base. Each cylinder includes a piston that performs reciprocating motion, a connecting rod that links the piston with the crosshead, and the crosshead that connects the piston-connecting rod system with the crankshaft, converting the reciprocating motion into rotary motion. Additionally, the frame includes liners within which the movement of the piston occurs and combustion takes place. The liners serve to better insulate the combustion chamber and protect the engine body from the high pressures and temperatures within the combustion chamber.

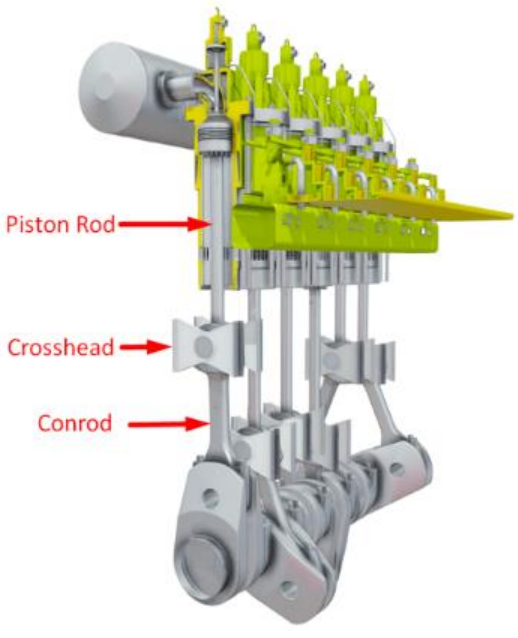

Figure 7: Piston rod-Crosshead-Conrod System

A diaphragm separates the cylinders from the crankcase chamber. This keeps the combustion products from getting into the crankcase chamber and changing the composition of the lubricating oil there. The diaphragm also serves as the lower limit of the scavenging air chamber, which envelops the lower part of the liner. A stuffing box allows the connecting rod to pass through the diaphragm while maintaining the seal between the scavenging air chamber and the crankcase chamber.

To convert the reciprocating movement of the piston-connecting rod assembly into the crankshaft's rotational movement, a bearing system supported by the crosshead is essential. The crosshead's top part attaches to the crosshead bearing, which is then bolted to the connecting rod. The crosshead's bottom part connects to the crankshaft. When the engine is running, the forces on the connecting rod and crosshead vary in accordance with the angular position of the crosshead as a result of crankshaft rotation. It's crucial to balance the side forces caused by the crosshead's angular movement. The crankshaft bearings directly handle the forces applied to it, while the forces on the crosshead require the use of shoes and guides.

Regarding the cylinder cover, this is where the fuel pumps and injectors are located, along with the exhaust valve for each cylinder, the intake for the electric blowers, and the air intake for starting the engine. The timing of the fuel injection and the exhaust valve is either mechanically synchronized using a camshaft, which is driven by the crankshaft through a chain in older engines, or in more modern engines by electronic means using hydraulic actuators, which tend to eliminate the use of the camshaft.

Lastly, the lubrication system of marine two-stroke engines is of particular interest. Unlike medium-speed engines without a crosshead, where a single lubricant is used for the entire engine necessitating compromises regarding its properties, in slow-speed engines, a different lubricant is used within the crankcase for the lubrication of its bearings, and a separate cylinder oil with alkaline properties to counteract the acidic residues of combustion is used for the lubrication of the combustion chamber. This cylinder oil is also burnt in the combustion chamber.

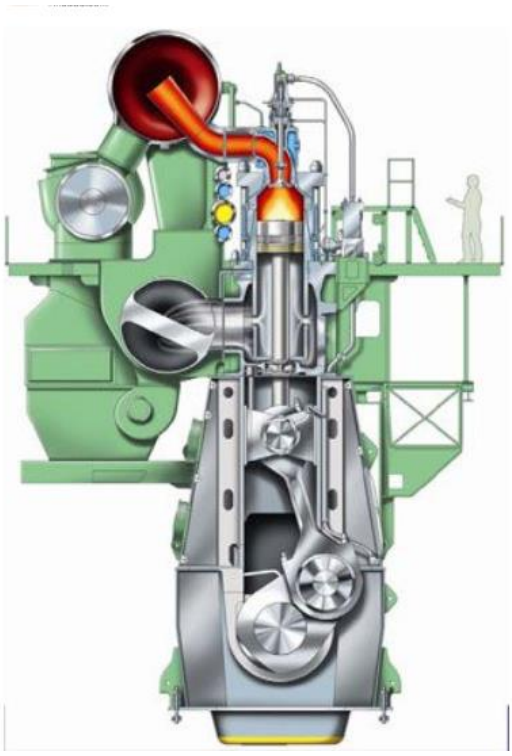

Figure 8: Section of Two Stroke Marine Engine

A pivotal role in the transitional response of a two stroke marine engine is played by the speed governor. The governor is a mechanism that controls the engine's revolutions in relation to its load and intervenes in the fuel supply by making the appropriate adjustments. This mechanism is responsible for maintaining steady revolutions during the engine's continuous operation and for changing (increasing or decreasing) the revolutions during transitional operation. Moreover, it limits the engine's maximum rotational speed and regulates the stability of its operation at minimum revolutions. The governor is crucial in adverse weather conditions with wave motion that can cause the propeller to ventilate. In such a case, the governor will limit the fuel supply to prevent an uncontrollable increase in the engine's operating revolutions due to a lack of load from the propeller, which could lead to damage to the shaft system and the support bearings due to high temperatures. The governor also sets the limits for engine operation in an overload condition, which are: torque limiter and scavenging air pressure limiter. The basic operating principle of the speed governor is presented in the image below.

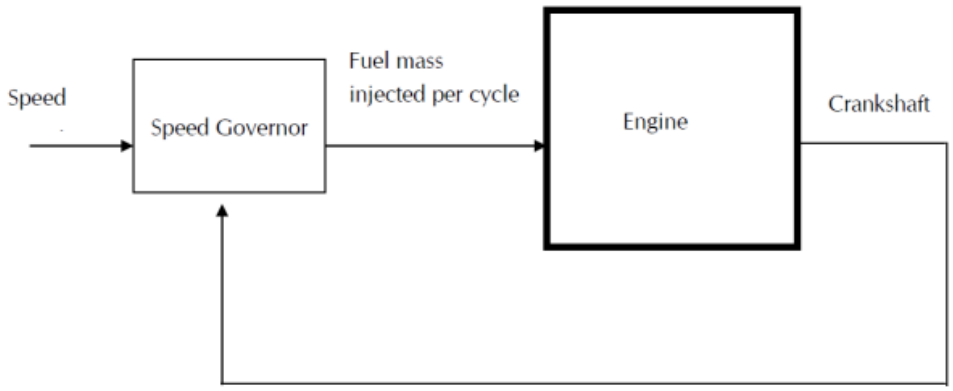

Figure 9: Governor's function schematic

2.2.2 Layout Diagram of a Two-Stroke Marine Engine

In two-stroke marine engines, the manufacturer provides the ability to adjust the power and operating revolutions according to the requirements of the respective vessel. The diagram showing the range of operating capabilities is called the Layout Diagram. The Operating Region Diagram is bounded by two mean effective pressure (MEP) lines L1 - L3 and L2 - L4, and by two lines cf constant engine speed, L1 - L2 and L3 - L4. Point L1 corresponds to the nominal maximum continuous power of the specific engine type. Within the operating field, there is complete freedom to choose and define any point within the diagram as the Maximum Continuous Rating (MCR). The choice of point is mechanically made through the amount of fuel supplied, the timing of the exhaust valves, the compression ratio, and the coupling of the supercharger. The ideal determination of the MCR point is a critical factor for the operation of the ship. It should be made based on the characteristics of the ship and the estimated resistance, as well as the service speed required for the ship. A qualitative Layout Diagram of a two-stroke marine engine follows in the image below.

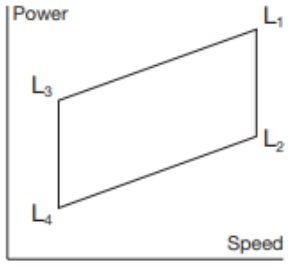

Figure 10: Layout Diagram of Two-Stroke Marine Engine

2.2.3 Loading Diagram of a Two-Stroke Marine Engine

The loading diagram of the engine (Loading Diagram) defines the limits of power and revolutions for continuous and transitional operating conditions, as well as for overloading conditions, of an installed engine that has an optimal operating point and a defined MCR corresponding to the ship's specifications.

The image below follows with a qualitative Loading Diagram of a two-stroke marine engine, along with propeller operation curves described in Section 2.2.4. This particular diagram is provided by the manufacturer of two-stroke marine engines WinGD and pertains to all engines manufactured by them.

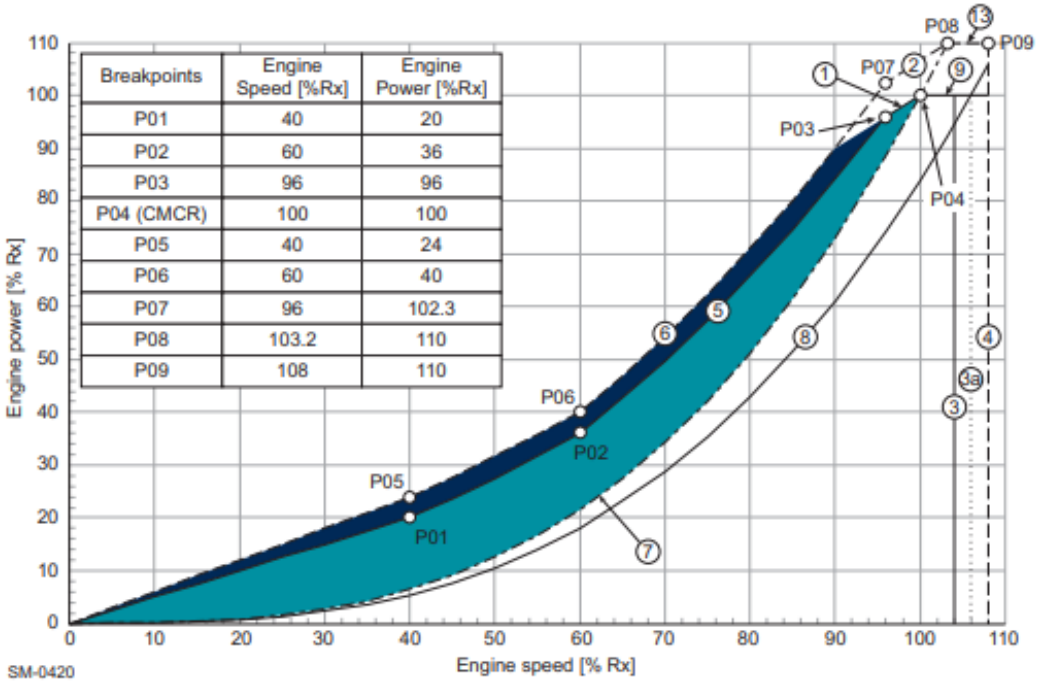

Figure 11: Loading Diagram of Two-Stroke Marine Engine

The curves of the Engine Loading Diagram are explained as follows:

- Line 1: Line 1 represents the maximum mean effective pressure for continuous operation of the engine.

- Line 2: Line 2 pertains to the engine's overload. It represents the maximum mean effective pressure and is available during engine trials and emergency situations.
- Line 3: Line 3 represents the maximum rotational speed that can be accepted for continuous operation and is equal to 104% of the Maximum Continuous Rating (MCR).
- Line 4: Line 4 represents the engine's overspeed limit. During sea trials, and only then, the maximum speed can be extended to 108% of the MCR.
- Line 5: Line 5 represents the limit of continuous operating power. Line 5 is a curve divided into individual curves to form the whole. The factors for its creation and the method of construction are described in detail below.
- Line 6: Line 6 represents the maximum power limit under transient conditions. Line 6 is a curve divided into individual curves to form the whole. The factors for its creation and the method of construction are described in detail below.
- Line 7: Line 7 corresponds to the propeller curve passing through the MCR point and follows the propeller law. This line corresponds to the heavy operation curve of the propeller, i.e., for a fouled hull and adverse weather conditions.
- Line 8: Line 8 corresponds to the light operation curve of the propeller, i.e., for a clean hull and good weather conditions, and follows the propeller law.
- Line 9: Line 9 represents the maximum power for continuous operation of the engine.
- Line 13: Line 13 corresponds to 110% of the engine's maximum continuous power and is the overload limit. Line 13 is available during engine trials and emergency situations.

The following operating areas are defined in the Engine Loading Diagram:

- The area formed by lines 1, 3, 5, and 9 is where the engine should operate continuously without time limitations. This area allows for the engine's continuous operation.
- The area bounded by line 7, line 9, and line 3 pertains to the engine's continuous operation, while the area between line 7, line 5, and line 1 pertains to the engine's transitional operation.
- The area between line 1, line 5, and line 6, known as the "time-limited operating range," is available only for transient conditions, such as sea trials or during necessary emergency acceleration. The engine may operate in this area for limited periods only (1 hour every 24 hours).
- The area above line 1 and line 9 represents the engine's overload range. Operation within this range is permitted for a maximum duration of one hour during sea trials, in the presence of authorized representatives of the engine manufacturer.
- The area between lines 3 and 4 is the engine's overspeed range. Operation within this range is allowed only during the conduction of sea trials, in the presence of authorized representatives of the engine manufacturer.

The lines 2,6,13 represent the limitations imposed by the engine's load controller (governor) and they are the following:

1. **Torque Limiter**
   The purpose of the torque limiter function is to ensure the engine operates within the allowable region of the loading diagram. The algorithm of the torque limiter compares the calculated position of the fuel rack (i.e., the fuel quantity) and the actual measured engine speed with a reference curve provided by the limiter. This curve represents the maximum allowable position of the fuel rack for a given engine speed. If the calculated position of the fuel rack exceeds this curve, the resulting position of the fuel rack is appropriately reduced.

2. **Air Scavenge Pressure Limiter**
   The purpose of the air scavenge pressure limiter is to prevent over-fueling of the engine during acceleration, such as during maneuvers. The algorithm of the air scavenge pressure limiter compares the calculated position of the fuel rack and the measured air scavenge pressure with a reference curve provided by the limiter. This curve represents the maximum allowable position of the fuel rack for a given air scavenge pressure. If the calculated position of the fuel rack exceeds this curve, the resulting position of the fuel rack is reduced accordingly. The reference curve of the limiter is adjusted to ensure that sufficient air is always available for complete combustion.

2.2.4 Propeller Law

The law of the propeller is stated as follows: "The necessary power absorbed by the propeller is proportional to the cube of the rotation rate."

The resistance R for low-speed ships is proportional to the square of the ship's speed V, that is, $R = cV^2$, where c is a constant. The required power P is proportional to the cube of the speed V and consequently: $P = RV = cV^3$.

For a ship with a fixed pitch propeller, that is, a propeller whose pitch cannot be changed, the ship's speed V will be proportional to the rate of rotation n of the propeller, that is: $V = kn$, where k is a constant. Thus, the following equation that defines the law of the propeller is ultimately derived:

$$P = cn^3$$

Real measurements have shown that the relationship between power and engine revolutions for a given weather condition is quite reasonable. The law of the propeller can, of course, be used for similar functions of the ship. For example, when the hull of the ship after some time of operation has been polluted and thus has become rougher, the field of the homogenous wake will be different from that of a ship with a smooth (clean) hull as it was in the acceptance tests. A ship with a polluted hull will face increased resistance, which will result in a "high loading of the propeller," that is, for the same power on the propeller, the rate of rotation will be lower. The law of the propeller applies to a different "higher" propeller curve from that which applies to a clean hull. The same proportional conditions also apply when the ship travels in bad weather or against the current. Additionally, if the ship sails in a lightened condition, that is with a lower draft, the law of the propeller applies to a "lower" propeller curve, that is, for the same propeller power, the rate of rotation will be higher.

The law of the propeller is a very useful approximation for the preliminary study and estimation of the thrust power required on a ship.

Therefore, for a ship with a fixed pitch propeller, the power can be expressed as an exponential function of the rotation speed n with an exponent i, that is: $P = cn^i$.

These exponential functions can be represented as linear on a logarithmic scale, transforming the above relationship into the form $y = ax + b$ as follows:

$$\log P = i \cdot \log n + \log c$$

Consequently, the curves of the propeller will be parallel to the straight lines with a slope $i = 3$. Thus in the field of operation and in the engine load diagram, logarithmic scale is used, turning the various

curves into simple straight lines.

For the determination of the constant c, a point $(P$ (power), n (rotations)) of the ship's operation is used.

The curve of the law of the propeller is presented in section 2.2.3 (Diagram of Marine Engine Loading). Curve 8 pertains to a clean hull and good weather conditions, while curve 7, which is shifted to the left relative to curve 8, pertains to a polluted hull and bad weather conditions.

2.2.5 Engine Shop Test

Engine shop tests, or Shop Test, are carried out on land before the engine is delivered to the ship. Instead of a propeller, the engine is connected to a hydraulic load that follows the law of the propeller for the required torque. In the shop tests of the engine under study, tests were carried out for the following loads: 25%, 50%, 75%, and 100%. The parameters studied from the shop tests are as follows:

- Engine power
- Engine rotation speed
- Load force
- Exhaust gas exit temperature from each cylinder
- Exhaust gas temperature at the inlet and outlet of the turbocharger
- Maximum pressure in each cylinder
- Compression pressure in each cylinder
- Cooling water and lubricant temperatures and pressures for each engine system
- Specific fuel and cylinder oil consumption
- Scavenging air pressure and temperature
- Pressure drop in the turbocharger air cooler

Based on the shop tests, the Cylinder Pressure-Crankshaft Angle diagrams are constructed for the four operating points (25%, 50%, 75%, and 100%).

The main elements of the shop tests of the engine under study (power, engine rotation speed) are presented below for the four loads of the tests.

Load Engine %	Engine Power (kW)	Rotational Speed (rpm)
25	1588	62.4
50	3175	78.6
75	4763	89.9
100	6350	99

Table 2.1: Engine Loads

2.3 Marine Propulsion System

The selection of the appropriate propulsion system for a specific ship is a rather complex process. It presupposes the examination of many alternative solutions, which are technologically available at the given time, in relation to the operating characteristics of the ship under study. The factors that affect the decision-making are many, while there are now also several alternative choices. The main options for propelling a commercial or passenger ship are the placement of a slow-speed two-stroke diesel engine with direct drive fixed pitch propeller, or a medium-speed four-stroke diesel engine with fixed or variable pitch propeller, connected to the engine through a reduction gear. In commercial ships, two-stroke marine engines are widely used because of their advantages, as analyzed in Section 2. Apart from the main engine of the ship, a propulsion installation also includes the shafting system of the ship which is responsible for transferring power from the engine and finally the propeller which is responsible for propelling it by converting the rotational motion of the engine into thrust force.

A typical propulsion installation of a ship follows in the image below. In it is presented the main engine of the ship, two-stroke or four-stroke, the reduction gear which in the case of two-stroke engines is absent, the thrust bearing which is usually located within the body of the main engine, the intermediate bearings or thrust bearings that support the weight of the shaft, the shafting system of the ship, the stern tube bearings, and the ship's propeller.

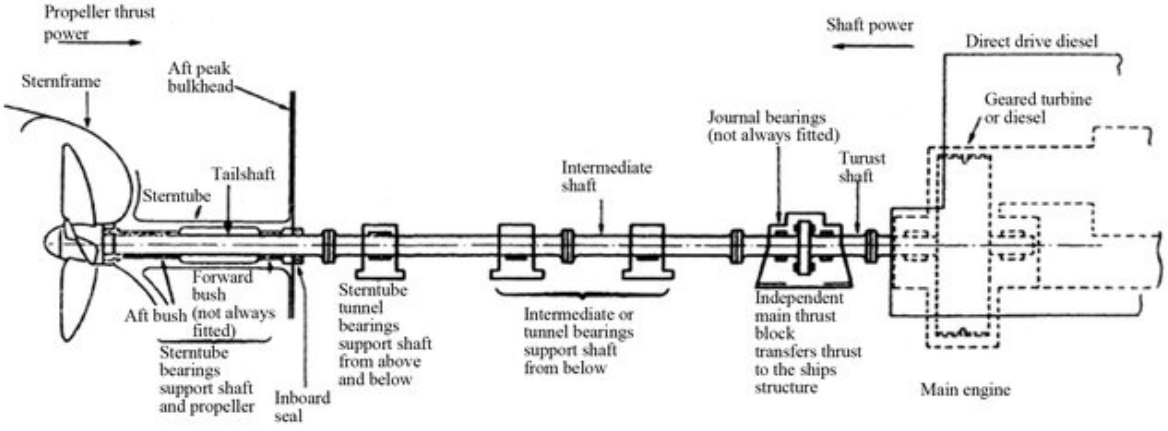

Figure 12: Typical Propulsion System of Merchant Vessel

2.4 Main Diesel Engine Components

The main propulsion engine is responsible for producing the required power to move the ship. The component responsible for the rotary motion is the crankshaft. The crankshaft can be divided into individual elements:

- A discrete mass system consisting of the part of the crankshaft that connects with the piston-rod-piston system.
- Damper
- Flywheel

The division of the crankshaft into the above individual sections is significant for determining the dynamic phenomena that are studied in this work, through the modeling of the propulsion installation as a system of discrete masses.

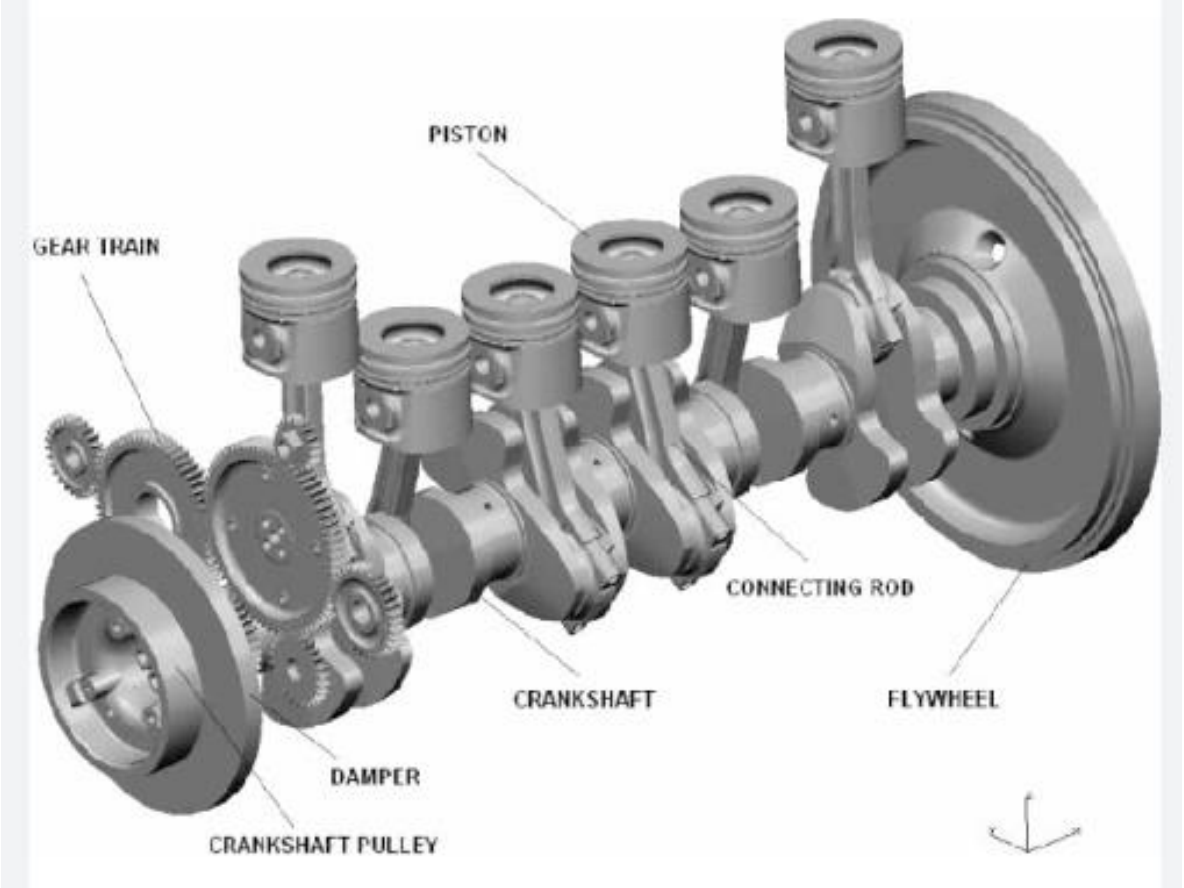

Figure 13: Engine Internals

2.4.1 Damper

Due to the time-varying forces applied to a two-stroke marine engine (forces due to combustion, inertial forces), torsional vibrations develop in the shafting system. The purpose of the damper is to reduce the amplitude of these torsional vibrations. The damper is usually placed at the free end of the crankshaft and consists of a primary and a secondary part. Between these parts are steel spring sheets forming chambers that are filled with pressurized oil. The steel springs are tuned to optimize the natural frequency of each system. The oil is used to reduce the torsional vibrations through hydraulic damping. The elasticity of the damper is determined by the shape and number of its springs. Thus, the torsional system is detuned, and the most critical resonance is eliminated, reducing the remaining torsional vibrations as well.

Figure 14: Torsional Damper (Geislinger)

2.4.2 Flywheel

The flywheel is a component with a large mass and a large moment of inertia. Its purpose is to contribute to the engine's effort to consistently supply kinetic energy to the ship's propulsion system. Due to its large inertia, the kinetic energy it acquires changes only slightly due to the uneven torque provided by the cylinders due to combustion, allowing the system to maintain a steady rotational speed. The usefulness of the flywheel is even greater in engines with a small number of cylinders (5,6), where the time interval between the combustion of cylinders is longer than in multi-cylinder engines. The following image presents a ship engine where the flywheel is clearly visible.

Figure 15: Flywheel

2.4.3 Reduction Gear

The reduction gear is used in medium-speed engines, consists of a gear system, and aims to reduce the revolutions received by the ship's propeller from the engine since the maximum efficiency of the propeller is presented at low operating revolutions. The reduction ratio of the reduction gear arises from the ideal operating revolutions of the engine and the ship's propeller.

Figure 16: Section of Reduction Gear

2.4.4 Shafting System

The ship's shafting system usually consists of 2 or more shafts depending on its length. One shaft is called the propeller shaft or propeller shaft, and the ship's propeller is connected to it. The forward end of it has an integrated flange for connection with the intermediate shafts, while the stern end of the shaft has a conical shape and ends in an appropriate thread. The propeller with the corresponding conical shape is fitted onto the shaft and tightened with an independent nut, the tightening direction of which is opposite to the direction of rotation of the propeller during forward motion. The torsional moment is transferred from the propeller shaft to the propeller by friction, due to the strong tightening force exerted by the nut.

Figure 17: Propeller Shaft & Intermediate Shaft

The other shaft is called intermediate and connects the ship's main engine with the propeller shaft. The intermediate shaft at its ends has integrated flanges that are made of soft forged steel. In case the main engine of the ship is not located completely at the stern of the ship, the existence of more than one intermediate shaft is deemed necessary. The ships where the existence of large shafting systems hence more than one intermediate shaft is more frequently encountered are container ships (containerships) where due to their sleek hull, the main engine is placed more forward compared to ships such as freighters or tankers.

2.4.5 Journal Bearings

The intermediate bearings or journal bearings are elements consisting of two cylindrical surfaces in motion, between which lubricant is supplied to reduce the developed friction and to conduct away the generated heat. Inside a journal bearing, there is a liner supported on the inside of a housing. The ship's shaft comes into contact with the liner. In simple journal bearings, the shaft moves relative to the stationary surface of the bearing. During the operation of the journal bearing, the following lubrication areas are distinguished:

1. Boundary lubrication: The roughness of the shaft and the bearing come into contact with each other. The lubricant has the thickness of a molecular layer.
2. Mixed lubrication (semi-fluid): Part of the load is taken by the lubricant through the developed pressure, while another part by the contact of the roughness of the shaft and the bearing.
3. Elastohydrodynamic lubrication: Existence of a lubricant wedge.
4. Hydrodynamic lubrication: With the rotation of the shaft, the incoming oil creates a lubricant film capable of lifting the shaft's load. The film is created due to the motion of the shaft.

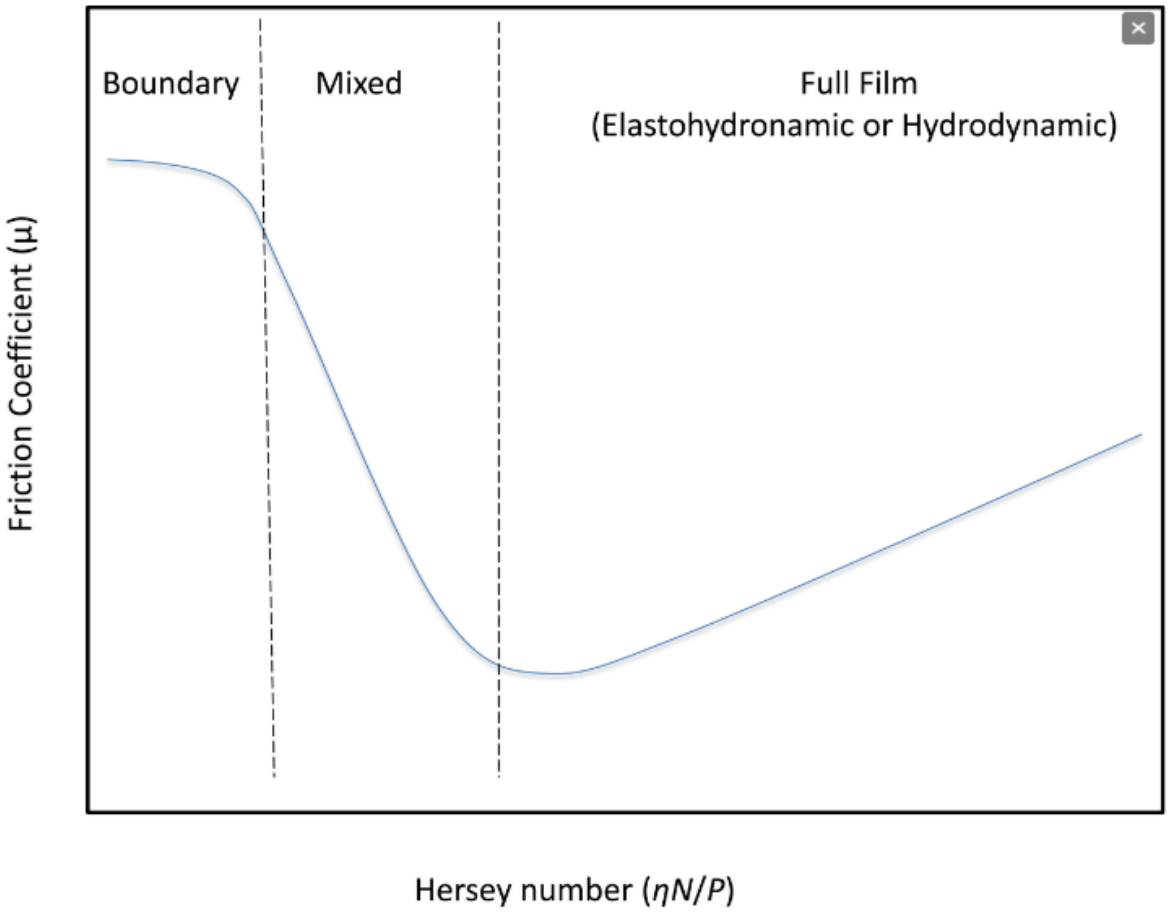

Figure 18: Journal Bearing Lubrication Regions

2.4.6 Thrust Bearing

The thrust bearing transfers the thrust from the propeller through the propeller shaft to the ship's hull, without allowing axial displacement. It is made of durable materials in order to withstand the thrust load and to transfer it to the metal structure of the ship. It is usually placed within the body of the main engine at its stern end so that thrust loads are not transferred from the propeller shaft to the crankshaft of the engine or to an installed reduction gear, which may be interposed. A thrust bearing is presented in the images below.

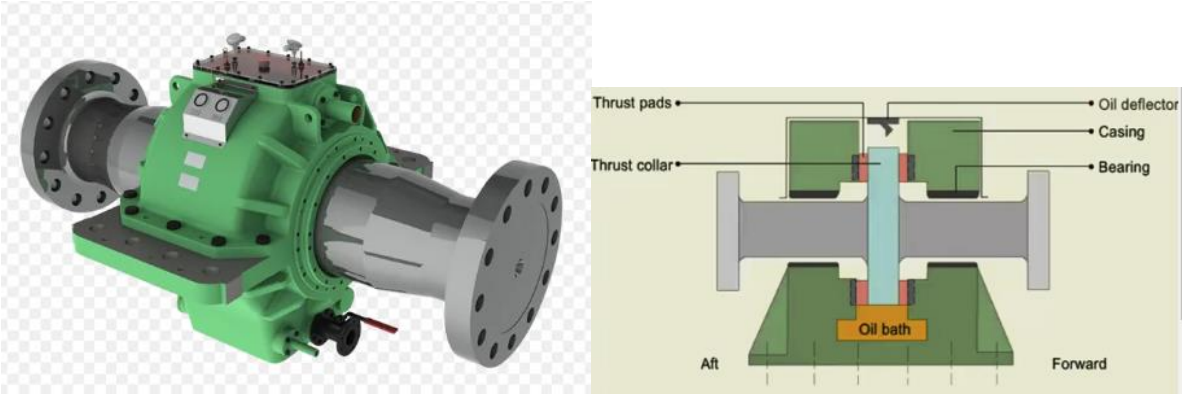

Figure 19: Thrust Bearing & Section of Thrust Bearing

2.4.7 Sterntube Bearings

The stern tube (stern tube) is the part of the ship's hull from which the propeller shaft exits. For the sealing of the stern tube, there are sealing systems that prevent the ingress of water into the interior as well as the outflow of lubricant that is inside for the lubrication of the shafting system. The stern tube bearings are responsible for receiving the weight of the propeller shaft. The propeller shaft is usually based on two journal bearings in the ship's stern tube. The sternmost bearing usually has a large length-to-diameter ratio to receive the large loads created due to the existence of the propeller as a cantilever beam.

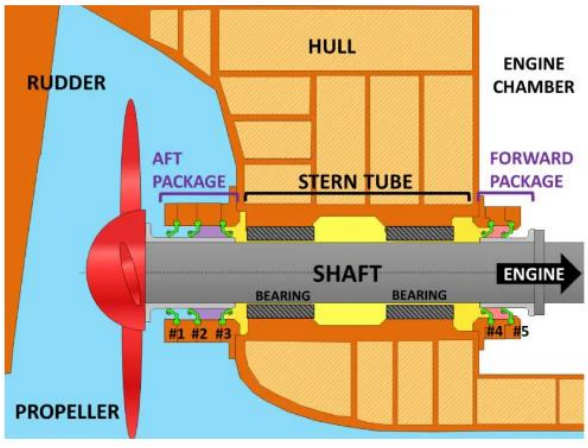

Figure 20: Stern Tube Bearing Section

2.4.8 Propeller

The ship's propeller is the most widespread propulsion system and is responsible for moving the ship. The propellers convert the mechanical energy on the propeller shaft into kinetic energy of the water. The rotational motion of the propeller increases the momentum of the water flowing between its

blades. At the same time, a force is induced on each blade by the fluid, which is resolved into a peripheral resisting component and an axial thrust force. The peripheral components of the forces of the blades create the opposing torque of the propeller, which is overcome by the torsional torque of the engine. The propeller can be fixed pitch (Fixed Pitch Propeller – FPP) or controllable pitch (Controllable Pitch Propeller – CPP). In the first case, reverse motion is achieved by reversing the direction of rotation of the engine, with poor efficiency of the propeller during reverse motion. In the second case, the blades have the ability to change their inclination relative to the axis of rotation, so the efficiency of the propeller can be optimized depending on the speed of the ship. By reversing their inclination, reverse motion is achieved, without the need to change the direction of rotation of the engine. Controllable pitch propellers are usually used in passenger-vehicle ferries and generally in ships where a large maneuvering capability is required. Conversely, in ocean-going ships, which move in open seas at a steady speed for long periods, fixed pitch propellers are usually used.

The power absorbed by the propeller at a given speed of the ship depends on the condition of the propeller, the condition of the ship's hull, the draft, the state of the sea, the currents, the speed and the direction of the wind. During the service of the ship, the absorbed power for a given speed increases, due to the increase in the roughness of the hull and the wear of the propeller. The above phenomenon is described in the law of the propeller through the coefficient ¨C¨.

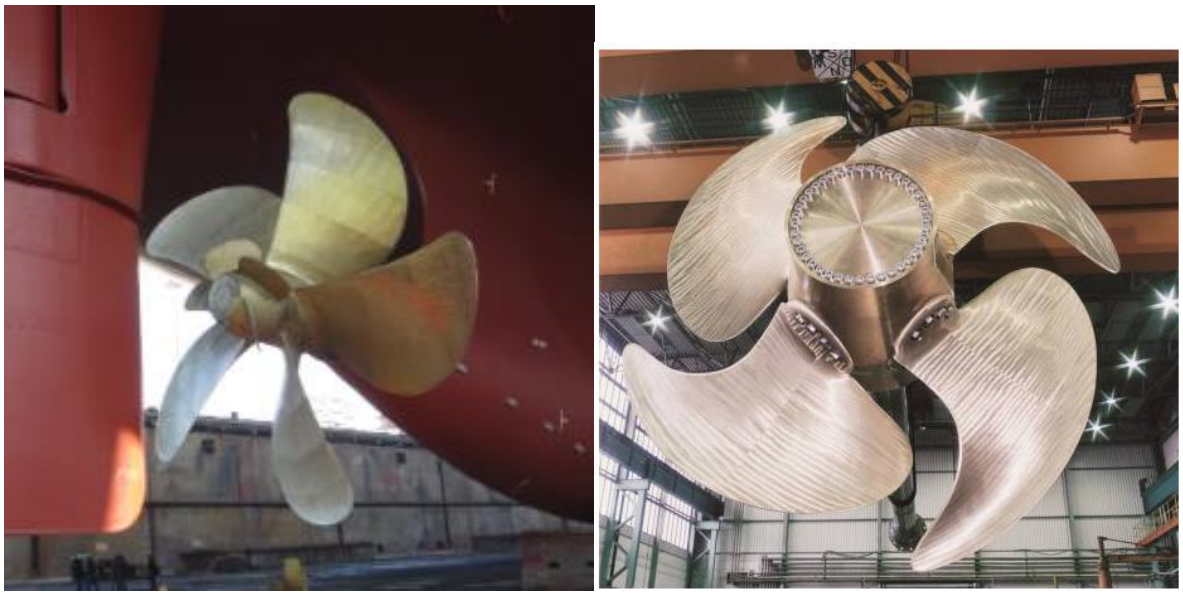

Figure 21: Fixed Pitch Propeller & Controlable Pitch Propeller

2.5 Basics of Dynamic Phenomena

2.5.1 General Aspects of Ship Oscillations

An oscillation is defined as any periodic motion of a body that occurs reciprocally around a position called the equilibrium position. That is, an oscillation is the periodic variation of a quantity around a value. The simplest oscillation system is presented in the image below. All oscillations, no matter how complex, are based on the following principle.

A mass M is connected to a stationary system through a spring with constant C and a damper with damping coefficient B. If mass M is displaced from its equilibrium position and released, it will begin to oscillate around its equilibrium position with a constant frequency of oscillation f_n, which is called the natural frequency or eigenfrequency of the system. This oscillation is called free oscillation. The eigenfrequency is characteristic of the system and depends on the mass M, the spring constant C, and the damping coefficient B. Usually, eigenfrequencies are calculated without taking into account the damping coefficients because, most of the time, they have a small contribution to the final result. Next, we will examine the case where the mass of the previous system is excited by an external periodic force T (exciting force). The oscillation that is caused is called forced oscillation.

The force T can in the general case be decomposed into a Fourier series in the form:

$$T(t) = \sum_{\nu} T_{\nu} \cdot \sin(\nu\omega t + \psi_{\nu})$$

where T_{ν} is the exciting force of order ν, ψ_{ν} is the phase angle of the corresponding force, ω is the angular frequency, and t is the time. The terms of the above sum are called harmonics of the exciting force. The response of the system (i.e., the instantaneous distance of mass M from the equilibrium position) is given in the corresponding form:

$$X(t) = \sum_{\nu} X_{\nu} \cdot \sin(\nu\omega t + \phi_{\nu})$$

where X_{ν} is the amplitude (or range) of the oscillation of order ν and ϕ_{ν} is the phase angle of order ν. The terms of the sum are called harmonics of the oscillation.

A ship (with all its equipment) actually constitutes an elastic metallic structure, which is subject to oscillations. Oscillations appear when the ship's system is excited by forces or moments, which vary periodically. In the case of a ship, the main sources of periodically varying forces and moments are the engine and the ship's propeller, as well as the wave motion. The induced oscillations, on the one hand, reduce the comfort of the transported passengers, on the other hand, they dangerously strain the equipment, but also the structure of the ship. For this reason, special care is taken to reduce the induced oscillations from the engine and the propeller. In two-stroke slow-speed engines, the problem of oscillations is more intense, especially in two-stroke engines with a small number of cylinders (5 or 6). Oscillations of a reciprocating internal combustion engine (RICE) are distinguished into internal and external. The internal oscillations refer to the relative motion of the various parts of the engine between them, causing internal stresses. The external oscillations refer to the oscillations of the engine as a whole, which are transferred to the ship's hull.
The internal oscillations in the propulsion system of a ship are the following three:

- Torsional oscillations (Torsional Vibration)
- Axial or longitudinal oscillations (Axial or Longitudinal Vibration)
- Lateral (bending) oscillations (Lateral Vibration)

Torsional Oscillations (Torsional vibration):
As for the torsional oscillations, they concern the entire system of the crankshaft, flywheel, intermediate shaft, propeller shaft, and propeller. They are caused by the corresponding exciting forces on the crankpins. The forces on each crankpin change over time, while they also vary from crankpin to crankpin. Thus, varying torques are created on the crankshaft, which tend to ”tune” and ”detune” the crankshaft, the intermediate, and the propeller shaft periodically. Since the torsional oscillations depend on the change in peripheral forces between the crankpins, the appropriate firing order is pivotal in reducing torsional oscillations. Their limitation is particularly important, because otherwise even destruction of the crankshaft or the ship's axial system may occur.

Axial or Longitudinal Oscillations (Axial or Longitudinal Vibration):
The axial oscillations concern the system of the crankshaft and the propeller shaft. They are induced by the combined action of the radial forces on each crankpin and the varying axial force of the propeller, causing tensile-compressive oscillations in the system. The radial forces on each crankpin cause periodic divergence-convergence of the crank cheeks, resulting in the appearance of the corresponding oscillations. A secondary axial excitation is caused by the action of the torsional oscillations, which ”tuning” and ”detuning” the crankshaft cause axial deformations. The latter phenomenon is particularly important when the corresponding critical rotational speeds of axial and torsional oscillations are very close to each other. The axial oscillations, on the one hand, increase the stress on the crankshaft, on the other hand, they are transferred (via the thrust bearing) to the ship's hull. To reduce the axial oscillations, a damper is placed at the free end of the crankshaft (in combination with a corresponding damper of torsional oscillations). With its adjustment, the critical speed of axial oscillations is shifted above the maximum rotational speed of the engine, while at the same time reducing the maximum width of the axial oscillations, i.e., the load on the crankshaft, as well as the thrust bearing.

Lateral (bending) Oscillations (Lateral Vibration):
The lateral oscillations mainly concern long propeller shafts and are due to the lateral forces from the propeller. They cause corresponding oscillations in the hull of the ship, reducing the comfort of the passengers. Especially in passenger ships, a special study is made to reduce them. The problem of bending oscillations consists of calculating the corresponding eigenfrequencies of the propeller shaft-intermediate shaft-propeller system. These eigenfrequencies are compared with the frequencies of the exciting forces from the propeller and it is determined whether there is a risk of resonance. The change in the eigenfrequencies of the shaft is made by the appropriate selection of the position and the number of bearings of the propeller shaft. In this way, its stiffness is increased, and its eigenfrequency is shifted to higher values, well above the basic frequency of the exciting forces.

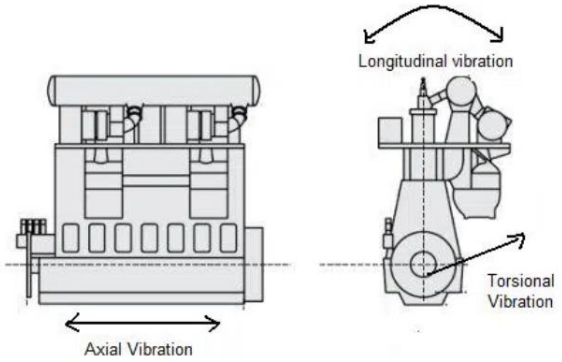

Figure 22: Internal Oscillations of Two-Stroke Engine

The forces of the gases, have a zero resultant force; therefore, they do not transfer external force to the base. However, they do cause an overturning moment on the engine, opposite to the torsional force on the propeller shaft. The overturning moment increases due to the presence of unbalanced reciprocat-

ing inertial forces. The overturning moment is received by the engine's mounting bolts. In addition to the overturning moment, the free (unbalanced) reciprocating and rotational inertial forces are also transferred. The above forces and moments, due to their periodic variation, cause external oscillations that are transferred to the ship's hull. Less frequently, the internal axial and torsional oscillations of the crankshaft can also transfer significant oscillations to the ship's hull. With an appropriate choice of firing order and proper engine design, the rotational inertial forces, as well as the reciprocating inertial forces, can have a zero resultant. However, their corresponding moments are not always nullified, resulting in 2 vertical moments in the general case. The vertical moments are so called because they can be associated with pairs of forces in the vertical plane. Their direction is horizontal, perpendicular to the engine's axis. The same applies to the horizontal moment, whose direction is vertical.

The above moments induce significant oscillations in the ship, in the following cases:

- If the frequencies of the moments are close to the corresponding natural frequencies of the ship's structure (resonance).
- If the engine is located near a node of the ship structure's oscillation (thus the position of the engine plays a significant role).
- If the amplitudes (maximum values) of the free moments are large, while the damping capacity of the ship's structure is not satisfactory.

2.5.2 Barred Speed Range

A very important part of the study of torsional oscillations is the aspect of resonance. The response of an oscillation can be described as a sum of harmonic oscillations. When the frequency of a harmonic becomes equal to the natural frequency of the system, resonance occurs. In the case of resonance, the amplitude of the oscillation increases excessively. This increase is limited only by the characteristics of the damper. This condition is particularly dangerous and should be avoided. Resonance exists within a specific range of engine speeds (Barred Speed Range – BSR). Passing through this speed range is critical and should be done quickly to avoid severe stresses.

An approximation of the upper limit of the speed range that creates resonance is given by MAN B&W in the image below.

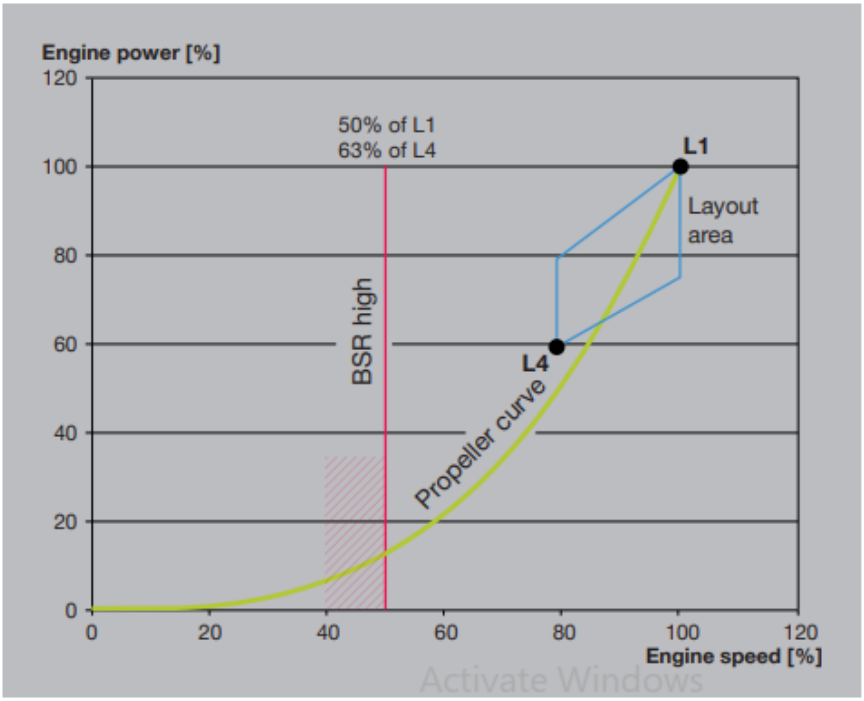

Figure 23: Barred Speed Range Approximation (MAN B&W)

The figure below presents a typical Torsional Stress-Speed operational diagram, highlighting the Barred Speed Range. This range indicates the speeds at which resonance is observed, leading to an increase in the amplitude of the torsional oscillations, and consequently, the torsional stresses applied to the axial system. The diagram illustrates the resonances for various harmonics as well as their composite effect, which is of particular interest for assessing the system's durability.

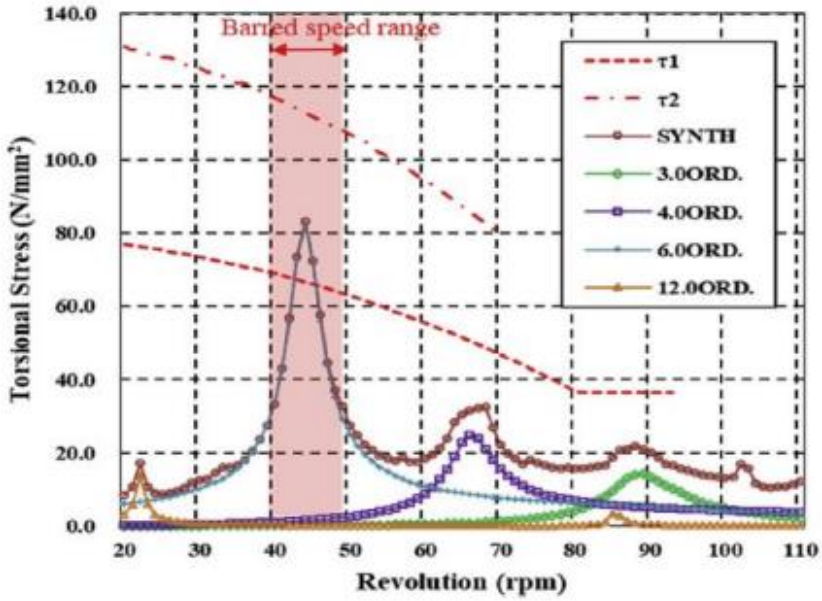

Figure 24: Torsional Stress-Rotational Speed Plot

According to the International Association of Classification Societies (IACS) M68, the limit $t1$ may be exceeded for a short period of time during changes in engine load (acceleration, deceleration). However, the limit $t2$ must not be exceeded under any circumstances. The Barred Speed Range (BSR) is defined by the following formula:

$$\frac{18 - \lambda_c \cdot n_c}{16 \cdot n_c} < n < \frac{18 - \lambda_c}{16} \tag{2.2}$$

Where:

- n_c is the resonant angular velocity,
- λ_c is the ratio of the resonant angular velocity to the maximum continuous operating angular velocity.

This formula establishes the boundaries of the BSR, indicating the critical range of speeds within which resonance effects become significant and thus should be carefully managed in the design and operation of marine engines.

2.6 Kinematics of the Motion Transmission Mechanism

The diagram below presents the schematic of the motion transmission mechanism from the piston to the crankshaft. Two principal points of the kinematic mechanism, whose kinematic characteristics are of concern, are the center of the piston pin (point E) and the center of the crank pin (point S). The center of the piston pin performs a straight-line accelerated motion (reciprocating between the Top Dead Center (TDC) and Bottom Dead Center (BDC)), while the center of the crank pin traces a circular path with a radius r and an angular velocity ω.

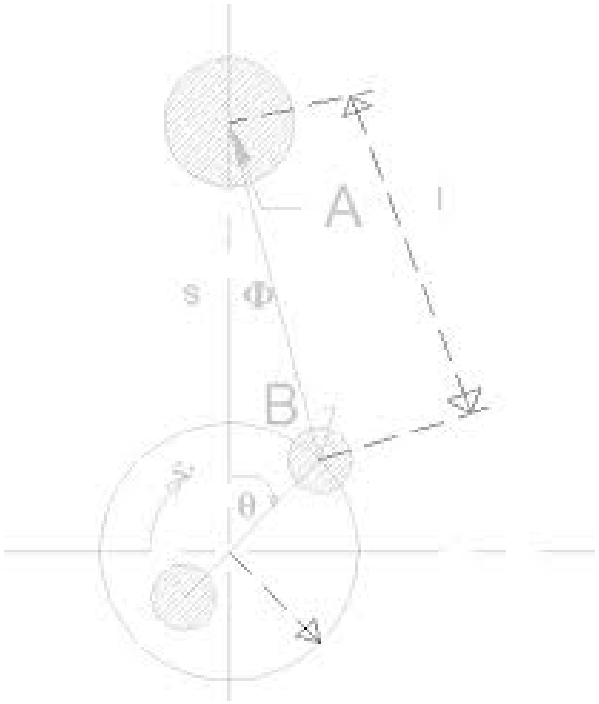

Figure 25: Kinematics of Marine Diesel Engine

As evident from the diagram, when the crank is at an angle ϕ from TDC (Top Dead Center), the displacement x of the piston from TDC is given by the following relation:

$$x(\phi) = \frac{r}{l} - l\cos(\beta) - r\cos(\phi)$$

where β is the angle formed by the connecting rod with the vertical direction, r is the radius of the crank, and l is the length of the connecting rod.

The ratio of the crank radius to the length of the connecting rod is denoted by λ:

$$\lambda = \frac{r}{l}$$

Performing trigonometric operations, the displacement x becomes:

$$x(\phi) = r(1 - \cos(\phi)) \left(\frac{l(1 - \sqrt{1 - \lambda^2 \sin^2(\phi)})}{r} \right)$$

The first derivative of the displacement x with respect to time yields the piston's velocity:

$$c = \frac{dx}{dt} = \frac{dx}{d\phi}\omega$$

where ω is the angular velocity of the crank rotation.

Differentiating the displacement equation with respect to ϕ, we obtain the piston's velocity:

$$c = \omega r \sin(\phi) \left(\frac{1}{\lambda \cos(\phi)} \right) \frac{1}{\sqrt{1 - \lambda^2 \sin^2(\phi)}}$$

The direction of the piston velocity c is taken as positive when directed from TDC towards BDC (Bottom Dead Center).

Differentiating the velocity with respect to time, the piston's acceleration b is obtained:

$$b = \omega^2 r \left\{ \cos(\phi) - \frac{\lambda \cos(2\phi) - 3\lambda^2 \sin^4(\phi)}{[1 - \lambda^2 \sin^2(\phi)]^2} \right\}$$

The positive direction of the acceleration, like the velocity, is from TDC towards BDC.

2.7 Combustion Gas Pressure in the Cylinders

The pressure of the gases within the cylinder, which results from compression during the piston's ascent and combustion, varies with the angle of the crankshaft. This variation is depicted in the corresponding indicator diagram of pressure versus crank angle ($P - \phi$). A typical cylinder pressure-angle diagram for a two-stroke marine engine is shown in the figure below.

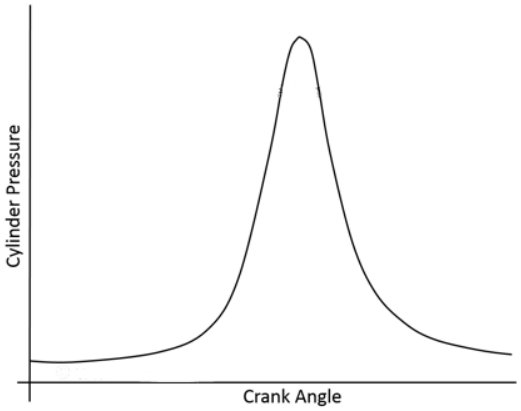

Figure 26: Cylinder Pressure vs Crank Angle

The variation of gas pressure is particularly large. Thus, the force on the piston, which results from the product of the gas pressure and the cylinder cross-section, also changes significantly. If p_g is the corresponding gas pressure, then the force on the piston is given by:

$$F_g = \pi \cdot \frac{D_p^2}{4} \cdot p_g$$

where D_p is the diameter of the cylinder.

This force is decomposed into two components, one perpendicular to the walls of the cylinder and one in the direction of the pushrod stem. In engines with a connecting rod (two-stroke marine engines), this analysis is carried out at the crankpin. The component F_{gN} perpendicular to the cylinder walls causes oval wear of the liner in non-connecting rod engines, while in connecting rod engines it is absorbed by the crankcase guides. The component F_{gS} in the direction of the pushrod stem is transferred to the

crankpin.

The two forces are given respectively by:

$$F_{gN} = F_g \cdot \tan(\beta)$$
$$F_{gS} = \frac{F_g}{\cos(\beta)}$$

where β is the angle formed by the pushrod with the vertical direction (between TDC and BDC).

The force F_{gS}, transferred to the crankpin, is decomposed into two components, one in the direction of the crank radius F_{gR} and one in the tangential direction F_{gT} (perpendicular to the previous one). The first is called the radial force of the crankshaft and the second the torsional force of the crankshaft, as the torsional torque on the crankshaft is due to the pressure of the gases. By applying trigonometric relations, the following results for the two components:

$$F_{gT} = F_g \cdot \frac{\sin(\phi - \beta)}{\cos(\beta)}$$
$$F_{gR} = F_g \cdot \frac{\cos(\phi - \beta)}{\cos(\beta)}$$

Obviously, the torsional torque due to the action of the gases is given as the product of the torsional force times the radius of the crankshaft:

$$T_{gT} = F_{gT} \cdot r = F_g \cdot \frac{\sin(\phi - \beta)}{\cos(\beta)} \cdot r$$

The torsional torque from all the cylinders is transferred via the crankshaft out of the engine, to the propeller of the ship.

The component F_{gS} is also transferred to the main bearing of the crankshaft (which it stresses) and then to the frame and the engine mount. The sum of the gas forces loading the frame, if transferred to one point, has a zero component (the force on the crown is opposite to the force on the piston, while the forces applied peripherally to the cylinder walls are also opposite). However, the torque on the frame from the gas pressure is not zero, but equal and opposite to the turning torque (cause of external vibrations). This torque tends to overturn the engine and is absorbed by the machine's mounting screws. Due to its temporal variation, the torsional torque also causes vibrations, which are transferred through the enginemount to the hull of the ship.

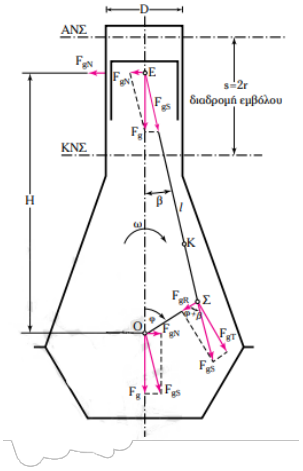

Figure 27: Combustion Gas Forces

2.8 Inertial Forces

The entire piston performs a rectilinear accelerated motion (together with the piston pin and springs). The crank (as a whole) performs a rotational motion with a constant angular rotation speed (in the steady-state operating condition of the engine). Conversely, the connecting rod performs a particularly complex motion. Its head, which is connected to the piston pin, performs rectilinear accelerated motion, its foot performs rotational motion along with the crank, while the connecting rod's shaft performs complex motion.

2.9 Rotational Inertial Forces

The rotating mass consists of the rotating mass of the connecting rod plus the rotating mass of the crank. The crank mass is not entirely concentrated at one radius. Due to the variation of the angle of the crankshaft, the rotating inertial forces cause vibrations, since their action is transferred to the bearing of the crank pin base and from there to the engine's frame and base. To be able to neutralize the action of the inertial force, a mass must be placed diametrically, which will act as a counterweight. Based on the above general principle, the counterweights, which are placed on the arms of the cranks, are calculated to neutralize the rotational inertial forces.

2.10 Reciprocating Inertial Forces

The reciprocating inertial forces are due to the reciprocating motion of the piston, the piston rod, and part of the connecting rod. The kinematic mechanism exerts a force on the mass of the piston (as well as on the other reciprocating masses) and accelerates (or decelerates) it. The piston correspondingly exerts the opposite force (reaction) on the kinematic mechanism (and naturally on the engine). This force is the inertial force F_l, given by Newton's law:

$$F_l = -m_l \cdot b$$

where b is the acceleration of the piston (at each position of the crank) and m_l is the reciprocating mass.

This force is applied in the vertical direction (the direction of motion and acceleration of the piston). It is analyzed like the gas force and results in a peripheral component at the connecting rod pin F_{lT}, called the torsional inertial force, which causes a torsional torque M_{lT} equal to:

$$M_{lT} = F_{lT} \cdot r$$

and obviously equal and opposite overturning torque (analogous to the corresponding force from the gases).

In contrast to the case of the forces from the gases, the reciprocating inertial force is transmitted to the frame and then to the base, since there is no opposite force at the top of the cylinder to neutralize it.

The trigonometric relations that give the components of the inertial force due to reciprocation are obviously analogous to those of the gases and are given as follows:

$$F_{lN} = F_l \cdot \tan(b)$$

$$F_{lS} = F_l \cdot \sin(f - b) / \cos(b)$$

$$F_{lT} = F_l \cdot \sin(f - b) / \cos(b)$$

$$F_l = F_l \cdot \cos(f - b) / \cos(b)$$

$$M_{lT} = F_{lT} \cdot r = F_l \cdot \sin(f - b) \cdot r / \cos(b)$$

The following image presents a sectional view of a reciprocating engine and the reciprocating inertial forces analyzed above.

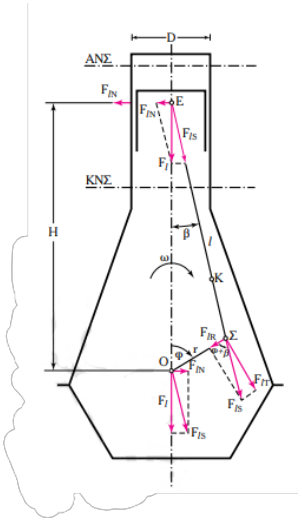

Figure 28: Inertial Forces

2.11 Superposition of the Forces

The total force on the piston pin results from the superposition of the inertial force due to the reciprocating motion and the gas force at each angle of the crankshaft. In engines with a connecting rod, this force is transferred to the big end bearing. In two-stroke engines, the total force does not reverse direction, resulting in a continuous hydrostatic pressure being required from the lower side of the big end bearing to maintain the lubricating film. The absence of force reversal means that the screws of the kinematic mechanism are not strained by tensile oscillating forces. This total force, along with the corresponding individual ones, is presented in the following diagram as a function of the crankshaft angle.

- F_g: Gas force
- F_i: Inertial reciprocating force
- F: Total force

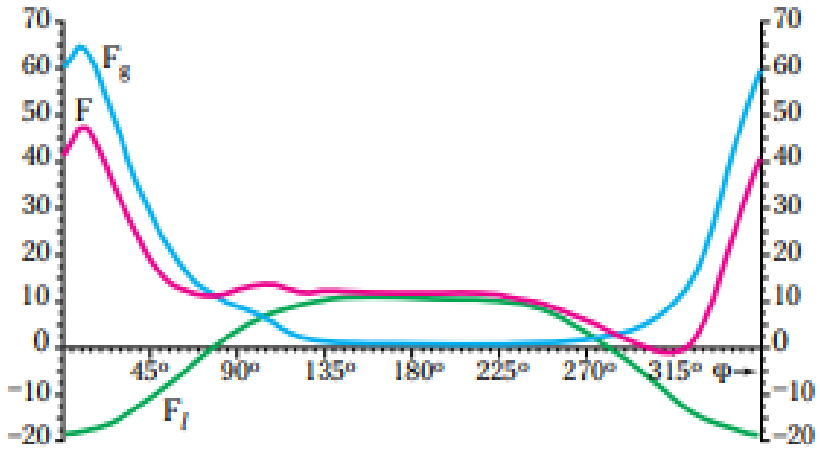

Figure 29: Superposition of Forces

3 Shaft Alignment

3.1 Definition

The propulsion system of traditional cargo ships consists of a large (2-stroke) marine engine linked to a propeller. In smaller vessels, two or four ”smaller” (4-stroke) engines drive the propeller through a gearbox, while passenger vessels might have multiple propellers. The ”shafting system” is a common feature across these configurations, transmitting power from the main engine(s) to the propeller(s). This system typically comprises three parts: the crankshaft, an intermediate shaft, and a propeller shaft, supported by different types of bearings based on the installation requirements. The crankshaft, bearing the load from the main engine, is usually supported by a number of crankshaft bearings, usually equal to the number of engine cylinders plus one. The intermediate shaft, bearing the least vertical load, is often supported by one or two intermediate bearings. The propeller shaft is usually supported by two stern tube bearings or by a substantial stern tube bearing along with an intermediate shaft. The aft stern tube bearing, heavily loaded due to propeller forces, is often long with L/D ratios around two (2). Given the potential for significant power losses in this transmission system, careful design is crucial.

The process of defining the parameters of the shafting system is termed as shaft alignment. This involves selecting the quantity and type of support points, and positioning them at predetermined longitudinal and vertical locations. A specific reference line is defined for vertical positioning. The angle at which bearings are placed concerning this reference line is also considered to minimize shaft/bearing misalignment. The type and dimensions of the bearings are chosen to adequately support the shaft load both in cold and operating conditions. The reaction forces at the support points are computed for these conditions to ensure they are within allowable bounds.

Proper shaft alignment helps in reducing shaft stress and system power losses, thereby ensuring a longer system lifespan, lesser wear and fatigue, and preventing system failures that could endanger the ship’s safety and operability. Good alignment is also crucial when coupling with a gearbox to prevent catastrophic gearbox failure and reduce gear teeth wear. Furthermore, effective shaft alignment can result in lower maintenance and repair costs.

3.1.1 ”Static” and ”Running” Condition

Ships experience two main conditions throughout their lifetime: moored (static) or seaworthy (running). Both conditions significantly affect the shaft, playing a crucial role in the Shaft Alignment procedure.

In static conditions:

- The main engine (ME) is inactive.
- No additional bending moment is considered as the propeller isn’t producing any thrust.
- Vertical motion is allowed at the support points (bearings) within the bounds of diametrical clearance as the shaft isn’t rotating.
- Hydrodynamic lubrication is not possible as there’s no fluid layer between the stationary shaft and bearing.
- Only static loading like gravitational forces and mechanical loads applied to the shaft are considered.

In running conditions:

- The operating ME adds more vertical loads and vibrations to the crankshaft bearings.
- Thermal expansion affects all crankshaft bearings due to the ME's high temperature.
- The rotating shaft experiences additional bending due to propeller's thrust.
- A fluid film forms at the support bearings, lifting the rotating shaft over the lower half of the bushing.
- Any misalignment causes a slight shift in the shaft's intended support point along the bearings.

This work primarily focuses on the running condition, where a fluid film forms and the shaft bends. Specifically, the thesis aims to simulate the entire shaft from engine to propeller with the engine turned on. Initially, a simplified condition is simulated, where the bearings operate under a constant given rotational speed, and the shaft experiences only the force and torque from the propeller, with the engine side being constrained – termed as the static condition. Following this, a fully dynamic FEA analysis is conducted considering acceleration and velocities – termed as the dynamic condition.

3.2 Regulations on Design & Analysis

The regulations pertaining to the alignment of shafts in rotating machinery, such as the primary propelling device of a vessel, exhibit a considerable degree of uniformity across the various classes established by the International Association of Classification Societies (IACS). The following are the most frequently encountered general requirements:

- A comprehensive shaft alignment plan, encompassing all relevant considerations and assumptions, is required to be submitted for approval.
- The findings of the analysis conducted prior to the implementation of the plan should be presented to the class.
- Analyses should be conducted to account for different ship operating conditions, such as hot and cold conditions, as well as various loading conditions including Ballast Arrival and Full Load Departure. These analyses should consider the corresponding hull deformations and main engine thermal expansion.
- The investigation of stern tube slope is imperative in any alignment plan. It is essential to thoroughly examine and apply single or multi-slope boring techniques as needed to avoid excessive misalignment of the shaft.
- The bearing reactions must adhere to the specified allowable limits.
- The class reviewer must have access to the details and procedures that were followed during the implementation of the plan.
- All the above must be checked and verified through testing by the class.

3.2.1 Reaction Forces

In the context of mechanics, reaction forces refer to the forces exerted by a body in response to an external force acting upon it. These forces are equal in magnitude and opposite in direction to the applied force.

The determination of allowable bearing reaction forces is established based on a set of specified criteria. In order to ensure proper functioning, it is imperative that bearings maintain contact with the shaft

within the lower half of their geometric structure. If the statement above is accurate, reaction forces are classified as "positive." Additionally, it is imperative that reaction forces remain within a predetermined range of acceptable limits. The mean pressure upper limit for white metal bearings is typically 0.8 MPa, while for composite anti-friction materials it is 0.6 MPa. The limit definition for maximum pressure exhibits variations across different classes. NK establishes the limit at 40MPa, while Bureau Veritas associates reaction forces with lubricant film thickness and sets a minimum film thickness limit of 30 μm (which is correlated to the roughness of the material). In contrast, ABS does not establish a precise threshold, but rather mandates the inclusion of solely affirmative responses and stipulates that a minimum of 10% of the permissible load must be maintained under all circumstances to mitigate the risk of unloading caused by unforeseen disruptions.
According to ABS, it is important to consider factors beyond reaction loads when determining alignment acceptance. The significance of relative misalignment between the shaft and the bearings is of equal importance.
Regarding the verification of reaction forces through experimental testing, it is permissible to have substantial discrepancies (within a range of ±20% deviation) between the calculated values and the measured reactions. This allowance is necessary due to the presence of considerable uncertainty in the measurements. In all instances, the prioritization is given to the measured reactions rather than calculations.

3.2.2 Deflection Curve

The latest class regulations incorporate details pertaining to this curve. To provide further clarification, the ABS guidance notes pertaining to the alignment of propulsion shafting make mention of:

> *"Relative misalignment between the bearing and the shaft may be evaluated from information defined by deflection curvature. Deflection curvature defines the angle of the shaft inclination at each node of the system. This angle is measured from the theoretical zero alignment angle.*"

Moreover, there exist guidelines pertaining to situations in which hull deflections are taken into consideration. These guidelines also suggest that if the misalignment angle is determined to be excessive, it may be necessary to conduct slope boring or adjust the inclination of the bearing. In the context of this study, it is imperative to provide a comprehensive explanation of the concept of 'bearing misalignment'.
The assessment of bearing misalignment between the shaft and bearings is a crucial parameter, as previously indicated. The inclination of the shaft within the bearing's length is a practical consideration. The stern tube bearing, by virtue of its considerable length, necessitates particular consideration; however, it is imperative not to neglect the other supporting points. According to the guidelines provided by Bureau Veritas, it is recommended that the elastic shaft alignment regulations be followed. Specifically, it is advised that the stern tube bearing be represented as a system consisting of at least five support points. This approach ensures a comprehensive representation of the misalignment of the bearing along its entire length. The restrictions imposed on the maximum angle of misalignment between the shaft and the bearing bushing are contingent upon the dimensions of the system. The maximum angle of contact between the shaft and the bearing bottom should not surpass the ratio of the radial clearance to the length of the bearing. This ensures that the shaft does not come into contact with the bearing bottom in practical terms. If the calculations yield different results, it is necessary to apply slope boring or bearing inclination to the bearing bush. Certain classes may discuss the potential application of multiple slope boring in certain instances, particularly in relation to the stern tube bearing, as a means to address extreme scenarios. This thesis will not take into account a sloped bearing.

3.2.3 Single or Two Point Contact

In the field of shaft analysis, it is customary to represent each bearing as a solitary point of contact for reaction forces. Since 2015, there has been increased attention on the two or multi-point modeling of bearings due to the implementation of more advanced requirements by various major classes. This tool holds significant potential, particularly in the examination of the stern tube bearing, as it facilitates the computation of multiple contact points rather than relying on the assumption of a single contact point. Typically, a contact point serves to indicate the location of the presumed bearing reaction. The determination of the contact intensity is contingent upon the positioning of the contact point, which in turn influences the slope between the shaft and the bearing's bush. There has been considerable debate surrounding the plausibility of two point contact, as the occurrence of genuine operational circumstances that facilitate such contact is exceedingly uncommon. However, utilizing a two-point contact approach simplifies the process of conducting initial calculations and validating the adherence to acceptance criteria in a given scenario. ABS and BV have made notable advancements in their efforts to model the contact between the bearing and shaft bush. The proposed models by ABS and BV are presented in this context.

> The ABS Stern Tube Bearing Evaluation program, as described in[34], employs the area contact method to assess the contact area and condition of the bearing in situations where the shaft remains stationary or rotates at extremely low velocities, prior to the formation of the oil film. In contrast, it is advisable to employ the single point contact methodology, while also taking into account the contact point positioned at a distance of D/3 (one third of the shaft diameter) from the edge of the subsequent bearing.

Figure 30: Single & Two Point Contact Models[35]

In the context of ESA modeling of the stern tube bearing, both the two-point contact and single point contact approaches are considered valid. However, it is important to ensure the verification of the single point contact before considering the two-point contact approach. Additionally, it is necessary to define the slope boring for the single point solution. In order to validate the efficacy of the two point method, the front-edge contact point is eliminated and a singular point scenario is examined.

[34] "Guide for Enhanced Shaft Alignment 2022," ABS.

3.2.4 Documentation & Results Verification

Consequently, due to the aforementioned regulations, the following list of items is required by major classes for submission and subsequent approval:

- Drawings of shafting arrangement and auxiliary systems
- General description of calculation model
- Assumptions
- List of investigated calculation conditions
- Input parameters
- Detailed results
- Conclusions
- Shaft alignment model
- Hull flexibility model
- Hull relative deformations
- View of FE model of aft part of ship structure
- Detailed alignment procedure

Further clarifying the above mentioned *Detailed Results*, the documents requested for the Elastic Shaft Alignment (ESA/ESA+)[36] are:

- Shaft Alignment Calculations:
  - Hull Deflections
  - Propeller Loads in Vertical & Transverse Directions
  - Optimization for Bearing Offsets & Slopes
- Required for ESA+ Notation
  - Final sighting to be conducted after engine, gearbox or other heavy machinery are installed onboard with the superstructure in place and all major steel works are completed
  - Gap and Sag not required
- Whirling Calculations Requirements
  - Required for all shaftline arrangements
  - Calculated with all bearings loaded
  - Calculated with forward sterntube bearing unloaded
- TCM Notation

[36] "Guide for Enhanced Shaft Alignment 2022," ABS.

3.3 Shaft Alignment Procedure

Executing the aforementioned procedures for designing, analyzing, and reporting the desired shaft alignment plan, the operational phase of the alignment process is initiated. The alignment that needs to be achieved in accordance with the specifications outlined by the designer. The absence of a standardized procedure often necessitates reliance on shipbuilder practices, experiences, and production schedules. While it is difficult to assess the validity of each approach, certain classes have established several examples of shaft alignment procedures. If these procedures are executed correctly, they have the potential to yield a high probability of success. The primary considerations for each proposal pertaining to shaft alignment are safety and practicality. This section will analyze several key parameters of the proper shaft alignment procedure.

3.3.1 Preliminary Calculations

The initial step involves conducting a series of preliminary calculations to determine the appropriate quantity and longitudinal placement of the support points. A rudimentary calculation using a ”straight-line” will be conducted to estimate the reaction forces, system’s influence factors, and shaft deformations. In the initial stage, the vertical offsets of the bearings are established as zero. However, it becomes necessary to redefine these offsets subsequently to attain a satisfactory distribution of reaction forces. The maximum load-bearing capacity of each individual bearing must not be surpassed. It is recommended to minimize shaft inclination and strive for minimal misalignment between the shaft and bushing. Achieving this objective can be particularly challenging, particularly in the domain of stern tube bearings. In these instances, it is recommended to employ solutions such as slope boring or bearing inclination, as discussed in preceding sections. The subsequent phase entails the implementation and assessment of the shaft alignment strategy.

3.3.2 Application

In accordance with the major classes, the commencement of shaft alignment is anticipated to occur subsequent to the completion of stern block welding for the vessel and the installation of all substantial structures. The initial procedure involves the establishment of a reference line that serves as a point of origin for the precise placement of bearings, shafts, gearbox, and the main engine. The various techniques for establishing the reference line will be further examined in the subsequent section, specifically focusing on measurements. During this phase, multiple provisional support points may be employed. Once the shafts are appropriately positioned, the propeller is typically attached, often accompanied by the application of a load on the forward end of the tail shaft. This load serves the purpose of maintaining contact between the forward stern tube bearing and the shaft before the assembly process. During this particular stage, it is customary to assess the Sag and Gap values in order to confirm adherence to the relevant analytically derived values. Ensuring precise and accurate Sag and Gap values between shaft segments is of utmost importance. During this phase, the assessment of misalignment between the bearing and shaft is conducted, followed by the implementation of appropriate measures to rectify the issue. In numerous instances, it may be necessary to make readjustments to the offset of the intermediate shaft bearing. Upon completion of the procedure, once the shafts have been connected, a comprehensive examination and assessment of the system’s parameters are carried out. This is done with the aim of aligning the actual reaction forces with the previously determined values obtained during the pre-alignment phase. Various measures can be implemented to address these disparities. Additional validation of the alignment condition should be conducted while the vessel is in a floating state. Ensuring compliance with the calculated alignment on a waterborne vessel poses greater challenges compared to other types of vessels. This is primarily due to the significant differences between the bearing reactions observed and the analytical predictions, which can be attributed to the deflections in the hull.

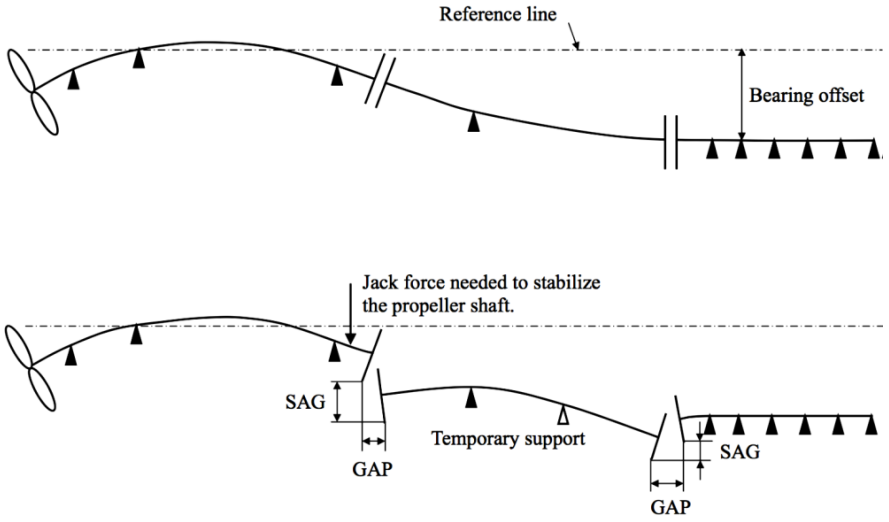

Figure 31: Sag & Gap Alignment Process[38]

According to ABS[37], it is preferable to carry out a significant portion of the alignment procedure while the vessel is situated in the dry dock. Therefore, if feasible, it is advisable to verify the reaction and bearing-shaft contact condition during the vessel's dry dock period. By implementing this approach, the shipyard can effectively maintain precise control over the alignment procedure in accordance with the analysis. It is crucial to emphasize that the matter of controlling the alignment is closely linked to the successful completion of the structural construction of the vessel.

Nevertheless, it is a general policy of the classification societies to accept any procedure that result in a satisfactory solution. In the following figure, the Sag and Gap alignment process is presented:
Additional important steps in the alignment process or calculations related to the hull stiffness, main engine, gear, and vibration analysis, which will not be extensively examined in this study but are crucial for achieving accurate alignment, are:

- Hull Girder Deflections
- Engine Bedplate pre-sagging
- Crankshaft Deflection Measurement
- Gear Contact Evaluation (if applicable)
- Gear-Shaft bearings reaction measurements
- Lateral Vibration (Whirling) Calculations
- Engine Shock Calculations
- Maintenance or Repair Practices
- Bearing wear-down issues

[37] "Guide for Enhanced Shaft Alignment 2022," ABS.

3.4 Measurements

3.4.1 Sag & Gap Values

As stated in the guidance notes on propulsion shafting alignment provided by ABS:

> *Sag and Gap is a shaft alignment method, commonly used to verify the preassembly condition of the propulsion shafting in new construction and repairs.*

The method is characterized by its simplicity and efficiency, as it does not necessitate the use of specialized equipment. However, its accuracy is subject to scrutiny. This method serves as a supplementary measure, yet it offers numerous benefits for the initial phases of the preassembly stage. During the preassembly phase, the individual segments comprising the shafting system are positioned onto their respective support bearings without being connected. In the present condition, the flanges are suspended without any support and require a substantial amount of force to be exerted in order to align them at the intended vertical and horizontal displacement for the purpose of coupling. Furthermore, it is imperative to note that when disassembling a shafting system, it is necessary to carefully position the flanges at precise vertical and horizontal distances. The parameters utilized for this measurement are SAG and GAP. The SAG refers to the vertical separation between the upper or lower edges of each flange, while the GAP represents the horizontal separation between the opposing edges of the flanges or between the upper and lower edges of each flange. The figure presented herein depicts various potential configurations and the corresponding measurements of SAG and GAP values.

39

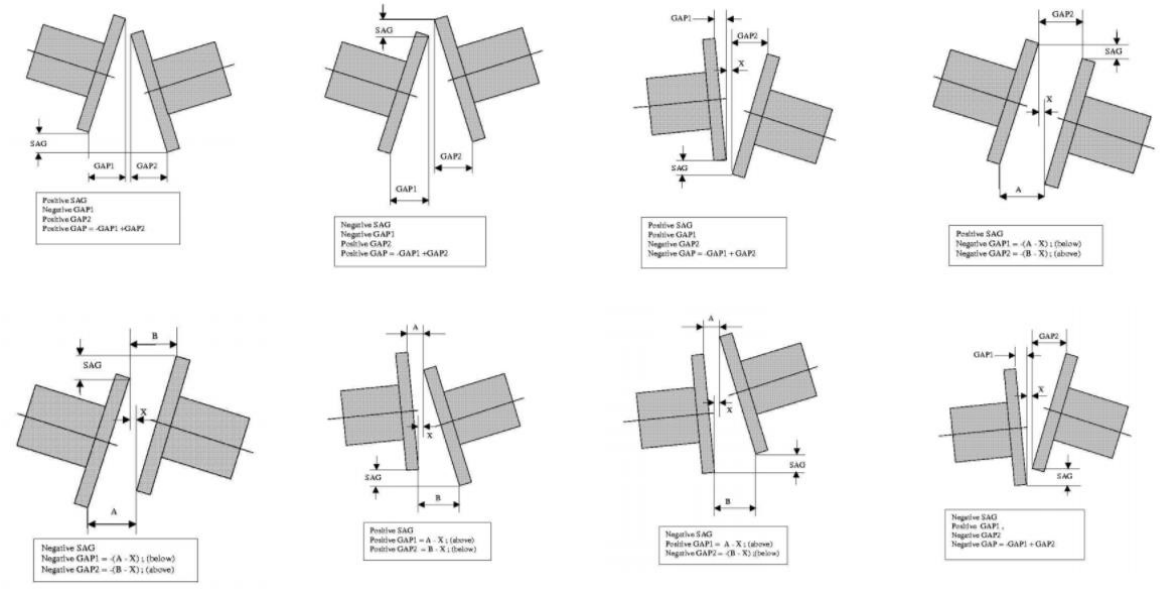

Figure 32: Sag & Gap Measurement Types

3.4.2 Sighting Through

The vertical positioning of the support point offsets in relation to a predetermined reference line is a crucial stage in the alignment application. There exist multiple methodologies for precisely delineating and establishing this reference line within the physical realm. The act of establishing a reference line is commonly referred to as sighting through or bore sighting, and it is often carried out using the piano wire method, optical instruments, or laser technology. Furthermore, it is imperative to establish a reliable methodology for quantifying distances relative to the reference line.

The sighting procedure is typically carried out in the following manner:

- Piano wire or optical method machinery is installed.
- The reference line is established to align with the central axis of the aft stern tube bearing.
- The target points are designated at the precise positions of the bearings.
- The target points are adjusted to align with the specified offsets for the dry dock condition.
- The bearings, gear box, and main engine are strategically positioned into their designated locations.
- The slope boring angles are designated or the inclination angle is applied to the stern tube bearing.

The Application of Piano Wire
This method involves securing a slender metallic string or wire to the rear position of the engine, positioned above the shaft. A weight is then attached to the opposite end of the string to maintain tension and promote straightness of the wire.
The methodology is depicted in the subsequent illustration:

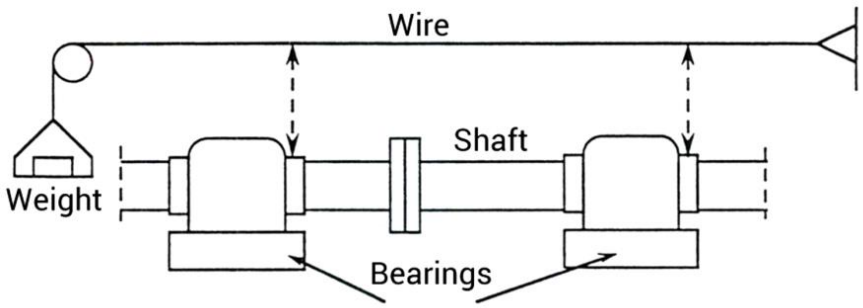

Figure 33: Piano Wired Method[40]

The vertical offset that is recommended is determined by measuring the distance between the wire and the specific location of the support point. The determination of the vertical offset and longitudinal position of the bearings is established by employing piano wire as a reference standard. However, it is necessary to account for the sagging of the piano wire in order to make accurate corrections.
Despite its simplicity, this method lacks accuracy for several reasons that are readily apparent.

- Firstly, it is challenging to measure the wire accurately without making contact with it, which in turn slightly alters the vertical position and measurement.
- Achieving optimal wire alignment is a challenging task.
- The sag of the wire may be influenced by any weight movement, such as the installation of shafts.
- Making corrections for the continuous small amplitude vibrations of the piano wire can be a challenging task.

Optical Methods
The utilization of optical techniques in scientific research and analysis has proven to be highly effective and advantageous. Optical methods encompass a wide range of the optical methods, namely the optical telescope and laser, are considered the most precise techniques for alignment implementation. The optical instruments utilized possess a high degree of accuracy, resulting in outcomes of superior quality. During the initial stage of the application, the telescope/laser is strategically placed at the posterior end of the shafting system. A reference target is placed at the opposite end, while multiple targets are

positioned at precise vertical offsets and longitudinal positions. The targets possess a centrally located aperture that facilitates the unobstructed transmission of laser beams. After establishing the reference line between the telescope/laser and the fore target, the measurement of support point offsets can be obtained by making adjustments to the telescopes dials. The targets are adjusted sequentially, beginning from the forward end and progressing towards the aft end of the shafting system.

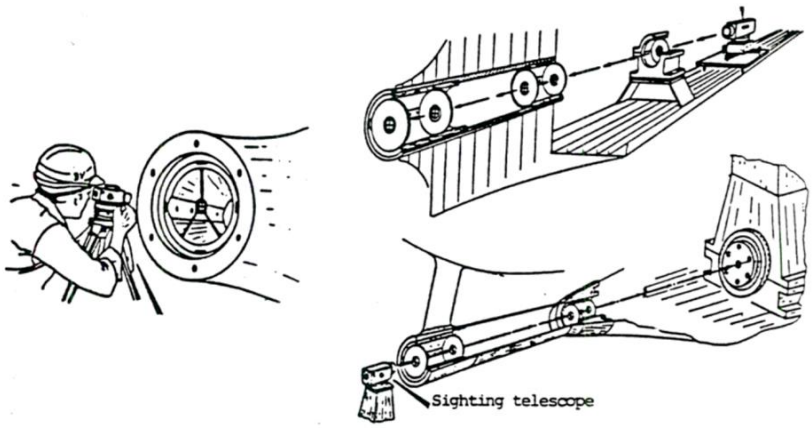

Figure 34: Alignment with Optical Methods[41]

Typically, the targets are adorned with concentric circles of varying diameters, serving the purpose of enhancing resolution, in addition to the presence of a scale on the graded dials. This approach offers the advantage of enhanced precision and also offers the added benefit of conveniently positioning objects or targets at predetermined locations by adjusting the telescope dials to a specific focus, distance, and offset, and aligning the object's position with the desired target. An additional benefit of significance for sloped stern tube bearings is the ability of lasers to establish a reference line at any desired angle. When considering the single or double slope boring or inclination of the stern tube bearing, the reference line is established based on the primary slope of the stern tube bearing. Consequently, the optical methods are the sole permissible approach for achieving precise shaft alignment.

3.4.3 Bearing Reaction Forces

After the completion of the alignment process and the coupling of the shafts, it becomes crucial to measure the actual reaction forces exerted on the remaining support points, following the removal of temporary support points. The prevailing methods employed for quantifying bearing reaction forces involve:

- Hydraulic Jacks
- Strain Gauges

Hydraulic Jack Test
The method described is widely utilized for the measurement of bearing reactions under cold conditions. The method is characterized by its simplicity and user-friendly nature, as it involves a straightforward measurement process that necessitates neither specialized expertise nor costly apparatus. The hydraulic jack is positioned beneath the shaft, precisely along the centerline, in close proximity to the bearing. The placement of the jack should be on a stable and rigid foundation throughout the entirety of the process. A micrometer or digital dial gauge is positioned atop the shaft, while a load shell is inserted between the jack and the shaft. Prior to commencing the test, it is advisable to elevate the shaft by a minimum of 0.5 mm to guarantee precise measurements. Subsequently, the shaft is elevated until it makes contact with the upper shell of the bearing bush, after which it is subsequently retracted

back to its original position. It is recommended to repeat this process multiple times in order to reduce systematic measurement errors. Simultaneous measurements of the reaction force exerted by the jack and the vertical displacement of the shaft are conducted during the process. The provided diagram depicts the graphical representation of the measurements' curve:

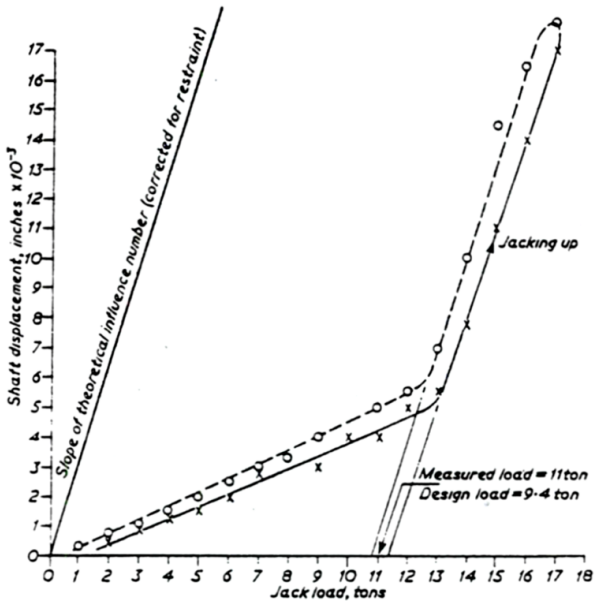

Figure 35: Jack-Up Test Measurement Curves[42]

In the first part of the curve, the gradual incline indicates that the load on the shaft continues to be sustained by the bearing. The occurrence of this phenomenon can be attributed to the elastic deformations exhibited by the bearing and shaft when subjected to substantial loads.
The subsequent section of the diagram, characterized by a pronounced incline, illustrates the complete application of load on the jack. The steepness of the slope corresponds to the influence factor associated with the support point, which in this case is the jack. The influence factor under consideration exhibits a strong resemblance to the influence factor associated with the bearing due to the close proximity of the jack to the bearing. Consequently, it is possible to employ correction factors in this scenario. The disparity is minimal due to the negligible longitudinal displacement of the support point in relation to the overall length of the shafting system. The final segment of the graph illustrates the measurements obtained during the descent of the jack. The minute discrepancy in values can be ascribed to the presence of friction. The determination of the bearing reaction's true value can be achieved by extrapolating the mean value between the ascending and descending curves (i.e., the steepest section) of the diagram towards zero shaft displacement.

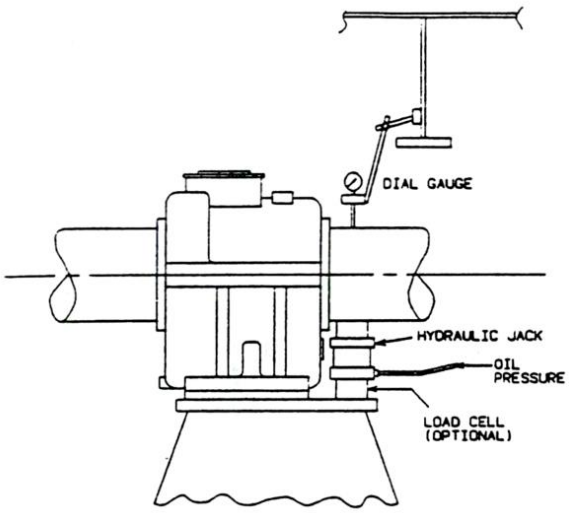

Figure 36: Hydraulic Jack Installation[43]

The jack-up method can also be employed for the assessment of permanent bending deformations in the shaft. This is achieved by conducting four measurements and subsequently rotating the shaft by 90 degrees after each measurement. By comparing these results, it can be inferred whether the shaft is misaligned.

Strain Gauge Test

This methodology employs strain gauges to quantify stress at any location along the shaft and subsequently derive the reaction forces. The method is highly precise and facilitates measurements at the precise location of the contact point, where the installation of jacks is not feasible. The system is capable of generating both vertical and horizontal loads, and has the capacity to simultaneously measure multiple bearing loads. In order to enhance measurement precision, it is common practice to install multiple gauges at a given longitudinal position. Typically, four gauges are positioned in pairs, with a separation of 180° between each pair, thereby forming a Wheatstone bridge configuration. Moreover, it can be readily replicated subsequent to the initial installation of the strain gauge. One additional benefit of this approach is that the provided data, specifically strains and bending moments, can be readily employed to accurately determine the curvature of the shaft and subsequently determine the precise position of the bearing. In contrast, the extended duration required for installation represents a prominent drawback of the approach, alongside the costly and intricate instrumentation essential for the measurement process. In addition, the measurement process necessitates the involvement of personnel with specialized expertise. Each strain gauge installation typically demands approximately one hour to complete, owing to the intricate nature of the procedure and the requisite precision. The accuracy of data in the strain gauge test is heavily reliant on the meticulous and precise modeling of the shafting system, as opposed to the hydraulic jack testing.
Telemetry enabled strain gauges have the potential to serve as monitoring devices in operational scenarios, including running conditions, and offer valuable insights during vessel operation and could be used in conjunction with this thesis as will be discussed in the future work section**??**.

4 Theoretical Background of FEA for Dynamic Simulations

This chapter presents the fundamental equations, addressing the coupling of structural dynamics and lubrication, laying down the theoretical foundation for the Finite Element Analysis (FEA) applied to solve these problems in the context of a ship's shafting system. Initially, the focus is on the structural model (Section 4.1), where the static model is the foundation, followed by a more intricate dynamic model which embodies the real-time dynamics of the vessel's shaft. Subsequently, the modeling of the bearings as springs is explained (Section 4.3).
The equations governing both the structural and the lubrication domains are discretized using finite element methods, translating the continuous problems into a discrete domain that is computationally tractable. This discretization leads to a finite element model that is distributed across all available CPU cores, leveraging the parallel processing capabilities to expedite the solution process. The PETSc solvers, discussed more extensively later in (Section 5.4.7), are employed to tackle the system of equations resulting from the discretization, ensuring an efficient and accurate solution.
The solution methodology is anchored on the robust Newton-Raphson method coupled with the HHT-a algorithm for time-stepping (Section 4.2.2). This approach ensures a systematic and convergent solution process, beginning with addressing the bearing lubrication problem predicated on the shaft's position, followed by delving into the structural dynamics of the shaft. The sequential tackling of the lubrication and structural problems, enriched by the FEA, provides a comprehensive understanding and solution to the complex interactions within the shafting system, paving the way for optimized design and operational strategies for maritime propulsion systems.

4.1 Structural Model

The structural analysis of the vessel's shafting system is essential to understanding the mechanics and ensuring the robustness of the design under various operational conditions. This section presents the theoretical framework and the computational methodology employed to analyze the structural integrity and dynamic behavior of the shafting system.

The structural model primarily consists of a static and a dynamic analysis. The static analysis provides insight into the stress distribution, deformation, and the overall behavior of the shaft under static or steady-state conditions. This analysis is crucial for evaluating the design under typical loading conditions, ensuring that the system can withstand the operational loads without experiencing failure or excessive deformation.

On the other hand, the dynamic analysis delves into the behavior of the shafting system under varying or transient conditions, encapsulating the effects of forces and moments induced by the engine, propeller, and the sea waves. The dynamic model accounts for the inertia effects, damping, and the time-varying nature of the applied loads and boundary conditions. This analysis is crucial for assessing the vibrational behavior, dynamic stresses, and the potential resonant conditions that might occur during the operational life of the vessel.

The Finite Element Analysis (FEA) serves as the computational backbone for both static and dynamic analyses. By discretizing the domain into finite elements, the continuous problem is translated into a discrete set of equations that can be efficiently solved using numerical methods. The FEA facilitates a detailed examination of the structural behavior under complex loading and boundary conditions, providing a comprehensive understanding of the stress distributions, deformation patterns, and dynamic responses of the system.

The subsequent sections will elaborate on the formulation of the static and dynamic models, the finite element discretization, and the solution techniques employed to analyze the structural behavior of the

vessel's shafting system. The discussion will also encompass the considerations and assumptions made to simplify the model without compromising the accuracy and reliability of the results.
The theory presented in the following is based on the works[44][45][46][47][48][49][50][51], which provide a more detailed overview.

4.1.1 Elasticity Relations

The field of continuum mechanics offers a theoretical framework for describing the dynamic behavior of a deformable body through a macroscopic model. The subsequent equations are presented to describe the behavior of linear elastic materials. The problem at hand is characterized by the utilization of kinematic relations, equilibrium equations, and the application of a constitutive model.
In the fixed reference system the position of a material (quadrature) point is given in a Cartesian Coordinate system with coordinates x, y, z and base vectors $\vec{e_x}$, $\vec{e_y}$, $\vec{e_z}$ as:

$$\vec{x}(t) = x(t)\vec{e_x} + y(t)\vec{e_y} + z(t)\vec{e_z} \tag{4.1}$$

The displacement of a material point can be formulated as the displacement vector $\vec{u}(t, \vec{x})$ as:

$$\vec{u}(t, \vec{x}) = \vec{u_x}(t, \vec{x}) + \vec{u_y}(t, \vec{x}) + \vec{u_z}(t, \vec{x}) \tag{4.2}$$

with the corresponding displacement components $\vec{u_x}$, $\vec{u_y}$, $\vec{u_z}$, respectively.

For the present study, the formulation considers **small deformations**, for which the strain for a given quadrature point can be described by the strain tensor:

$$\mathbf{E}(t, \vec{x}) = \frac{1}{2}[\nabla\vec{u}(t, \vec{x}) + \nabla^T\vec{u(t, \vec{x})}] \tag{4.3}$$

With its components:

$$\mathbf{E}(t, \vec{x}) = \begin{pmatrix} \frac{\partial u_x}{\partial x} & \frac{1}{2}\left(\frac{\partial u_x}{\partial y} + \frac{\partial u_y}{\partial x}\right) & \frac{1}{2}\left(\frac{\partial u_x}{\partial z} + \frac{\partial u_z}{\partial x}\right) \\ \frac{1}{2}\left(\frac{\partial u_y}{\partial x} + \frac{\partial u_x}{\partial y}\right) & \frac{\partial u_y}{\partial y} & \frac{1}{2}\left(\frac{\partial u_y}{\partial z} + \frac{\partial u_z}{\partial y}\right) \\ \frac{1}{2}\left(\frac{\partial u_z}{\partial x} + \frac{\partial u_x}{\partial z}\right) & \frac{1}{2}\left(\frac{\partial u_z}{\partial y} + \frac{\partial u_y}{\partial z}\right) & \frac{\partial u_z}{\partial z} \end{pmatrix} = \begin{pmatrix} \varepsilon_x & \varepsilon_{xy} & \varepsilon_{xz} \\ \varepsilon_{xy} & \varepsilon_y & \varepsilon_{yz} \\ \varepsilon_{xz} & \varepsilon_{yz} & \varepsilon_z \end{pmatrix} \tag{4.4}$$

The strain tensor is symmetric and thus contains six different strain components, three normal strain components ε_{ii} and three shear strain components ε_{ij}.

The equilibrium conditions are given as:

$$\nabla \cdot \mathbf{T}(t, \vec{x}) + \varrho(\vec{x})\vec{k} + \vec{t} = \varrho(\vec{x})\ddot{\vec{u}}(t, \vec{x}) + c(\vec{x})\dot{\vec{u}}(t, \vec{x}), \tag{4.5}$$

With the stress tensor $\mathbf{T}$, the density of the material ϱ, the extrenal forces per mass $\vec{k}$, the external forces per area $\vec{t}$. The stress tensor $\mathbf{T}$, akin to the strain tensor $\mathbf{E}$, exhibits symmetry and comprises three normal components σ_{ii} and three shear components τ_{ij}.

[44] *Πεπερασμένα Στοιχεία στην Ανάλυση Κατασκευών*, Χ. Γ. Προβατιδης.
[45] "The ÿnite volume solution of the Reynolds equation of lubrication with ÿlm discontinuities," M. Arghir *et al.*
[46] "The Finite Element Method for the Analysis of Non-Linear and Dynamic Systems," D. E. Chatzi.
[47] *The Finite Element Method: Linear Static and Dynamic Finite Element Analysis*, T.G. Hughes and T. Hughes.
[48] "NONLINEAR CONTINUUM MECHANICS," J. T. Oden.
[49] *Metal fatigue analysis handbook*, Y.-L. Lee *et al.*
[50] "Goal-oriented error estimation and mesh adaptivity in three-dimentional elasticity problems," S Sh Ghorashi *et al.*
[51] *The deal.II Library: The step-44 tutorial program.*

As per the Voigt notation, the quantities of displacement, strain, and stress are converted into a column matrix format:

$$\mathbf{u} = [u_x\ u_y\ u_z], \tag{4.6}$$

$$\mathbf{E} = [\varepsilon_{xx}\ \varepsilon_{yy}\ \varepsilon_{zz}\ 2\varepsilon_{yz}\ 2\varepsilon_{xz}\ 2\varepsilon_{xy}]^{\mathrm{T}}, \tag{4.7}$$

$$\mathbf{T} = [\sigma_{xx}\ \sigma_{yy}\ \sigma_{zz}\ \tau_{yz}\ \tau_{xz}\ \tau_{xy}]^{\mathrm{T}} \tag{4.8}$$

The differential operator matrix $\mathbf{D} \subset \mathbb{R}^{6x3}$ provides the relation between the strain vector $\mathbf{E} \subset \mathbb{R}^6$ and the displacement vector $\mathbf{u} \subset \mathbb{R}^3$,

$$\mathbf{E} = \mathbf{Du}, \text{ with } \mathbf{D} = \begin{pmatrix} \frac{\partial}{\partial x} & 0 & 0 \\ 0 & \frac{\partial}{\partial y} & 0 \\ 0 & 0 & \frac{\partial}{\partial z} \\ 0 & \frac{\partial}{\partial z} & \frac{\partial}{\partial y} \\ \frac{\partial}{\partial z} & 0 & \frac{\partial}{\partial x} \\ \frac{\partial}{\partial y} & \frac{\partial}{\partial x} & 0 \end{pmatrix} \tag{4.9}$$

Using the stress and strain vector, linear elastic material behavior of the continuum can be modeled through:

$$\mathbf{T} = \mathbf{CE} \tag{4.10}$$

The symmetric elasticity matrix $\mathbf{C} \subset \mathbb{R}^{\mathbf{6x6}}$ relates stress and strain in a continuum. For isotropic material behavior for small deformations, the inverse of the elasticity matrix is given as:

$$\mathbf{C}^{-1} = \frac{1}{E} \begin{pmatrix} 1 & -\nu & -\nu & 0 & 0 & 0 \\ -\nu & 1 & -\nu & 0 & 0 & 0 \\ -\nu & -\nu & 1 & 0 & 0 & 0 \\ 0 & 0 & 0 & 2(1+\nu) & 0 & 0 \\ 0 & 0 & 0 & 0 & 2(1+\nu) & 0 \\ 0 & 0 & 0 & 0 & 0 & 2(1+\nu) \end{pmatrix}$$

Hence, the isotropic linear elastic material behavior is governed by only two parameters, Young's Modulus E and Poisson′s ratio ν.
However, in this particular study the symmetric elasticity matrix is defined using the Lam$\acute{e}'$s constants, namely λ and μ. Consequently, the final form of the elasticity matrix $\mathbf{C}$ is the following:

$$\mathbf{C} = \begin{pmatrix} 2\mu+\lambda & \lambda & \lambda & 0 & 0 & 0 \\ \lambda & 2\mu+\lambda & \lambda & 0 & 0 & 0 \\ \lambda & \lambda & 2\mu+\lambda & 0 & 0 & 0 \\ 0 & 0 & 0 & \mu & 0 & 0 \\ 0 & 0 & 0 & 0 & \mu & 0 \\ 0 & 0 & 0 & 0 & 0 & \mu \end{pmatrix} \tag{4.11}$$

This assumed elastic behavior of the material will in higher strain values generate falsely high stresses. This behavior can be tamed using an elastoplastic formulation, where certain points of the domain enter the plastic region of deformation, while others remain in the linear stress-strain region. This will not be examined in this present study.

4.1.2 Finite Elements Method

In most cases, the linear elasticity relations shown above cannot be solved analytically for complicated geometries. Consequently, the solution is estimated by employing the finite element method.

The subsequent section provides an overview of the derivation of the equations used and will present the methods utilised to solve the system of differential equations given the limitations in computation power and data.

The starting point of the derivation is the elastic wave equation for solids Equation 4.5 which is integrated over the domain:

$$\int_V \delta\vec{u} \cdot \rho\ddot{\vec{u}} dV + \int_V \delta\vec{u} \cdot c\dot{\vec{u}} dV + \int_V \delta\mathbf{E} \cdot \mathbf{T} dV - \int_V \delta\vec{u} \cdot \rho\vec{k} dV - \int_A \delta\vec{u} \cdot \vec{t} dA = 0 \tag{4.12}$$

where:

- $\delta\vec{u}$ is the virtual displacement,
- $\delta\mathbf{E} = \frac{1}{2}(\nabla\delta\vec{u} + \nabla^{\mathbf{T}}\delta\vec{u})$, the virtual strain
- $\vec{t} = T \cdot \vec{n}$ the normal surface load density and
- $\vec{n}$ the surface normal vector

The above equation is approximated by small, simply shaped 3D elements, and specifically in this current study hexagonal elements. This approximation converts the volume of the solid into the discrete domain Ω_s which is subdivided into subdomains Ω_e. Similarly, the surface A is approximated by Γ. The column matrix $x \subset \mathbb{R}^3$ contains the coordinates of a point in the discrete three-dimensional domain.

The interpolation from the local domain (element) to the discrete domain, shape functions are utilized. The shape functions can be organized in a matrix $\mathbf{N}_e(\mathbf{x}) \subset \mathbb{R}^{3\times n_{en}}$. This matrix contains the value of the shape functions evaluated at $\mathbf{x} \subset \mathbb{R}^3$ for all nodes n_{en} of an element e.
In this study, the shape functions $\mathbf{N}_e$ will not be explored further, as they are a part of the computational library used and they can provide all the essential parts of the building blocks of the solution.

The interpolation from the element to the discretized domain for the diplacement $\mathbf{u}^h \subset \mathbb{R}^3$ is given as:

$$\mathbf{u}^h(t, \mathbf{x}) = \mathbf{N}_e(\mathbf{x})\mathbf{u}_e(t), \tag{4.13}$$

where the superscript h indicates the discretized domain. The element displacement vector $\mathbf{u}_e \subset \mathbb{R}^{3\times n_{en}}$ contains the three displacement components of all nodes of an element. The approximated diplacements $\mathbf{u}^h$ are inserted into Equation 4.9 to approximate the strains:

$$\mathbf{E}^h = \mathbf{D}\mathbf{N}_e(\mathbf{x})\mathbf{u}_e = \mathbf{B}_e(\mathbf{x})\mathbf{u}_e \tag{4.14}$$

With the strain-displacement matrix $\mathbf{B}_e(\mathbf{x}) \subset \mathbb{R}^{6\times 3\cdot n_{en}}$. The aforementioned approximation is also applied to the accelerations $\ddot{\mathbf{u}}^h$, the velocities $\dot{\mathbf{u}}^h$, the virtual displacements $\delta\mathbf{u}^h$, and virtual strains $\delta\mathbf{E}^h$.

Utilising the approximated variables and the constitutive relation (Equation 4.9), the weak form Equation 4.12 can be rewritten for each element e as:

$$\delta\mathbf{u}_e^{\mathbf{T}}\{\int_{\Omega_e} \mathbf{N}_e^{\mathbf{T}}(\mathbf{x})\rho\mathbf{N}_e(\mathbf{x})d\Omega\ddot{\mathbf{u}}_e(t) + \int_{\Omega_e} \mathbf{N}_e^{\mathbf{T}}(\mathbf{x})c\mathbf{N}_e(\mathbf{x})d\Omega\dot{\mathbf{u}}_e(t) + \int_{\Omega_e} \mathbf{B}_e^{\mathbf{T}}(\mathbf{x})\mathbf{C}\mathbf{B}_e(\mathbf{x})d\Omega\mathbf{u}_e(t) - \int_{\Omega_e} \mathbf{N}_e^{\mathbf{T}}(\mathbf{x})\rho\mathbf{k}d\Omega - \int_{\Gamma_e} \mathbf{N}_e^{\mathbf{T}}(\mathbf{x})\mathbf{t}(\mathbf{x}, t)d\Gamma\} = 0 \tag{4.15}$$

The virtual displacements are considered to be arbitrary in nature. Therefore, in order to satisfy Equation 4.15, it is necessary for the equation within the brackets to equate to zero. The equations representing the element mass matrix, the element damping matrix, the element stiffness matrix and the element force vector are provided below:

$$\mathbf{M}_e = \int_{\Omega_e} \mathbf{N}_e^{\mathbf{T}}(\mathbf{x}) \rho \mathbf{N}_e(\mathbf{x}) d\Omega \tag{4.16}$$

$$\mathbf{C}_e = \int_{\Omega_e} \mathbf{N}_e^{\mathbf{T}}(\mathbf{x}) c \mathbf{N}_e(\mathbf{x}) d\Omega \tag{4.17}$$

$$\mathbf{K}_e = \int_{\Omega_e} \mathbf{B}_e^{\mathbf{T}}(\mathbf{x}) \mathbf{C} \mathbf{B}_e(\mathbf{x}) d\Omega \tag{4.18}$$

$$\mathbf{F}_e = \int_{\Omega_e} \mathbf{N}_e^{\mathbf{T}}(\mathbf{x}) \rho \mathbf{k} d\Omega + \int_{\Gamma_e} \mathbf{N}_e^{\mathbf{T}}(\mathbf{x}) \mathbf{t}(\mathbf{x}, t) d\Gamma \tag{4.19}$$

The global (system) matrices are created as a combination of all the element matrices. For each element, a coordinate transformation is performed using the Jacobian matrix, while the integrals are approximated using Gauss Quadrature. The resulting element matrices are distributed to the global matrix in accordance to the degrees of freedom that they contribute. Simplified, the assembly process can be illustrated as follows.
The local matrices of element 1 and element 2 are denoted as $[K]_1$ and $[K]_2$ respectively. The global matrix $[K]$ is assembled by summing the contributions of these local matrices at corresponding degrees of freedom. The general expression for the assembly process is given by:

$$[K] = [K] + [K]_1 + [K]_2 \tag{4.20}$$

For simplicity, assume that each element contributes to two nodes. The assembly process can then be visually represented as:

$$\begin{pmatrix} K_{11} & K_{12} \\ K_{21} & K_{22} \end{pmatrix} = \begin{pmatrix} K_{11}^{(1)} & K_{12}^{(1)} \\ K_{21}^{(1)} & K_{22}^{(1)} \end{pmatrix} + \begin{pmatrix} K_{11}^{(2)} & K_{12}^{(2)} \\ K_{21}^{(2)} & K_{22}^{(2)} \end{pmatrix} \tag{4.21}$$

where the superscripts (1) and (2) denote element 1 and element 2 respectively, and K_{ij}, $K_{ij}^{(1)}$, and $K_{ij}^{(2)}$ are the elements of the global and local matrices.

In summary, the system matrices are assembled as shown below,

$$\mathbf{M} = \bigcup_{e=1}^{n_{el}} \mathbf{M}_e, \quad \mathbf{C} = \bigcup_{e=1}^{n_{el}} \mathbf{C}_e, \quad \mathbf{K} = \bigcup_{e=1}^{n_{el}} \mathbf{K}_e, \quad \mathbf{F} = \bigcup_{e=1}^{n_{el}} \mathbf{F}_e, \tag{4.22}$$

where $\bigcup$ indicates the assembly process, n_{el} is the number of elements and $\mathbf{M} \subset \mathbb{R}^{n_u \times n_u}$, $\mathbf{C} \subset \mathbb{R}^{n_u \times n_u}$, $\mathbf{K} \subset \mathbb{R}^{n_u \times n_u}$, $\mathbf{F} \subset \mathbb{R}^{n_u}$ are the global mass, damping, stiffness matrices and the global force vector, respectively. The element displacement vectors $\mathbf{u}_e \subset \mathbb{R}^{n_{en}}$, element velocity vectors $\dot{\mathbf{u}}_e \subset \mathbb{R}^{n_{en}}$ and element acceleration vectors $\ddot{\mathbf{u}}_e \subset \mathbb{R}^{n_{en}}$ are also assembled to their respective global vectors $\mathbf{u} \subset \mathbb{R}^{n_u}$, $\dot{\mathbf{u}} \subset \mathbb{R}^{n_u}$, $\ddot{\mathbf{u}} \subset \mathbb{R}^{n_u}$, where n_u denotes the degrees of freedom.
In summary, the system of differential equations is the following:

$$\mathbf{M}\ddot{\mathbf{u}} + \mathbf{C}\dot{\mathbf{u}} + \mathbf{K}\mathbf{u} = \mathbf{F} \tag{4.23}$$

4.1.3 Rayleigh Damping

Introduction

The analysis of damping in dynamic finite element analysis (FEA) is crucial for the accurate simulation of real-world systems. However, the calculation of the damping values of a solid is very complex and, especially on larger systems, not always feasible, so several methods of approximating this value have been developed. A common method employed is Rayleigh damping, which provides a simplistic linear representation of damping through a combination of mass and stiffness proportional damping. This method is mathematically expressed as:

$$\mathbf{C} = \mu_{Rayleigh}\mathbf{M} + \lambda_{Rayleigh}\mathbf{K}, \tag{4.24}$$

where $\mathbf{C}$ is the damping matrix, $\mu_{Rayleigh} \in (0, 0.5)$ and $\lambda_{Rayleigh} \in (0, 0.5)$ are the Rayleigh damping coefficients.

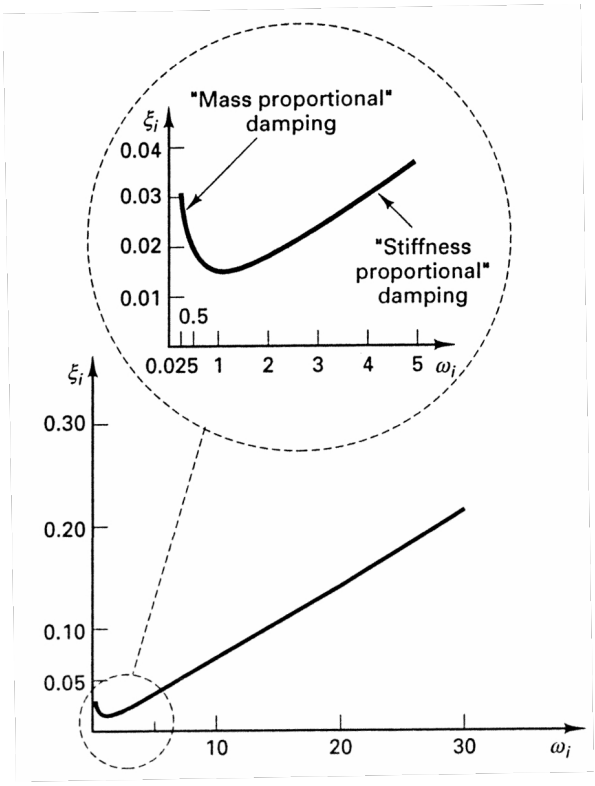

Figure 37: Rayleigh Damping- Frequency vs Damping Ratio[52]

The scalars $\mu_{Rayleigh}$ and $\lambda_{Rayleigh}$ are real scalars with units 1/sec and sec respectively. This approach is based on two main assumptions:

- The model used for the damping of the structure is viscous and
- the approach is formulated for the linear response of the structure, which is the case for the small deformations assumed for the shafting system.

The damping ration for the n^{th} mode of the system is:

$$\zeta_n = \frac{\mu_{Rayleigh}}{2}\frac{1}{\omega_n} + \frac{\lambda_{Rayleigh}}{2}\omega_n \tag{4.25}$$

The Rayleigh damping coefficients are calculated based on the desired damping ratio, ζ, for two target modes of vibration with angular frequencies ω_i and ω_j. The coefficients are determined by the following equations:

$$\mu_{Rayleigh} = \frac{2\zeta(\omega_i\omega_j)}{\omega_i + \omega_j} \tag{4.26}$$

$$\lambda_{Rayleigh} = \frac{2\zeta}{\omega_i + \omega_j} \tag{4.27}$$

These relationships ensure that the damping ratio ζ is accurately represented at the two selected frequencies, which is crucial for the correct simulation of structural behavior under dynamic loading.

Problems with Rayleigh Damping
The Rayleigh damping approach can be problematic in some cases. On of the main considerations when using Rayleigh damping is when applying it in structures with added dampers or base isolators. In this case if the damping matrix is constructed using the properties of the relatively stiff superstructure alone, the damping ratio imposed on the total system will be very high as a result of the mass-proportional damping term. The solution to this is the use of the stiffness-proportional damping term alone.

Another consideration, which is not applicable to this study, is the large mass-proportional damping forces that can develop when a structure breaks loose and therefore develops a high velocity[53]. This is the result of the assumption that proportional stiffness damping corresponds to linear viscous dampers. Especially, in a non-linear analysis, where the non-linearities, such as buckling, yielding, cracking, reduce the total stiffness, whereas the structure's velocity augments, driven by these very non-linearities. Yet, the motion equation, formulated using the initial high stiffness values, leads to an overestimation of the damping forces. This overestimation is further exacerbated by the linearity assumption intrinsic to the damping forces, which dictates a constant proportionality to the velocities, regardless of their magnitude .

Several Solutions have been proposed to remedy the aforementioned problems, namely:

- Eliminate the mass-proportional damping contribution and Bound the stiffness proportional damping contribution
- Basing the damping matrix only on the diagonal terms of the initial stiffness
- Updating the damping matrix for each time step (as used in this study)
- In addition to the above, update the proportionality coefficients for each time step
- Use only mass-proportional damping, which will satisfy the static equilibrium, but displacement responses will exhibit significant higher-frequency responses, not observable in real structures, due to the small damping rations at the higher modes.
- Modelling each beam element with a combination of an elastic beam element and rotational end springs, which will result in stiffness proportional damping and eliminates the effect of forces resulted from nonlinear phenomena
- As an extension of the above, updating the stiffness matrix of the modeled beams in each timestep.

[53] "Problems encountered from the use (or misuse) of Rayleigh damping," J. F. Hall.

4.2 Solution of Dynamic Systems

The analytical solution of dynamic systems is often unattainable, necessitating the use of numerical integration methods to approximate system behavior over time. These methods are critical in analyzing the system's evolution under varying conditions, with the method's choice greatly influencing the solution's accuracy, stability, and computational efficiency. We detail several numerical integration techniques prevalent in dynamic system analysis, focusing on the method employed in this study referenced in Equation 4.23:

- **Euler's Methods:** Including explicit and implicit variants, these are fundamental first-order integration techniques offering rapid solutions with lower accuracy.
- **Runge-Kutta Methods:** These provide a higher accuracy level than Euler's methods, with the 4th order variant being particularly favored for its accuracy and computational efficiency balance.
- **Newmark-Beta Method:** Prevalent in structural dynamics and earthquake engineering, this method supports both implicit and explicit integration schemes, allowing for robust step-by-step system integration over time.
- **Wilson-Theta Method:** Known for unconditional stability, it is especially useful for analyzing highly damped or nonlinear systems.
- **Central Difference Method:** A straightforward method offering a moderate accuracy level, ideal for linear systems.
- **Houbolt Method:** Efficient for stiff systems, this multistep integration method balances computational efficiency and accuracy.

Each method is selected based on the problem's specific needs, considering accuracy, system nature, and computational resources. This study employs the **Newmark-Beta** method, which provides sufficient accuracy with limited computational resources. It also allows incorporation into the HHT-α algorithm for enhanced convergence through additional algorithmic damping.

4.2.1 Newmark-Beta Method

The Newmark-Beta method, established by Nathan M. Newmark in 1959, is a cornerstone numerical technique for differential motion equations in structural dynamics. It predicts system responses under diverse load conditions with a time-stepping mechanism controlled by parameters β and γ, influencing the solution's dissipation and accuracy. This method unifies implicit and explicit schemes, offering a comprehensive analysis framework.
The linear equation for each time step is:

$$\mathbf{M}\ddot{\mathbf{u}}_{k+1} + \mathbf{C}\left(\dot{\mathbf{u}}_{k+1} + \gamma\Delta t\ddot{\mathbf{u}}_{k+1}\right) + \mathbf{K}\left(\mathbf{u}_{k+1} + \beta\Delta t^2\ddot{\mathbf{u}}_{k+1}\right) = \mathbf{f}(t_{k+1}) \tag{4.28}$$

Predictors for the next time step depend on the current and previous states:

$$\tilde{\mathbf{u}}_{k+1} = \mathbf{u}_k + \Delta t\dot{\mathbf{u}}_k + \Delta t^2(\frac{1}{2} - \beta)\ddot{\mathbf{u}}_k, \tag{4.29}$$

$$\dot{\tilde{\mathbf{u}}}_{k+1} = \dot{\mathbf{u}}_k + \Delta t(1-\gamma)\ddot{\mathbf{u}}_k. \tag{4.30}$$

The correctors for the current time step are:

$$\mathbf{u}_{k+1} = \tilde{\mathbf{u}}_{k+1} + \beta\Delta t^2\ddot{\mathbf{u}}_{k+1}, \tag{4.31}$$

$$\dot{\mathbf{u}}_{k+1} = \dot{\tilde{\mathbf{u}}}_{k+1} + \gamma\Delta t\ddot{\mathbf{u}}_{k+1}. \tag{4.32}$$

The method can be explicit ($\beta = 0$) or implicit (requiring inversion of $\mathbf{K}$ when $\beta \neq 0$). Stability and accuracy are governed by β and γ, typically chosen within $\frac{1}{4} \leq \beta \leq \frac{1}{2}$ and $\frac{1}{2} \leq \gamma \leq \frac{3}{2}$ to ensure stability. Without damping, the Newmark method's stability criterion is:

$$\gamma \geq \frac{1}{2}, \quad \beta \leq \frac{1}{2}, \quad \Delta t \leq \frac{1}{\omega_{max}\sqrt{\frac{\gamma}{2} - \beta}}, \tag{4.33}$$

where ω_{max} is the highest natural frequency. The method is unconditionally stable if:

$$2\beta \geq \gamma \geq \frac{1}{2}, \tag{4.34}$$

although $\gamma \geq \frac{1}{2}$ introduces numerical damping and period elongation errors. Its unconditional stability, particularly for the average acceleration method, makes it robust for large, complex structures with numerous high frequencies.
Newmark-Beta Non-Linear IVP

The Newmark-Beta method is adept at handling nonlinear problems that are typical in dynamic systems. The discretization of the initial value problem (IVP) with a time step $\Delta t = t_{k+1} - t_k$ involves the dynamic equilibrium equation at the timestep $k+1$:

$$\mathbf{M}\ddot{\mathbf{u}}_{k+1} + \mathbf{r}(\mathbf{u}_{k+1}, \dot{\mathbf{u}}_{k+1}) = \mathbf{f}(t_{k+1}) \tag{4.35}$$

The initial conditions are specified as $\mathbf{u}(t_0) = \mathbf{u}_0$ and $\dot{\mathbf{u}}(t_0) = \dot{\mathbf{u}}_0$. At each timestep, a nonlinear problem is formulated and solved as follows:

$$\mathbf{M}\ddot{\mathbf{u}}_{k+1} + \mathbf{r}(\tilde{\mathbf{u}}_{k+1} + \ddot{\mathbf{u}}_{k+1}\beta\Delta t^2, \dot{\tilde{\mathbf{u}}}_{k+1} + \ddot{\mathbf{u}}_{k+1}\gamma\Delta t) = \mathbf{f}(t_{k+1}) \tag{4.36}$$

The implicit nature of the Newmark-Beta method requires the use of an iterative solution strategy, such as the Newton-Raphson method, to solve the nonlinear equations at each timestep. The algorithm is as follows:

$\ddot{\mathbf{u}}_{k+1} \leftarrow \mathbf{0}$

$\mathbf{u}_{k+1} \leftarrow \mathbf{u}_k + \dot{\mathbf{u}}_k \Delta t + \ddot{\mathbf{u}}_k \left(\frac{1}{2} - \beta\right) \Delta t^2 + \ddot{\mathbf{u}}_{k+1} \beta \Delta t^2$

$\dot{\mathbf{u}}_{k+1} \leftarrow \dot{\mathbf{u}}_k + \ddot{\mathbf{u}}_k (1 - \gamma) \Delta t + \ddot{\mathbf{u}}_{k+1} \gamma \Delta t$

$\epsilon \leftarrow \mathbf{f}(t_{k+1}) - \mathbf{r}(\mathbf{u}_{k+1}, \dot{\mathbf{u}}_{k+1}) - \mathbf{M}\ddot{\mathbf{u}}_{k+1}$

while $\|\epsilon\| \geq$ Tol **do**

$\Delta\ddot{\mathbf{u}}_{k+1} \leftarrow (\mathbf{M} + \mathbf{C}\gamma\Delta t + \mathbf{K}\beta\Delta t^2)^{-1}\epsilon$

$\ddot{\mathbf{u}}_{k+1} \leftarrow \ddot{\mathbf{u}}_{k+1} + \Delta\ddot{\mathbf{u}}_{k+1}$

$\dot{\mathbf{u}}_{k+1} \leftarrow \dot{\mathbf{u}}_{k+1} + \Delta\ddot{\mathbf{u}}_{k+1}\gamma\Delta t$

$\mathbf{u}_{k+1} \leftarrow \mathbf{u}_{k+1} + \Delta\ddot{\mathbf{u}}_{k+1}\beta\Delta t^2$

$\epsilon \leftarrow \mathbf{f}(t_{k+1}) - \mathbf{r}(\mathbf{u}_{k+1}, \dot{\mathbf{u}}_{k+1}) - \mathbf{M}\ddot{\mathbf{u}}_{k+1}$

end while

The assembly of the restoring force and the stiffness matrix is performed by looping over the elements, which is crucial for understanding the behavior of the system under dynamic loading:

for $i = 1$ to I **do**

$\mathbf{r}_{i,k+1} \leftarrow$ elementForce$(\mathbf{Z}_i \mathbf{u}_{k+1})$

$\mathbf{r}_{k+1} \leftarrow \mathbf{r}_{k+1} + \mathbf{Z}_i^T \mathbf{r}_{i,k+1}$

end for

for $i = 1$ to I **do**

$\mathbf{K}_{i,k+1} \leftarrow$ elementStiff$(\mathbf{Z}_i \mathbf{u}_{k+1})$

$\mathbf{K}_{k+1} \leftarrow \mathbf{K}_{k+1} + \mathbf{Z}_i^T \mathbf{K}_{i,k+1} \mathbf{Z}_i$

end for

These steps ensure that the Newmark-Beta method can be effectively applied to solve complex dynamic problems in a robust and reliable manner, as it is depicted in the plot below:

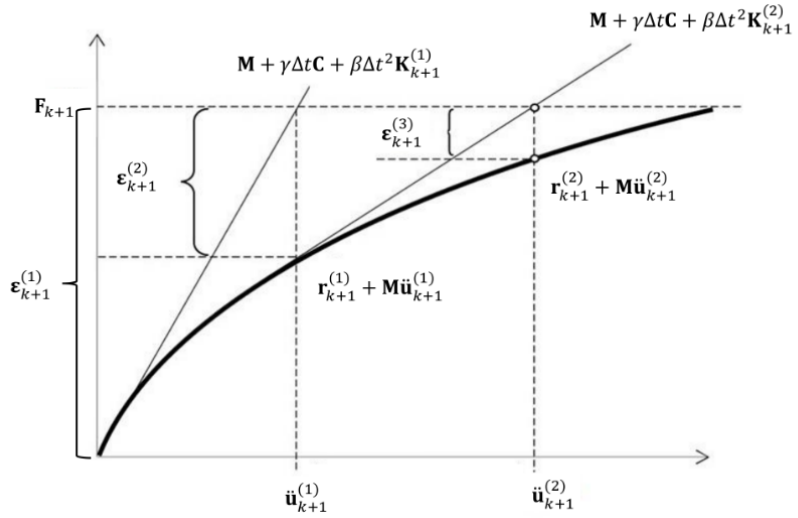

Figure 38: Full Newton-Raphson Iteration

4.2.2 HHT-a Algorithm

The Hilber-Hughes-Taylor (HHT-α) algorithm[54] is an extension of the Newmark-Beta method designed to enhance numerical stability and convergence by introducing algorithmic damping. This is particularly beneficial when dealing with high-frequency response components that might induce numerical instabilities in the solution process.

The HHT-α algorithm, developed by Hilber, Hughes, and Taylor, was introduced to the field of computational structural dynamics through their seminal 1977 paper. This paper, titled "Improved Numerical Dissipation for Time Integration Algorithms in Structural Dynamics"[55] was a breakthrough in the numerical analysis of structures subjected to dynamic loading. The algorithm's inception was driven by the need to control numerical dissipation effectively, thereby improving both the stability and the accuracy of the transient response obtained from time integration methods.

The Hilber-Hughes-Taylor (HHT-α) algorithm is an implicit method notable for its ability to introduce controlled numerical damping without compromising second-order accuracy. This characteristic is particularly advantageous when dealing with the dynamic analysis of structures, as it allows for energy dissipation, which is not achievable with the standard Newmark method. The HHT-α method can also be configured to be unconditionally stable for linear problems, depending on the choice of input parameters, which is an essential property for ensuring the reliability of the numerical solution.

Additionally, the HHT-α method preserves the accuracy of the Newmark's approximations while modifying the time-discrete momentum equation to increase numerical damping. This modification is crucial as it dampens high-frequency response components that can cause instability in the solution process. The intermediate displacements and velocities are adjusted by the α parameter, leading to a set of linear equations that can be efficiently solved, ensuring accurate results and convergence to the correct solution.

The α-shifted equation of motion is given by:

$$\mathbf{M}\ddot{\mathbf{u}}_{k+1} + (1+\alpha)\mathbf{r}(\mathbf{u}_{k+1}, \dot{\mathbf{u}}_{k+1}) - \alpha\mathbf{r}(\mathbf{u}_k, \dot{\mathbf{u}}_k) = (1+\alpha)\mathbf{f}(t_{k+1}) - \alpha\mathbf{f}(t_k) \tag{4.37}$$

The initial conditions remain the same as $\mathbf{u}(t_0) = \mathbf{u}_0$ and $\dot{\mathbf{u}}(t_0) = \dot{\mathbf{u}}_0$. The integration parameters β and γ, and the interpolation equations for displacement and velocity are given by:

$$\mathbf{u}_{k+1} = \mathbf{u}_k + \dot{\mathbf{u}}_k\Delta t + \ddot{\mathbf{u}}_k\left(\frac{1}{2} - \beta\right)\Delta t^2 + \ddot{\mathbf{u}}_{k+1}\beta\Delta t^2 \tag{4.38}$$

$$\dot{\mathbf{u}}_{k+1} = \dot{\mathbf{u}}_k + \ddot{\mathbf{u}}_k(1-\gamma)\Delta t + \ddot{\mathbf{u}}_{k+1}\gamma\Delta t \tag{4.39}$$

$$\beta = \frac{(1-\alpha)^2}{4}, \quad \gamma = \frac{1-2\alpha}{2} \tag{4.40}$$

Here, α modulates the algorithmic damping and lies in the range $[-1/3, 0]$.
The implicit Newton-Raphson iterations are used for the implementation:

[54] *The Finite Element Method: Linear Static and Dynamic Finite Element Analysis*, T.G. Hughes and T. Hughes.
[55] "Improved numerical dissipation for time integration algorithms in structural dynamics," H. M. Hilber *et al.*

Initialize $\ddot{\mathbf{u}}_{k+1}$ to zero

Compute the displacement: $\mathbf{u}_{k+1} \leftarrow \mathbf{u}_k + \dot{\mathbf{u}}_k \Delta t + \ddot{\mathbf{u}}_k \left(\frac{1}{2} - \beta\right) \Delta t^2 + \ddot{\mathbf{u}}_{k+1} \beta \Delta t^2$

Compute the velocity: $\dot{\mathbf{u}}_{k+1} \leftarrow \dot{\mathbf{u}}_k + \ddot{\mathbf{u}}_k (1 - \gamma) \Delta t + \ddot{\mathbf{u}}_{k+1} \gamma \Delta t$

Compute the effective force: $\epsilon \leftarrow \hat{\mathbf{f}}_{k+1}$

while $\|\epsilon\| \geq$ Tol **do**

Solve for acceleration increment: $\Delta \ddot{\mathbf{u}}_{k+1} \leftarrow \hat{\mathbf{M}}^{-1} \epsilon$

Update the acceleration: $\ddot{\mathbf{u}}_{k+1} \leftarrow \ddot{\mathbf{u}}_{k+1} + \Delta \ddot{\mathbf{u}}_{k+1}$

Update the velocity: $\dot{\mathbf{u}}_{k+1} \leftarrow \dot{\mathbf{u}}_{k+1} + \Delta \ddot{\mathbf{u}}_{k+1} \gamma \Delta t$

Update the displacement: $\mathbf{u}_{k+1} \leftarrow \mathbf{u}_{k+1} + \Delta \ddot{\mathbf{u}}_{k+1} \beta \Delta t^2$

Re-evaluate the effective force: $\epsilon \leftarrow \hat{\mathbf{f}}_{k+1}$

end while

The modified mass matrix $\hat{\mathbf{M}}$ and the effective force $\hat{\mathbf{f}}_{k+1}$ used in the iterations are defined as:

$$\hat{\mathbf{M}} = \mathbf{M} + \mathbf{C}\gamma\Delta t(1+\alpha) + \mathbf{K}\beta\Delta t^2(1+\alpha) \tag{4.41}$$

$$\begin{aligned} \hat{\mathbf{f}}_{k+1} = {} & (1+\alpha)\mathbf{f}_{k+1} - \alpha\mathbf{f}_k - (1+\alpha)\mathbf{r}(\tilde{\mathbf{u}}_{k+1}) \\ & + \alpha\mathbf{r}(\tilde{\mathbf{u}}_k) - (1+\alpha)\mathbf{C}\dot{\tilde{\mathbf{u}}}_{k+1} + \alpha\mathbf{C}\dot{\tilde{\mathbf{u}}}_k + \alpha(\mathbf{C}\gamma\Delta t + \mathbf{K}\beta\Delta t^2)\ddot{\mathbf{u}}_k \end{aligned} \tag{4.42}$$

The assembly of the restoring force and the stiffness matrix follows the same procedure as in the Newmark method, ensuring that the HHT-α algorithm is consistent with the established framework but enhanced for better performance in dynamic analysis.

4.3 Bearings' Model as a Mechanical System

The dynamic behavior of a journal bearing can be effectively modeled by simplifying the bearing into a mechanical system comprising spring and damper elements along with a frictional torque component. This abstraction allows for the study of the bearing's response to external loads and its inherent damping characteristics in a more analytically tractable form.In this model, the journal bearing is represented by two spring constants: one along the vertical z axis and the other for the lateral axis. These springs mimic the stiffness of the bearing material and the hydrodynamic forces generated by the lubricant film. The spring constants are determined by the geometry of the bearing and the properties of the lubricant, which influence the load-carrying capacity of the bearing and its ability to maintain a film of lubricant between the journal and the bearing surfaces and are given as inputs to the calculation.

In Finite Element Analysis (FEA), springs are integrated into the system stiffness matrix $\mathbf{K}$ to model elastic resistance to deformation. The springs are typically represented by their stiffness coefficients, which quantify the relationship between the force exerted on the spring and the resulting displacement. For an individual spring, this relationship is given by Hooke's Law, which can be expressed as $F = k \cdot x$, where F is the force, k is the spring constant, and x is the displacement.

When incorporating springs into the FEA model, each spring's stiffness coefficient is placed into the global stiffness matrix $\mathbf{K}$ at the degrees of freedom that the spring affects. For a system with multiple springs, the contributions of each spring are assembled into the matrix by adding their stiffness coefficients to the corresponding entries in $\mathbf{K}$.

$$\mathbf{K} = \begin{bmatrix} k_1 + k_2 & -k_2 & 0 & \cdots & 0 \\ -k_2 & k_2 + k_3 & -k_3 & \cdots & 0 \\ 0 & -k_3 & k_3 + k_4 & \cdots & 0 \\ \vdots & \vdots & \vdots & \ddots & \vdots \\ 0 & 0 & 0 & \cdots & k_{n-1} + k_n \end{bmatrix} \tag{4.43}$$

The weak form of the finite element discretization is modified to include the effect of spring stiffness per area, denoted by k'. This term represents the distributed spring support, which adds to the internal virtual work due to the elastic resistance of the springs. The modified weak form, accounting for this stiffness, is given by:

$$\delta \mathbf{u}_e^{\mathbf{T}} \left\{ \int_{\Omega_e} \mathbf{N}_e^{\mathbf{T}}(\mathbf{x}) \rho \mathbf{N}_e(\mathbf{x}) d\Omega \ddot{\mathbf{u}}_e(t) + \int_{\Omega_e} \mathbf{N}_e^{\mathbf{T}}(\mathbf{x}) c \mathbf{N}_e(\mathbf{x}) d\Omega \dot{\mathbf{u}}_e(t) + \int_{\Omega_e} \mathbf{B}_e^{\mathbf{T}}(\mathbf{x}) \mathbf{C} \mathbf{B}_e(\mathbf{x}) d\Omega \mathbf{u}_e(t) \right.$$
$$\left. - \int_{\Omega_e} \mathbf{N}_e^{\mathbf{T}}(\mathbf{x}) \rho \mathbf{k} d\Omega - \int_{\Gamma_e} \mathbf{N}_e^{\mathbf{T}}(\mathbf{x}) \mathbf{t}(\mathbf{x}, t) d\Gamma + \int_{\Omega_e} k' \mathbf{N}_e^{\mathbf{T}}(\mathbf{x}) \mathbf{N}_e(\mathbf{x}) d\Omega \mathbf{u}_e(t) \right\} = 0 \tag{4.44}$$

In equation (4.44), the newly added term $\int_{\Omega_e} \mathbf{N}_e^{\mathbf{T}}(\mathbf{x}) k' \mathbf{N}_e(\mathbf{x}) d\Omega \mathbf{u}_e(t)$ accounts for the work done by the spring forces in the domain Ω_e. This term incorporates the spring stiffness per area into the internal virtual work of the system, thus modifying the stiffness matrix accordingly. The presence of this term ensures that the spring effects are properly represented in the FEA model, allowing for a more comprehensive analysis of the system's behavior under various loading conditions.

Here, σ represents the stress tensor, f denotes the body force per unit volume, and t represents the traction on the boundary $\partial\Omega$ with $d\Gamma$ as the boundary element. The first integral on the left-hand side corresponds to the internal virtual work due to stress, the second integral corresponds to the virtual work by the spring forces, and the right-hand side represents the external virtual work done by body forces and tractions.

The inclusion of the spring stiffness per area in the weak form allows the FEA system to simulate the effect of distributed spring supports or elastic foundations, providing a more accurate and comprehensive understanding of the mechanical behavior under various load conditions.

Accompanying the springs are two damper elements, also aligned with the z and lateral axes. These dampers represent the energy dissipation mechanisms of the system, primarily the viscous shear within the lubricant film. The damping coefficients are crucial in modeling the phase lag between the applied load and the displacement response of the bearing, which is essential for predicting the onset of vibrational instability. In this study, the damping is handled using Rayleigh Damping Section 4.1.3, so the added damping is handled exactly as the damping of the original solid, which also avoids several problems described in Section 4.1.3

By combining these elements into a coherent model, the dynamic response of a journal bearing to various operating conditions can be simulated. This model enables the analysis of critical parameters such as the system's natural frequencies, resonance conditions, and transient behaviors.

5 Software Design and Development

The primary objective of the software is to deliver a robust and reliable Finite Element Analysis (FEA) simulation platform that specializes in the parametric modeling of ship propulsion shafting systems. It is designed with a focus on scalability, adaptability, and user accessibility, ensuring that it remains intuitive while offering advanced features for experienced users. The software is architected to facilitate verification through simplified analytical methods, providing a means to validate the FEA results for enhanced reliability and accuracy.

The selection of the core software that will serve as the basis of the present study is of utmost importance. The core will determine the features that the final software will contain, regarding the parametric design, the user interface, the HPC components, the ability to change the core software, as well as the real world cost of obtaining the core software. Below the core software that were considered are introduced:

Introduction to the Software considered

- **ANSYS**: A comprehensive simulation software enabling complex simulations.
- **Abaqus**: Known for advanced mechanics simulations and material modeling.
- **CalculiX**: An open-source FEA software for three-dimensional linear and nonlinear calculations.
- **FEniCS**: Another open-source computing platform for solving PDEs using finite element methods.
- **deal.II**: Open-source C++ library used for solving PDEs with finite element methods.

Comparison Criteria

- **Parametric Design:**
  - ANSYS provides robust parametric design capabilities integrated with its simulation environment.
  - Abaqus offers parametric optimization with the use of additional plugins or software.
  - CalculiX has limited parametric design features compared to commercial software.
  - FEniCS allows parametric studies through scripting but lacks a dedicated parametric design interface.
  - deal.II, while not having a built-in parametric design interface, supports parametric studies through flexible scripting and programming.
- **User Interface:**
  - ANSYS offers a user-friendly and feature-rich graphical interface.
  - Abaqus' interface is less intuitive but highly functional for experienced users.
  - CalculiX provides a basic GUI via third-party tools.
  - FEniCS primarily operates through Python scripts without a native GUI.
  - deal.II focuses on library capabilities, with no dedicated GUI, targeting developers and researchers, but provides the ParametersGUI for parameters input.
- **HPC Components:**
  - ANSYS and Abaqus both offer advanced HPC capabilities for large-scale simulations.

  - CalculiX's HPC support is growing but still behind commercial options.
  - FEniCS supports parallel computing through MPI.
  - deal.II has extensive support for HPC with adaptive mesh refinement and parallel computing.

- **Core Software Customization:**
  - ANSYS customization is possible but can be complex and requires knowledge of its scripting language, while risking breaking the total functionality of the software.
  - Abaqus allows user subroutines for customization, which is powerful but has a steep learning curve.
  - CalculiX being open-source, provides more flexibility for users to modify the core.
  - FEniCS is highly customizable via Python scripting.
  - deal.II is designed to be a flexible and customizable library, with extensive library of documentation and an enganged community, making it ideal for developers needing custom solutions.

- **Cost:**
  - ANSYS and Abaqus have significant licensing fees, which can be a barrier for small companies and individual users.
  - CalculiX and FEniCS are free and open-source, with no acquisition cost.
  - deal.II is also free and open-source, aligning with the trend towards accessible computational tools.

- **Advantages & Disadvantages:**
  - **ANSYS**
    - **+** It provides the user with a well rounded FEA package, containing comprehensive graphical interface and proven multiphysics support.
    - **-** ANSYS has significant licensing fees and while it presents with many advantages, it is also a black box, so when encountering an error that is attributed on the mathematical core, the user is not able to pinpoint its origin.
  - **Abaqus**
    - **+** It allows the manipulation of the input and output files with external software, while providing with a stable FEA core.
    - **-** Like ANSYS, Abaqus has significant licensing fees and it is also a black box, while also having a less intuitive interface comparing to ANSYS. Also, regarding the parametric design, it will require the synergy of external software for this feature.
  - **Calculix**
    - **+** It is a proven and functional open-source software.
    - **-** Although it is open-source, the mathematical core is very convoluted and it does not provide the user with parametric design or stable HPC features, also limiting the total DoFs to 1 million.
  - **FEniCS**
    - **+** It is an open-source FEA package with the advantage of the scripting language being Python and it supports parallel computing through MPI

* **-** The main disadvantage is the dependency to a great number of external libraries not written in Python, which leads to the software not being stable and it requires the user to spend quite a lot of time maintaining its basic functionality. Furthermore, it does not support natively distributed mesh and it does not provide a GUI.

– **deal.II**

* **+** It is an open-source FEA package, created by academic researchers with the purpose of providing a research tool, with many choices for parallel computing and it allows the seamless integration of a lengthy list of external libraries, while providing a rudimentary GUI and allowing the user to built the whole mathematical foundation of the problem. Additionally, it is accompanied by a great volume of tutorials and documentation, attributed to the vibrant community and forums, where its developers are active and answer any questions provided. Finally, it is coupled with the ParametersGUI, which allows the parameter manipulation.
* **-** deal.II is a C++ scripting software with all the complexity that entrails. Moreover, while it is open-source and well documented, the amount of core scripts can be daunting. Finally, it requires external software for the visualisation of the results and post-processing.

Conclusion While each software has its strengths, deal.II stands out for users who require a customizable and open-source FEA solution with strong HPC capabilities. Its lack of an extensive GUI is offset by its powerful library functions and adaptability to complex computational problems.

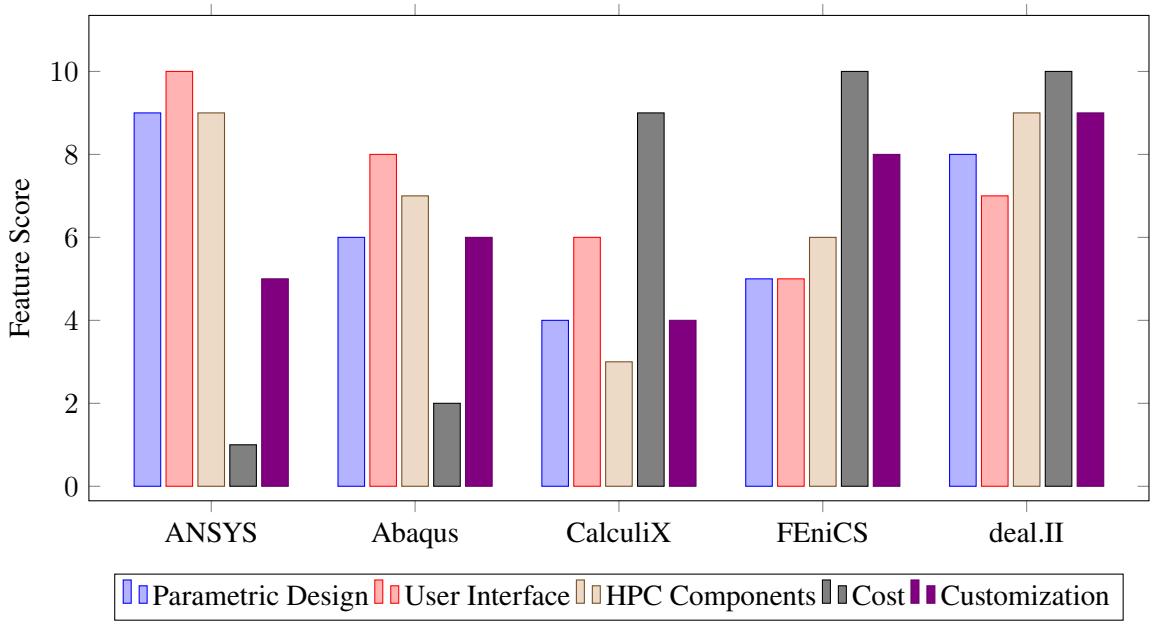

Figure 39: Comparison of FEA Core Software on Different Criteria

5.1 Systems Development Life Cycle Models considered

Software development is a structured process that involves several stages from conception to deployment and maintenance. Systems Development Life Cycle (SDLC) models provide a framework for breaking down the complexity of software creation into manageable phases, ensuring that the end product meets quality standards and user expectations. The choice of an SDLC model can significantly influence the efficiency, cost, and success of software development projects. Various models have been proposed, each with its own set of advantages and challenges, catering to different project needs. The following subsections discuss some of the prominent SDLC models considered in the industry today, including their methodology, benefits, and potential drawbacks[56].

5.1.1 V Model (Verification and Validation Model)

The V Model is a strict, sequential upgrade of the traditional waterfall model that emphasizes the early detection and correction of defects. Each development phase, such as requirements specification or design, is directly associated with a testing phase, allowing for early verification and validation. This structured approach ensures a high level of discipline and control over the project lifecycle.
Pros/Cons:
Advantages:

- Promotes early detection and correction of defects, reducing the cost and effort required for remediation later in the development cycle.
- Facilitates clear and well-defined requirements, which aids in creating a solid foundation for the development process.
- Ensures comprehensive test coverage as every phase has a corresponding testing activity.
- Supports a structured and methodical approach to software development, which can enhance the clarity and quality of the process.
- Emphasizes rigorous verification and validation, which are integral to quality assurance.

Disadvantages:

- Its highly rigid structure can make it unsuitable for projects where requirements are not clearly defined or are expected to evolve.
- Limited flexibility and adaptability can be a hindrance in accommodating changes late in the development cycle.
- Can be time-consuming and costly due to the high upfront planning and documentation required.
- May not be suitable for agile development environments that require rapid adaptation and stakeholder involvement.
- The iterative process of error detection and correction can lead to significant updates to both test and requirement documentation, increasing the workload.

[56] "Software Development Life Cycle Models-A Comparative Study," G. Gurung *et al.*

5.1.2 Spiral Model

The Spiral Model is a sophisticated software development methodology that merges the iterative nature of prototyping with the systematic aspects of the Waterfall model, making it particularly well-suited for large projects requiring significant risk management and planning. It operates in a repeating four-phase cycle: planning, risk analysis, engineering, and evaluation, allowing for continual refinement and progression.

Pros/Cons:
Advantages:

- Offers a high degree of flexibility and is adaptable to changes throughout the project lifecycle.
- Provides early development of software, which can be cost-effective in the long term.
- Enhances risk management, with each cycle focusing on the most significant risks.
- Produces a highly customized end product with strong client involvement and approval.
- Well-suited for complex and large scale projects that require thorough monitoring and documentation.

Disadvantages:

- Can be costly, particularly if there are numerous iterations without a clear endpoint.
- Requires specialized knowledge for effective risk analysis, which may not be readily available.
- May not be the best fit for smaller or less risky projects due to its complexity and documentation requirements.
- The success of the project is heavily dependent on the accuracy and effectiveness of the initial risk analysis.
- The structure of the process can be complex, demanding strict adherence to rules and protocols throughout the development.

5.1.3 Iterative Model

The Iterative Model is a cyclic software development process that allows software to evolve through repeated cycles (iterations). It involves the gradual improvement of detailed software specifications through multiple iterations, typically resulting in a new or refined version of the software at the end of each one. This model is characterized by repeated cycles of analysis, design, implementation, and testing, making it flexible and responsive to changes.

Pros/Cons:
Advantages:

- Facilitates a quick launch of the project, allowing the business to realize returns earlier.
- Reduces risks by resolving issues in each iteration before they accumulate.
- Offers the flexibility to prioritize and implement changes or new functionalities during the project lifecycle.
- Encourages regular releases and continuous advancement of the project.
- Ensures quality through feedback and repeated testing, leading to a robust software architecture.

Disadvantages:

- Lacks fixed budgeting and deadlines, which can lead to uncertainties in project timelines and costs.
- Requires strong customer involvement, which may not always be feasible or preferable.
- May encounter issues with software architecture due to the evolving nature of requirements and lack of a global plan.

This approach is particularly suitable for large projects with undefined requirements or those that are innovative in nature. However, for small projects with limited functionality, the iterative approach may be excessive and not cost-effective.

5.1.4 Agile Model

The Agile Model is a responsive, iterative, and incremental approach to software development that emphasizes flexibility, collaboration, customer feedback, and rapid delivery. It's designed to accommodate change and deliver working software quickly through a series of iterative sprints, each resulting in an increment of the final product. This methodology is structured around several key principles, including customer satisfaction through early and continuous delivery, welcoming changing requirements, frequent iteration, and maintaining a sustainable pace for the development team.

Pros/Cons:
Advantages:

- Agile methodologies allow for rapid adaptation to changing requirements, which is critical in a dynamic business environment.
- Communication with stakeholders is integral, ensuring that the software meets their needs and priorities accurately.
- It fosters continuous improvement, with lessons learned from one iteration applied to the next, improving the project incrementally.
- Agile methods emphasize direct communication, knowledge sharing, and frequent feedback, ensuring alignment with business goals and user needs;.
- The focus on delivering functional software in small increments enables quicker realization of project benefits and return on investment.

Disadvantages:

- Agile development can involve substantial planning and require constant communication, which can be time-consuming and demands a high level of management skill.
- It necessitates a team with high-level skills and exceptional communication abilities, which may increase the demand for more experienced and therefore potentially more expensive personnel.
- Agile's iterative nature can lead to scope creep, as ongoing changes may extend the project's timeline and budget.
- Documentation can sometimes be de-emphasized, which might cause issues for new team members or when maintaining and scaling the software;.
- Without careful management, iterations can become overloaded, leading to rushed deliveries and potential quality issues.

Agile is particularly effective for projects where requirements are not fully known in advance or are expected to change. It allows for a more nuanced and flexible approach to software development, with an emphasis on customer collaboration and team empowerment. However, it also requires a well-coordinated team and effective ongoing communication to manage the complexities inherent in this dynamic environment.

5.1.5 Proposed Software Development Model

The proposed Systems Development Life Cycle Model is a **hybrid of Agile and Iterative** Models. Given the relatively undefined final goal of the software, as it is expected to be refined more extensively in the future, as detailed in Section 8.2, the combination of the Agile and Iterative models will result in functional software quickly in the development, which will then gradually be refined with both software features and regarding the mathematical foundation. A visual representation of the model is presented below and regarding the actual Iterations, they will be discussed further into this section:

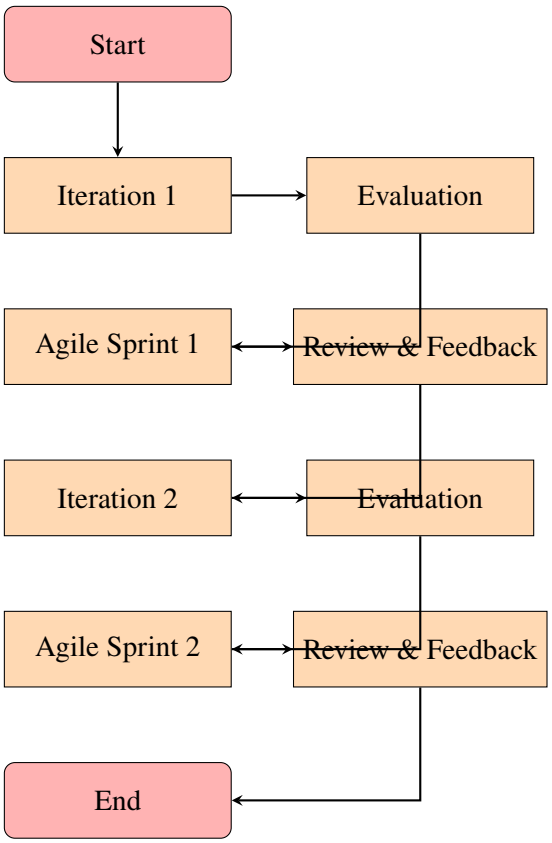

Figure 40: SDLC Model Schematic

5.1.6 Software Refinement Iterations

This proposed approach of a hybrid of Iterative and Agile Software Development Cylce Models allows for rapid and continuous improvement. Within this framework, the software refinement process for Finite Element Analysis (FEA) tool involves a series of iterative cycles, each aimed at enhancing functionality, performance, and user experience. These iterations are characterized by short development cycles, known as sprints, which enable incremental augmentation of the software's capabilities while frequently reassessing and validating the software produced. This subsection presents the specifics of each iteration, detailing the evolution of the software from its initial conception through to its current state, highlighting key developments.

The following pseudocode presents the iterations, as well as the gradual refinement of the software's capabilities:

while 1st Iteration do
Calculation of weak form of the equation, Stiffness Matrix, RHS and Stress-Strain Tensors
Simple Cylinder Body model under compression due to Neumman's Boundary condition (constant movement of *propeller side*) (static)
Conversion of Neumman Boundary to Distributed Pressure
Creation of autonomous mesh refinement
end while
while 2nd Iteration do
Integration of ParametersGUI for inputs
Introduction of Marine Diesel Engine and calculation of the appropriate thrust
end while
while 3rd Iteration do
Introduction of Gravity as a Body Force
Distributed Torque at the propeller section of the cylindrical body
end while
while 4th Iteration do
Calculation of the Mass Matrix
Preliminary Eigenvalues solver
end while
while do5th Iteration
Calculation of Damping Matrix with Rayleigh Damping
Introduction of Newmark-Beta integration Method, solving the system for the acceleration
end while
while 5th Iteration do
Parellisation of the software using MPI and ensuring distributed mesh and matrices
end while
while 6th Iteration do
Introduction of Newton-Raphson iterative solver and HHT-α algorithm
end while
while 7th Iteration do
Introduction of Bearings as Dirichlet Boundaries in the z axis
end while
while 8th Iteration do
Conversion of Bearings as springs in the Stiffness Matrix
end while
while 9th Iteration do
Creation of Bearing, Shaft and cylinder Structs for parametric number for each
Introduction of Parametric Shaft Design, including shafts with up to 5 different radii Section 5.4.1, and 4 different sets of bearings, up to 40 bearings
end while
while 10th Iteration do
Creating framework to use shaft elements as input fig. 41, refining mesh to match the inputted shaft
Creating inputs for added masses that affect the polar mass moment of inertia (Flywheel, Flanges, Cylinders, Propeller)
end while
while 11th Iteration do
Application of distributed Torque and thrust over the propeller shaft with the shaft being non-constant radius
Application of distributed torque over the cylinders and over the bearings
Creating the framework to output a visual representation of EigenModes and Case Study
end while

5.2 Software Requirements

The software is expected to perform simulations that accurately reflect the dynamics of the shafting system, as dictated by user-defined parameters. It must efficiently harness the available computational resources to deliver results expeditiously. The solver at the core of the software is required to be robust enough to achieve convergence reliably for any given set of parameters defining the shaft. Upon convergence, the software should compute and present the eigenvalues corresponding to the specific shaft configuration. The results must be rendered in a format that is not only legible and structured for ease of parsing but also conducive to seamless integration with visualization tools. This dual-format output should grant users the convenience of interpreting complex data arrays while providing a clear graphical representation of the shafting system's behavior under various simulated conditions. All these capabilities should be encapsulated within a user interface that simplifies the complex process of FEA, making it accessible even to those who may not be experts in the field.

5.2.1 Functional Requirements

Parametric Design Features
The parametric design capabilities of the software are a cornerstone of its functional requirements. These features must enable users to define and manipulate a wide array of parameters that influence the shafting system of a ship's propulsion plant. Users should be able to specify geometric dimensions, material properties, and boundary conditions which are the key variables in the shaft design. The software shall provide a flexible interface for the input of these parameters, allowing for rapid adjustments that dynamically update the model. To facilitate a robust design process, the software will also support the creation of parametric relationships between different elements of the shafting system, ensuring that changes to one parameter intelligently cascade through related features. This should include constraints and expressions that govern the behavior of the model under various loading conditions. In addition, the software must be capable of generating and displaying 3D models that accurately reflect the parametric inputs, allowing users to visually assess the changes. This interactive modeling environment is critical for engineers to iterate designs quickly, evaluate multiple scenarios, and make informed decisions about the optimization of the shafting system's performance. To cater to the needs of advanced users, the software shall also include scripting capabilities for automating repetitive tasks and enabling complex parametric studies. All these features aim to empower users with the tools necessary for a sophisticated and comprehensive design process that is both time-efficient and highly customizable to the unique requirements of marine propulsion systems.

Dynamic Simulation Capabilities
The field of Dynamic Simulation represents a cutting-edge frontier in the field of marine engineering's application of FEA. This software aims to overcome the industry's reliance on oversimplified models—models that often reduce complex mechanisms to mere torsional springs for the estimation of natural frequencies within the shafting system in torsion. In this current approach, each element of the propulsion shaft is designed and modelled in a way that it equivalent to its real counterpart in regards to its affect on the whole rotating system.
The software is engineered with the capability to perform sophisticated simulations of the rotating components within the shafting system, taking into account the myriad of external forces acting upon these elements. The dynamic simulation module is adept at computing and rendering a vivid visualization of the system's eigenvalues and the respective eigenmodes. It enables a comprehensive analysis that extends beyond mere frequency calculations, including the visualization of stress distributions across the mesh points, as well as the associated displacements.

Users will have the ability to observe and analyze the harmonic and transient responses of the shafting system, providing invaluable insights into the vibrational characteristics and potential resonance issues. Such detailed simulations are indispensable for the design of safer, more reliable, and efficient

marine propulsion systems.

User Interaction
The software is meticulously crafted to offer users a seamless and intuitive interface for accurately delineating the shafting system. It is designed to accommodate direct input of shaft elements based on specific guidelines and standards, such as those outlined in shipyard vibration manuals. For example:

Mass elements

node	m [kg]	jx [kgm²]	l_fwd [m]	l_aft [m]	c
EngDE	8160	8000			
node1	640	0			

Shaft elements

node		type	l [m]	d_inner [m]
EngDE	node17	FLANGE	0.080	0
node17	temp2	SHAFT	1.197	0
temp2	node16	SHAFT	2.400	0
node16	node15	SHAFT	0.255	0
node15	IB1	SHAFT	0.145	0
IB1	node14	SHAFT	0.145	0
node14	node13	SHAFT	0.255	0
node13	jk2	SHAFT	0.050	0
jk2	temp1	SHAFT	1.550	0
temp1	flan1_f	SHAFT	0.670	0
flan1_f	flange1	FLANGE	0.080	0
flange1	node12	FLANGE	0.100	0
node12	jk1	SHAFT	0.270	0
jk1	node11	SHAFT	0.409	0
node11	FSTB	SHAFT	0.170	0
FSTB	node10	SHAFT	0.170	0
node10	node9	SHAFT	0.081	0
node9	node8	CONE	0.385	0
node8	node7	SHAFT	1.720	0
node7	node6	CONE	0.385	0
node6	node5	SHAFT	0.152	0
node5	ASTB	SHAFT	0.660	0
ASTB	node4	SHAFT	0.330	0
node4	node3	SHAFT	0.363	0
node3	prop	CONE	0.449	0
prop	node2	CONE	0.581	0
node2	node1	SHAFT	0.170	0
node1	End	SHAFT	0.170	0

Bearing elements

node	cy_stat [N/m]	cz_stat [N/m]	cy_dyn [N/m]	cz_dyn [N/m]
mb7	4.0e+09	2.8e+09	1.5e+09	1.5e+09

Figure 41: Sample from Vibration Manual for Shaft Elements Input

Moreover, the user interface (UI) of the software is not only user-friendly and easily navigable but also customizable, catering to a wide range of user preferences and expertise levels. The software is compatible with various input methods, capable of interpreting data from straightforward text files to more complex data formats, ensuring versatility and accessibility.

5.2.2 Computational Requirements

At the core of the software's design is scalability and universality, with a preference for open-standard libraries and data structures over proprietary alternatives. It is constructed to leverage parallel computing, efficiently distributing data across processes and optimizing memory usage to prevent overlap and bottlenecks. The software is rigorously tested to ensure that it is devoid of random bugs, with the ex-

pectation that any instance of non-convergence can be traced back to user input errors, thus upholding the integrity and reliability of the simulation results.

5.3 System Architecture and Algorithmic Foundation

The architecture of the FEA software is meticulously crafted, comprising an array of high-level modules and sophisticated algorithms. Each component is meticulously designed to fulfill specific roles within the simulation process, ensuring a harmonious and efficient performance.

5.3.1 System Architecture Modules

Core Engine The nucleus of the software is the deal.II library, a powerful and open-source finite element analysis toolkit renowned for its adaptability in crafting intricate simulations. It stands out for its extensive customization capabilities, encompassing a comprehensive suite of tools for geometry definition, finite element spaces, and operations. Moreover, deal.II offers seamless interfaces with a plethora of auxiliary libraries, including the advanced linear algebra libraries PetsC and SLePC, and data output frameworks such as VTK and HDF5. The integration of deal.II provides the foundation for advanced numerical methods, tapping into a vibrant community and a wealth of documentation, thereby enhancing the software's robustness and user support.

Data Management Module The data management module is ingeniously devised to interpret XML files, transforming their contents into actionable simulation inputs. Harnessing the native capabilities of deal.II, this module takes parameter file inputs and, through sophisticated data structures, generates distinct instances for elements such as shaft components, bearings, cylinders, and additional masses. These instances are pivotal, given the parametric nature of the simulations, allowing for the specific properties of each element to be readily accessible within the FEA framework. The architecture of this module is exemplified by the following structured algorithm:

---

struct Element
std::string name;
std::string type;
double length;
double start_position;
double diameter_start;
double diameter_end; This is optional and is utilized for conical shapes.
double density, G, lambda, poissons;
;

User Interface (UI) An integral part of the software is the ParameterGUI, synergized with deal.II, which presents a user-friendly graphical interface facilitating the input of predefined parameters. This interface significantly diminishes the error margin commonly associated with text file inputs. ParameterGUI enhances user interaction by incorporating Object-Oriented Programming principles, enabling parameters to be part of classes, thus offering a structured and intuitive input experience. The following visual exemplifies the ParameterGUI in action:

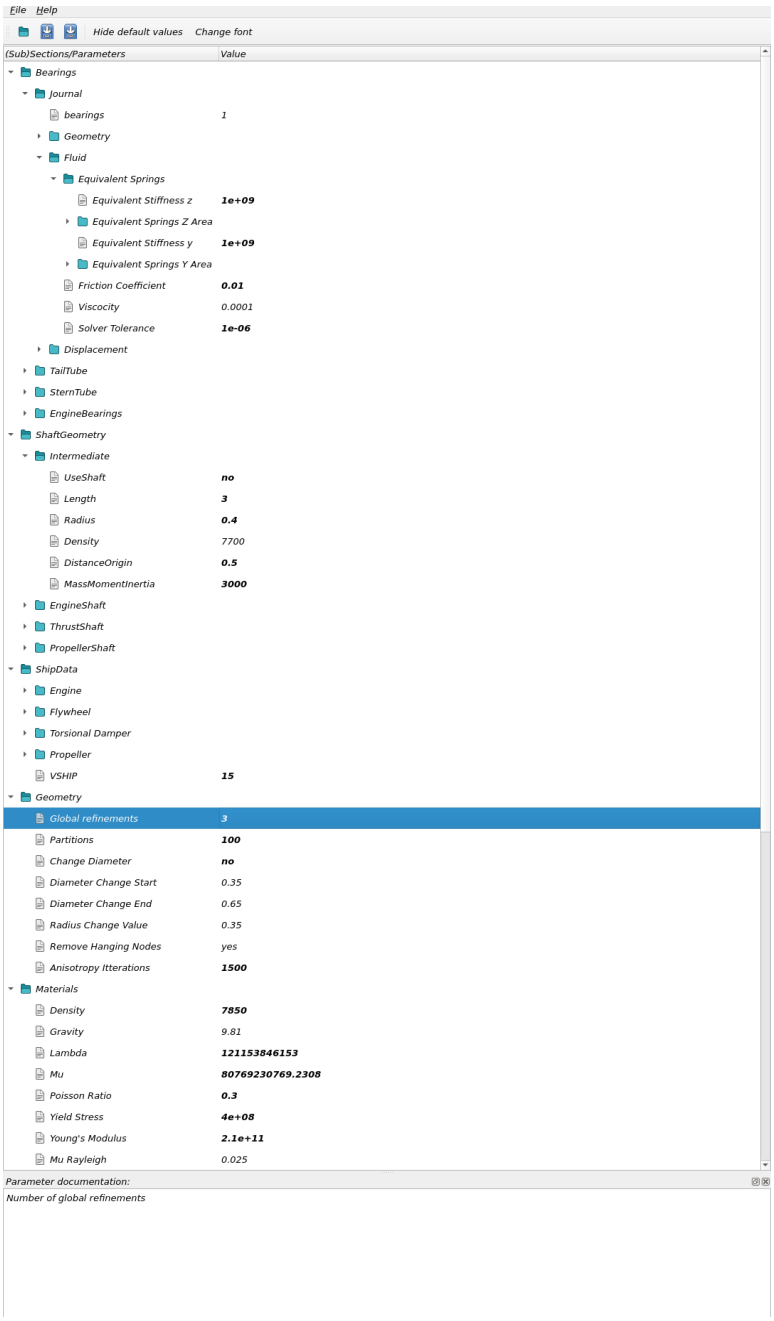

Figure 42: Sample Screenshot of the ParametersGUI

5.4 Algorithms

The algorithmic foundation of the software is rooted in the finite element method (FEM), which is enhanced by the latest advancements in numerical analysis and computational mechanics. The key algorithms include:

- Mesh Generation Algorithm
- System Setup Algorithm
- System Assembly Algorithm
- Solver Algorithm
- Eigenvalues Analysis Algorithm
- Stress-Strain Computation Algorithm
- Dynamic Analysis Algorithms
- Parameter Parsing Algorithm
- Data Parsing and Visualization Algorithms
- Parallel Processing and High-Performance Computing Algorithms

The Libraries used are:

- deal.II for the framework and core of the software
- PetsC and MPI for the parallel components of the software
- PetsC and SlepC for the solvers and preconditioners used
- HDF5 to create an easily and rapidly parsable output file, and the accompanying h5py for reading the output with Python
- Python with matplotlib for the post-processing script
- VTK to create an output file to be used in ParaView for the purposes of visualization

5.4.1 Mesh Generation Algorithm

The deal.II library provides with several algorithms to generate simple geometrical shaped meshes, such as a hyperball, a parallelogram hexahedron, pipe and cylinder, which will be used in this present software. The provided function uses as inputs the length, radius of the cylinder and the number of subdivisions that will be created on the length axis.
The resulting cylinder consists of regular mesh cells and constant radius in all of its length, which is not proper for the simulation of the shafting system that consists of several cylinders with different radii. This is remedied with the manipulation of the quadrature points so that the outer radius equals the appropriate radius derived from either the ParameteGUI or an input file like the one portrayed in fig. 41. This algorithm is described below:

Calculate the nodes to correspond to the given shaft like in fig. 41

for i in Nodes-1 **do**

$x_1 = x$ coordinate of $node[i]$

$x_2 = x$ coordinate of $node[i+1]$

$R_1 = z$ coordinate of $node[i]$

$R_2 = z$ coordinate of $node[i+1]$

for q in Quadrature Points **do**

if $x(q) \in [x_1, x_2]$ && q point is untouched **then**

move point to: $\frac{R_1 + \frac{x-x_1}{x_2-x_1} \cdot (R_2 - R_1))}{\text{original radius of cylinder}}$ · original radius of point

end if

end for

end for

The mesh generation algorithm also includes the distribution of the mesh to the appropriate parallel process. The *partitioning* of the mesh in this software is done manually, subdividing the cylindrical body into a number of regions equal to the number of parallel processes, with each region constituting the mesh from $x_i \rightarrow x_{i+1}$, where $x_i = n_{process} * \delta x$ and $\delta x = L/N_{processes}$.

The mesh generation algorithm also has the responsibility to assign the appropriate boundary ID to all the faces in the mesh. This boundary ID allows the user to apply boundary conditions or boundary forces to a specific set of faces. This is especially useful given the plethora of different boundary forces and conditions exerted onto the shafting system. The boundary IDs used in this software are described below:

- **Boundary ID 0: Engine End**, the circular section of the cylindrical body that has the *x coordinate* equal to the length of the shafting system and is constraint in all 3 dimensions
- **Boundary ID 1: Propeller End** the circular section of the cylindrical body that has the *x coordinate* equal to 0. When the length and position of the propeller is not given as an input, the total torque and thrust produced by the propeller is exerted in this area.
- **Shafts** this provides the user with the ability to create 4 different shafts with different properties:
  - **Boundary ID 2: Intermediate Shaft** all the faces on the perimeter of the cylindrical body not belonging to boundary IDs 0 & 1.

  - **Boundary ID 3: Thrust Shaft** the faces on the perimeter of the cylindrical body from $x^0_{thrustshaft}$ to $x^{final}_{thrustshaft}$
  - **Boundary ID 4: Engine Shaft** the faces on the perimeter of the cylindrical body from $x^0_{engineshaft}$ to $x^{final}_{engineshaft}$
  - **Boundary ID 5: Propeller Shaft** the faces on the perimeter of the cylindrical body from $x^0_{propellershaft}$ to $x^{final}_{propellershaft}$

- **Boundary ID 6: Propeller** all the faces on the perimeter of the cylindrical body from $x^0_{propeller}$ to $x^{final}_{propeller}$, where a uniform pressure simulating the propeller torque and a uniform pressure simulating the thrust is applied

- **Boundary ID 60: Torsional Damper** all the faces of the cylindrical body from x^0_{damper} to the end of the shaft, where the Lame's constants change in accordance to the inputs.

- **Boundary IDs 61,62:ME Flanges** the first ME Flange is also considered as the thrust bearing and in this study the the faces on the perimeter are constraint using Dirichlet boundary conditions on the x axis, allowing torsion, as in reality, although this simplification does not allow the axial vibrations to be calculated accurately.

- **Boundary IDs 7 to 46: Bearings** all the faces on the perimeter of the cylindrical body belonging to the bearing, where each category of bearings is assumed to have the same characteristics and be at a defined distance from each other, constant over the category of bearings

  - **Boundary IDs 7 to 16: Intermediate Bearings**
  - **Boundary IDs 17 to 26: Tailtube Bearings**
  - **Boundary IDs 27 to 36: Sterntube Bearings**
  - **Boundary IDs 37 to 46: Engine/Main Bearings**

- **Boundary IDs 70 to number of Cylinders: Cylinders on the Crankshaft**

A visual representation of the shaft with the boundary IDs is shown below:

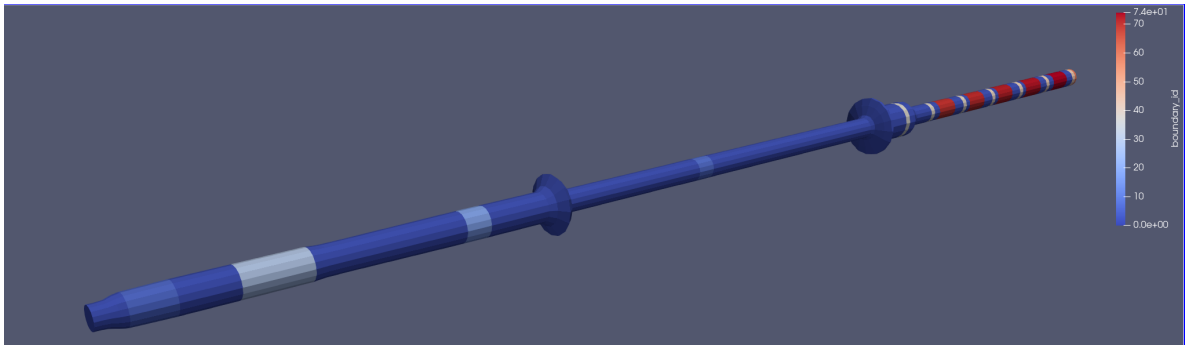

Figure 43: Boundary IDs Visual Representation

5.4.2 System Setup Algorithm

The system setup algorithm is a critical component of the software, designed to initialize and prepare the matrices for the execution of FEA tasks. This algorithm follows a series of steps to ensure that the model is accurately constructed and the boundary conditions are correctly applied.

Initialization
The algorithm begins by initializing the system matrices in and distributes them to the appropriate parallel processes. For the system vectors, this is straightforward, as each value of the vector acts on a specific degree of freedom, whereas regarding the system matrices, a value acts on 2 degrees of freedom, that might not belong to the same parallel process. This issue is resolved distributing the matrix based on the relevant DoFs, not only the ones owned by the parallel process.

Applying Dirichlet Constraints In deal.II, the application of Dirichlet constraints, which are essential for specifying known values of a function on the boundary of the domain (often referred to as boundary conditions), is an integral aspect of setting up a finite element analysis. This is managed by the AffineConstraints class, which is designed to handle constraints that can be expressed in the form of linear relations between degrees of freedom. When applying Dirichlet boundary conditions, this class allows for the specification of exact values at the nodal points on the boundary of the mesh. During the system assembly process, the AffineConstraints object is used to modify the global system matrix and the right-hand side vector to ensure that the solution satisfies the prescribed values at the Dirichlet boundaries. This modification involves adjusting the corresponding rows in the system matrix to zero out off-diagonal entries and setting the diagonal entry to one, while the right-hand side vector is adjusted to reflect the known value at the constraint. By doing so, deal.II ensures that the finite element solution honors the boundary conditions at the discrete level, which is pivotal for the accuracy and stability of the simulation results.

5.4.3 System Assembly Algorithm

In deal.II, the assembly of system matrices is a critical step in the finite element analysis process, where the local contributions of each element are integrated into a global system that represents the entire computational domain. The assembly process is orchestrated by traversing through all the cells (elements) in the mesh and calculating their local stiffness matrices and force vectors based on the governing equations of the physical problem being solved, material properties, and the chosen finite element discretization.

During this process, a local-to-global mapping is employed to ensure that the contributions of each element are accurately placed in the corresponding locations of the global matrix and vector. This is done using the DoFHandler object, which keeps track of the degrees of freedom associated with each element and the entire mesh. As the algorithm iterates over the mesh, it invokes the FEValues class to evaluate the necessary shape functions and their derivatives at quadrature points within each cell, which are then used to compute the local matrices and vectors.

Once the local contributions are computed, they are distributed into the global system matrix and right-hand side vector using the distribute_local_to_global function. This function takes into account the connectivity of the nodes and ensures that the assembly process respects the continuity of the solution across element boundaries. The assembly algorithm also incorporates any necessary boundary conditions or constraints at this stage, adjusting the global matrix and vector as required to accommodate them.

Initialize system matrix A and right-hand side vector b to zero

Create a DoFHandler object associating degrees of freedom with mesh cells

Initialize FEValues object to access shape functions and their derivatives

for each cell in DoFHandler **do**

    Initialize local matrix A_{local} and vector b_{local} to zero

    Apply quadrature formula to integrate over the cell

    for each quadrature point in the cell **do**

        Evaluate shape functions and their derivatives

        Compute local matrix and vector contributions

    end for

    Map local contributions to global matrix and vector

    Apply constraints, such as Dirichlet boundary conditions

    Distribute local contributions to global system A and b

end for

Apply final constraints and close system matrix A and vector b

---

5.4.4 Solver & EigenValues Analysis

In deal.II, solving the linear system that arises from the finite element discretization of a partial differential equation is a pivotal stage of the simulation process. The framework provides a variety of solver classes that can be employed to address this task. The choice of a specific solver and preconditioner is often governed by the nature of the system matrix: whether it is sparse or dense, symmetric or non-symmetric, and well- or ill-conditioned.

Once the system matrix and right-hand side vector are assembled, the solver is tasked with finding the vector of unknowns that satisfies the equation Ax=b. The deal.II library integrates with state-of-the-art linear algebra solvers like PETSc and Trilinos, which offer a range of iterative methods such as Conjugate Gradients or GMRES, known for their efficiency in handling large, sparse systems. For these iterative methods, selecting an appropriate preconditioner is crucial for improving convergence rates and reducing computational efforts.

The solving process is encapsulated within a try-catch block to handle any exceptions that may arise during the computation, ensuring that the software can provide informative feedback on solver performance or potential issues. Upon successful completion, the solver yields the solution vector, which represents the distribution of the field of interest (displacement or acceleration) across the domain. This vector is then often post-processed to extract meaningful physical quantities and visualize the results for interpretation and analysis.

Define system matrix A, right-hand side vector b, and solution vector x

Choose appropriate linear solver and preconditioner

Initialize solver control with tolerance and maximum iteration parameters

Create solver object with solver control

Set up the solver (e.g., CG or GMRES)

Set up the preconditioner (e.g., Jacobi, SSOR, AMG)

Attempt to solve the linear system $Ax = b$

if solution converges **then**

    Output the solution vector x

else

    Report convergence failure

end if

Handle exceptions and provide diagnostic information

Linear Solver
The solver used in this particular problem is the Conjugate Gradient provided by the PetsC library and the chosen preconditioner is the Block Jacobi.

In deal.II, the Conjugate Gradient (CG) solver is a popular choice for solving large, symmetric, and positive-definite linear systems that frequently arise in finite element analyses. The CG solver is particularly favored for its efficiency and scalability when dealing with sparse matrices, making it well-suited for problems in structural mechanics, fluid dynamics, and other areas of computational physics.

The effectiveness of the CG solver is often significantly enhanced when coupled with a suitable preconditioner, such as the Block Jacobi preconditioner. The Block Jacobi preconditioner is an iterative

method that accelerates convergence by solving smaller block-diagonal systems derived from the main system matrix. Each block corresponds to a subset of the equations and is solved independently, which is particularly advantageous in parallel computing environments. This preconditioner is adept at dealing with matrices that exhibit block structures, often encountered in problems where the domain is decomposed into subdomains, such as in multi-material simulations or domain decomposition methods.

The combination of the CG solver with the Block Jacobi preconditioner in deal.II thus provides a powerful tool for efficiently tackling complex linear systems, reducing computational time while maintaining accuracy.

Eigenvalues Analysis
Given a mechanical system governed by the equation of motion $M\ddot{u} + Ku = 0$, where M is the mass matrix, $\ddot{u}$ is the acceleration vector, K is the stiffness matrix, and u is the displacement vector, an eigenvalue analysis can reveal the system's natural frequencies and mode shapes.

The analysis proceeds by assuming a harmonic solution of the form $u(t) = \phi e^{i\omega t}$, leading to the eigenvalue problem $(K - \omega^2 M)\phi = 0$. Here, ω represents the angular frequency and ϕ the mode shape of the system. The eigenvalues $\lambda = \omega^2$ and eigenvectors ϕ correspond to the square of the natural frequencies and the displacement patterns at these frequencies, respectively.

To solve this eigenvalue problem computationally, the SLEPc library is employed, which is designed for the efficient solution of large scale sparse eigenvalue problems. The integration of SLEPc with deal.II facilitates the handling of complex finite element discretized systems. A typical workflow using SLEPc in deal.II is as follows:

1. Define the mass and stiffness matrices M and K within the deal.II environment, as shown above.
2. Initialize the SLEPc solver, configuring the appropriate solver type and parameters for the problem at hand.
3. Invoke the SLEPc routines to solve the eigenvalue problem, obtaining the eigenvalues λ and eigenvectors ϕ.
4. Output and Post-process the results to interpret the natural frequencies and mode shapes, which are critical for understanding the dynamic response of the system.

5.4.5 Parameter Parsing

The foundation of a parametric and dynamic simulation software lies in its ability to accurately interpret and process user input. To achieve this, a robust input and parsing algorithm is implemented, serving as the inteface between the user's requirements and the software's core functionality. This algorithm is designed to handle inputs both from the ParametersGUI, as well as text files describing the shaft geometry and material properties, validate the data against predefined criteria, and translate the input into a structured format that the simulation engine can utilize. The versatility of the input mechanism accommodates both novice users, through a guided graphical interface, and advanced users, through direct file manipulation. This subsection outlines the algorithmic approach employed to ensure that the parameter input and parsing process is only efficient, reliable and user-friendly.

The structure of the Parameter Parsing Algorithm follows the structure of the ParametersGUI file. The structure is divided into classes or sections of Parameters that can facilitate standalone parameters, as well as other sections. Each Parameter is considered a structure with the following members:

---

struct Parameter
std::string Parameter Name;
std::string Parameter Documentation;
value This can be double, integer, Boolean or string;
int pattern number ;This is an integer for the ParametersGUI xml file and a function for the algorithm (ie *get_bool*).
;

The structure of the Parameters Input File is the following:

- Bearings
  - Journal
    - Number of Bearings
    - Geometry
      - Bearing Distance from Origin Point (zero in the x coordinate)
      - Length
      - Radius of the Bearing (not utilised currently)
      - Distance from each other
      - Bearing Eccentricity (not utilised currently)
      - Maximum Eccentricity angle (not utilised currently)
    - Fluid
      - Equivalent Springs (separate inputs for z and y springs)
      - Equivalent Stiffness
      - Spring Area of effect
      - Distance from the first point of the bearing (x axis)
      - Distance from the last point of the bearing (x axis)
      - Distance from the center right (y axis)
      - Distance from the center left (y axis)
      - Distance from the Bottom minimum (z axis)
      - Distance from the Bottom maximum (z axis)
      - Friction in percentage of Total Torque
      - Viscocity (not utilised currently)
      - Solver Tolerance for Reynolds (not utilised currently)

        - Bearing Displacement
            - bearing ID for which the displacement is defined (up to 2 displacements for each bearing category)
            - Displacement value in m
            - Direction of Displacement (1 for x, 2 for y, 3 for z)
            - Displacement Endtime
    - Taitube (with subsections the same as journal)
    - Sterntube (with subsections the same as journal)
    - EngineBearings (with subsections the same as journal)
- ShaftGeometry
    - Intermediate Shaft
        - UseShaft Boolean
        - Length
        - Radius
        - Density
        - Distance from Origin
        - Mass Moment of Inertia (optional if Radius>0)
    - Engine Shaft
    - Thrust Shaft
    - Propeller
- Ship Data
    - Engine
        - Use Separate Cylinders Boolean
        - MCR
        - RPM
        - RPM^{MCR}
        - Total Mass Moment of Intertia (Optional)
        - Total Torsional Stiffness (Optional)
        - Cylinders
        - Cylinder Rotating Mass
        - Cylinder Density
        - Cylinder Length

    - Cylinder distance from each other
    - Cylinder Distance from Origin
    - Cylinder Mass Moment of inertia
    - Cylinder Torsional Stiffness
    - Use ME Flanges boolean
    - ME Flanges Mass
    - ME Flanges Mass Moment of Inertia

- Flywheel
    - UseFlywheel Boolean
    - Flywheel Mass
    - Flywheel Mass Moment of Inertia
    - Flywheel Radius
    - Flywheel Density
    - Flywheel Length
    - Flywheel Distance from Origin

- Torsional Damper
    - UseTorsionalDamper Boolean
    - Torsional Damper Mass
    - Torsional Damper Mass Moment of Inertia
    - Torsional Damper Stiffness
    - Torsional Damper Damping
    - Torsional Damper Length
    - Torsional Damper Distance from Origin

- Propeller
    - UsePropeller Boolean
    - Propeller Weight
    - Propeller Length
    - Propeller Mass Moment of Inertia
    - Propeller distance for Origin

- Velocity of the Ship in knots

- Geometry
  - Global Refinement Cycles (Final Cell Count = Original Cell Count$^{\text{Global Refinement Cycles}}$
  - Partitions (Subdivisions in the length of the shaft)
  - Change Diameter Boolean
  - Diameter Diameter Change Start x coordinate
  - Diameter Diameter Change End x coordinate
  - Radius Final
  - Remove Hanging Nodes Boolean (ensures smooth mesh with isotropical cells)
  - Anisotropy Iterations (Cycles of Removal of hanging Nodes)
- Materials
  - Density (used if now other density is provided)
  - Gravity coefficient (gravity acceleration)
  - Lame's Lambda
  - Lame's Mu
  - Poisson Ratio
  - Yield Stress (not utilised currently)
  - Young's Modulus
  - Rayleigh Mu
  - Rayleigh Lambda
- Solver
  - Maximum Iterations per Timestep
  - Number of Refinement Cycles with Kelly Error Estimator
  - Solver Tolerance
  - Newton Method Tolerance
  - Maximum Iterations of Newton Method
  - HHT-α absolute value
  - Eigenvalues Calculation Boolean
  - Eigenvalues Number
  - Eigenvalue Problem Solver [Lanczos, KrylovSchur, Arnoldi, Generalized Davidson, jacobi Davidson]
  - Eigenvalue Problem Preconditioner [BlockJacobi, jacobi,Boomer]

  - path for postprocessing script
  - Newmark-Beta β value
  - Newmark-Beta γ value
  - Dynamic Problem Boolean
  - Output Folder
  - UseReynolds Boolean (not utilised currently)
  - Use Newton-Raphson Method Boolean
  - Use Input File for Elements Boolean
  - Path for Elements Input File

- Time
  - EndTime
  - Timestep δt

The Parameters parsing algorithm reads the parameters XML file and assigns the parameter values accordingly. It is worth mentioning that the if the added masses are used (Flywheel, ME Flanges, Propeller), but not density or radius is provided in the input file, then the algorithm calculates a density value required for the equivalent cylinder to have the same polar mass moment of inertia and a different density value required for the weight added to the rigth hand side vector.

5.4.6 Data Parsing and Visualization Algorithm

In deal.II, data parsing and visualization are crucial steps that transform raw simulation output into comprehensible and actionable information. Data parsing involves interpreting the output data from the simulation, which includes parsing solution vectors and derived quantities into a format that can be readily processed for visualization or further analysis. deal.II provides robust tools and interfaces to facilitate this process, such as the DataOut class, which serves as a bridge between the raw data and various output formats suitable for visualization software.

For visualization, deal.II can export data into formats compatible with high-end visualization software like ParaView or VisIt. These tools can read the exported data files, enabling the user to visualize and interact with the simulation results in 3D. For example, users can inspect the deformation, stress distribution, or temperature gradient within a simulated material. The graphical representation is not just for aesthetic appeal; it provides insights into the physical phenomena under investigation, such as identifying regions of high stress or visualizing the mode shapes from an eigenvalue analysis.

In this software parses through the data and outputs the following values:

- Von Mises stress
- Maximum Stress encountered within the cell
- Norm of Stress
- Deformation per timestep and total in each dimension
- δ of velocity and acceleration from the constant rotational velocity rotation
- The parallel process to which the cell belongs and
- the Eigenmodes normalized to 1

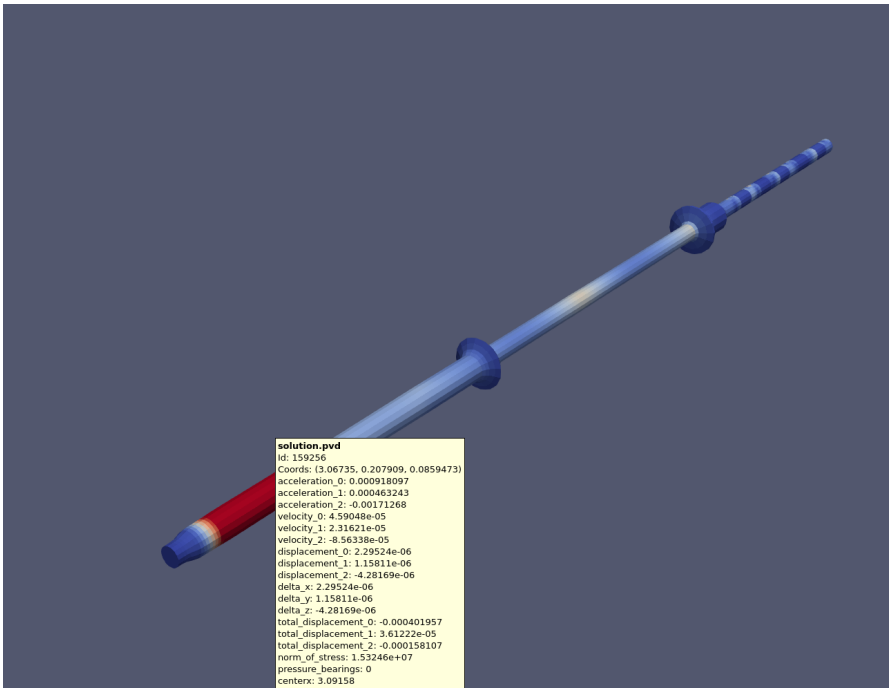

Figure 44: Visualization Sample from ParaView

5.4.7 High-Performance Computing in Finite Element Analysis using deal.II

High-Performance Computing (HPC) has become a cornerstone in conducting large-scale Finite Element Analysis (FEA), enabling researchers and engineers to solve complex physical phenomena with unprecedented precision and speed. The deal.II software library[57], with its recent extensions for distributed computing, presents an advanced ecosystem for conducting FEA within a massively parallel computing environment.

Challenges in Parallel FEA
One of the primary challenges in parallel FEA is the management of adaptive meshes across multiple processors. As simulations become more detailed and meshes become finer, the computational load must be distributed efficiently to prevent bottlenecks and ensure scalability. Furthermore, maintaining data consistency and minimizing global communication are critical to achieving high performance on large computing clusters.
Data Distribution
The cornerstone of parallel FEA is the ability to distribute the data associated with the mesh, boundary conditions, and material properties across multiple processors. Ensuring that each processor has the necessary data to perform its computations without excessive duplication is key. deal.II handles this by integrating with p4est, which provides a distributed mesh framework. However, maintaining a balance between data locality and the minimization of inter-processor data transfer is an ongoing challenge.

Computational Load Balancing
Distributing the computational workload equitably among processors is crucial to optimize resource utilization and prevent performance degradation. The adaptive nature of FEA meshes, where elements are refined or coarsened based on error estimates, can lead to uneven work distribution. Dynamic load balancing algorithms are required to redistribute the workload as the simulation progresses and the mesh evolves.

Inter-Process Communication
Parallel FEA involves a significant amount of communication between processors, especially during the assembly of the global system matrix and the application of boundary conditions. Minimizing these communications to avoid latency is essential, as excessive communication can negate the benefits of parallelization. deal.II minimizes global communication by localizing as much of the computation as possible and using efficient algorithms for the necessary global operations.

Consistency and Synchronization
Maintaining consistency across distributed data structures is another challenge. As the mesh is refined and the solution progresses, ensuring that all processors have a consistent view of the global mesh and solution state is non-trivial. This requires synchronization mechanisms that can quickly become a performance bottleneck if not handled optimally.

Scalable Algorithms and Data Structures
Developing algorithms and data structures that scale with the number of processors is fundamental to successful parallel FEA. deal.II's algorithms are designed to scale linearly with the problem size, but achieving this in practice requires careful implementation and testing. The scalability of preconditioners and solvers, in particular, is critical for large-scale simulations.

Heterogeneous Computing Environments
Modern HPC clusters are increasingly heterogeneous, combining traditional CPUs with accelerators like GPUs. This heterogeneity introduces additional complexity in the parallelization of FEA, as dif-

[57] "Algorithms and data structures for massively parallel generic adaptive finite element codes," W. Bangerth *et al.*

ferent parts of the computation may be optimized for different types of hardware. deal.II's architecture must therefore be flexible enough to accommodate these different computing paradigms.

Addressing these challenges is essential for the effective use of HPC in FEA. The deal.II library's approach to parallelization serves as a model for how to manage these complexities, providing a platform that can be extended and optimized as computational resources and algorithms evolve.

Scalable Linear Algebra

The assembly and solution of linear systems are key operations in FEA. deal.II leverages state-of-the-art linear algebra packages like PETSc and Trilinos to handle these operations in parallel. It employs a scalable approach to create sparsity patterns and distribute the workload during the assembly phase. For the solution phase, it interfaces with solver packages to utilize advanced preconditioning and iterative methods that are optimized for HPC environments.

Efficient Postprocessing

After solving the linear systems, postprocessing steps such as mesh refinement and error estimation are crucial for the validation and enhancement of simulation accuracy. deal.II facilitates these operations in a distributed manner, ensuring that the refinement process does not become a bottleneck in the simulation pipeline.

Numerical Results and Scalability

Numerical experiments conducted with deal.II demonstrate the linear scalability of the library's parallel operations. The tests, which include solving the Laplace equation and thermal convection simulations, show that both the setup and solve phases can scale effectively with the number of processors and degrees of freedom, as long as the problem size is sufficiently large.

6 Validation Against Analytical Solutions

The validation of Finite Element Analysis (FEA) software against analytical solutions is an indispensable step in the verification process, serving as a benchmark for ensuring the software's accuracy and reliability. Analytical solutions, derived from exact mathematical formulations, provide a ground truth against which the numerical approximations of the FEA can be compared. This comparison is crucial because it helps to identify any discrepancies that may arise from numerical methods, discretization errors, or implementation issues within the software. Validation with analytical solutions not only instills confidence in the software's capability to produce precise results but also helps in calibrating the FEA models for improved fidelity. It is particularly important in scenarios where the FEA software will be used to make critical decisions in design, analysis, and safety evaluations of engineering systems. Without such rigorous validation, the risk of errors in simulation results could lead to suboptimal designs, increased costs, or even catastrophic failures in engineering applications. Therefore, validation acts as a quality assurance measure, ensuring that the FEA software adheres to the highest standards of computational accuracy and is capable of delivering reliable insights for engineering challenges.

The validation of the FEA software developed took place for a cylindrical cantilever beam for four different conditions: compression, torsion, bending, and the Eigenvalues calculated with Euler Beam Theory and with Timoshenko's beam theory. The cylinder, as well as the engine characteristics, used as inputs are the following:

E $\{N/m^2\}$	2.10E+11
$\nu\{-\}$	0.3
G=$\mu_{\text{Lame's}}\{N/m^2\}$	8.08E+10
$\lambda_{\text{Lame's}}\{N/m^2\}$	1.21E+11
Diameter{m}	0.4
Length{m}	3
Power of Engine {kW}	6350
Vessel's Speed{kn}	15
Rotations per Minute{RPM}	99
Axial Force{N}	855894
Torsional Torque {Nm}	612505
Weight of Propeller(force perpendicular to the axis of the beam) {N}	411447

Table 6.1: Validation Model Parameters

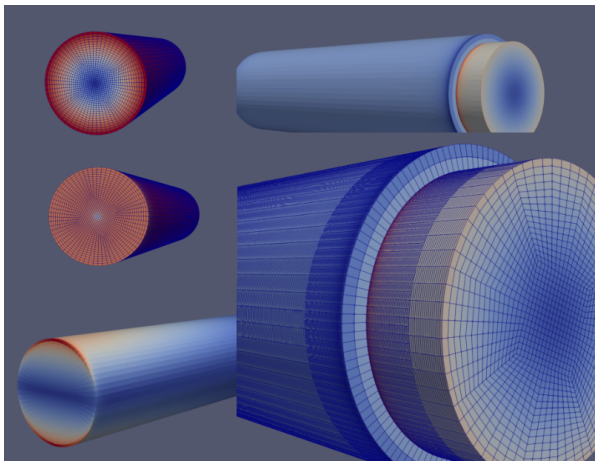

Figure 45: Validation Cases, Torsion, Bending, Combined Torsion and Compression for Cylinder with Varying Radius

6.1 Compression

The software was tested for its ability to simulate the compression of a cylindrical column. The analytical solution for axial compression was used as the benchmark, derived from the material's constitutive relationships under uniform compressive loads. The FEA software needed to demonstrate its proficiency in predicting the correct axial stress distribution and deformation under such loading scenarios.

For a column in compression, the stress is given by:

$$\sigma = \frac{P}{A}, \tag{6.1}$$

where σ is the axial stress, P is the axial load, and A is the cross-sectional area.
The maximum stress in a column under axial compression is simply the applied axial load P divided by the cross-sectional area A, assuming uniform stress distribution:

$$\sigma_{\text{max}} = \frac{P}{A}. \tag{6.2}$$

The deformation, assuming a linear elastic material and that buckling does not occur, is given by:

$$\delta_{\text{max}} = \frac{PL}{AE}, \tag{6.3}$$

where L is the length of the column, and E is the Young's modulus of the material.

	Analytic Calculation		**deal.II Calculation**		**% Deviation**	
Force Applied	**Stress**	**Deformation**	**Stress**	**Deformation**	**Stress**	**Deformation**
822894 N	1.64E+06 Pa	2.34E-05 m	1.64E+06 Pa	2.34E-05 m	0.38%	0.07%

Table 6.2: Compression Comparison

The expected behavior in compression is for the stress to be uniform and equal to the maximum in the whole mesh. The displacement is maximum at the face where the force is applied and is linearly reduced to zero over the length of the cylinder, as shown below:

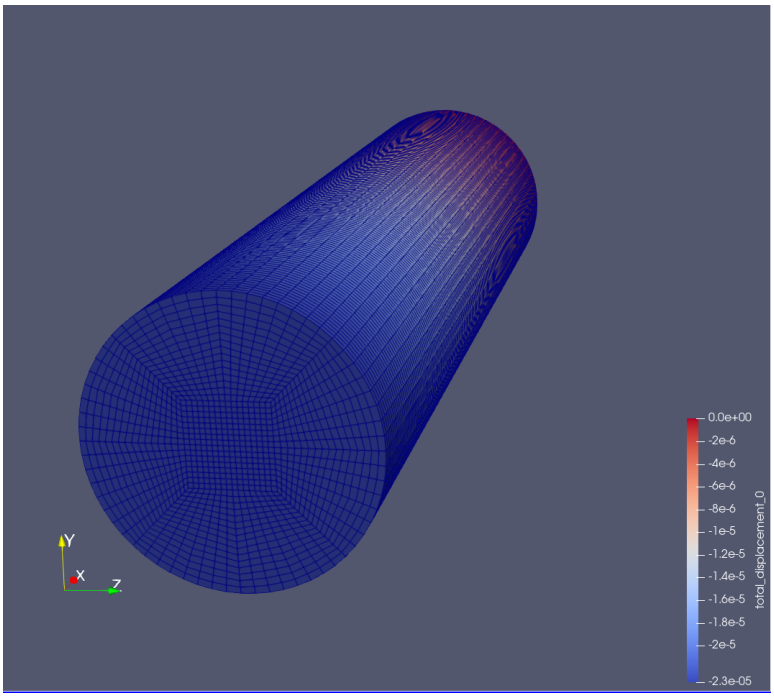

Figure 46: Compression Displacement

6.2 Torsion

The torsional behavior of a cylindrical shaft was analyzed, with the FEA software's results compared to the analytical solution given by the classical torsion theory. This theory predicts the stress distribution and angular displacement in a shaft subjected to a twisting moment, assuming a linear elastic material and pure torsion. The validation focused on ensuring that the software correctly calculates the shear stress and angle of twist, which are directly related to the eigenvalues representing the torsional rigidity of the cylinder.

The analytical solution for the torsion of a cylindrical shaft is given by:

$$\tau(r) = \frac{T}{J}r, \tag{6.4}$$

where τ is the shear stress, r is the radial distance from the center, T is the applied torque, and J is the polar moment of inertia of the cross-section.
For a cylindrical shaft subjected to torsion, the maximum shear stress occurs at the surface of the shaft and is given by:

$$\tau_{\text{max}} = \frac{T}{J}r_{\text{out}}, \tag{6.5}$$

where r_{out} is the outer radius of the shaft. The maximum angle of twist, θ_{max}, for a shaft of length L is:

$$\theta_{\text{max}} = \frac{TL}{GJ}, \tag{6.6}$$

where G is the shear modulus of the material.

	Analytic Calculation		**deal.II Calculation**		**% Difference**	
Torque Applied	**Stress**	**Deformation**	**Stress**	**Deformation**	**Stress**	**Deformation**
612505 Nm	6.09E+06 Pa	5.66E-04^o	6.10E+06 Pa	5.66E-04^o	0.12%	0.01%

Table 6.3: Torsion Comparison

The expected behavior of the stress and deformation are quite similar, minimum at the center of the circular section and maximum at the radius. The torque applied is translated into a uniformly distributed pressure vectors perpendicular to the radius of each point. This results into the cell that is located into the center of the section to have a Von Misses stress smaller than the rest of the section, as the displayed stress is calculated per cell, where inside of this cell the stresses at points negate each other.

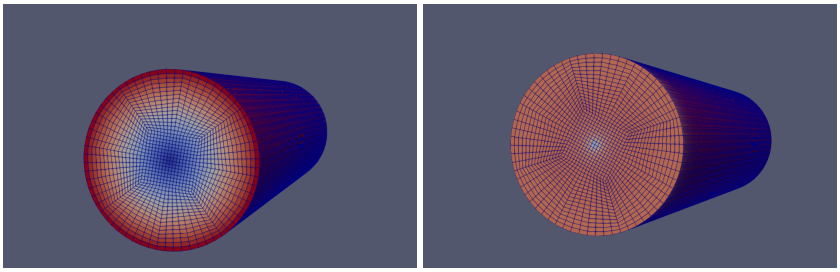

Figure 47: Torsion Contraint Side & Torque Application Side

6.3 Bending

Bending analysis was performed on a cylindrical beam to validate the software against the analytical bending solution. The comparison was based on Euler-Bernoulli beam theory, which describes the relationship between the bending moment and the curvature of the beam. The software's accuracy was evaluated by comparing the calculated deflection and bending stresses with those predicted by the theory for various loading conditions.

The bending of a beam under a uniform load is described by the elastic line equation:

$$\frac{d^2}{dx^2}\left(EI\frac{d^2u}{dx^2}\right) = q, \tag{6.7}$$

where E is the Young's modulus, I is the moment of inertia of the beam's cross-section, u is the deflection, and q is the distributed load.
The maximum deflection y_{max} of a simply supported beam with a uniformly distributed load of total F the applied force is given by:

$$z_{\text{max}} = \frac{FL^3}{3EI}, \tag{6.8}$$

and the maximum bending stress is at the outermost fiber of the beam and can be calculated as:

$$\sigma_{\text{max}} = \frac{FLR_{\text{out}}}{I} \tag{6.9}$$

	Analytic Calculation		deal.II Calculation		% Deviation	
Force Applied	**Stress**	**Deformation**	**Stress**	**Deformation**	**Stress**	**Deformation**
411447 N	2.46E+07 Pa	8.77E-04 m	2.50E+07 Pa	8.83E-04 m	1.81%	0.69%

Table 6.4: Bending Comparison

The expected behavior of the cantilever beam in bending is that the maximum stress is located at the top and at the bottom of the constraint side of the cylinder, as shown below. The maximum stress, according to the analytical solution, should be equal both the bottom and top, but in this test case the bending force is always perpendicular to the original xy plane, so when the section is deformed, the top is extended more in relation to the compression of the bottom.

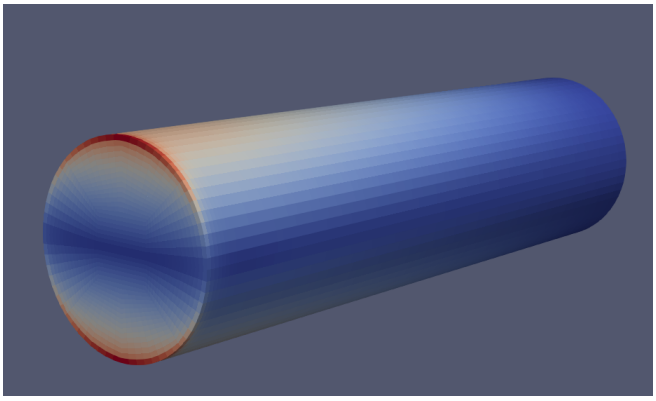

Figure 48: Bending Constraint Side

6.4 Change of Radius in combined Torsion and Compression

This test case is performed in order to verify the ability of the software to handle the change of radius in the length of the cylindrical body, which is commonly encountered in the shafting system, for instance, in the transition from the intermediate shaft to the propeller shaft using a flange. The anticipated behavior of the maximum stress, in a sufficient distance from the point of changing radius, where there is a concentration of stress, equals the anticipated stress in a cylindrical body of constant radius subjected to the same loading conditions.

The main challenge is the convergence of the system if the change in radius is not gradual and there is no chamfer or fillet. This is addressed by instead of the change being instant, a chamfer is used, with a length equal to the length of a cell. When using appropriately refined mesh, the angle is close to 90 degrees, which avoids non-linearities without impacting the solution significantly, especially away from the changing radius area, ensuring the convergence of the system.

		Stress		
Force Applied	**Torque Applied**	**Analytic Calculation**	**deal.II**	% Difference
411447 N	612505 Nm	1,22E+07 Pa	1,21E+07 Pa	-0,71%

Table 6.5: Torsion & Compression with Radius change Comparison

The solution of this test case presents a concentration of stress at the point where the bigger radius changes into the smaller and the smaller radius presents a maximum stress significantly close the expected.

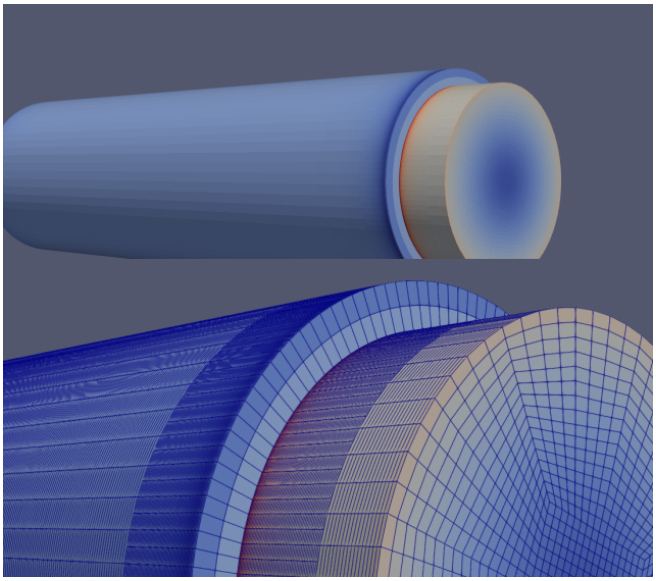

Figure 49: Torsion & Compression with Radius change Comparison

6.5 Convergence Study

The test cases for a constant radius beam reveal a convergence to the analytical solution with the use of 256 thousand DoFs while the beam with the radius change requires for the convergence detailed above approximatily 1.5 million DoFs, so the 2 radii test case is used for this convergence study.

6.5.1 Convergece Study Results

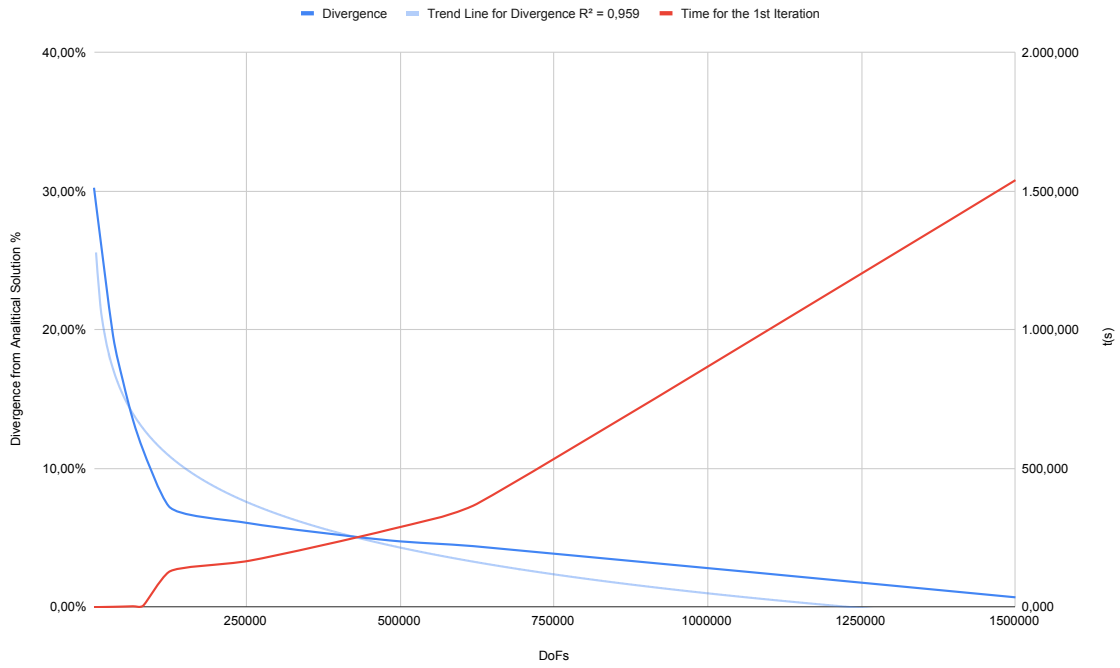

Figure 50: Convergece Study Visualisation

The software presents a logarithmic convergence (light blue curve), which is commonly associated with this kind of problem with numerical solution.

Up to 120,000 Degrees of Freedom (DoFs), the discretization along the axis, which particularly benefits the accuracy for the beam that is subjected to torsion, is increased. However, this simultaneously increases the initial norm of the right-hand side of the system, which, if this discretization is increased significantly, will lead to non-convergence.

Immediately after the corner, the discretization is increased overall, which leads to the convergence of the problem, provided that the necessary computational power is available. This increase in mesh size is quadratic in the total number of cells.

Initially, the time is essentially zero, as the sequential part of the algorithm, which achieves the correct discretization, is very small. However, as the overall discretization increases, the sequential part increases proportionally with the increase in cells.

6.5.2 Amdahl's Law & Gustafson's Law for Parallelization Efficiency

Amdahl's Law
Amdahl's Law provides the theoretical speedup in latency of the execution of a task at a fixed workload due to improved system resources. Formally, it is presented by Gene Amdahl and can be formulated as follows:

$$S_{\text{latency}}(s) = \frac{1}{(1-p) + \frac{p}{s}}$$

where:

- S_{latency} is the theoretical speedup of the execution of the whole task,
- s is the speedup of the part of the task that benefits from improved system resources,
- p is the proportion of execution time that the part benefiting from improved resources originally occupied.

The law underlines that the maximum speedup of a program is limited by its serial portion. For instance, if 30% of the execution time can be sped up ($p = 0.3$) and the improvement makes the affected part twice as fast ($s = 2$), then the overall speedup is:

$$S_{\text{latency}} = \frac{1}{1 - p + \frac{p}{s}} = \frac{1}{1 - 0.3 + \frac{0.3}{2}} = 1.18$$

This reflects that the speedup of the entire program is less than the speedup of the individual part. Amdahl's Law applies when the problem size is fixed and becomes less optimistic as the parallelizable portion's time grows compared to the serial work.

Optimizations of the non-parallelizable part can lead to significant speedup improvements. For example, optimizing a task that has two parts A and B, where part B is optimized to be 5 times faster, might result in a smaller overall speedup compared to optimizing part A to be twice as fast, despite the fact that the latter requires less work.

Gustafson's Law
While Amdahl's Law assumes a fixed problem size, Gustafson's Law provides a more optimistic view by considering the scaling of the problem size with the number of processors. Gustafson's Law suggests that the potential speedup of a program using multiple processors is not strictly limited by the serial portion of the program, because as more processors are added, it is practical to work on larger problems, which can increase the parallel portion of the work proportionately.

The law is formulated as:

$$S_{\text{scaled}} = p + (1 - p) \cdot s$$

where:

- S_{scaled} is the scaled speedup,
- s is the number of processors,
- p is the proportion of the parallelizable part of the task.

Gustafson's Law counters the pessimistic view of Amdahl's Law, showing that computing efficiency can scale effectively with the addition of more processors by increasing the problem size rather than by simply reducing the time to solve the same problem.

The parallel efficiency of the developed software will be evaluated using Gustafson's Law and compared with the theoretical speed up for 3 different sizes of the same problem.

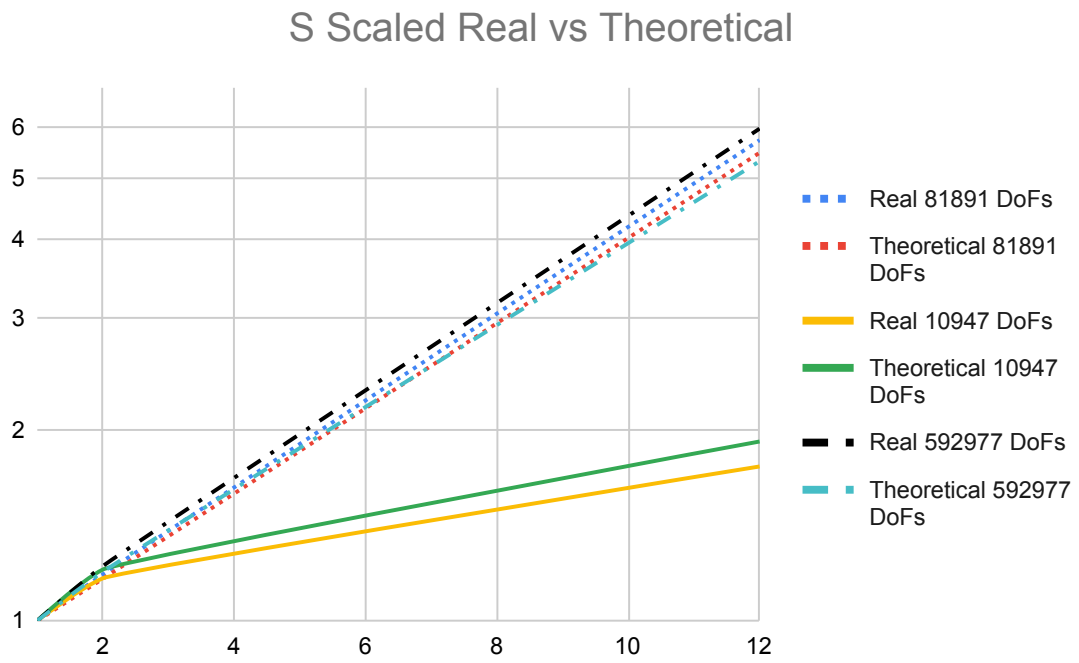

Figure 51: Parellisation Efficiency Real vs Theoretical

The S_{scaled} is calculated by adding the time the software spends on the serial and parallel functions, which is logged in each timestep as presented below:

Setup	Serial
Assembly	Parallel
Create Coarse Grid	Serial
Solve	Parallel
all the rest	Serial

Figure 52: Functions Serial vs Parallel

```
+-----------------------------------------+------------+------------+
| Total wallclock time elapsed since start |       128s |            |
|                                         |            |            |
| Section                         | no. calls |  wall time | % of total |
+---------------------------------+-----------+------------+------------+
| Setup: constraints              |         1 |  1.56e-06s |         0% |
| Setup: distribute DoFs          |         1 |  1.05e-06s |         0% |
| assembly                        |         1 |      42.4s |       33% |
| create_coarse_grid              |         1 |     0.621s |      0.49% |
| setup                           |         1 |      6.51s |       5.1% |
| setup_quadrature_point_history  |         1 |    0.0574s |         0% |
| solve_problem                   |         1 |      75.2s |       59% |
| update_quadrature_point_history |         1 |     0.279s |      0.22% |
+---------------------------------+-----------+------------+------------+
```

Figure 53: Wall-Clock Time per Function

As depicted by the fig. 51, for low number of DOFs, the theoretical efficiency exceeds the calculated, as is to be expected, but for high number of DOFs the real surpasses the theoretical, with their difference growing further for a growing number of DOFs. This can be attributed to the fact that the theoretical does not take into account the distribution of the DOFs to the MPI processes, which significantly affects the time the software spends in serial for higher number of MPI processes.

Also, noteworthy is the fact that the RAM memory usage is not affected by the number of parallel processes, which allows for a computer with 64GB of RAM to run up to 2.5 million DOFs problems.

6.6 Euler-Bernoulli & Timoshenko's Beam Theory

Euler-Bernoulli Beam Theory
The eigenvalue analysis of the software was compared to the analytical solutions provided by the Euler-Bernoulli beam theory for free vibrations of a cantilever beam. The natural frequencies and mode shapes of the beam, which are the key characteristics in dynamic analysis, were calculated and compared to the classical solutions. The focus was on ensuring the software accurately determines the eigenvalues that represent the square of the natural frequencies of the beam.

The classical solution for the eigenvalues of a beam in free vibration (Euler-Bernoulli theory) is:

$$\omega_n^2 = (\beta_n \cdot L)^4 \cdot \frac{EI}{\rho \cdot \pi \cdot R^2 \cdot L^4}, \tag{6.10}$$

where ω_n are the natural frequencies, ρ is the density of the material, R is the radius of the section, L is the length of the beam, and E, I retain their earlier meanings. The β_n is derived from theory and it is the solution of the equation: $cos(\beta L) \cdot cosh(\beta L) = 1$ and the solutions βL are the following:

Eigenmode 1	1.875
Eigenmode 2	4.694
Eigenmode 3	7.853
Eigenmode 4	10.995
Eigenmode n	…

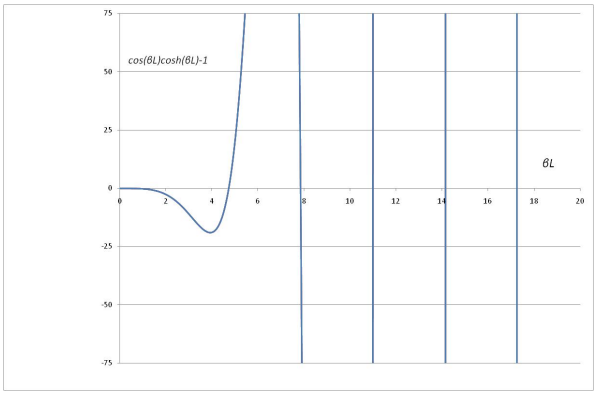

Figure 54: Euler Beam $cos(\beta L) \cdot cosh(\beta L) = 1$ Solutions

Timoshenko's Beam Timoshenko beam theory is an improvement over the classical Euler-Bernoulli beam theory as it accounts for shear deformation and rotational effects, which are significant in short and deep beams. The eigenvalue analysis for Timoshenko beams involves solving the coupled differential equations governing bending and shear deformations.

The governing equations for vibration analysis of a Timoshenko beam can be expressed as a system of second-order differential equations:

$$EI\frac{d^2\phi}{dx^2} - \kappa AG\left(\frac{d\phi}{dx} - \frac{du}{dx}\right) = \rho I\frac{d^2\phi}{dt^2}, \tag{6.11}$$

$$\kappa AG\left(\frac{d\phi}{dx} - \frac{du}{dx}\right) = \rho A\frac{d^2u}{dt^2}, \tag{6.12}$$

where ϕ is the rotation of the cross-section, u is the transverse displacement, E is the modulus of elasticity, G is the shear modulus, A is the area of the cross-section, I is the second moment of area, ρ is the density, κ is the Timoshenko shear coefficient, and x and t denote the spatial and temporal variables, respectively.

Eigenvalue Problem for Timoshenko's Beam
The eigenvalues for the free vibration problem are found by assuming harmonic motion such that

$u(x,t) = \hat{u}(x)e^{i\omega t}$ and $\phi(x,t) = \hat{\phi}(x)e^{i\omega t}$, where ω is the angular frequency of vibration. Substituting these into the governing equations leads to the following eigenvalue problem:

$$EI\frac{d^2\hat{\phi}}{dx^2} - \kappa AG\left(\frac{d\hat{\phi}}{dx} - \frac{d\hat{u}}{dx}\right) = -\omega^2\rho I\hat{\phi}, \tag{6.13}$$

$$\kappa AG\left(\frac{d\hat{\phi}}{dx} - \frac{d\hat{u}}{dx}\right) = -\omega^2\rho A\hat{u}. \tag{6.14}$$

The eigenvalues and eigenmodes can be obtained by discretizing the beam and solving the resulting algebraic eigenvalue problem. Various numerical methods, such as the finite element method or the spectral element method, can be employed for this purpose. The eigenvalues give the squared natural frequencies of the beam, and the eigenmodes correspond to the mode shapes. For the purposes of this test case the [42] FEM code is utilized.

Results

Below the comparison of Euler-Bernoulli, Timoshenko beam theory with the calculation from deal.II is presented:

	Values[rad/s]			Deviation from deal.II	
eignevalue	Euler	Timoshenko	deal.II	Euler	Timoshenko
1	404,0356434	442,993	250,1	30,95%	-11,56%
2	2532,607499	1328,98	1444	42,98%	-8,65%
3	7088,514053	3101	3343	52,84%	-7,80%
4	13896,34607	3987,2	4248,23	69,43%	-6,55%
5	22974,13623	4873,25	5487	76,12%	-12,59%

Table 6.6: Eigenvalues Theory Comparison

The deal.II presents a significant divergence from the Euler beam theory, which is the simpler theory and detached from reality, whereas the software converges towards the Timoshenko beam theory. Furthermore, the eigenmodes provided from the developed software closely resemble the theoretical eigenvectors, as demonstrated below:

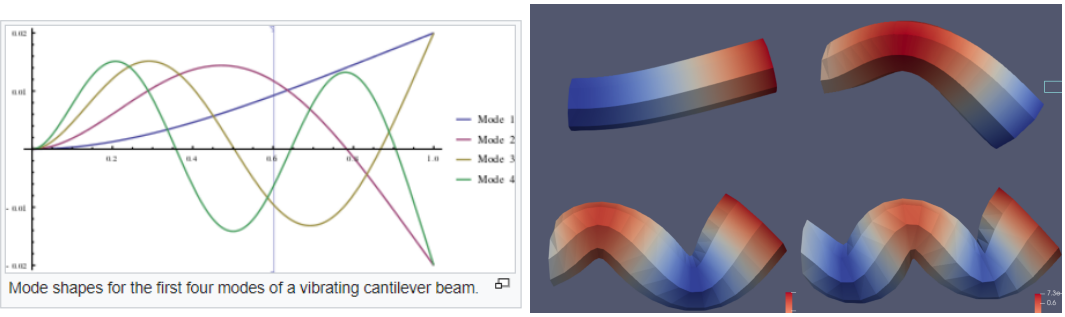

Figure 55: Theoretical Eigenvectors

6.7 Comments on the Validation Cases

The developed software converges to the analytical solution with sufficient accuracy. The maximum divergence from the analytical solution is reported for the bending test case, with an almost 1.8% difference. Regarding the eigenvalues of the cantilever beam calculated with Euler's Beam, the divergence in the natural frequencies is in the area of 70%, but the eigenmodes produced by Timoshenko's beam are located closer to the ones provided by the software, with the eigenmodes being significantly close. The divergence reported can be attributed to the following:

- The Euler-Bernoulli theory of beam bending cannot be exactly be translated into three dimensions, especially the boundary conditions,
- The Euler theory does not consider the shear stress that are present in the 3 dimensional model
- According to this theory, every section of the beam is perpendicular to the line, which is not the case in the 3D model, which especially affects the eigenvalue analysis.
- Regarding the Timoshenko's beam eigenvalues analysis, the divergence can be attributed to the fact that the area of each section is considered to be constant, however as it apparent for the fig. 55 that is not the case in the developed software.
- In the software, the bending force is not parallel to the face of the cylindrical section, but it is perpendicular to the xy plane.
- The constitutive model used by the software considers small deformations

The aforementioned divergence in bending is not considered significant, as it remains below the arbitrary imposed threshold of 2% and the software can be considered accurate as far as displacement and stresses are concerned.

Lastly, the theoretical eigenvalue analysis considers a two dimensional domain, whereas the developed software runs in three dimensions and therefore torsional eigenvalues appear as the 3rd and 5th eigenvalues, and their corresponding eigenmodes are presented below:

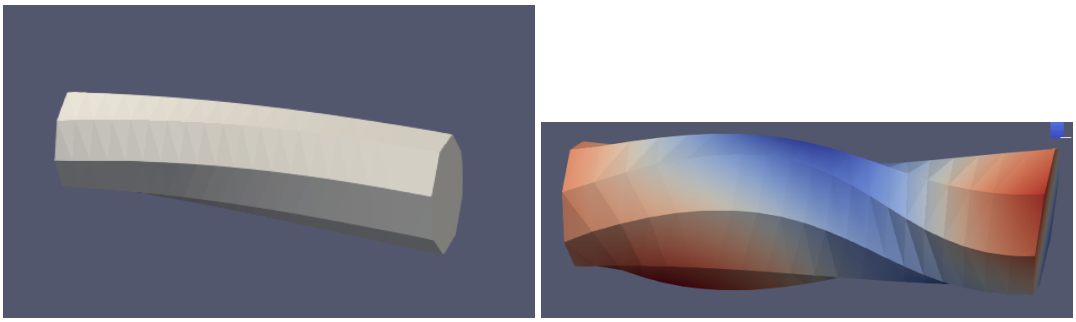

Figure 56: Torsional Eigenmodes for Cantilever Beam

7 Case Study

The dynamic analysis model for the propulsion installation of a ship is of vital importance for many aspects of the engine regarding the timely diagnosis of faults that may occur during its operation, as well as the improvement of its performance. Specifically, by studying the dynamic phenomena that develop due to the time-varying forces during the operation of a two-stroke marine engine, conclusions can be drawn about the stresses received by the individual parts of the engine, as well as the entire ship propulsion system. Knowing the stresses that the system undergoes, proper planning of its maintenance can be carried out, and undesirable faults that lead to increased repair costs can be avoided. Equally important is the optimal design of the parts of the propulsion system, which aims to maximize the system's endurance at the lowest possible cost.

The software is used to simulate the dynamic behavior of the shafting system with a two-stroke diesel marine engine for a constant rotational speed. The goal of this case study is to assess the behavior of a real diesel engine in regards to the Von Mises stresses developed, as well as the deformation it presents. The torque applied on the cylinders varies with the angle of the crankshaft and the phase difference of each cylinder, as will be detailed below. Finally, the lateral vibration eigenvalues will be calculated and compared with the values provided by the Lateral Vibration Manual of the Shafting System.

The methodology of this case study is the following:

- **Real world Reference Ship**, a two-stroke engine with its respective shafting system is chosen and their parameters are presented
- **Input of Parameters to the software**,
- **Creation of Cylinder Torque Models**, the combustion gases, friction and inertial torque models are integrated into the software.
- **Comparison of Results**

7.1 Reference System

The reference system examined in this study is a real propulsion system of a ship, consisting of a two-stroke marine engine that drives a propeller as in every typical propulsion system of a commercial ship. The power transmission from the engine to the propeller is done through the axial system which includes an intermediate and a propeller shaft. The characteristics of the ship and the propulsion system are presented below:

7.1.1 Reference Ship Characteristics

- Ship Category: Bulk Carrier
- Bulk Carrier Category: Handysize
- Overall Length (LOA): 180 m
- Length Between Perpendiculars (LBP): 176.75 m
- Width (B): 30 m
- Design Draft (Tdes): 10.304 m
- Depth (D): 14.7 m
- Block Coefficient (Cb): 0.82
- Displacement at Design Draft (Δ): 46073.6 t
- Deadweight (DWT): 36056 t
- Lightship (LS): 10017.6 t

7.1.2 Main Engine Characteristics

- Engine: 5RT-flex50-D
- Manufacturer: Doosan Engine (Wartsila)
- Maximum Continuous Power: 6350 kW
- Maximum Continuous Operating Speed: 99 rpm
- Number of Cylinders: 5
- Piston Diameter: 0.5 m
- Piston Stroke: 2.050 m
- Connecting Rod Length: 2.050 m
- Mean Effective Pressure (MEP) at Maximum Continuous Rating (MCR): 19.12 bar
- Mean Indicated Pressure (MIP) at Maximum Continuous Rating (MCR): 19.97 bar
- Cylinder Firing Order: 1-4-3-2-5

7.1.3 Main Axial System Characteristics

- Length of Intermediate Shaft: 6.827 m
- Diameter of Intermediate Shaft: 340 mm
- Mass of Intermediate Shaft: 5555 kg
- Ultimate Tensile Strength (UTS) of Intermediate Shaft: 800 N/mm^2
- Length of Propeller Shaft: 6.565 m
- Diameter of Propeller Shaft: 450 mm
- Mass of Propeller Shaft: 7396 kg
- Ultimate Tensile Strength (UTS) of Propeller Shaft: 600 N/mm^2

7.1.4 Main Propeller Characteristics

- Propeller Diameter: 5.9 m
- Pitch-to-Diameter Ratio: 0.87
- Number of Blades: 4
- Expanded Area Ratio AE/AO: 0.4
- Mass of Propeller: 11960 kg

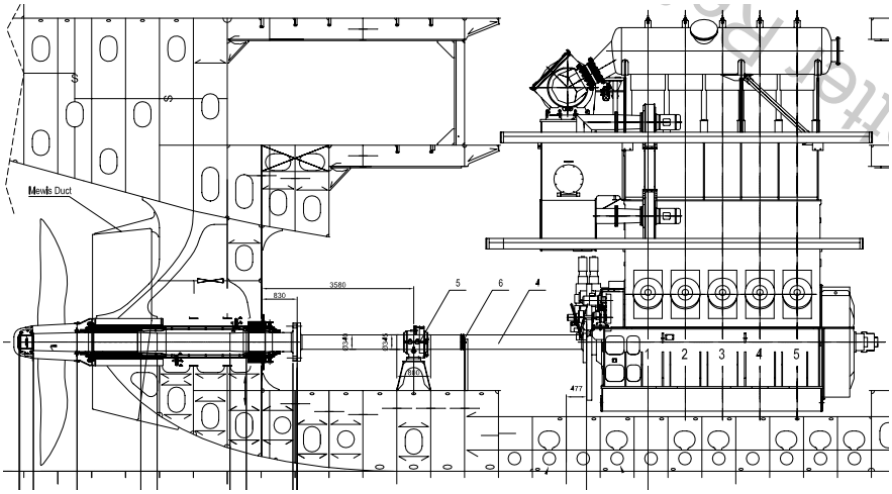

Figure 57: Reference Propulsion System

7.1.5 Reference Shaft System Inputs

The reference system is translated to the software using the following shaft elements, as well as the polar mass of inertia required:

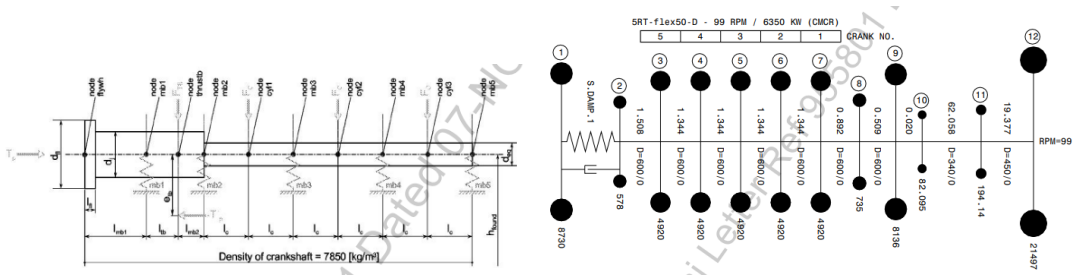

Figure 58: Engine Shaft Inputs

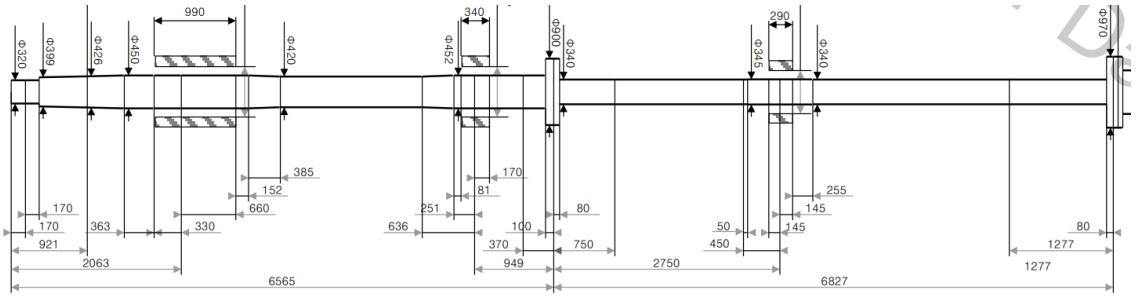

Figure 59: Shaft Input

The shaft is inputted as shaft element as described in fig. 41, and the additional polar mass moment of inertia values attributed to the cylinders, the flywheel, the torsional damper and the propeller are used to calculate the density required for the equivalent cylindrical sections.

The bearings equivalent springs stiffness constants are presented in fig. 60, while the spring area for all bearings is chosen to be located at the whole length of the bearing and ten centimeters at each side and from the bottom of the bearing for the vertical spring and ten centimeters from the radius of the bearing, and 10 centimeters the center of the shaft in height for the lateral bearings.

Bearing elements

node	cy_stat [N/m]	cz_stat [N/m]	cy_dyn [N/m]	cz_dyn [N/m]
mb7	4.0e+09	2.8e+09	1.5e+09	1.5e+09
mb6	4.0e+09	2.8e+09	1.5e+09	1.5e+09
mb5	4.0e+09	2.8e+09	1.5e+09	1.5e+09
mb4	4.0e+09	2.8e+09	1.5e+09	1.5e+09
mb3	4.0e+09	2.8e+09	1.5e+09	1.5e+09
mb2	4.0e+09	2.8e+09	1.5e+09	1.5e+09
mb1	4.0e+09	2.8e+09	1.5e+09	1.5e+09
IB1	1.0e+09	1.0e+09	1.0e+09	1.0e+09
FSTB	5.0e+09	5.0e+09	5.0e+09	5.0e+09
ASTB	5.0e+09	5.0e+09	5.0e+09	5.0e+09

Figure 60: Bearings Equivalent Springs Inputs

Regarding the friction torque in each bearing, the torque is calculated to be 1% of the Propeller Torque for all the bearings, which is distributed analogous to the area of the bearing.

7.2 Right Hand Side Forces

The moments exerted during the operation of a two-stroke marine engine and introduced into the dynamic analysis model developed in this diploma thesis are analyzed below.

7.2.1 Combustion Torque

The combustion torque of each cylinder of the engine results from considering the variation of pressure in the cylinder and the characteristics of the engine's kinematic mechanism. The combustion torque is given by the following formula.

$$T_{gas}(\theta) = D_s(\theta) \cdot \frac{\pi}{4} \cdot B^2 \cdot p(\theta) \tag{7.1}$$

Where:

- θ: the angle of the crankshaft
- B: the diameter of the cylinder's piston
- $p(\theta)$: the pressure developed within the combustion chamber as a function of the crankshaft angle
- $D_s(\theta)$: the derivative of the piston displacement from the top dead center as a function of the crankshaft angle. It is determined according to the following equation taking into account the characteristics of the kinematic mechanism, which are shown in the figure following the equation.

$$D_s(\theta) = \frac{ds(\theta)}{d\theta} = r \cdot \sin(\theta) \cdot (1 + \frac{\cos(\theta)}{\sqrt{\left(\frac{l}{r}\right)^2 - (\sin(\theta))^2}} \tag{7.2}$$

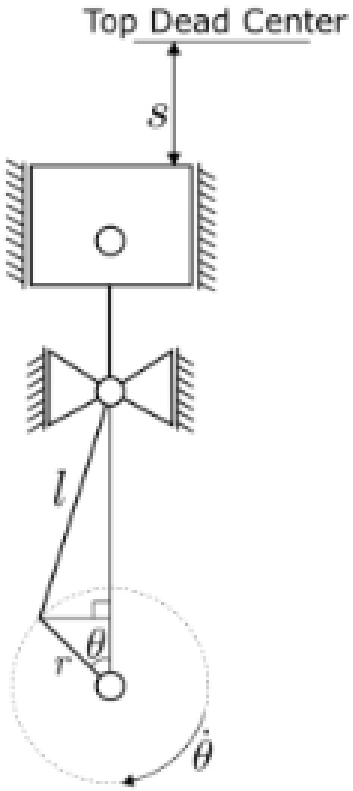

Figure 61: Kinematic Mechanism of two-Stroke Marive Engine

The distribution of pressure as a function of the angle θ of the crankshaft within the combustion chamber is qualitatively presented in the diagram below.

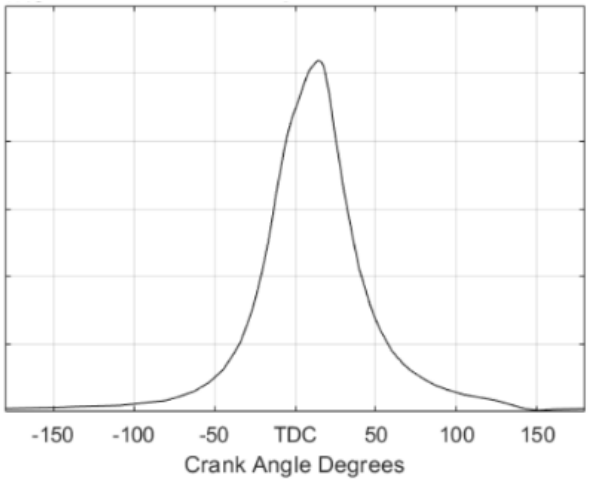

Figure 62: Pressure Angle Diagram for Marine Two-Stroke Diesel Engine

The Pressure-Angle (P-θ) diagrams for the engine under study were provided by the company CLEOS. They were constructed using the AVL company's CRUISE M software. This program performs thermodynamic modeling of the engine with the introduction of appropriate data. Data from the factory tests of the engine and geometric characteristics of the engine were used to construct the indicator diagrams. Specifically, the data used from the shop tests are the following:

- Ambient pressure
- Ambient temperature
- Scavenging air pressure
- Scavenging air temperature
- Fuel Flow (calculated from the specific consumption and engine power)

The geometric characteristics of the engine used are as follows:

- Piston diameter
- Piston stroke
- Connecting rod length
- Number of cylinders
- Firing order of cylinders
- Volume of scavenging air space
- Volume of exhaust manifold

The verification of the indicator diagrams is carried out through the software with the following elements provided in the shop tests:

- Maximum cylinder pressure
- Compression pressure

- Mean effective pressure
- Exhaust gas temperature after the turbocharger

The CRUISE M software for constructing the indicator diagrams is based on the Woschni-Anisits combustion model. It is a phenomenological model used for simulating combustion in direct injection engines. This model relies on the single S-curve equation, which calculates the fraction of the burned fuel mass m_b and the total mass of fuel injected into the cylinder m_{total}. The main equation of this method (Weibe function) is:

$$x_b(\theta) = \frac{m_b}{m_{total}} = 1 - \exp\left[-a \cdot \left(\frac{\theta - \theta_0}{\Delta\theta}\right)^m\right] \tag{7.3}$$

Where:

- a: constant representing the efficiency of combustion, $a = 6.9$
- θ: the angle of the crankshaft
- θ_0: the angle of the crankshaft at the start of combustion for each cylinder
- $\Delta\theta$: the total duration of combustion measured in angle
- m: constant affecting the shape of the P-θ indicator diagram, $m = 0.5 - 2$

The pressure curve using the Weibe function is generated from the following equations:

$$\frac{dQ_n}{d\theta} = \frac{dx_b(\theta)}{d\theta} \cdot m_{fuel} \cdot LHV_{fuel} \cdot n_{comb} - \frac{dQ_{ht}}{d\theta} \tag{7.4}$$

Where:

- $\frac{dQ_n}{d\theta}$: the rate of heat release
- $\frac{dx_b(\theta)}{d\theta}$: the derivative with respect to the angle θ of the Weibe function
- m_{fuel}: the mass of fuel injected into the cylinder
- LHV_{fuel}: the lower heating value of the fuel
- n_{comb}: the efficiency of combustion
- $\frac{dQ_{ht}}{d\theta}$: the rate of heat transfer

The pressure is obtained as follows:

$$\frac{dP}{d\theta} = \gamma - 1 \cdot \frac{dQ_n}{d\theta} \cdot \frac{P}{V} - \gamma \cdot \frac{P}{V} \cdot \frac{dV}{d\theta} \tag{7.5}$$

Where:

- P: the pressure at each angle of the crankshaft
- V: the displacement volume of the cylinder
- γ: the thermodynamic constant of gases
- $\frac{dP}{d\theta}$: the change of pressure with the angle of the crankshaft (P-θ indicator diagram)
- $\frac{dV}{d\theta}$: the change of displacement volume with the angle θ of the crankshaft

The combustion torque is applied uniformly on the area of the cylindrical body section that belongs to each cylinder. The calculation of the surface traction applied on each element will be presented in the **??**.

7.2.2 Engine Friction Torque

The engine's friction torque is calculated as the friction coefficient 'times' the engine's angular velocity.

$$T_{friction} = f \cdot \omega \tag{7.6}$$

The friction coefficients are calculated through the friction pressure ($P_{friction}$) given at the point of maximum continuous operation by the manufacturer and the formula:

$$P_{friction} = T_{friction} \cdot \omega \tag{7.7}$$

It is considered that the friction coefficients remain constant for any operating speeds, and the friction increases proportionally to the angular velocity.

7.2.3 Inertial Mass Torque

The variation of inertia during the rotational motion of the engine is the result of the rotational and reciprocating motion of the pistons, connecting rods, crossheads, and cranks of the engine. The elements of variable inertia correspond to the engine cylinders, and the produced torque is calculated using the following equation:

$$T_j = M_{rec} \cdot \left(\frac{ds}{d\theta}\right)^{\prime 2} \cdot \left(\frac{d\theta}{dt}\right)^2 \tag{7.8}$$

Where:

- M_{rec}: the reciprocating mass of each cylinder
- $\frac{ds}{d\theta}$: $Ds(\theta)$, as described in Section 7.2.1
- $\frac{ds}{d\theta}^{\prime}$: the derivative of $Ds(\theta)$ which equals:

$$\left(\frac{ds}{d\theta}^{\prime}\right) = r \cdot \frac{3 \cdot r^2 \cdot \cos(\theta) \cdot \left(\left(\frac{l}{r}\right)^2 - (\sin(\theta))^2\right) + r^2 \cdot (\sin(\theta))^4 - l^2 \cdot (\sin(\theta))^2 + l^2 \cdot (\cos(\theta))^2}{\left(\left(\frac{l}{r}\right)^2 - (\sin(\theta))^2\right)^{3/2}} \tag{7.9}$$

- $\left(\frac{d\theta}{dt}\right)^{\prime}$: the angular velocity of the engine

The torque applied to each cylinder is the sum of the Combustion, Friction and Inertial Mass Torque.

7.2.4 Propeller Torque

The expression of the load torque depends on the type of load that is moved by the engine shaft. For a two-stroke marine engine connected to a propeller, the load torque is determined based on the law of the propeller, as described in Section 2.2.4, according to the following formulas:

$$P = c \cdot n^3, \quad P = T_{prop} \cdot \omega \tag{7.10}$$

7.2.5 Bearing Friction Torque

The bearing's friction torque is calculated by multiplying the calculated Propeller Torque by the weighted average of the bearing friction percentages. The friction torque is the distributed to the bearings accordingly. The friction percentages do not have a physical meaning, but for the current level of the software refinement it is deemed sufficient.

7.2.6 Propeller Thrust

The thrust exerted on the propeller shaft perimeter area is calculated as below:

$$F_{Thrust} = P/V_{Ship} \tag{7.11}$$

Where P is the Horsepower for the input RPM and V_{Ship} is the vessel speed as calculated in the sea trials and presented in the EEXI Technical File.

7.2.7 Body Force-Gravity

The Gravitational pull in each point is calculated by multiplying the density of the material with the volume of associated with each point.

7.3 Case Study Results

7.3.1 Dynamic Simulation Results

The results presented in this section consider the rotational velocity of the engine to be constant at 100% Load (MCR) where the load is considered to be the maximum and all the data required are known. Two cases will be presented, the first with the torque being constant and equal for all the cylinders, where the shaft reaches a state of dynamic equilibrium. This case study does not exist in reality, but it is used as a test to ensure that the software converges. The second case study uses the torques presented in Section 7.2.1, and are variable with the rotation of the shaft. This model does not converge to an equilibrium, as it is expected, and the shafting system is subjected to constant oscillations.

The initial value conditions are those of constant rotational speed with the rotational velocity being equal to the RPM_{MCR} and the initial acceleration being equal to the radial (centripetal) acceleration. If the radial acceleration is considered equal to zero, then the model does not converge; instead, the whole cylindrical body seems to gain volume, which agrees to the Newmark-Beta theory, where the initial conditions are of utmost importance.

The results for each case study will be presented in the following plots for 2 timesteps:

- ParaView screenshots:
  - Boundary IDs
  - Partitioning
  - Von Mises
  - Maximum Displacement in the x axis for the present timestep
  - Maximum Displacement in the y axis for the present timestep
  - Maximum Displacement in the z axis for the present timestep
  - Maximum Displacement in the x axis total from the elastic line being a straight line
  - Maximum Displacement in the y axis total from the elastic line being a straight line
  - Maximum Displacement in the z axis total from the elastic line being a straight line
- Plots presented describe the following for every dx in the length of the shaft
  - Maximum Von Mises Stress
  - Maximum z Displacement for the present timestep
  - Maximum y Displacement for the present timestep
  - Total Displacement from the first timestep
  - Maximum and Minimum Z & Y Displacement over the total Time

All the following Results are in S.I. units unless stated otherwise

- Length & Displacement in metres
- Von Mises & Norm of Stress in Pascal
- Eigenvalues in radians per second

Constants over all Test Cases

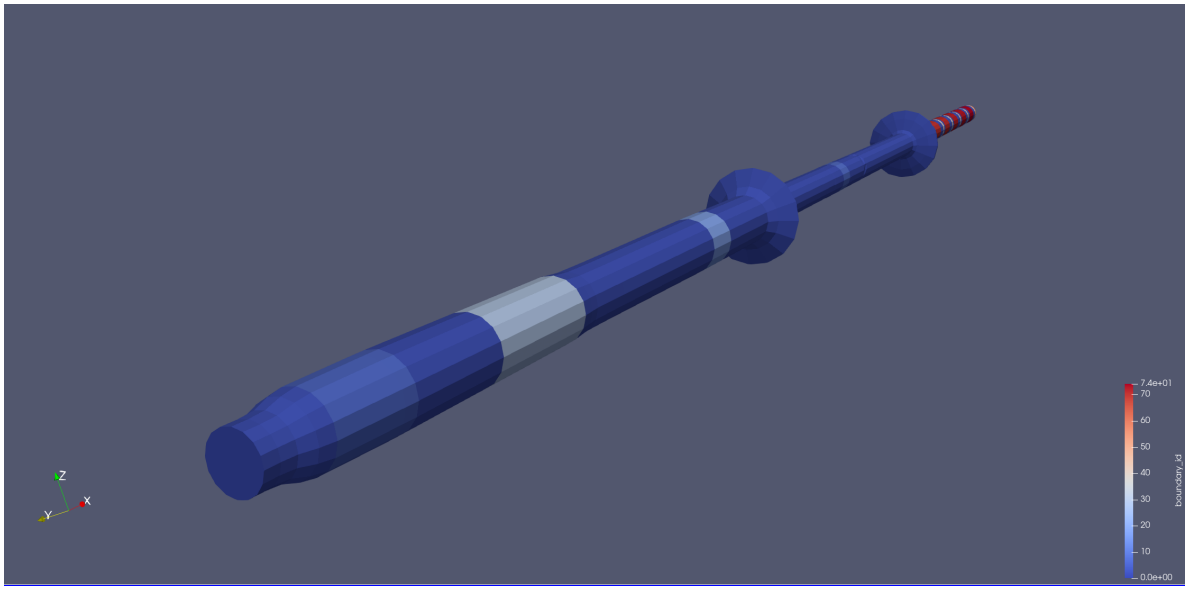

Figure 63: Boundary IDs for Constant Torque

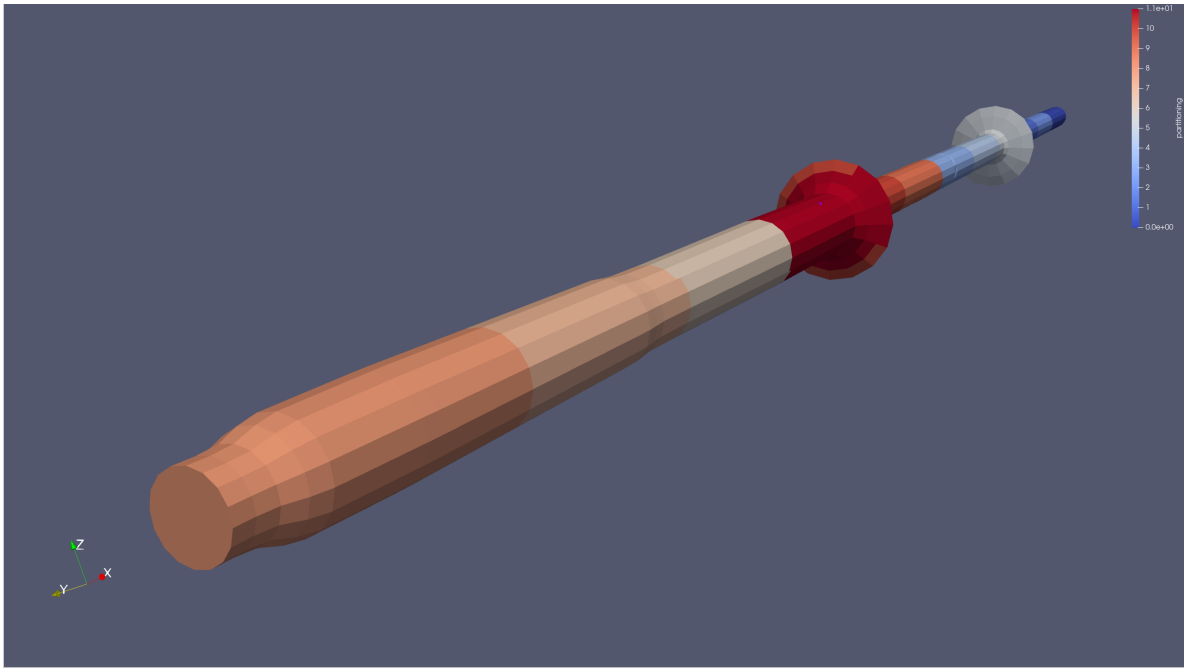

Figure 64: Partitioning of Mesh over MPI Processes

Constant Torque

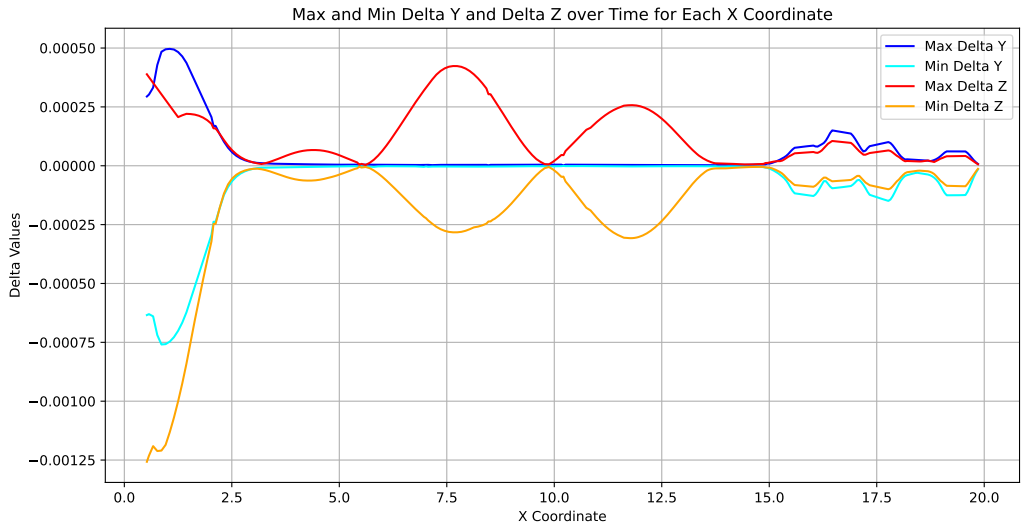

Figure 65: Range of z and y displacement

Timestep=0.01s

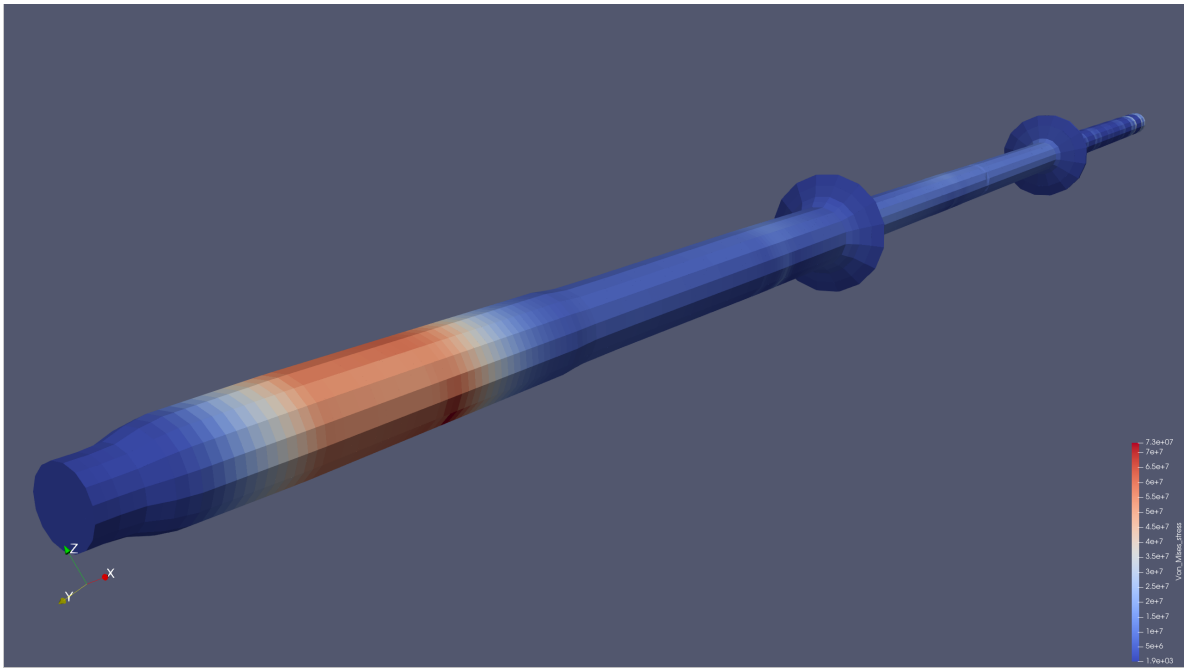

Figure 66: Von Mises for Constant Torque in timestep 1, t=0.01s

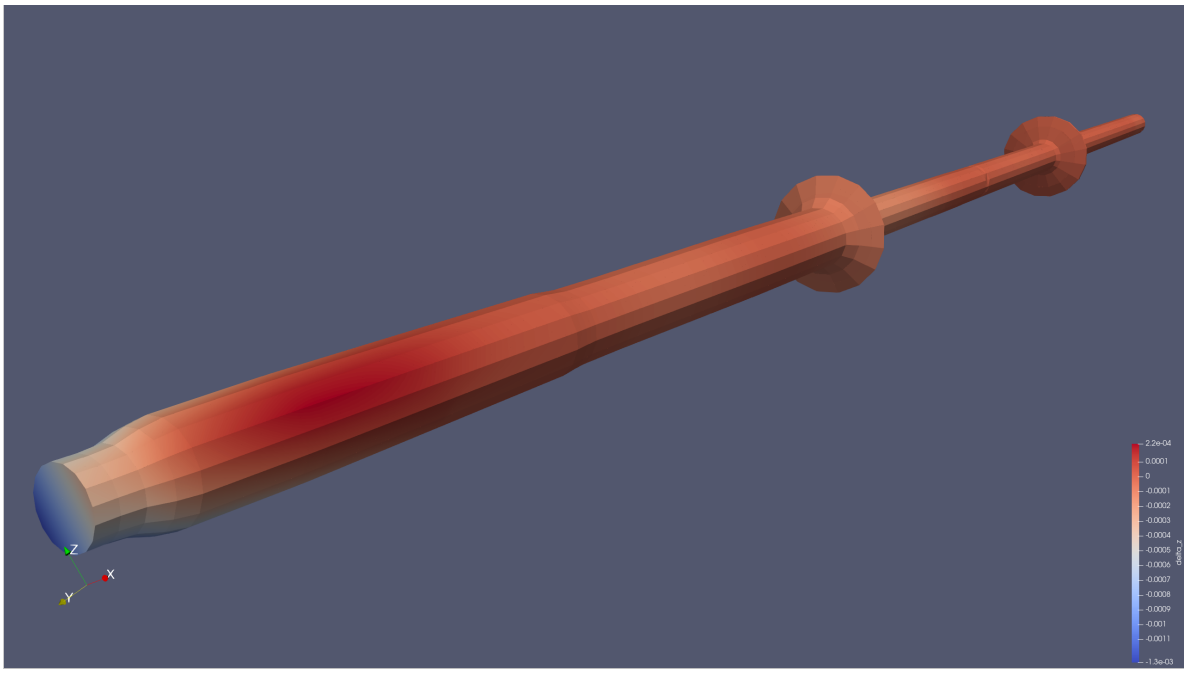

Figure 67: Delta Z for Constant Torque in timestep 1, t=0.01s

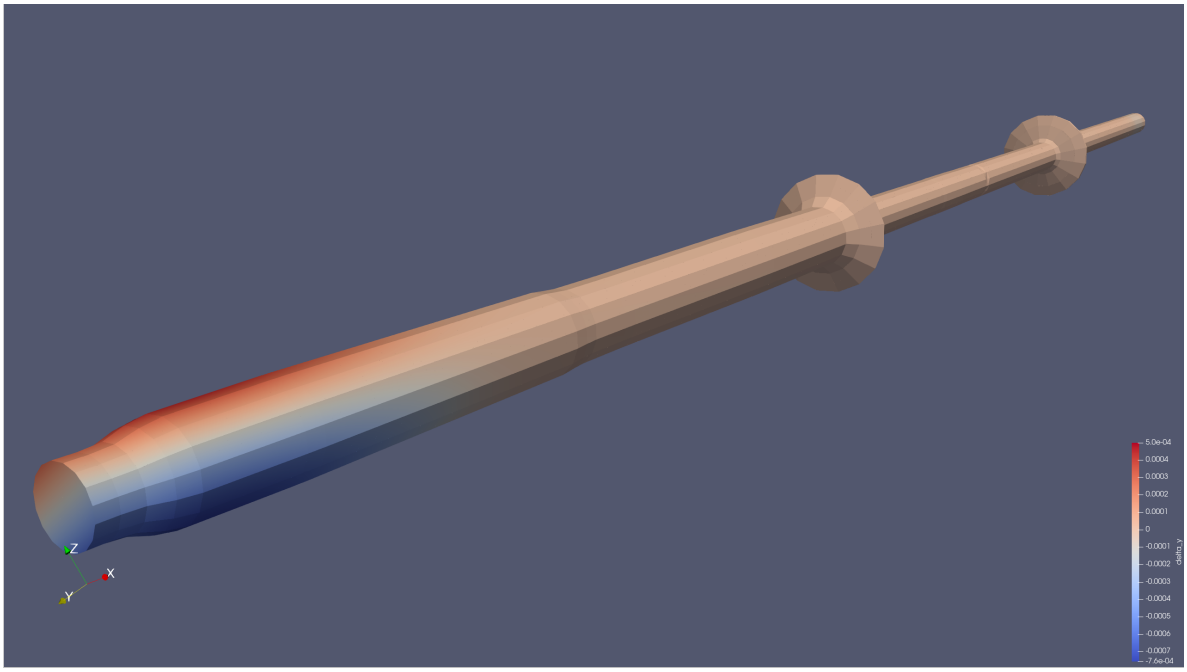

Figure 68: Delta Y for Constant Torque in timestep 1, t=0.01s

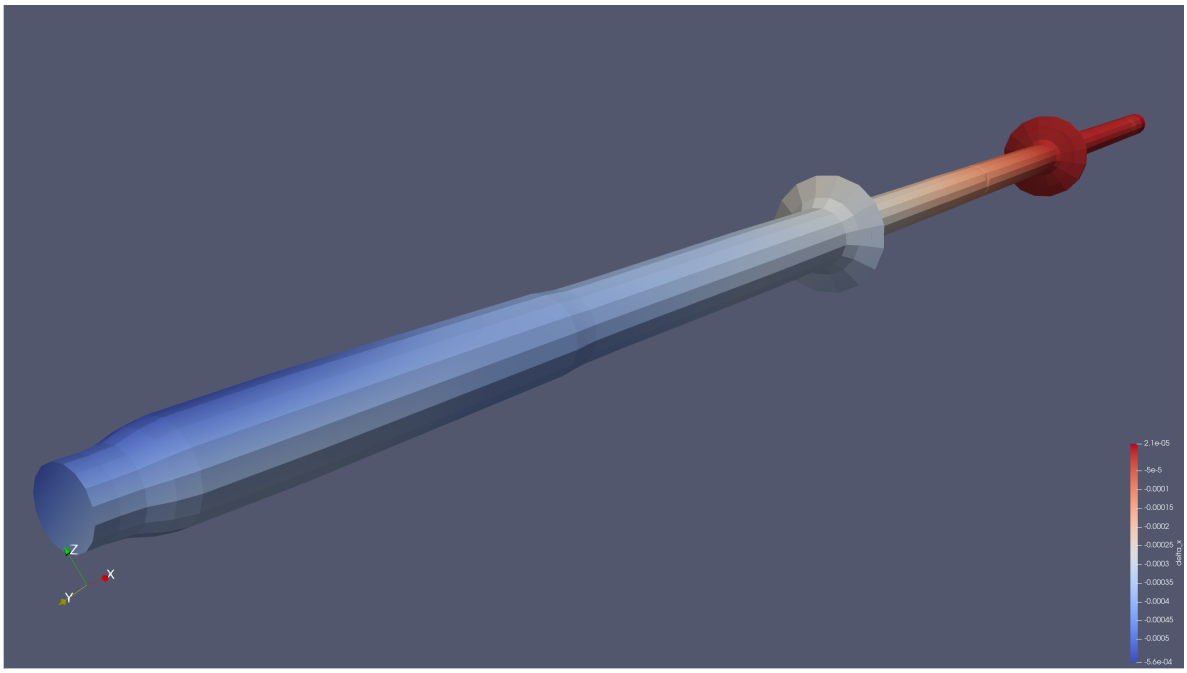

Figure 69: Delta X for Constant Torque in timestep 1, t=0.01s

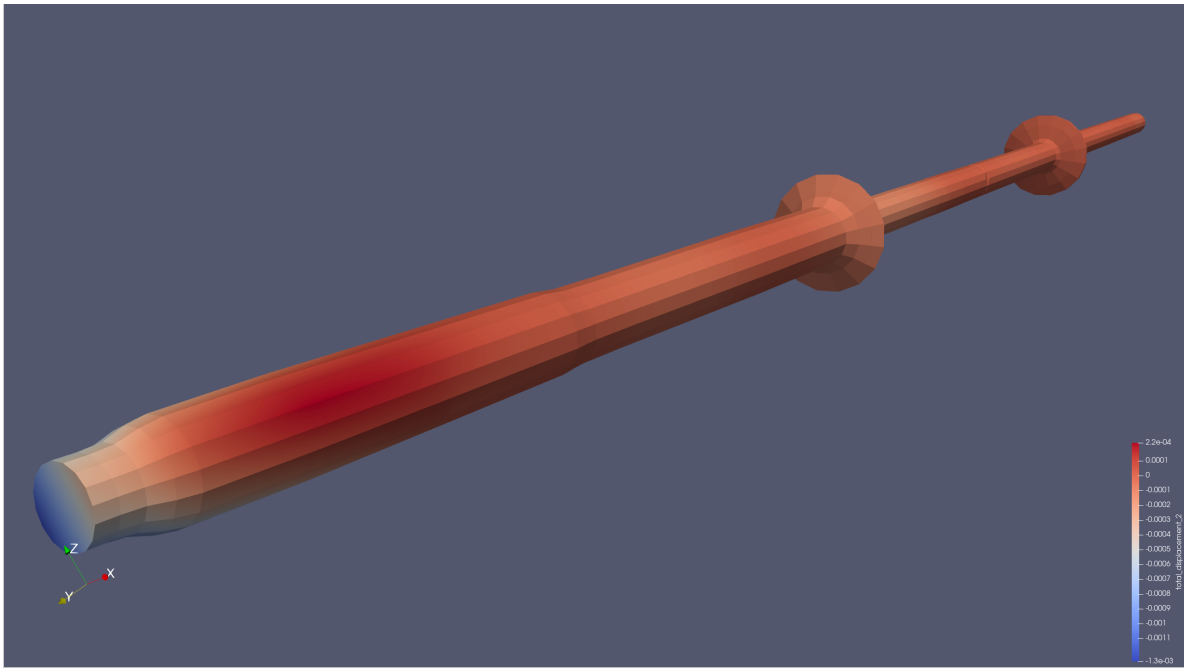

Figure 70: Total Delta Z for Constant Torque in timestep 1, t=0.01s

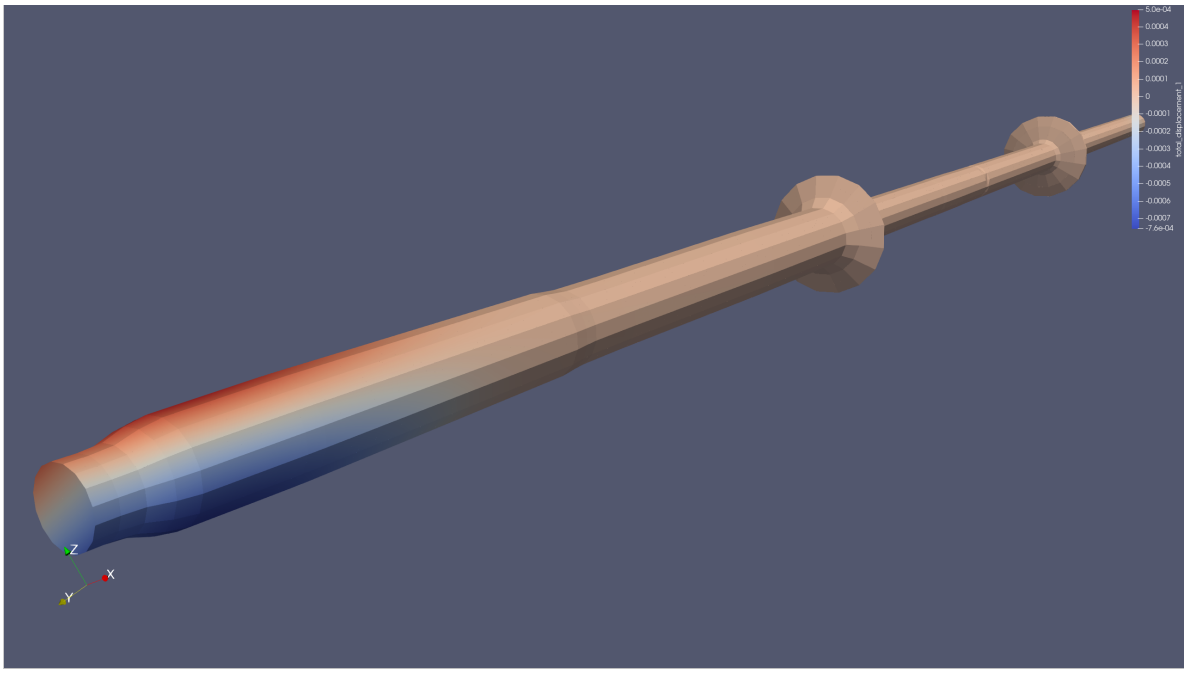

Figure 71: Total Delta Y for Constant Torque in timestep 1, t=0.01s

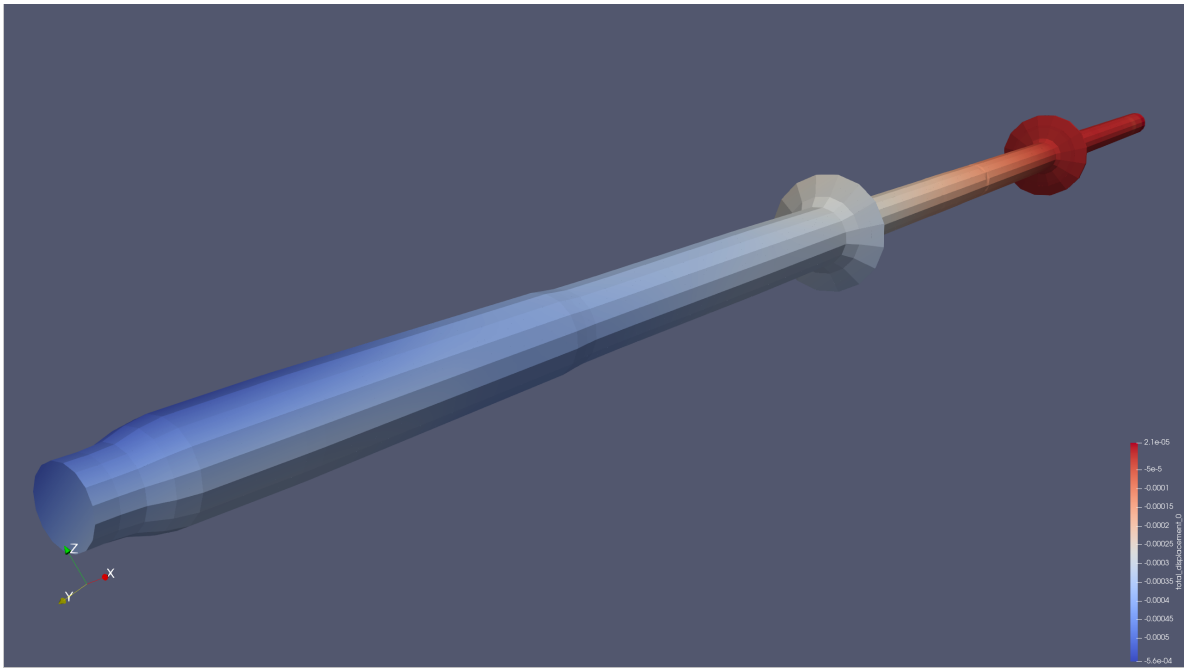

Figure 72: Total Delta X for Constant Torque in timestep 1, t=0.01s

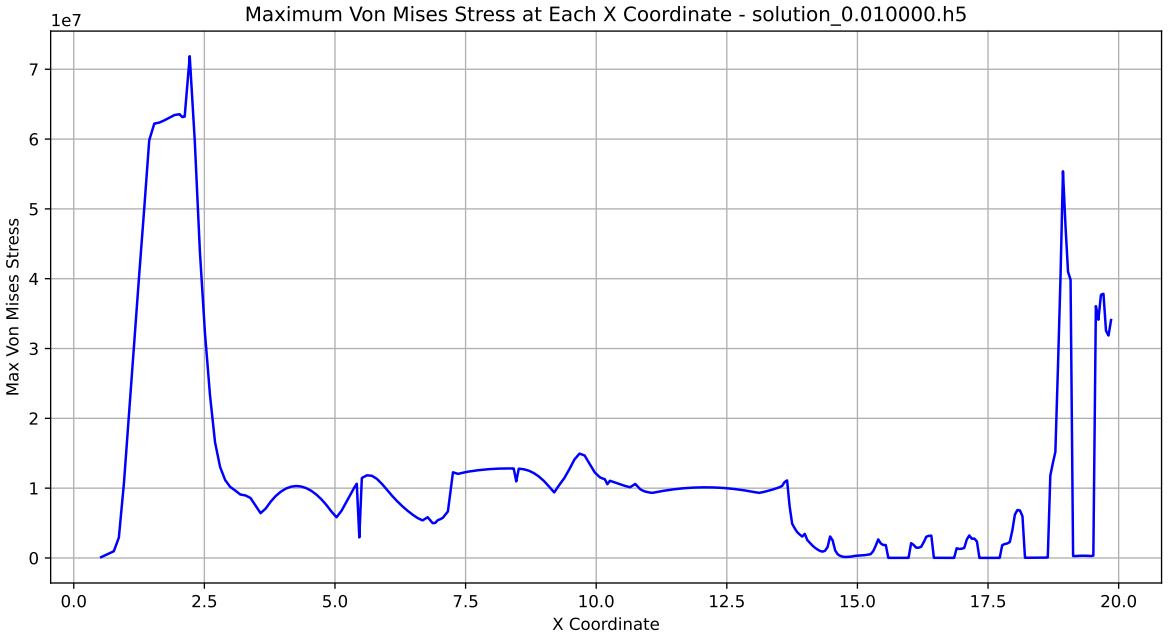

Figure 73: Von Misses Stress over Length in timestep 1, t=0.01s

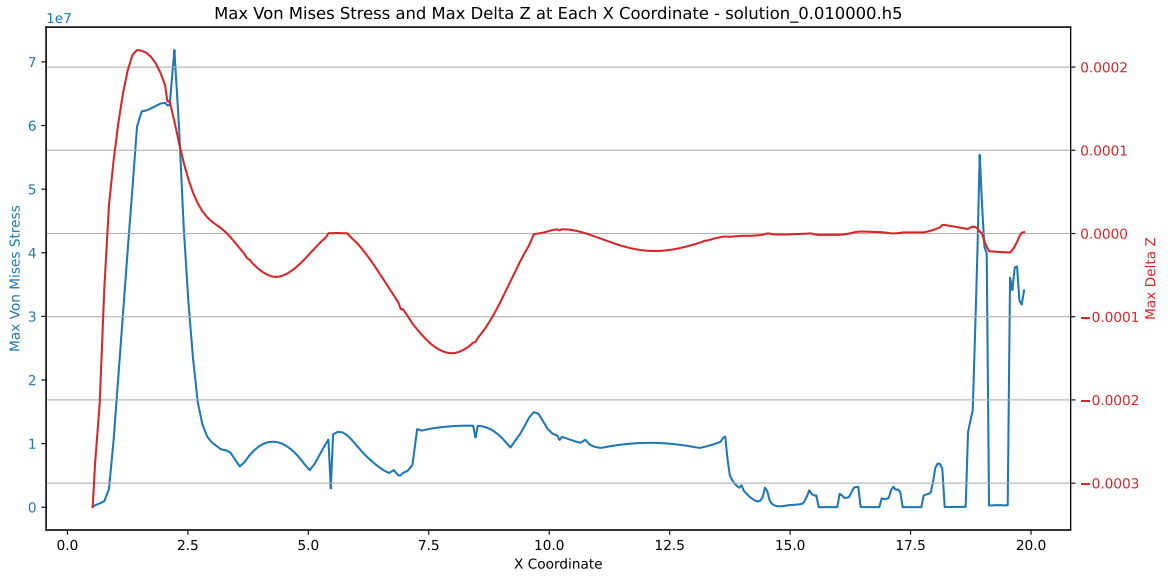

Figure 74: Delta Z over Length in timestep 1, t=0.01s

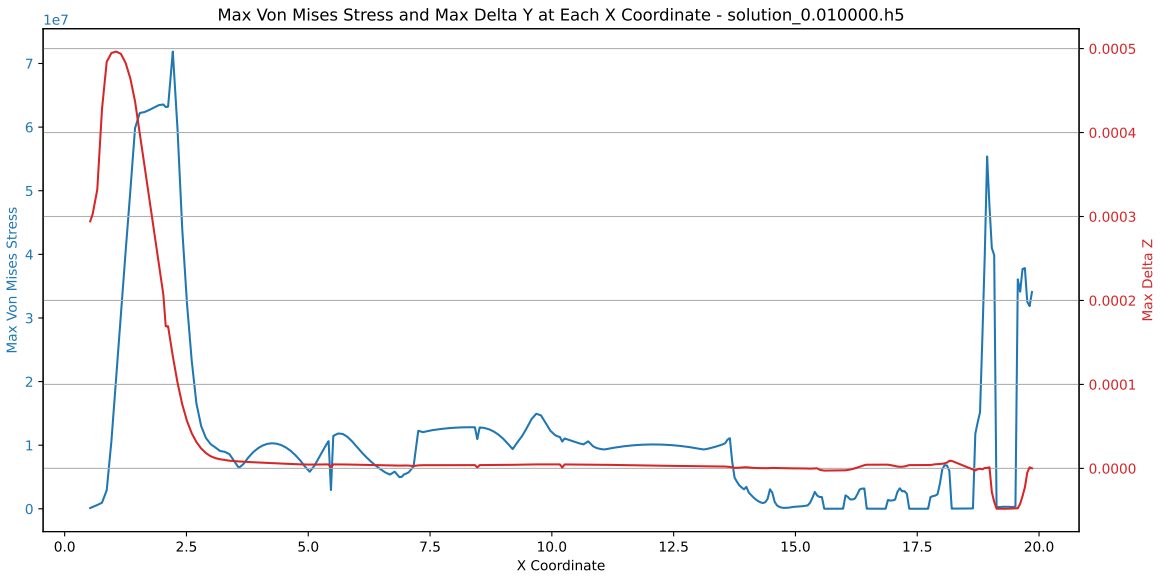

Figure 75: Delta Y over Length in timestep 1, t=0.01s

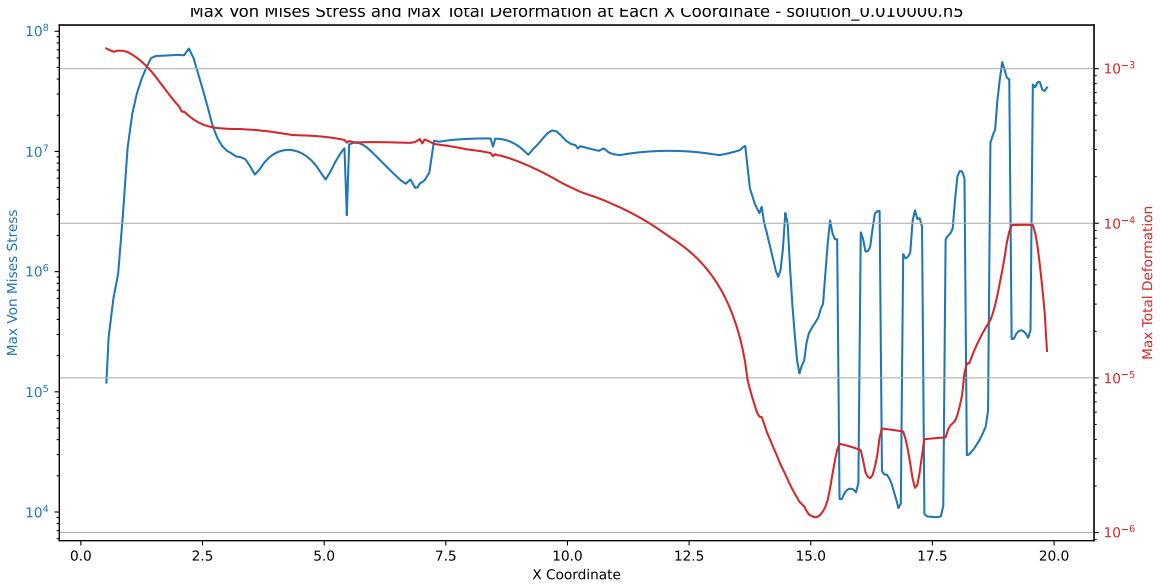

Figure 76: Displacement over Length in timestep 1, t=0.01s

Timestep=0.55s Convergence of System

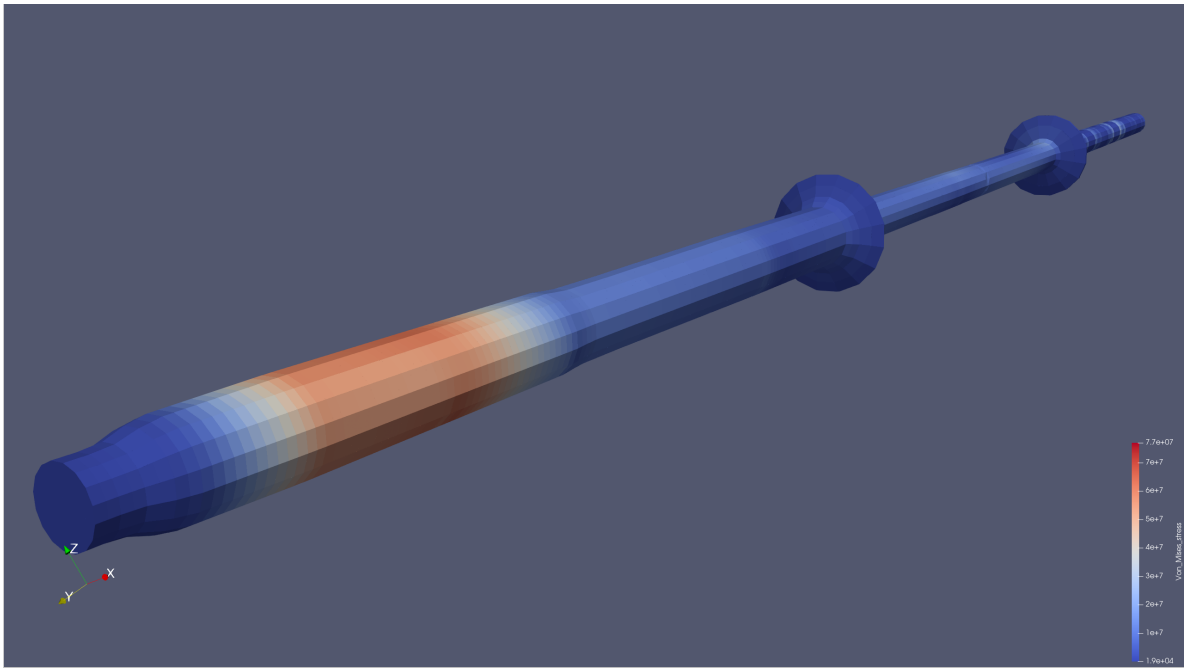

Figure 77: Von Mises for Constant Torque in timestep 55, t=0.55s

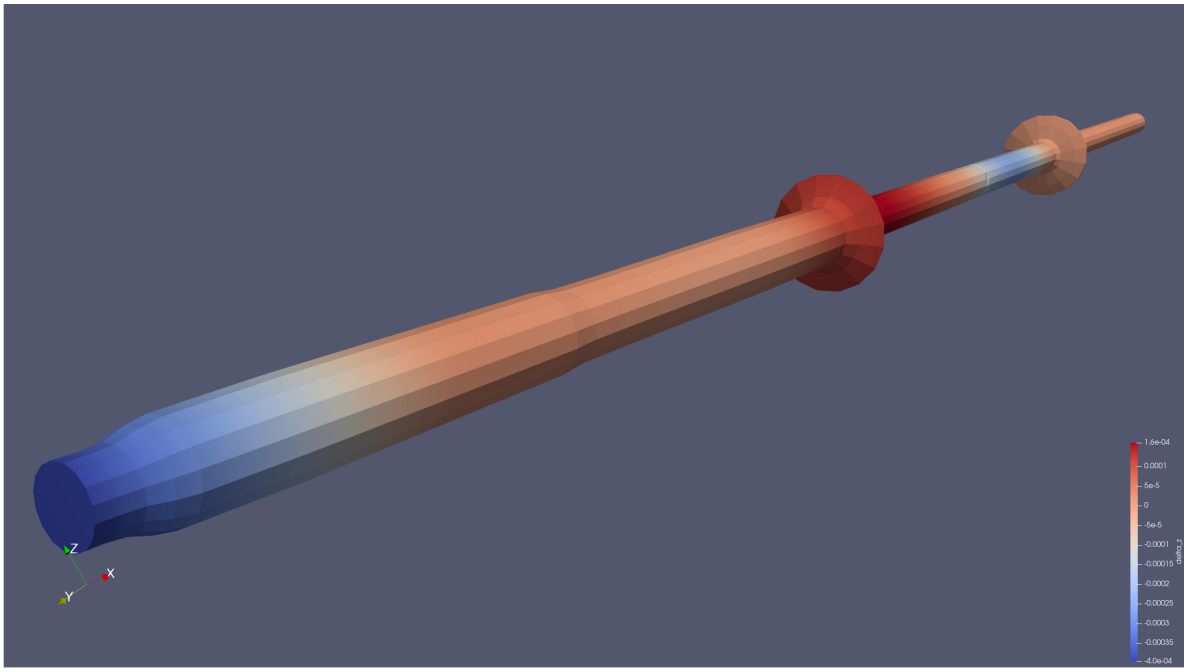

Figure 78: Delta Z for Constant Torque in timestep 55, t=0.55s

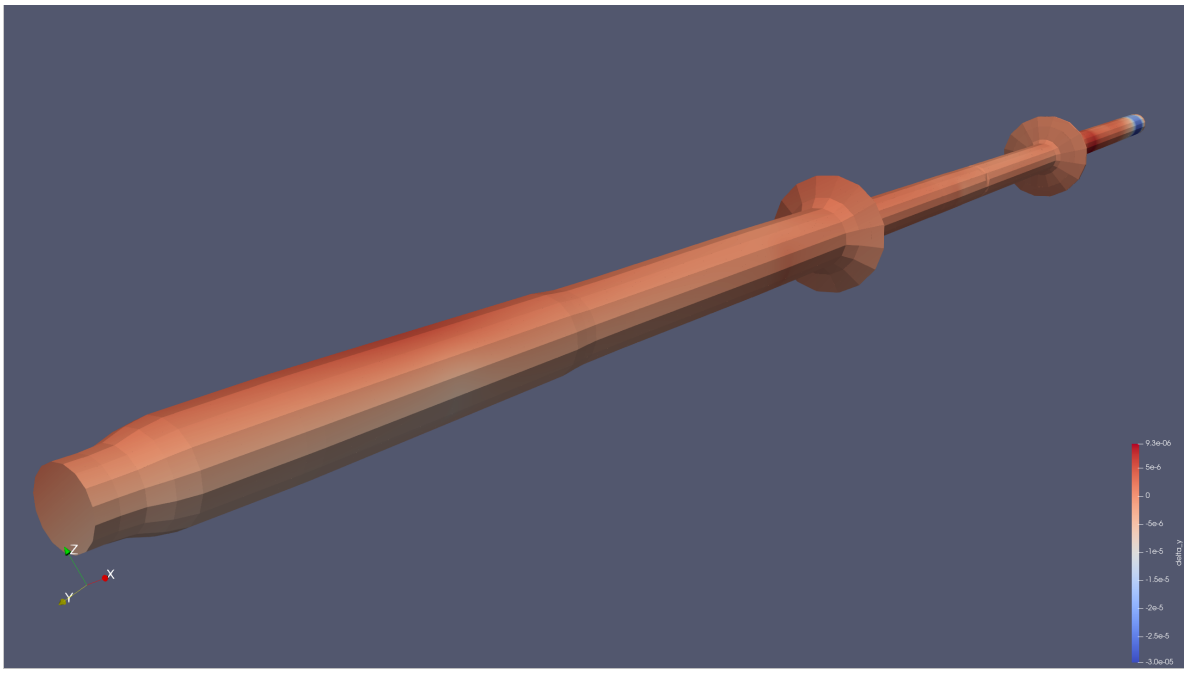

Figure 79: Delta Y for Constant Torque in timestep 55, t=0.55s

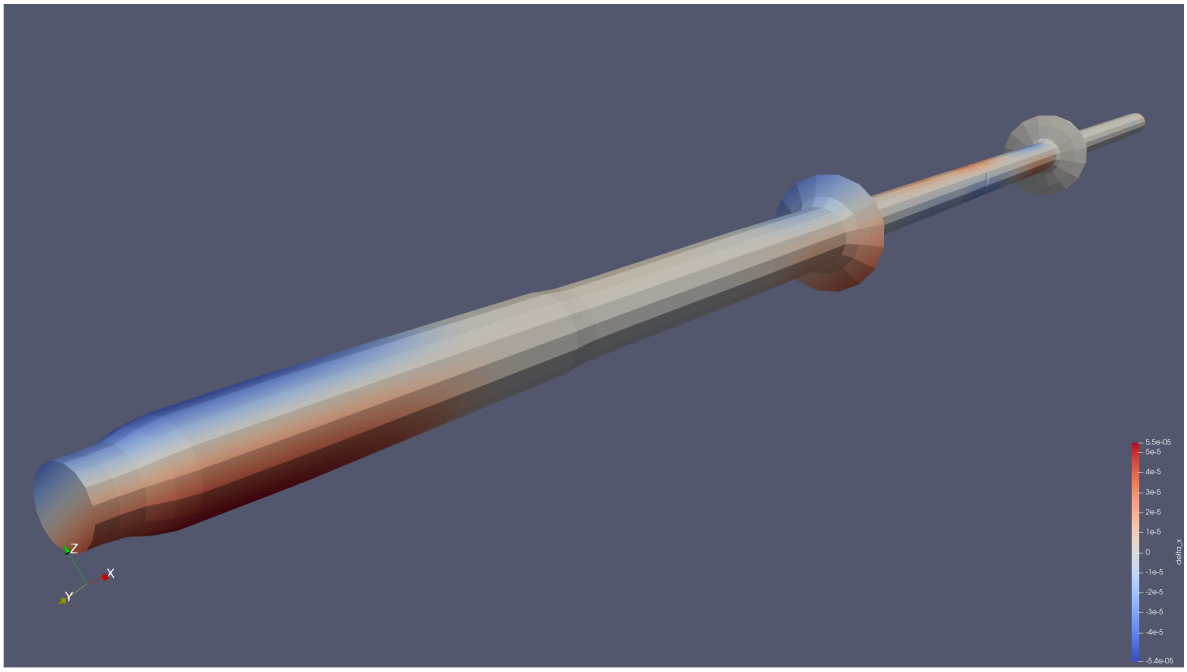

Figure 80: Delta X for Constant Torque in timestep 55, t=0.55s

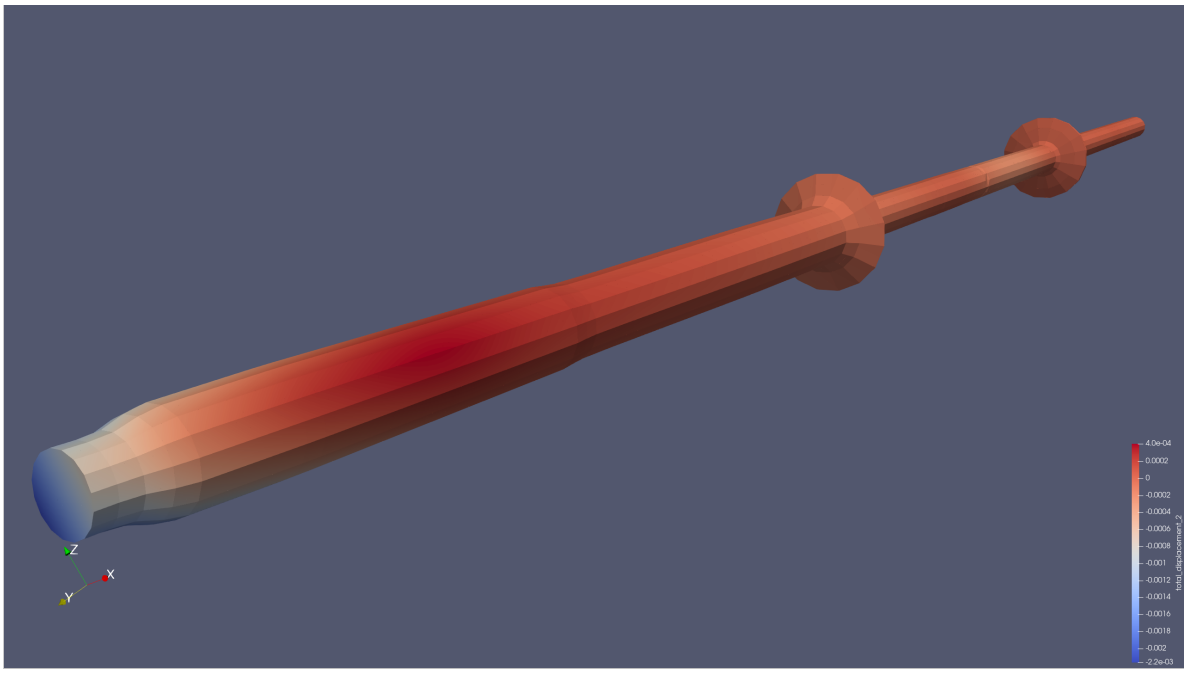

Figure 81: Total Delta Z for Constant Torque in timestep 55, t=0.55s

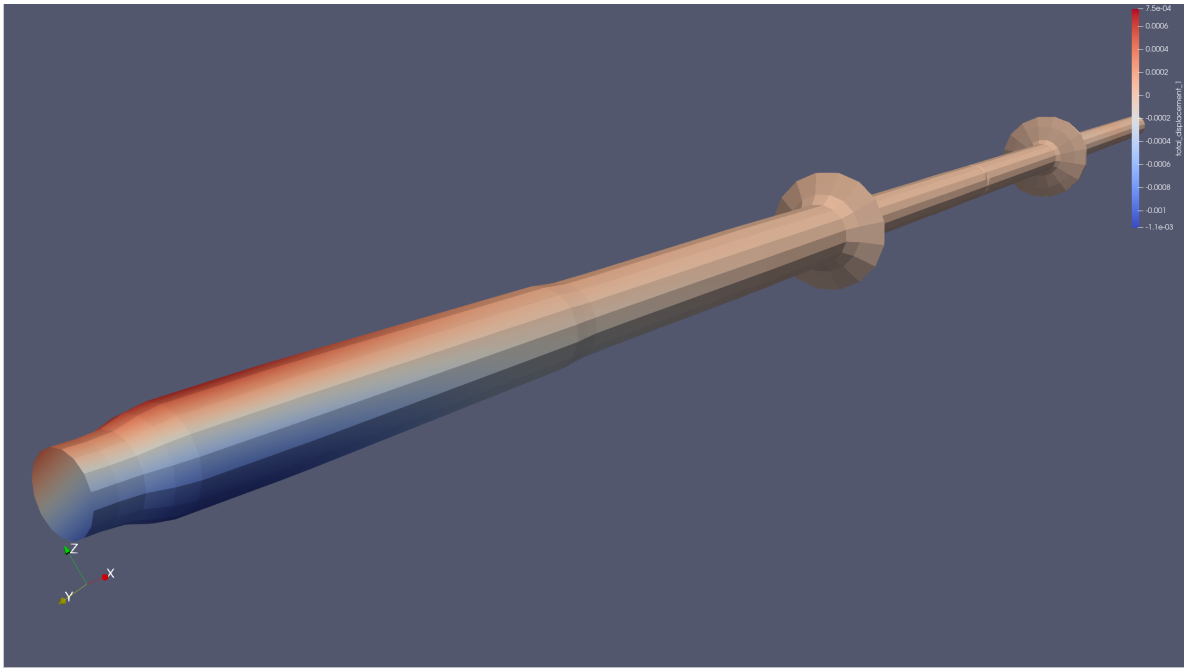

Figure 82: Total Delta Y for Constant Torque in timestep 5, t=0.55s

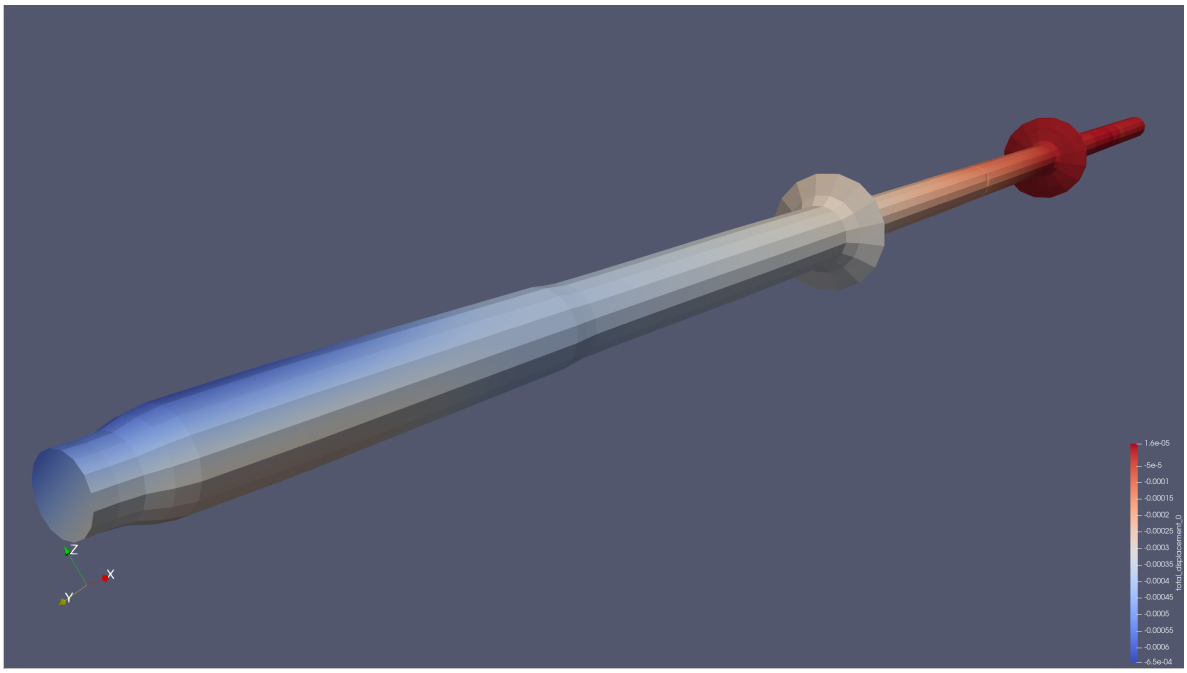

Figure 83: Total Delta X for Constant Torque in timestep 55, t=0.55s

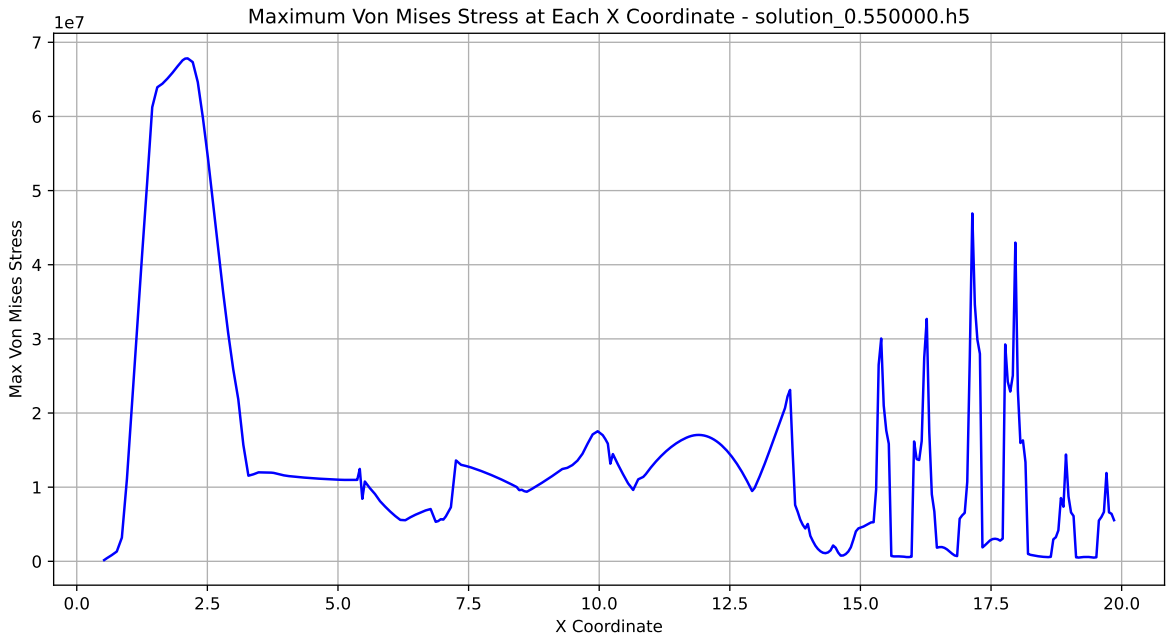

Figure 84: Von Mises over Length in timestep 55, t=0.55s

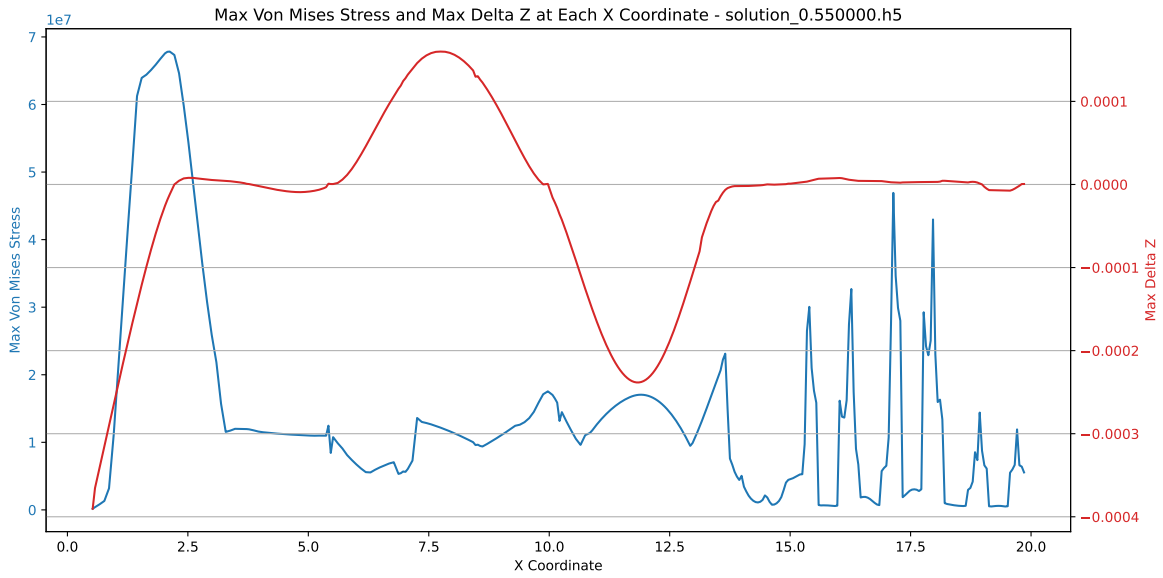

Figure 85: Delta Z over Length in timestep 55, t=0.55s

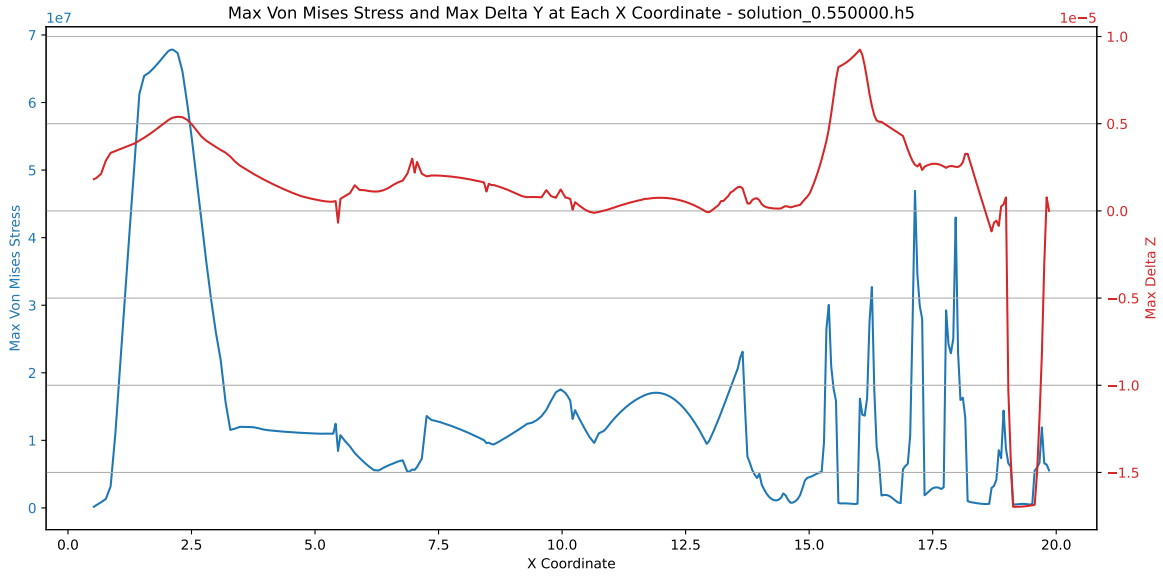

Figure 86: Delta Y over Length in timestep 55, t=0.55s

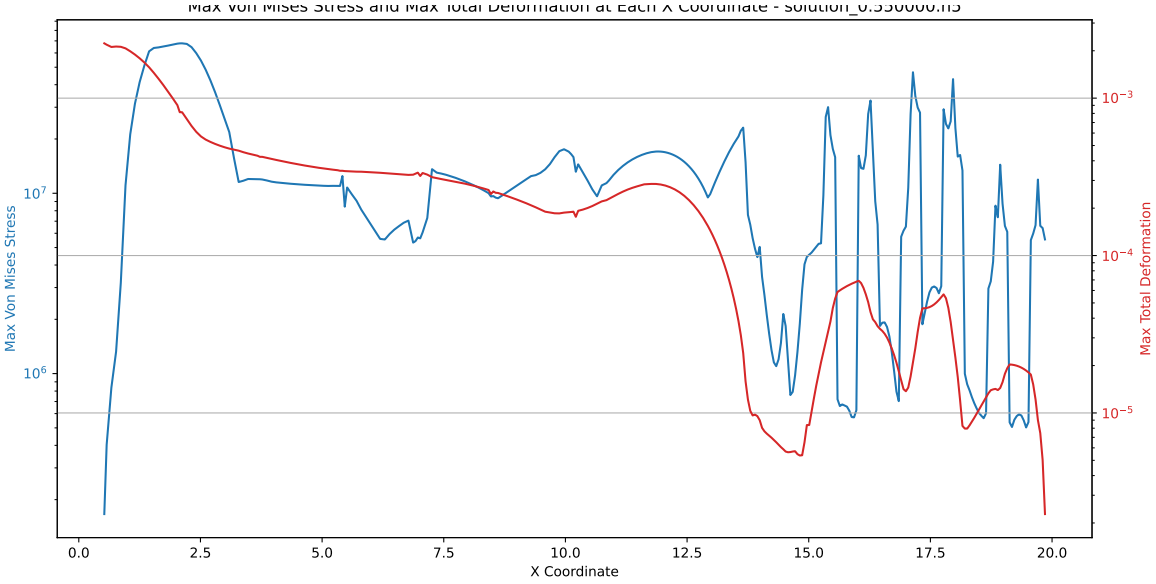

Figure 87: Displacement over Length in timestep 55, t=0.55s

Variable Torque on the Cylinders

Given the large difference in stresses between the cylinders, the refinement of the mesh was executed in comparison to the Constant Torque Case Study.

The oscillations observed on the plots, are attributed to the refinement of the mesh.This presents a difficulty for the postprocessing script, which parse through the mesh in the x axis, and so it takes into account for a small δx only points that do not belong on the perimeter, where the maximum values of the examined deformations and stresses.

Timestep=0.05s

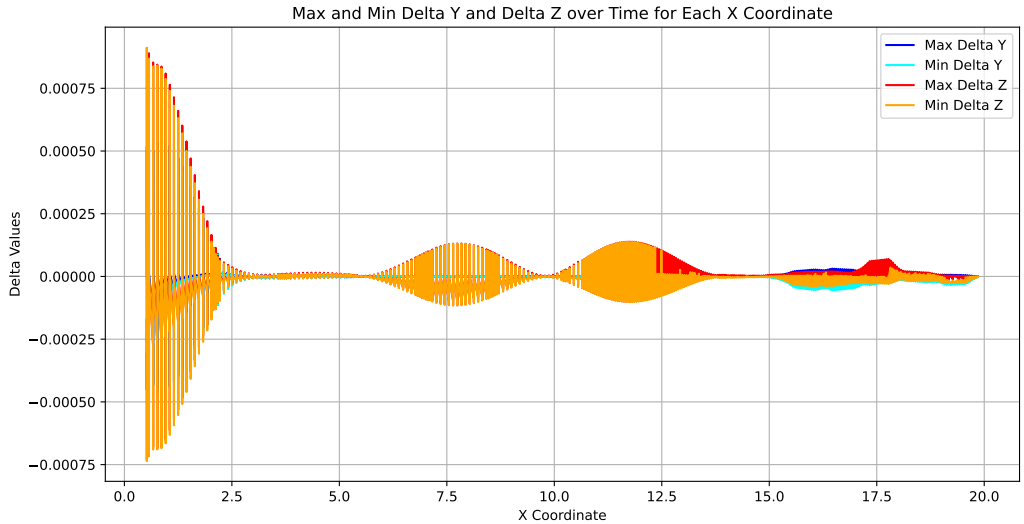

Figure 88: Range of z and y displacement for Variable Torque

Timestep=0.05s

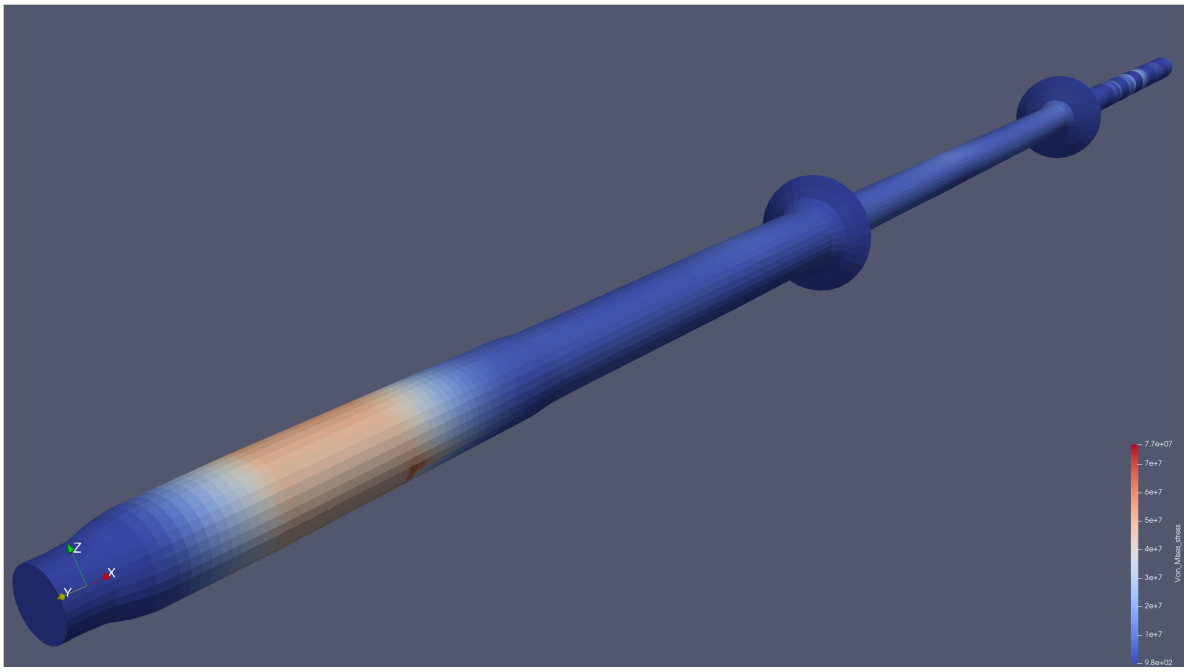

Figure 89: Von Mises for Variable Torque in timestep 5, t=0.05s

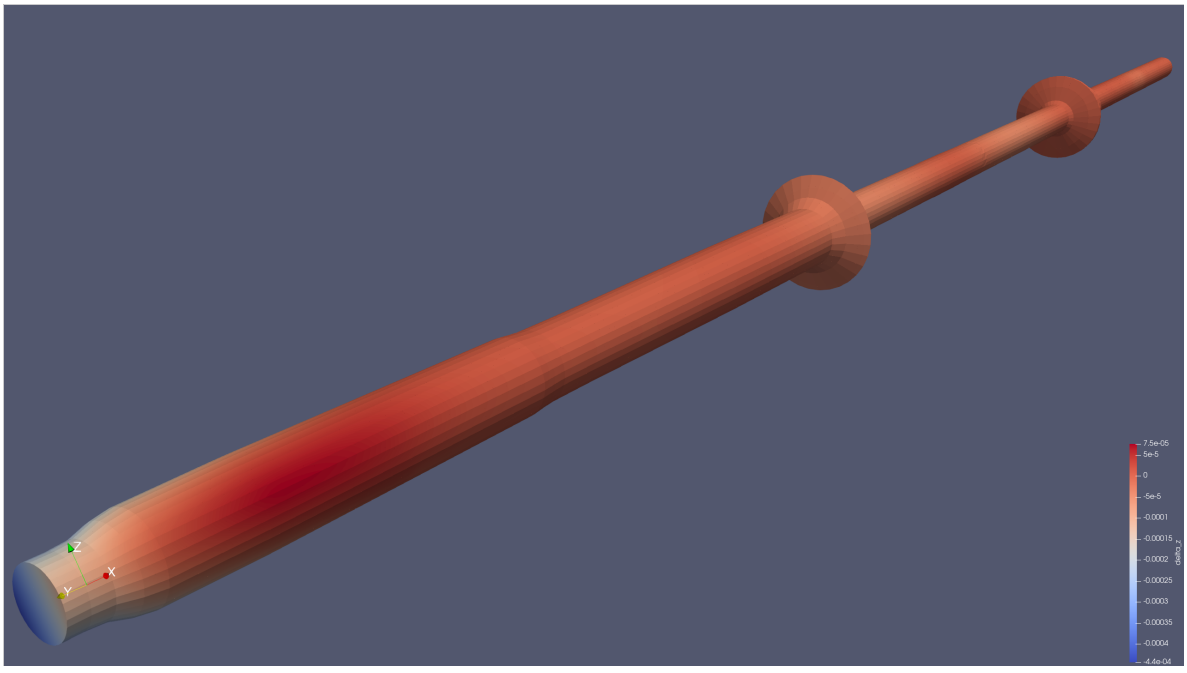

Figure 90: Delta Z for Variable Torque in timestep 5, t=0.05s

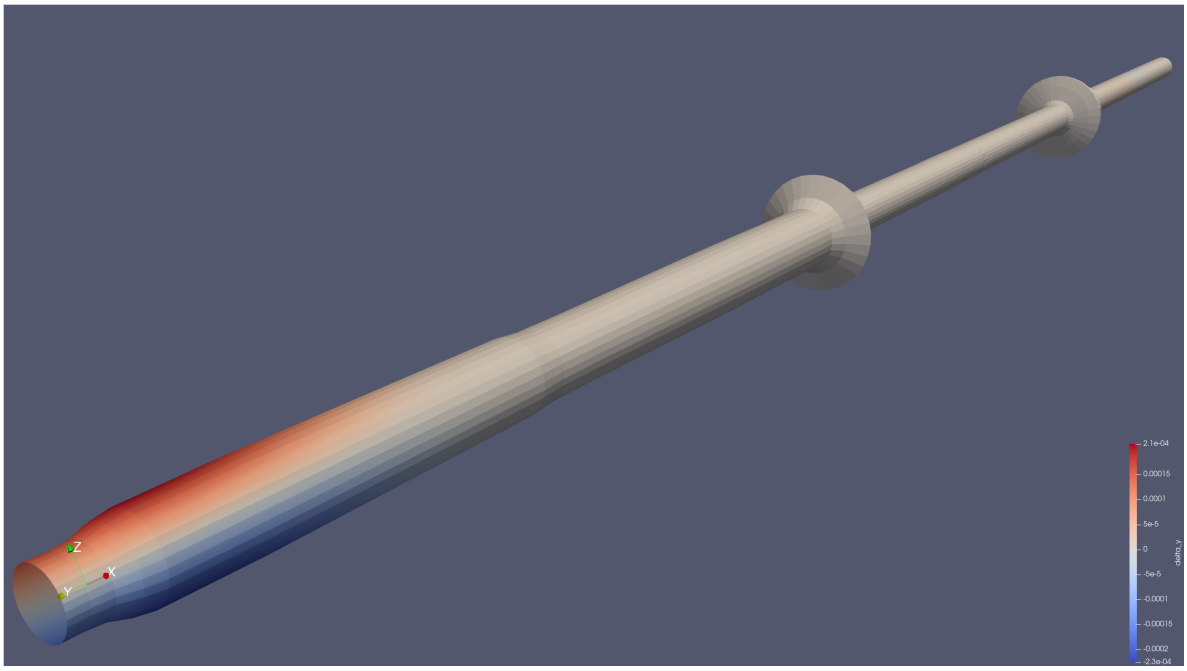

Figure 91: Delta Y for Variable Torque in timestep 5, t=0.05s

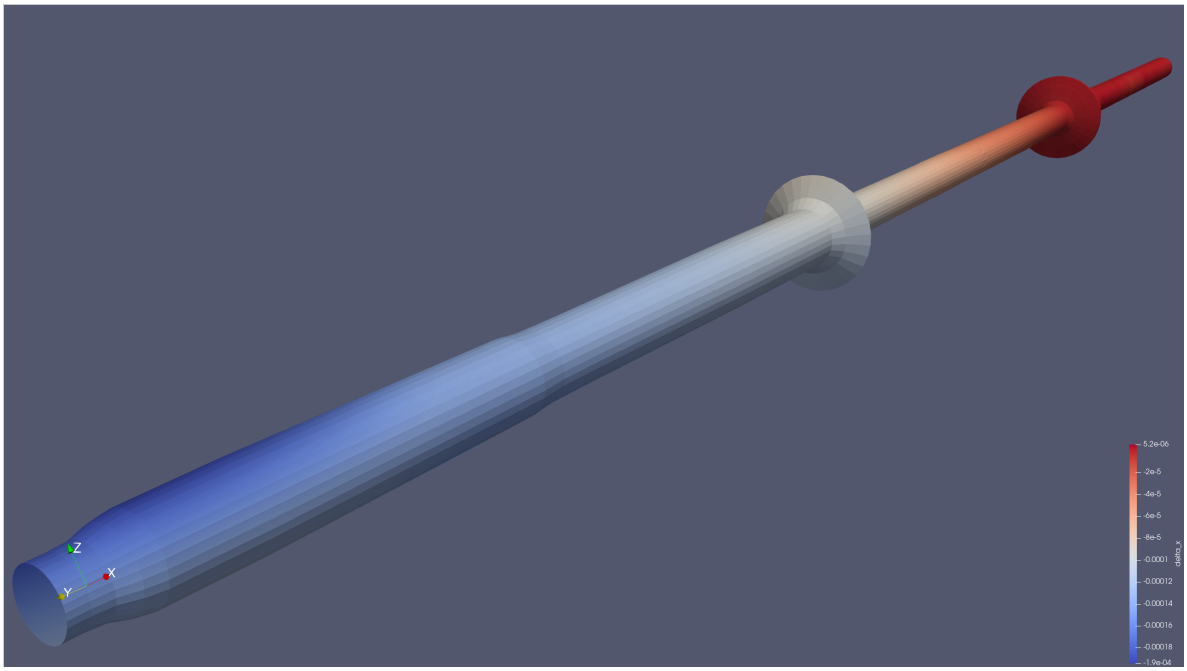

Figure 92: Delta X for Variable Torque in timestep 5, t=0.05s

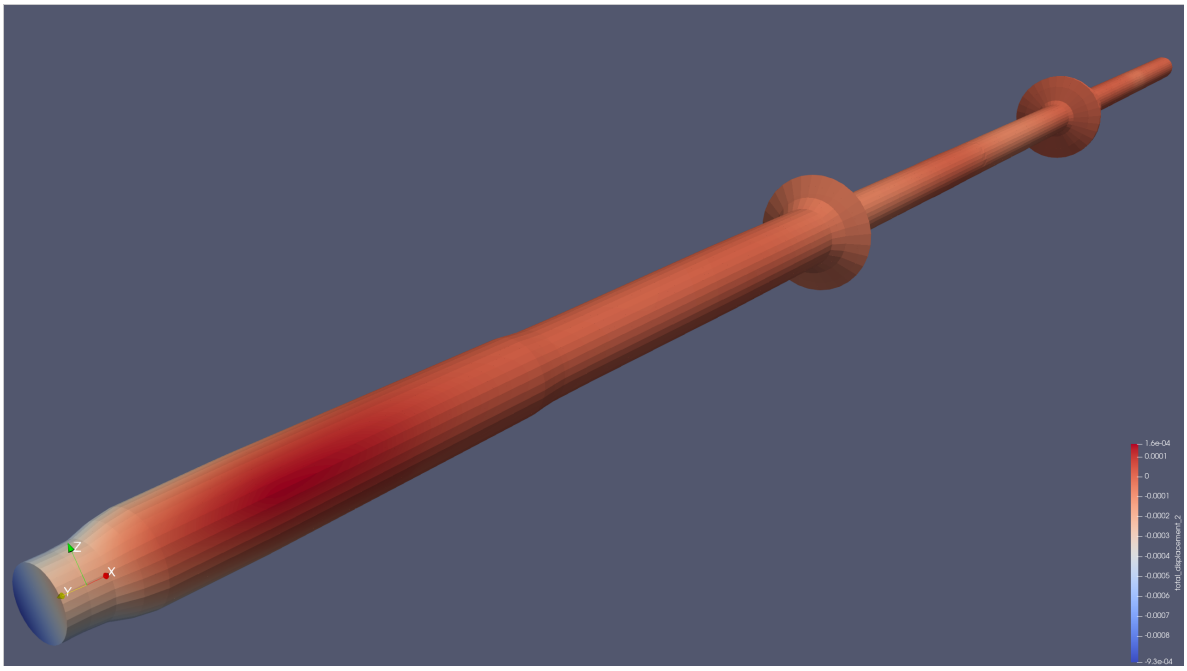

Figure 93: Total Delta Z for Variable Torque in timestep 5, t=0.05s

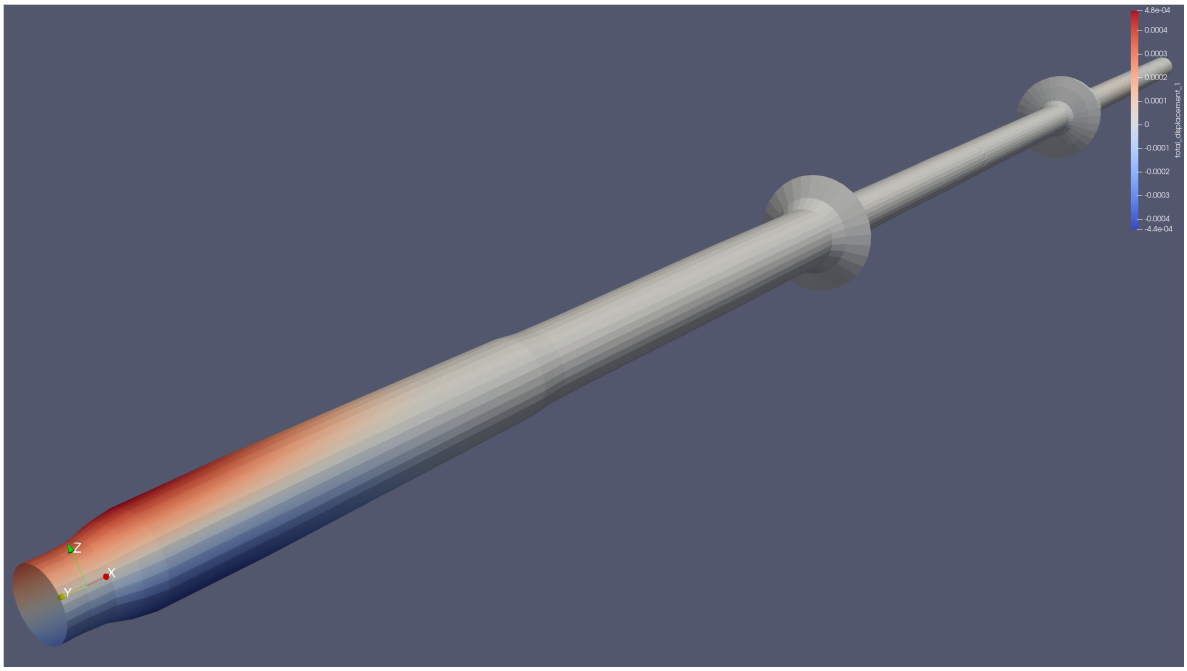

Figure 94: Total Delta Y for Variable Torque in timestep 5, t=0.05s

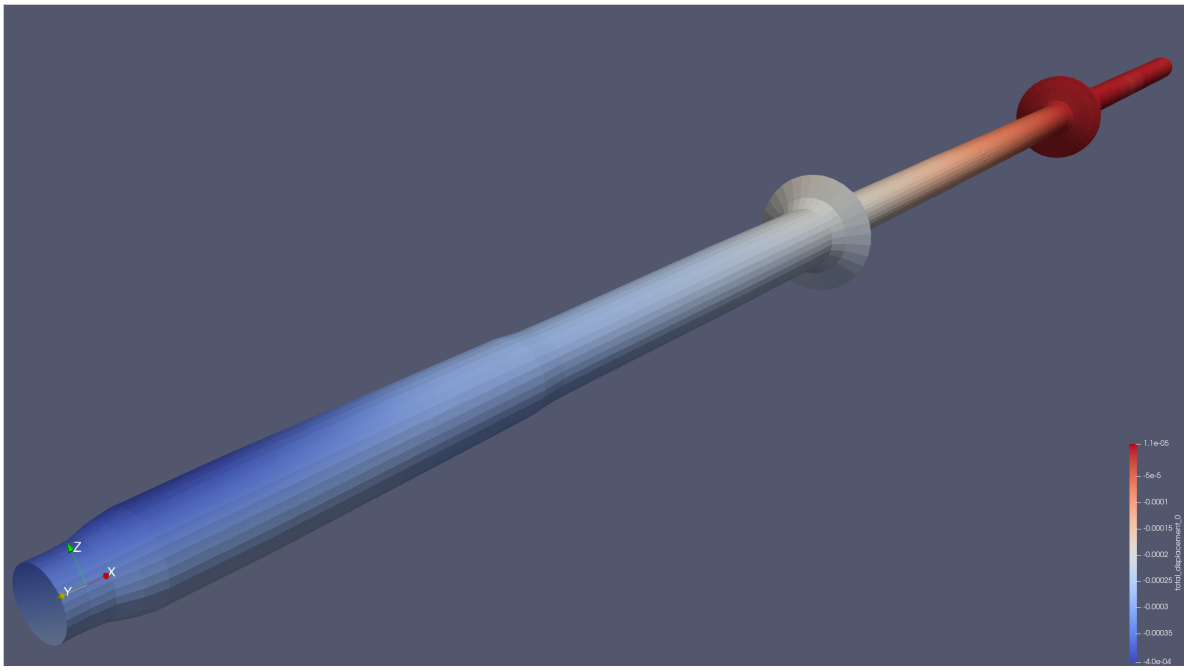

Figure 95: Total Delta X for Variable Torque in timestep 5, t=0.05s

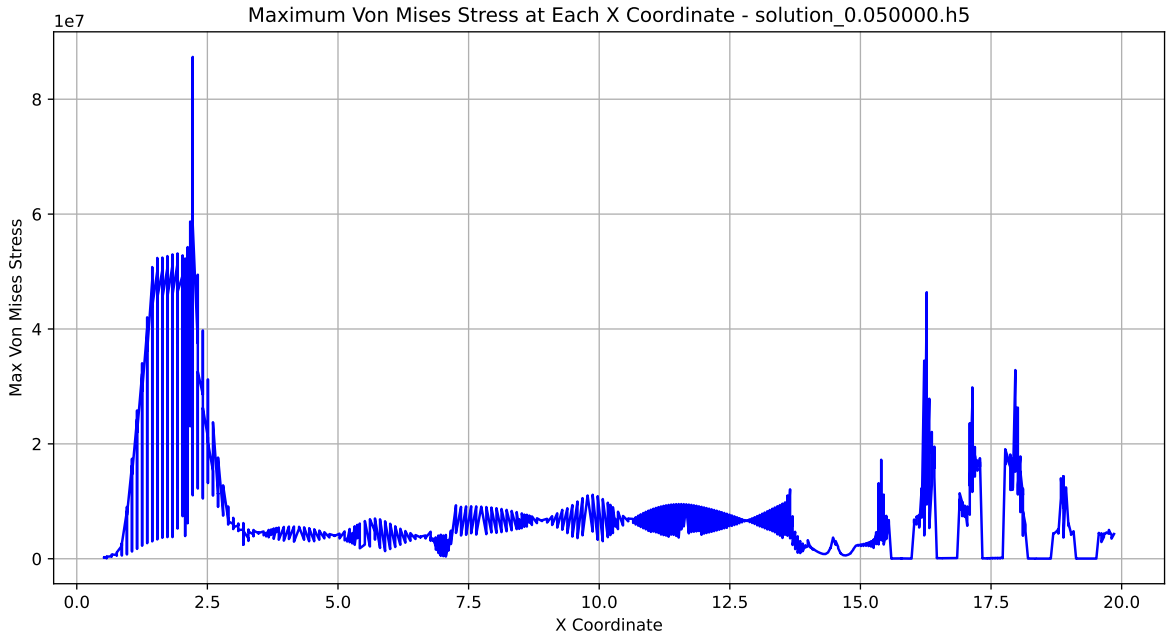

Figure 96: Von Misses Stress over Length for Variable Torque in timestep 5, t=0.05s

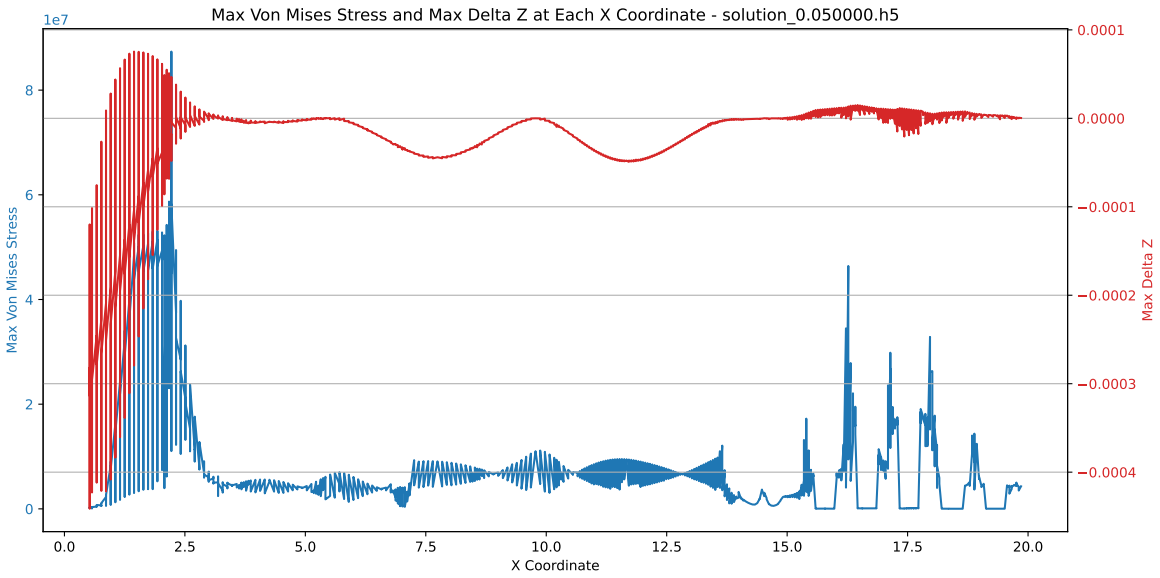

Figure 97: Delta Z over Length for Variable Torque in timestep 5, t=0.05s

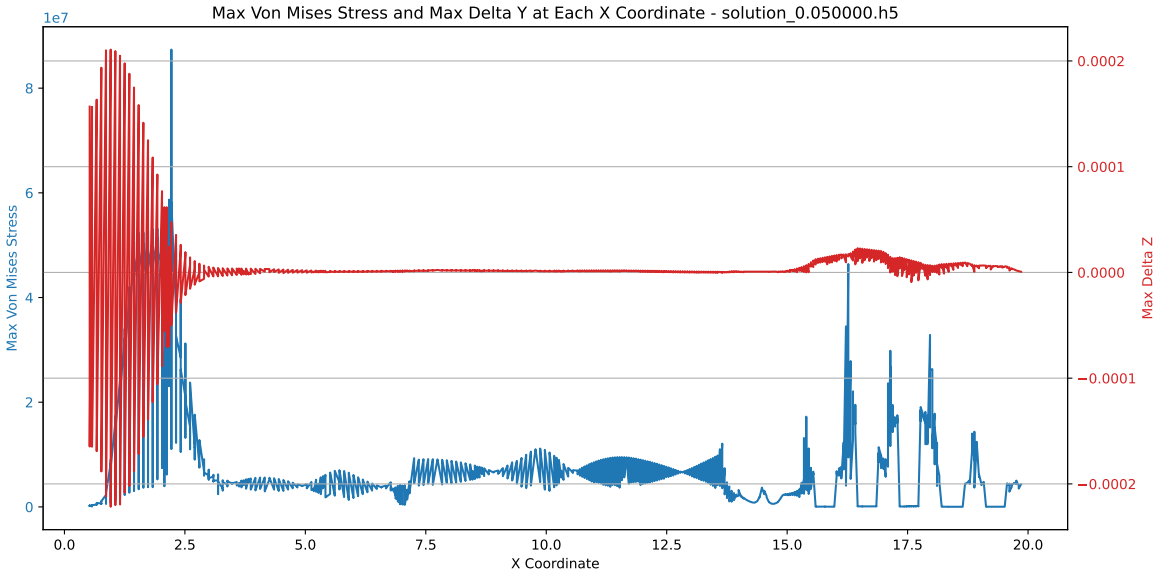

Figure 98: Delta Y over Length for Variable Torque in timestep 5, t=0.05s

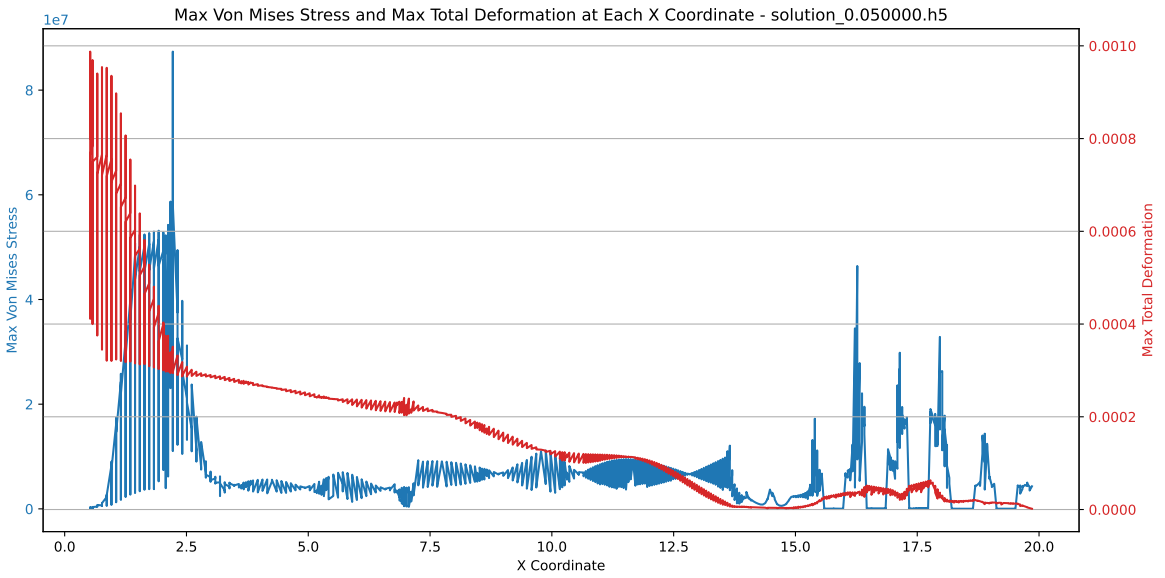

Figure 99: Displacement over Length for Variable Torque in timestep 5, t=0.05s

Timestep=1.5s Steady State of System

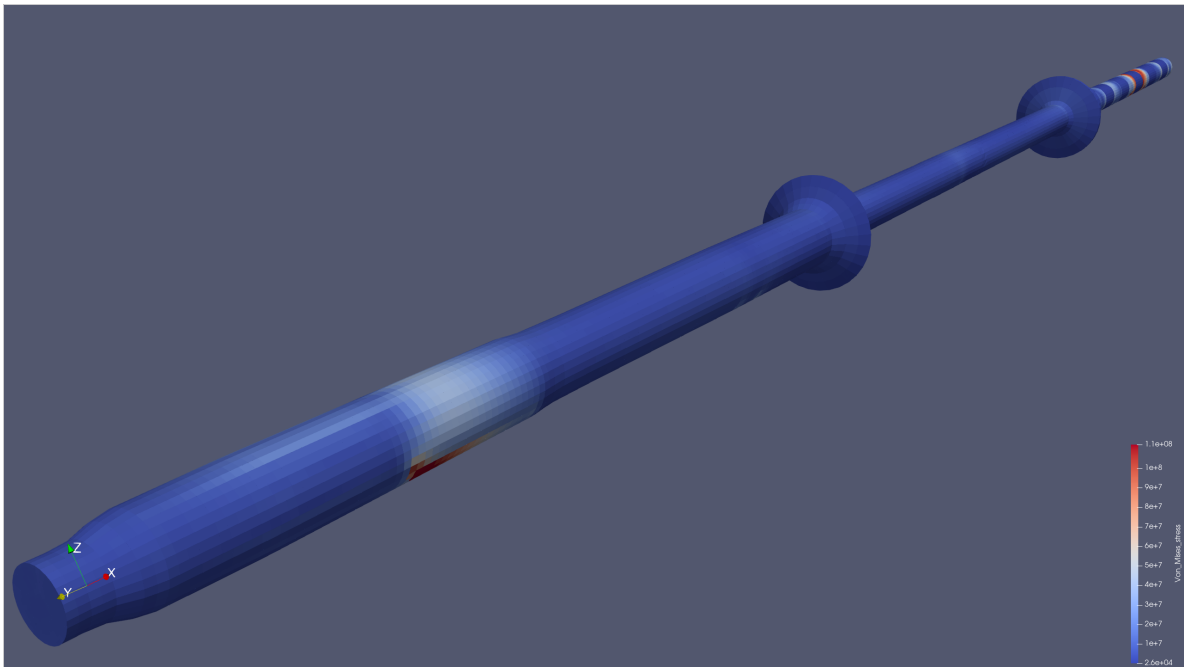

Figure 100: Von Mises for Constant Torque for Variable Torque in timestep 150, t=1.50s

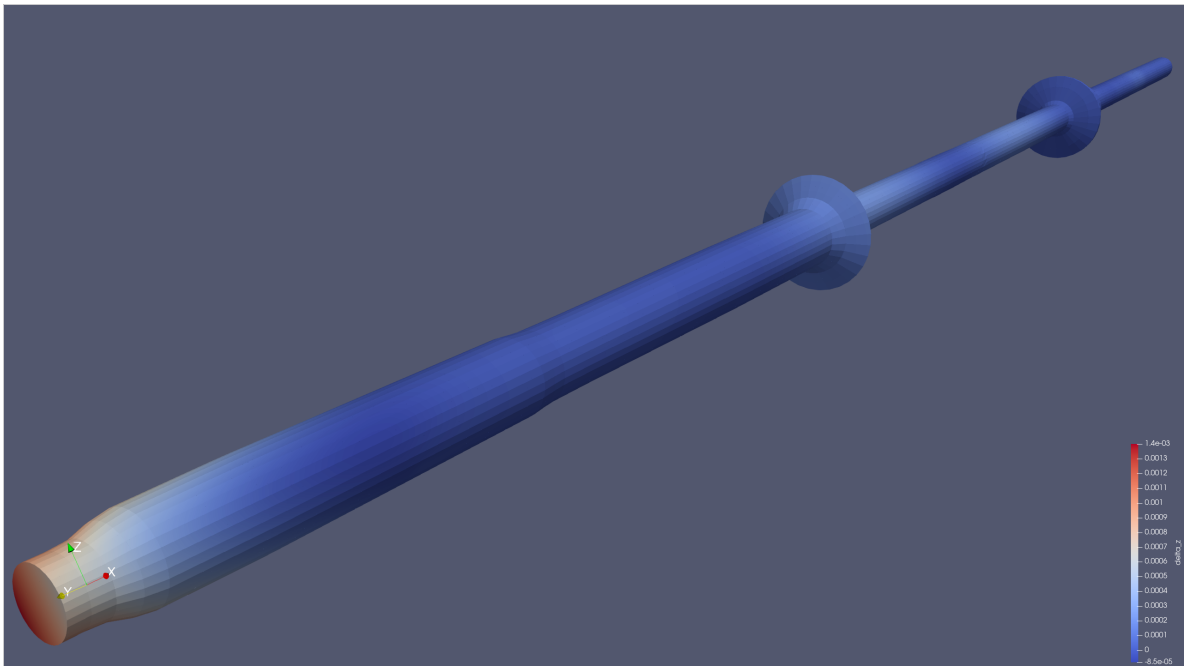

Figure 101: Delta Z for Variable Torque in timestep 150, t=1.50s

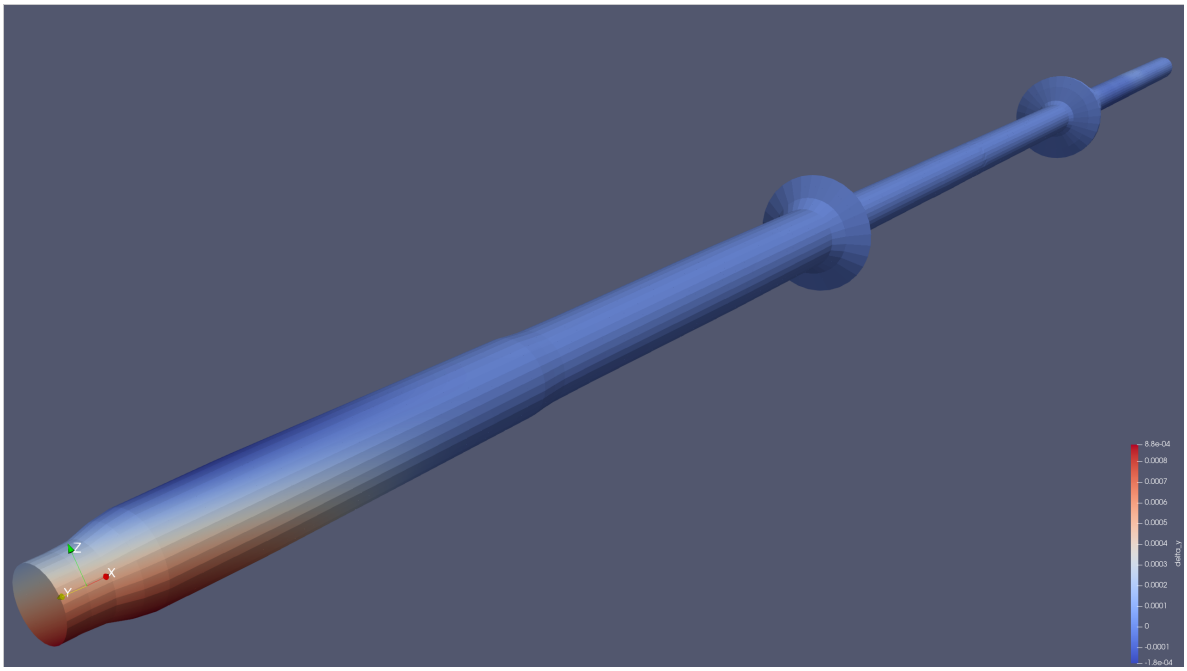

Figure 102: Delta Y for Variable Torque in timestep 150, t=1.50s

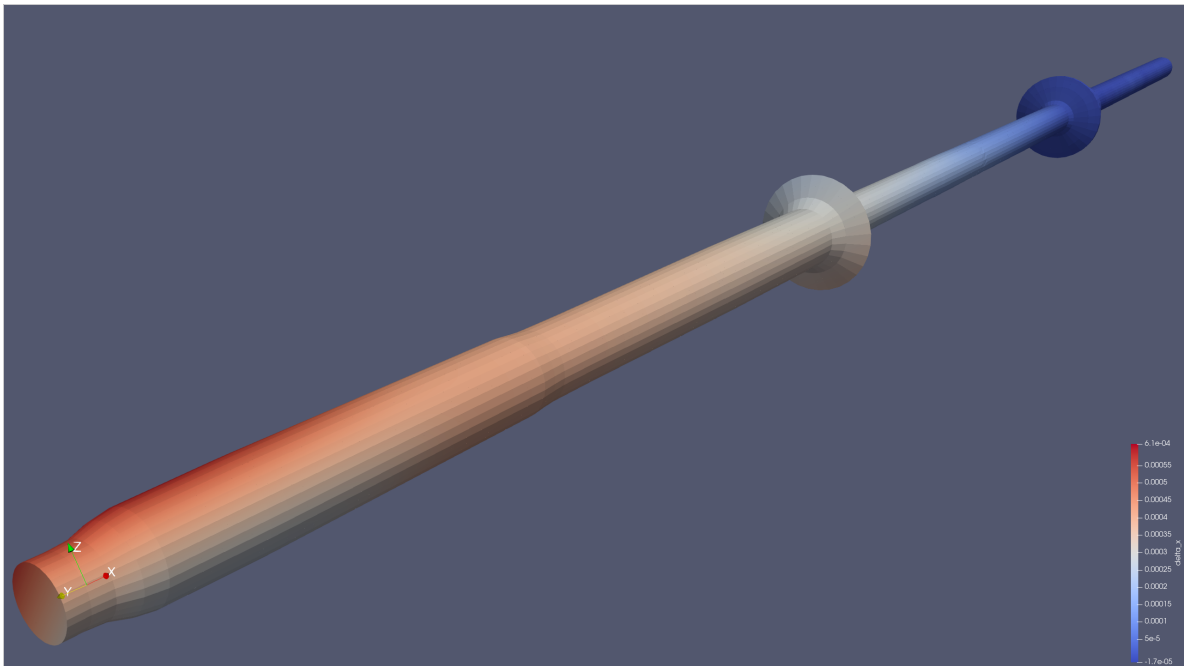

Figure 103: Delta X for Variable Torque in timestep 150, t=1.50s

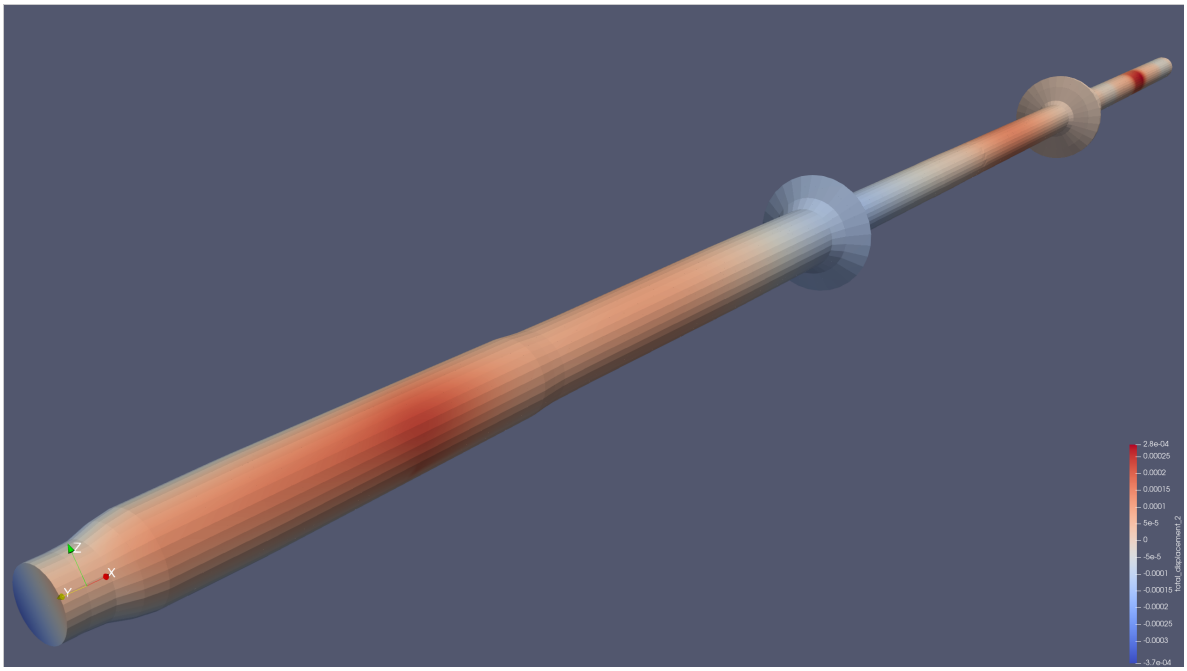

Figure 104: Total Delta Z for Variable Torque in timestep 150, t=1.50s

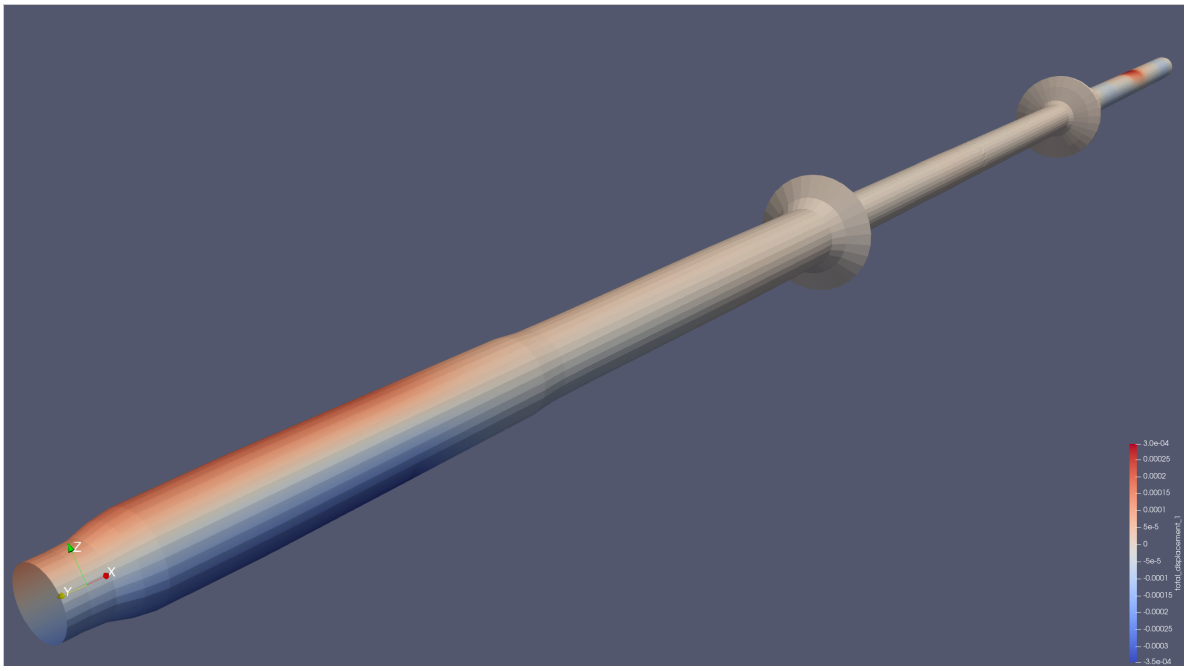

Figure 105: Total Delta Y for Variable Torque in timestep 150, t=1.50s

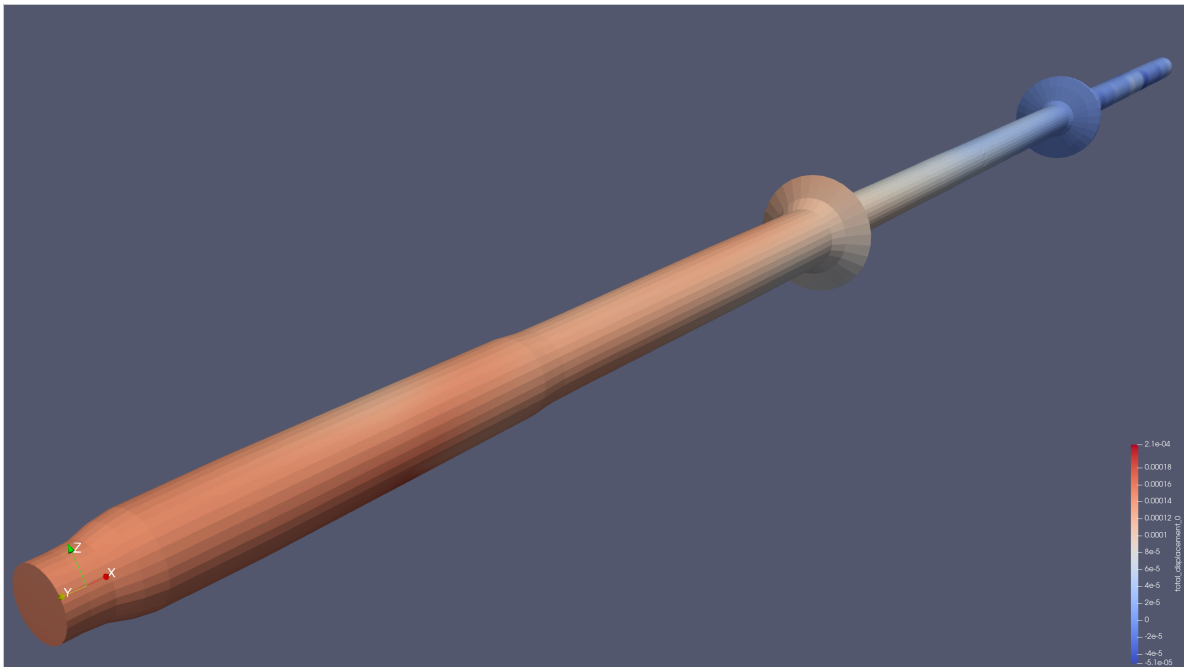

Figure 106: Total Delta X for Variable Torque in timestep 150, t=1.50s

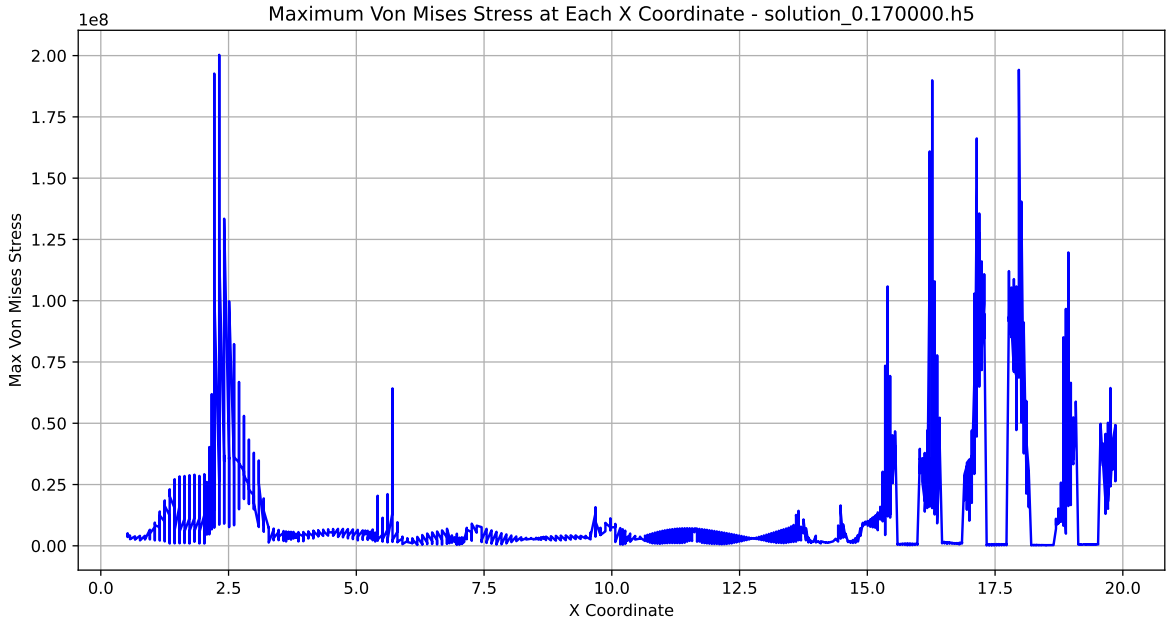

Figure 107: Von Mises over Length Variable Torque in timestep 150, t=1.50s

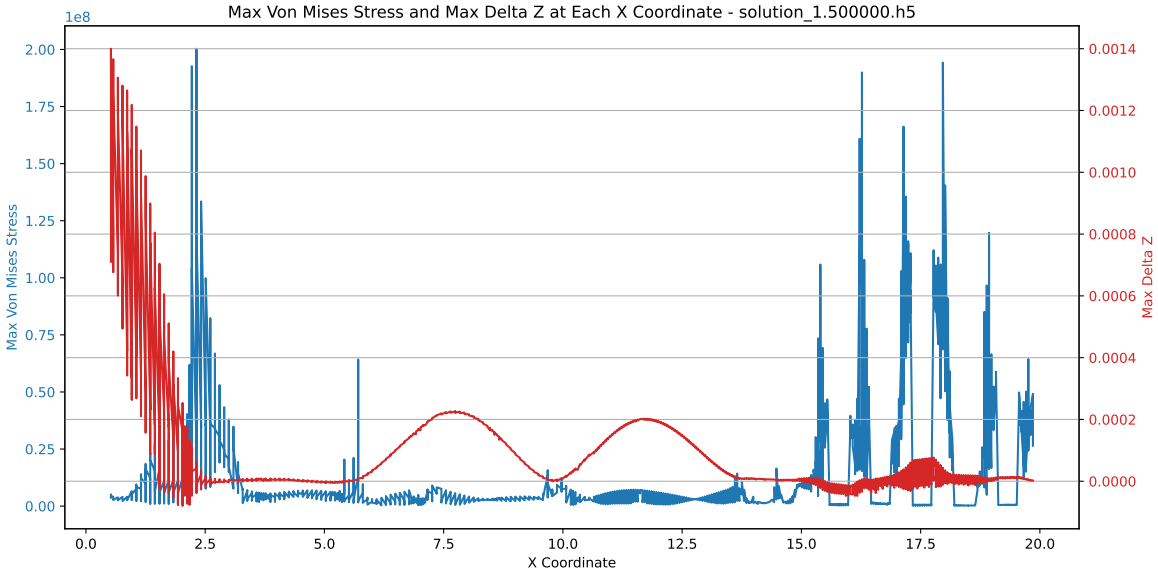

Figure 108: Delta Z over Length Variable Torque in timestep 150, t=1.50s

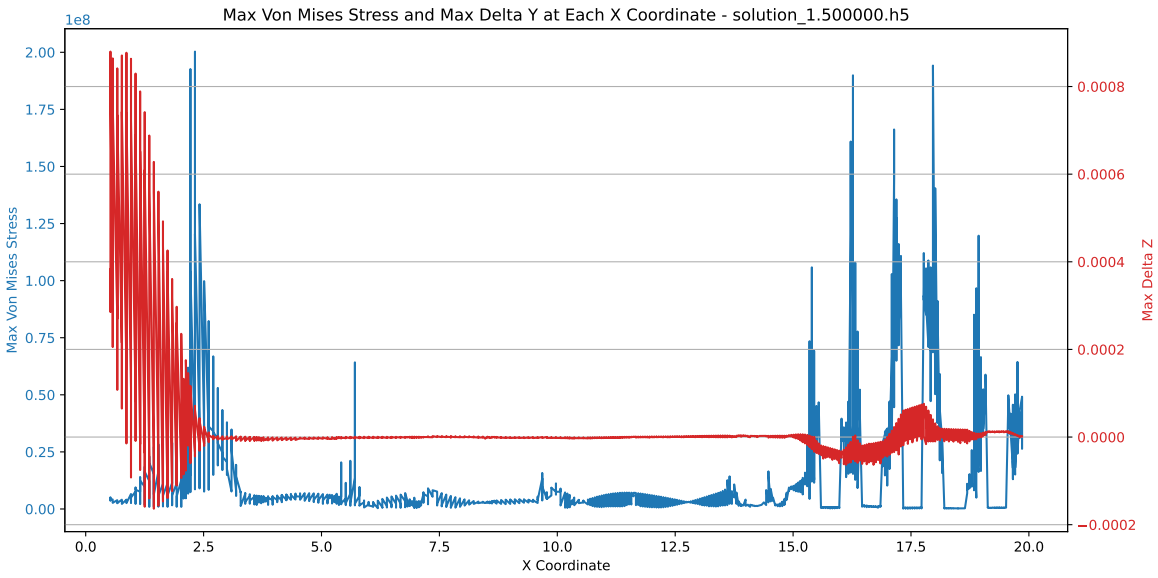

Figure 109: Delta Y over Length Variable Torque in timestep 150, t=1.50s

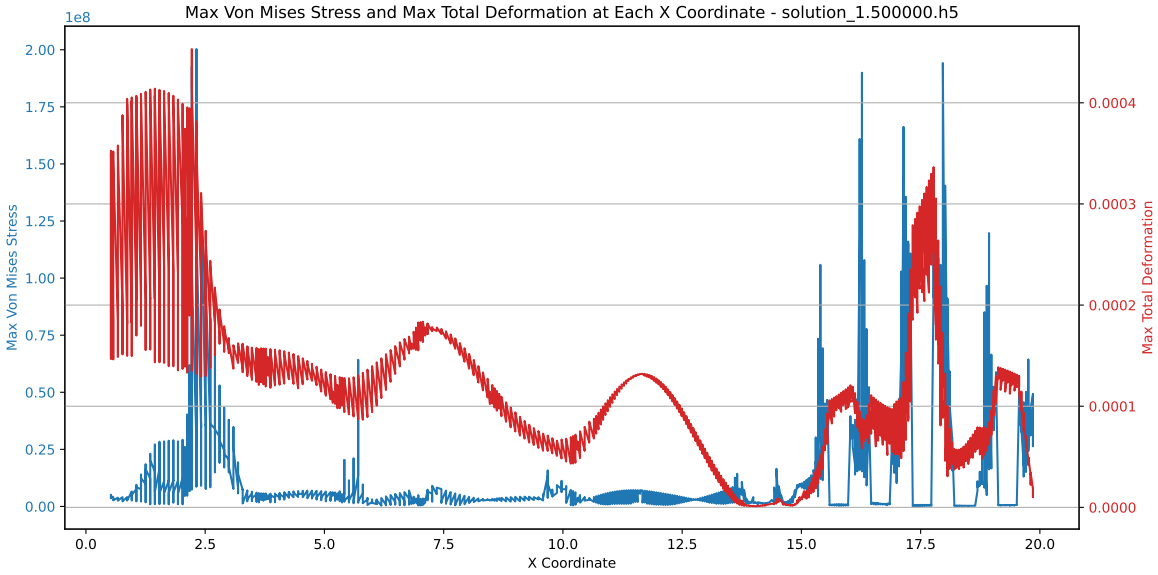

Figure 110: Displacement over Length Variable Torque in timestep 150, t=1.50s

7.3.2 Comments on the Results

The plots presented above, especially the figs. 97 and 108, portrait the maximum deformation in the vertical axis (red curve) and the maximum Von Mises Stress produced (blue curve) at each point of the x axis of the shafting system. These lead to the following conclusions:

- The maximum stress is developed at the end of the sterntube (x Coordinate=2.5m)
- The maximum stress developed due to the variable torque at each cylinder is significant, but due to the fact that the full geometry of the crankshaft is not used here, these high values could be erroneous and should be validated
- The maximum deformation occurs at the tip of the propellershaft, while the internal deformation of the engine is significant and should be accounted for, but also further studies should take place, as noted above

- The flywheel (x Coordinate=15m) flattens the deformations resulting from the engine, as demonstrated by figs. 108 and 109
- It is noted that all the Stresses are either maximum or momentary, and the fatigue from any oscillation in the stresses values is not considered in this study, although for the complete overview of the shafting system's structural behavior it should be calculated, as it will be a big factor in a possible failure of the material.

7.4 Eigenvalues Analysis

In this subsection the results of the eigenvalues calculation are presented. The focus will be on the lateral oscillations, which will be compared to the eigenmodes and eigenvalues provided by the Lateral Vibration Manual for the shafting system used as reference in this study.

Firstly, the eigenvalues position in the eigenspectrum will be discussed and then the produced eigenmodes will be compared to the provided ones.

The Eigenmodes presented are normalized to one.

7.4.1 Eigenvalues

	Calculation			
Eigenvalue #	rad/s	Hz	Provided[Hz]	Difference
1	55,5845	8,846547934	12	-26,28%
2	153,026	24,35484432	23,2	4,98%
3	208,99	33,26179156	29,1	14,30%
4	233,773	37,20612851	30,6	21,59%
5	249,844	39,7639076		
6	271,104	43,14754169		
7	287,905	45,82150389		
8	409,488	65,17203934		
9	445,275	70,86771729		
10	463,859	73,82545275		

Table 7.1: Eigenvalues Comparison for the Case Study

7.4.2 Eigenmodes

In this subsection the Comparison of the Eigenmodes will thake place first and then the total eigenmodes calculated will be presented.

1st Eigenmode

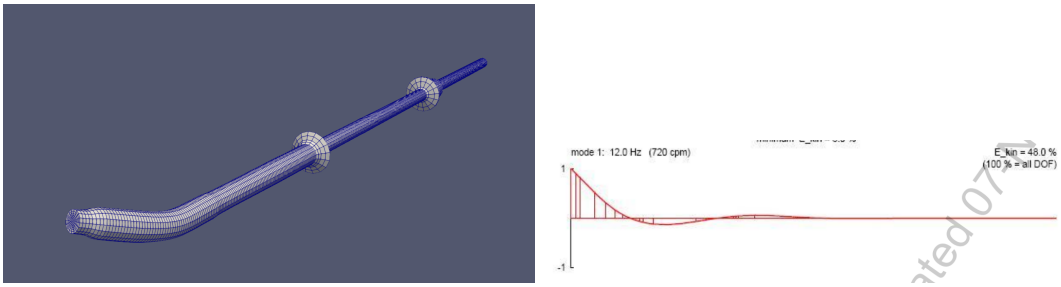

Figure 111: 1st Eigenmode Comparison

2nd Eigenmode

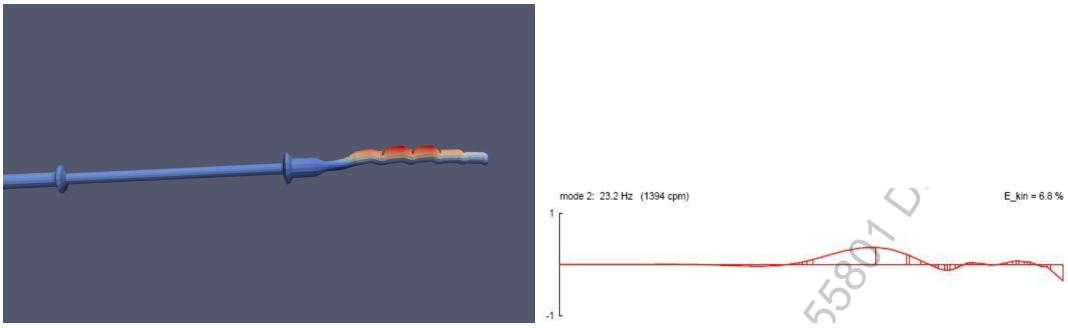

Figure 112: 2nd Eigenmode Comparison

3rd Eigenmode

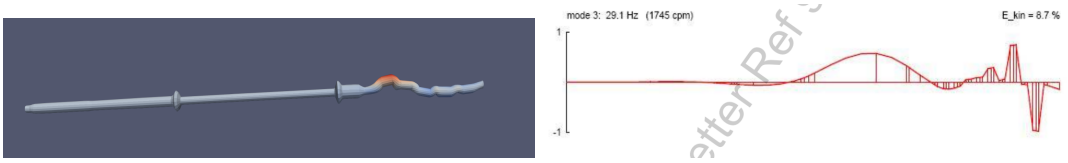

Figure 113: 3rd Eigenmode Comparison

4rth Eigenmode

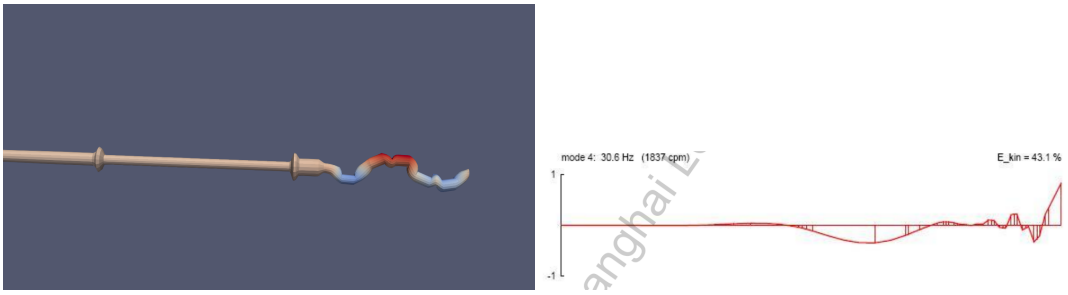

Figure 114: 4rth Eigenmode Comparison

Eigenmodes Presentation

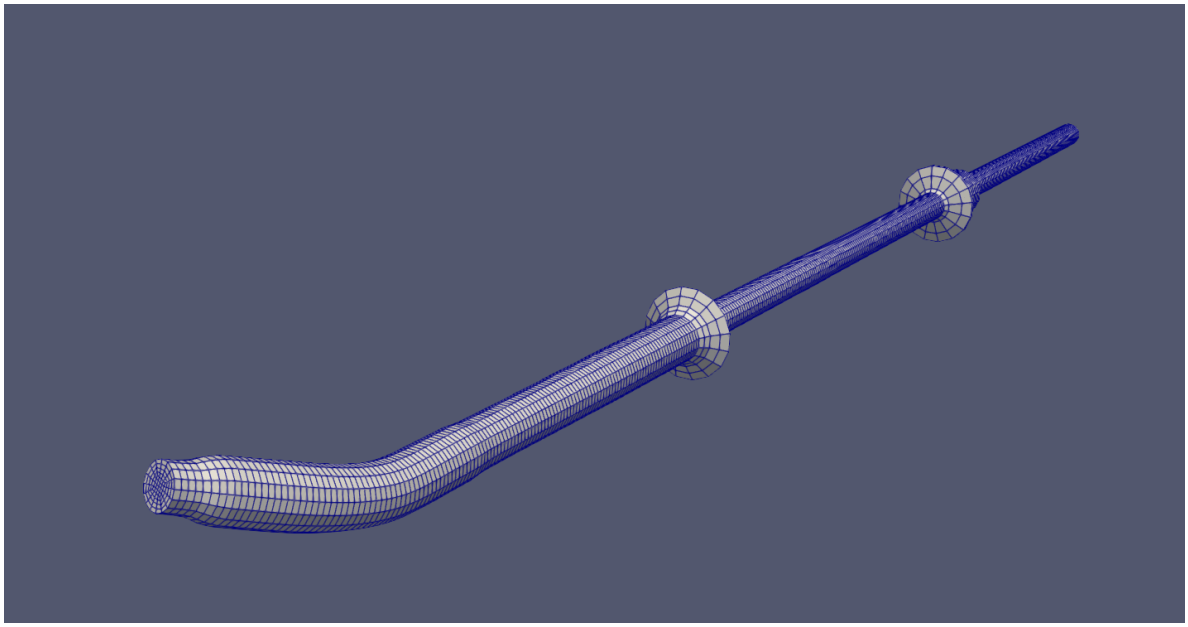

Figure 115: 1st Eigenmode

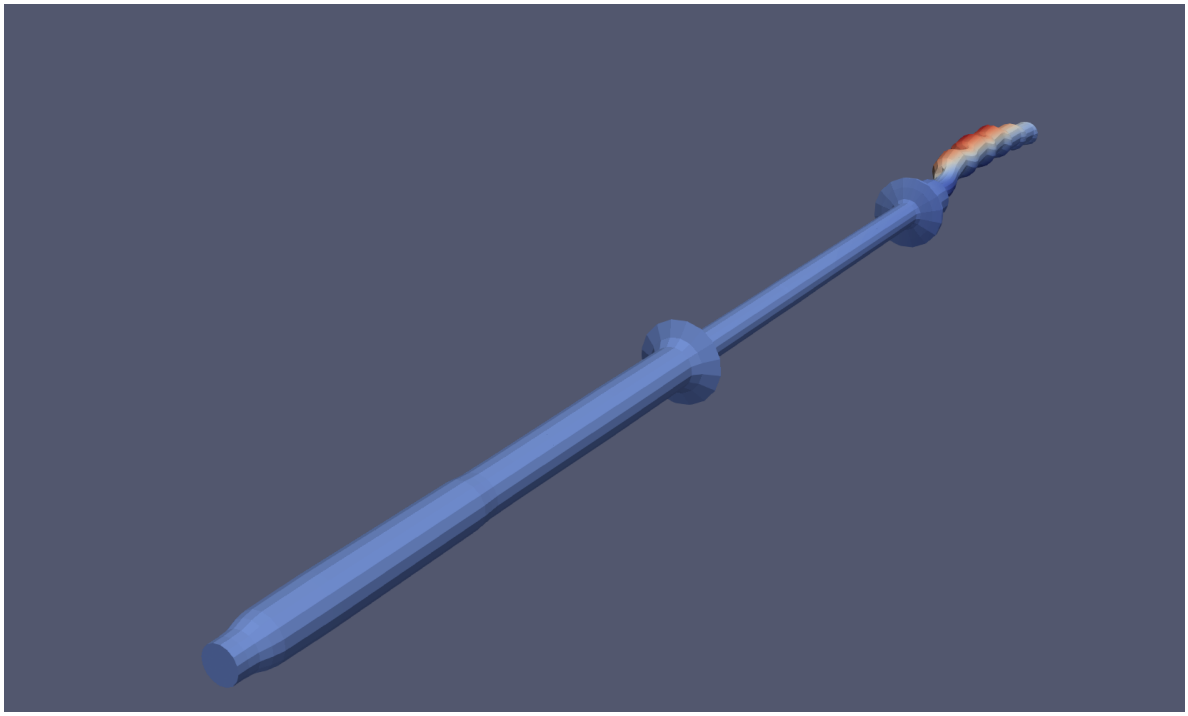

Figure 116: 2nd Eigenmode

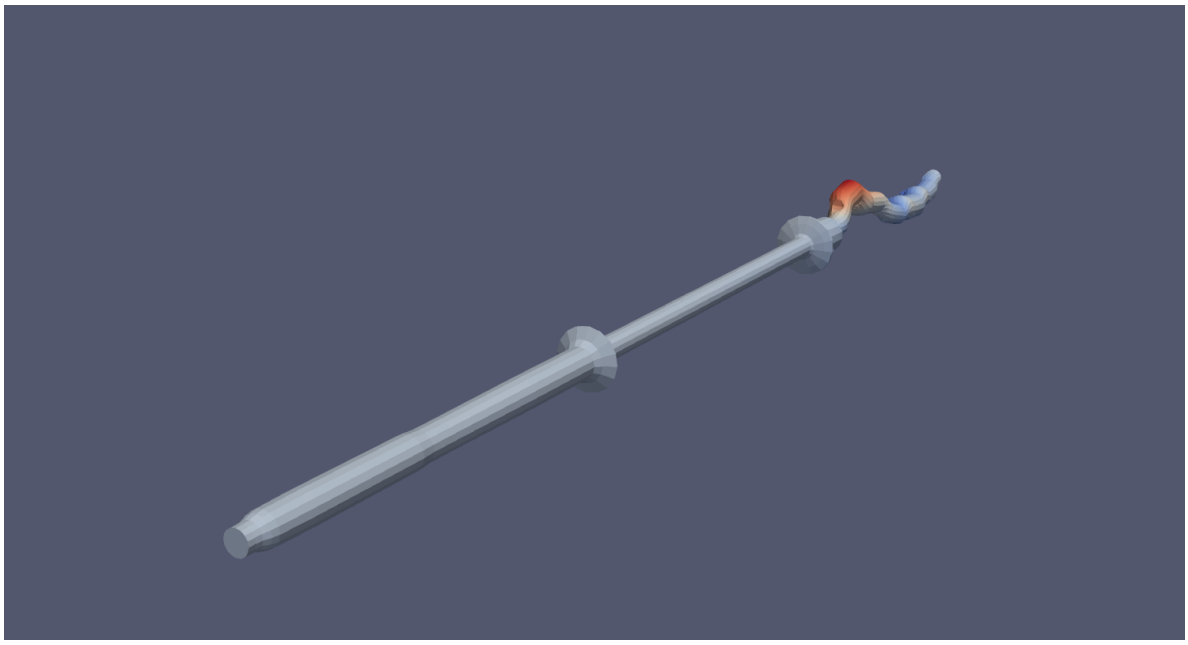

Figure 117: 3rd Eigenmode

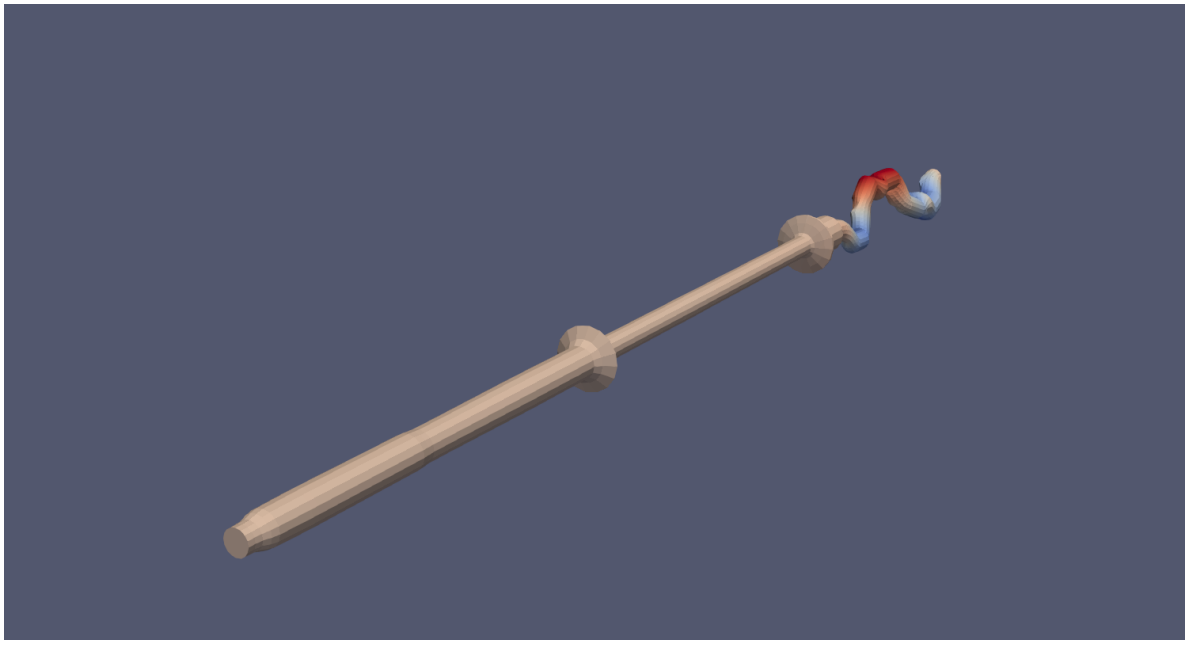

Figure 118: 4rth Eigenmode

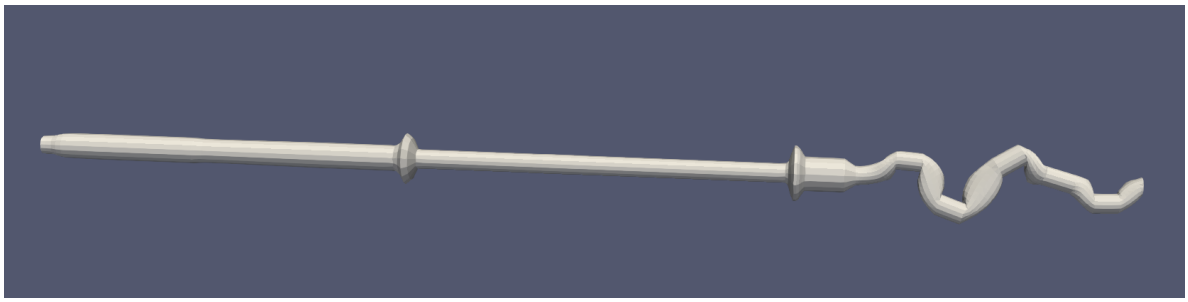

Figure 119: 5th Eigenmode

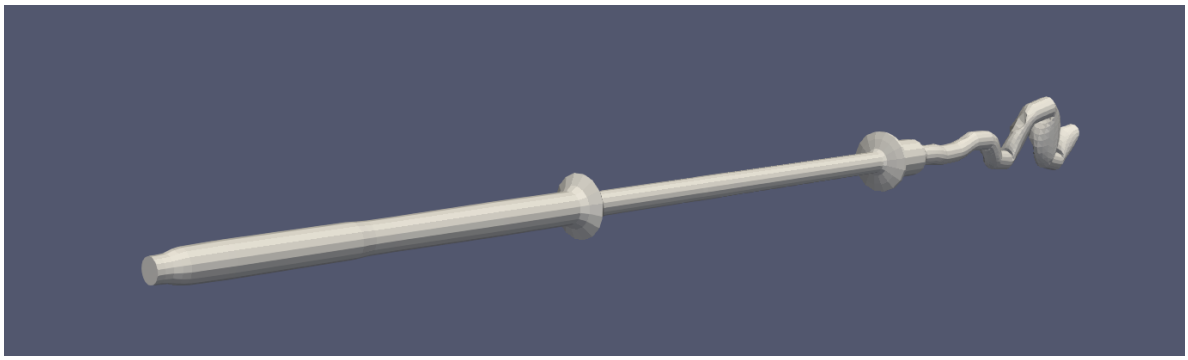

Figure 120: 6th Eigenmode

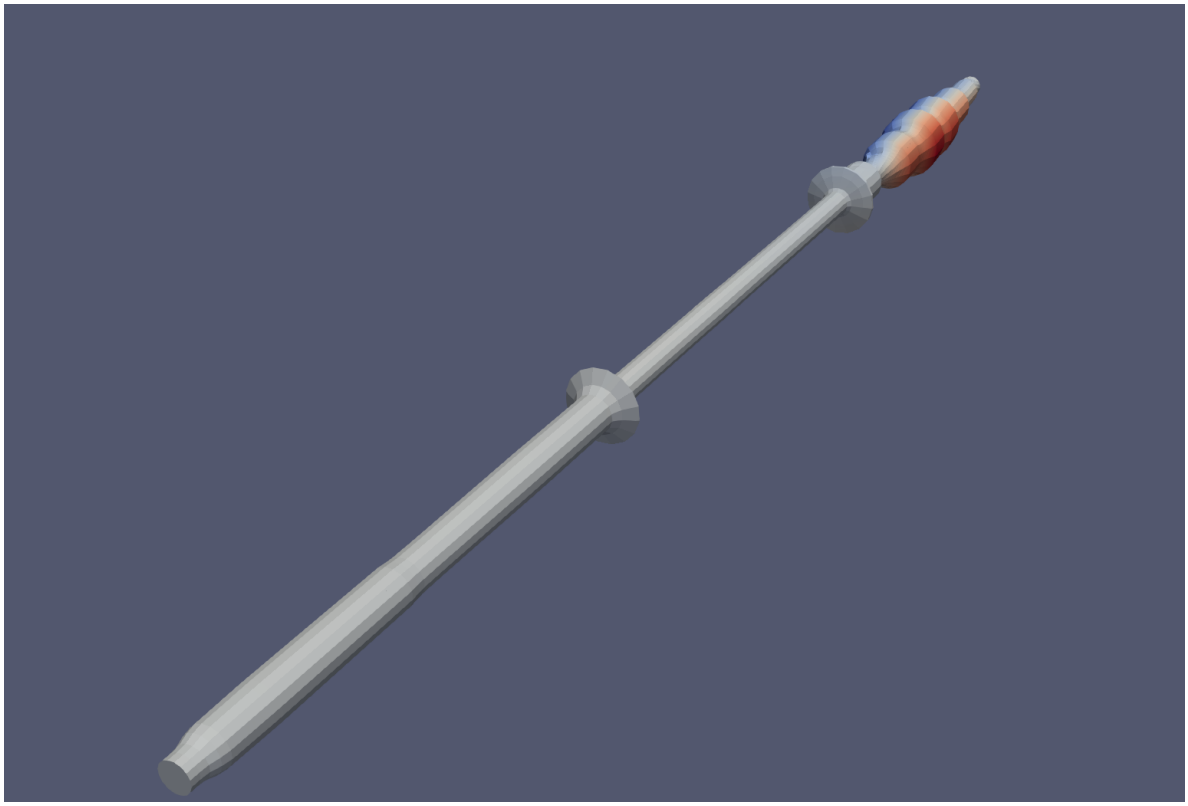

Figure 121: 7th Eigenmode

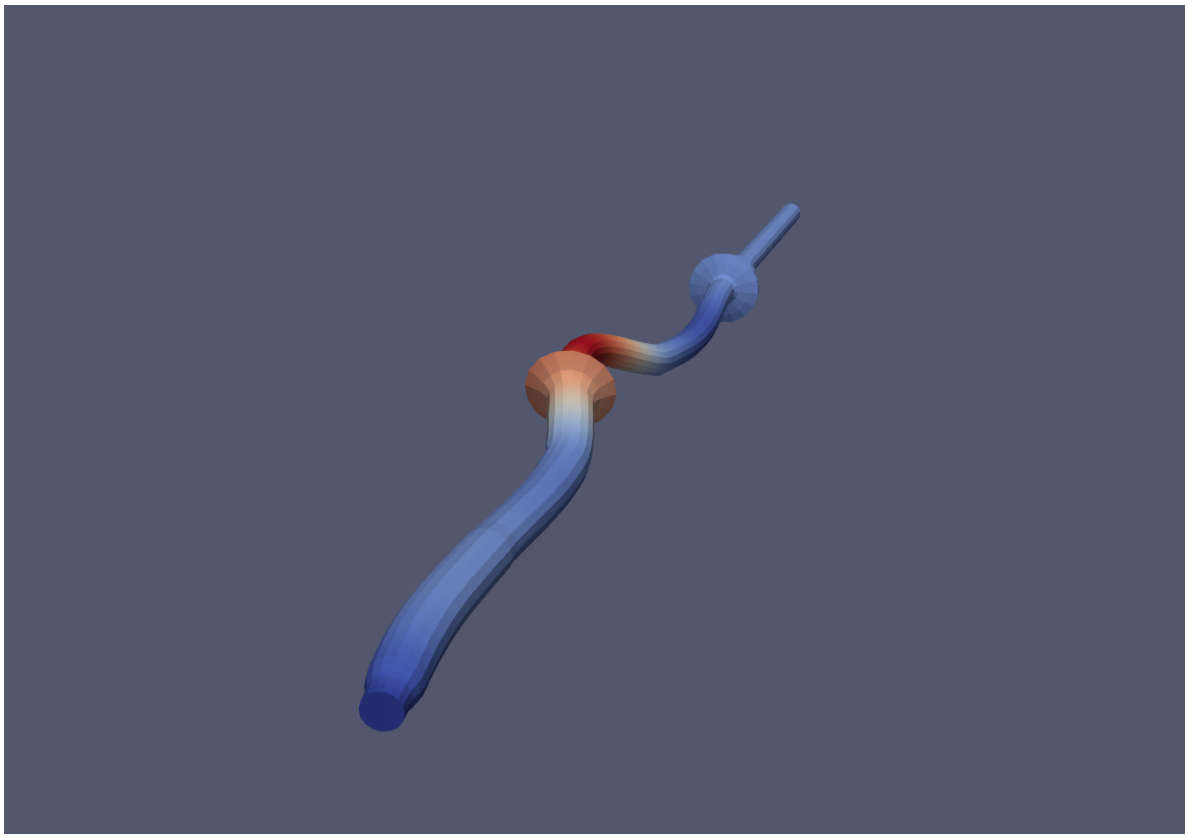

Figure 122: 8th Eigenmode

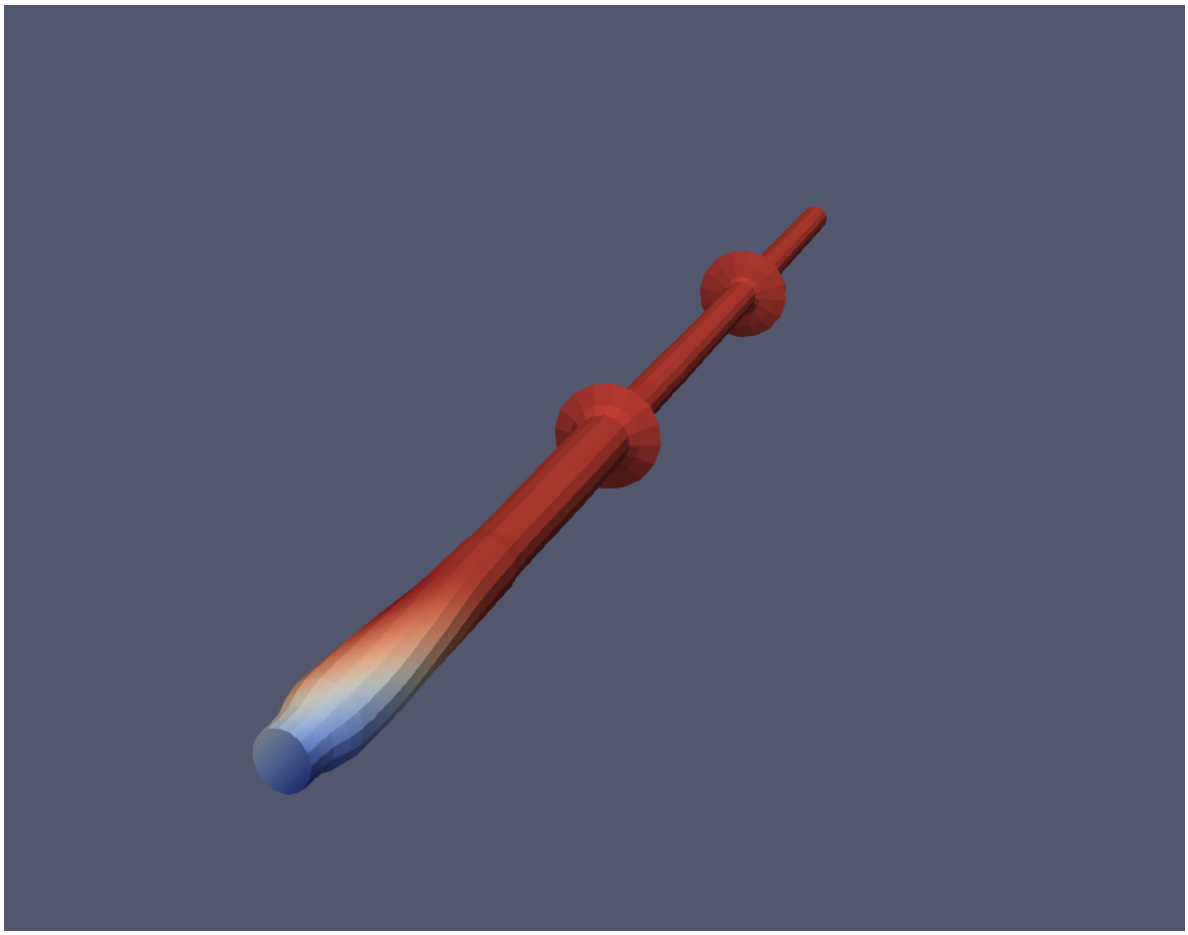

Figure 123: 9th Eigenmode

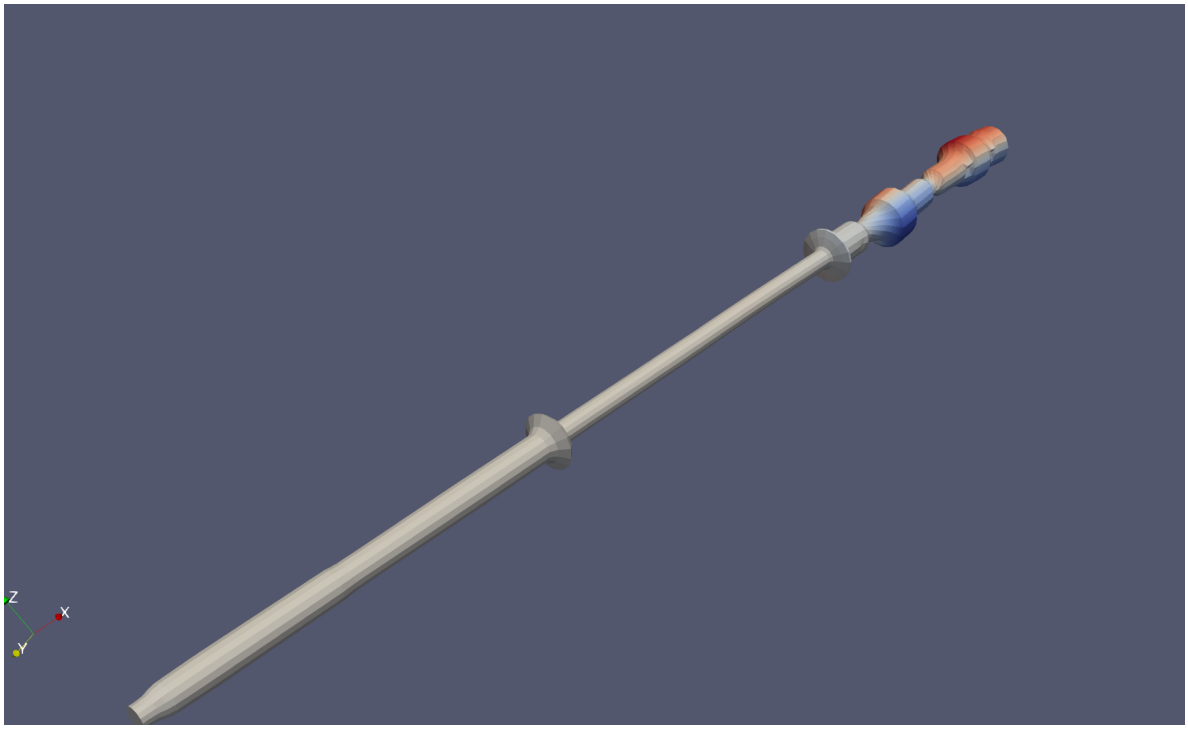

Figure 124: 10th Eigenmode

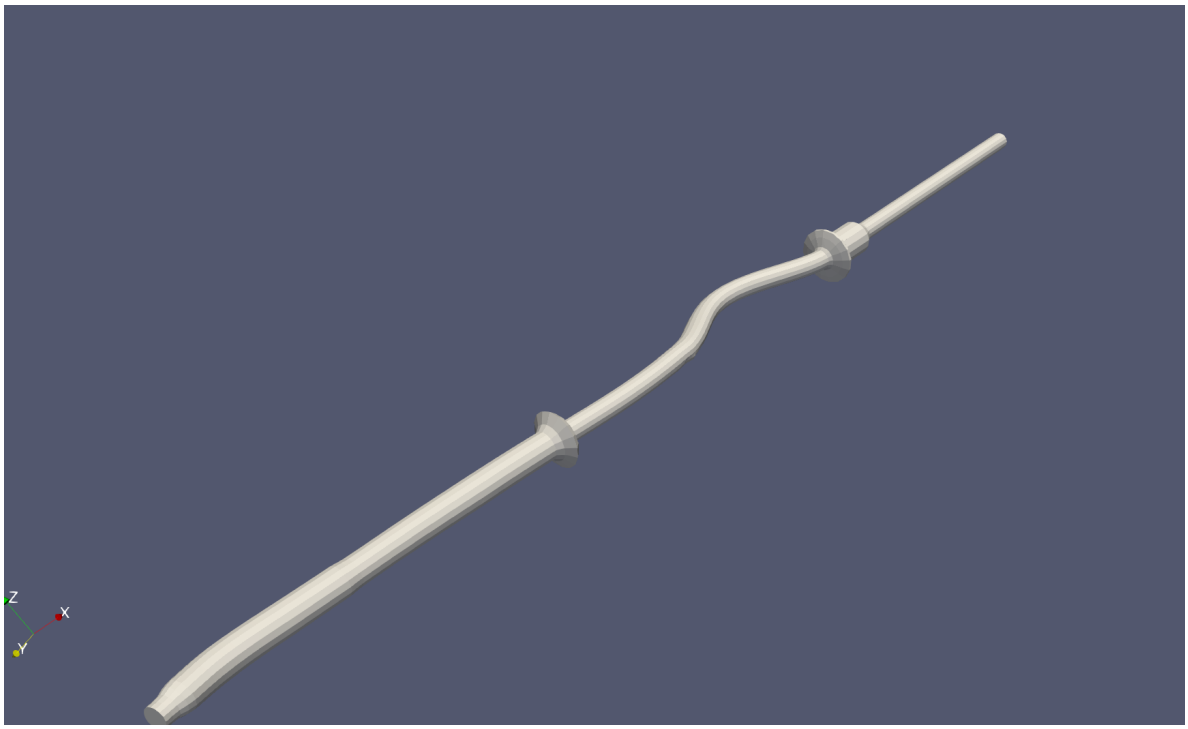

Figure 125: 11th Eigenmode

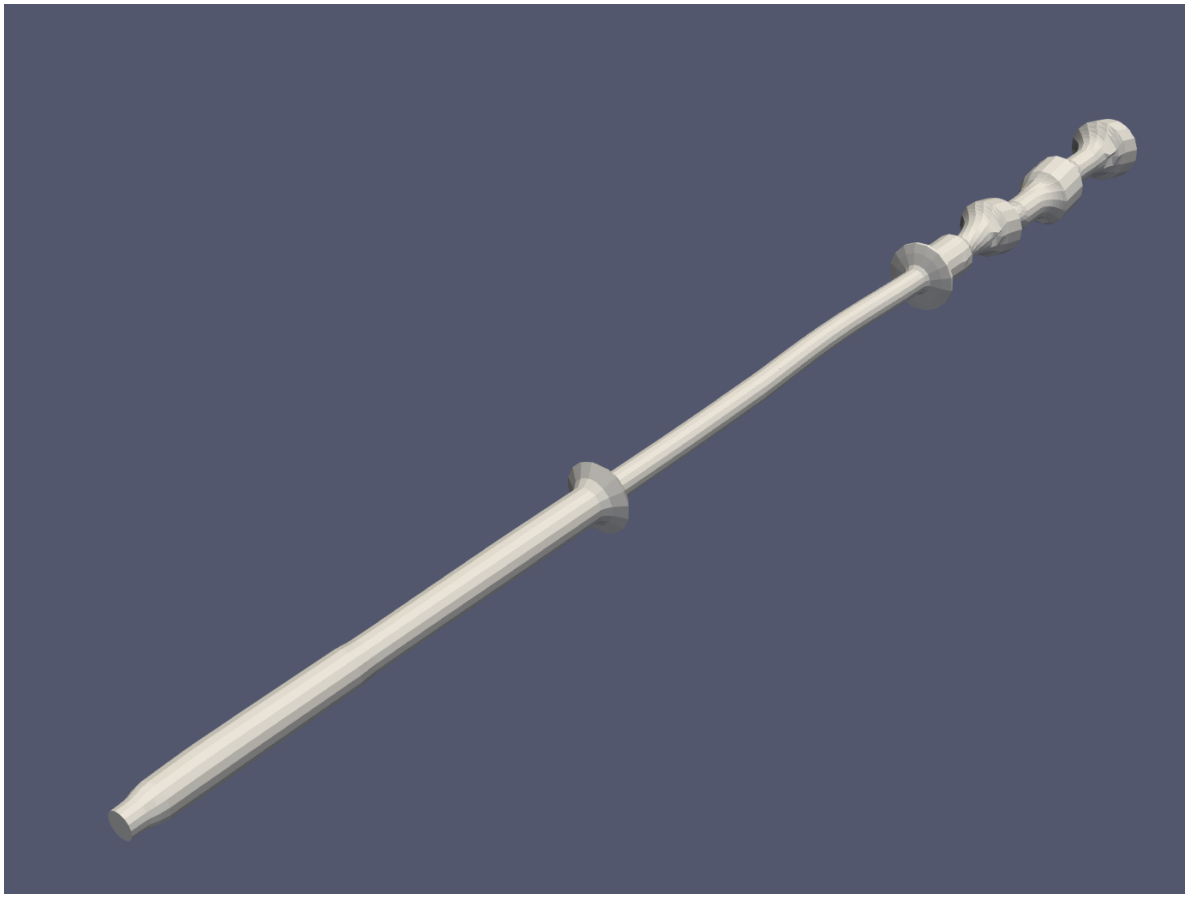

Figure 126: 12th Eigenmode

Figure 127: 13th Eigenmode

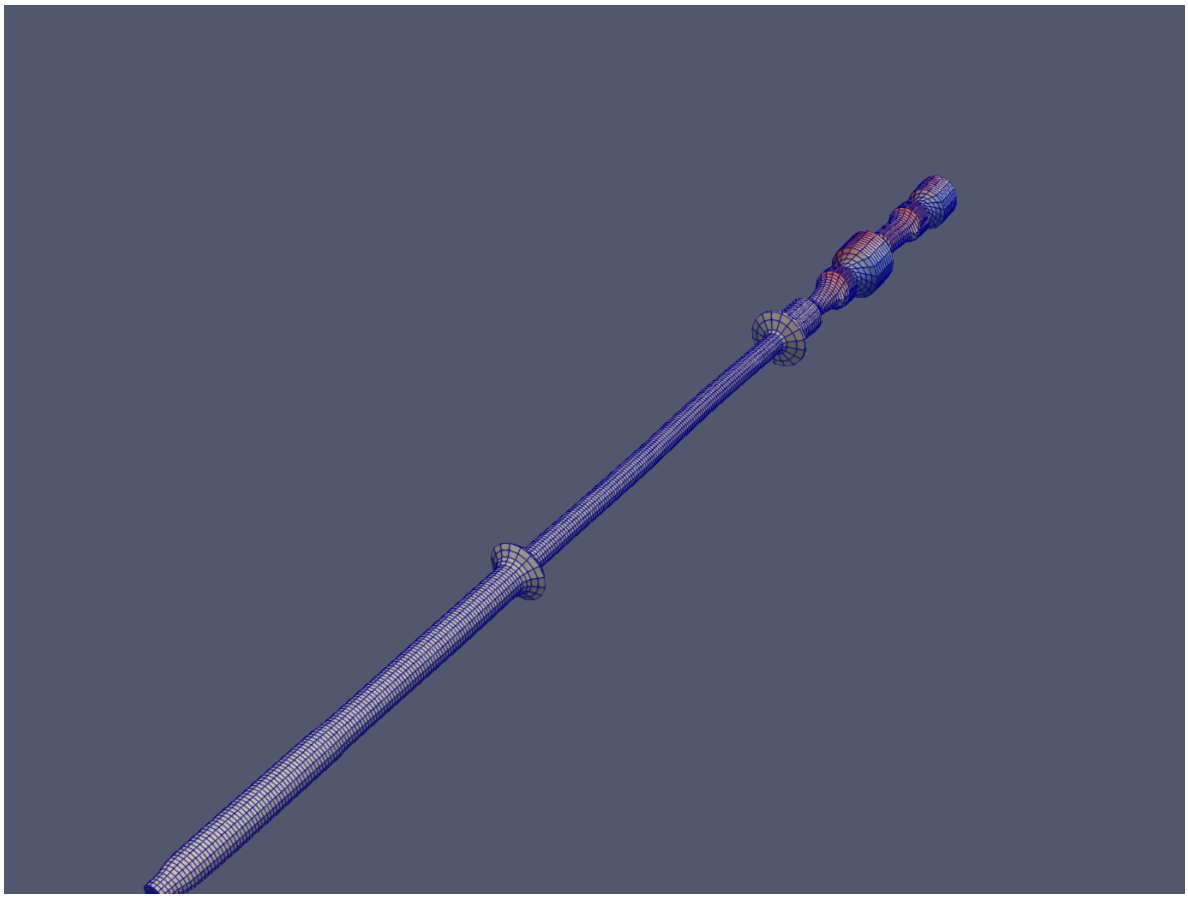

Figure 128: 14th Eigenmode

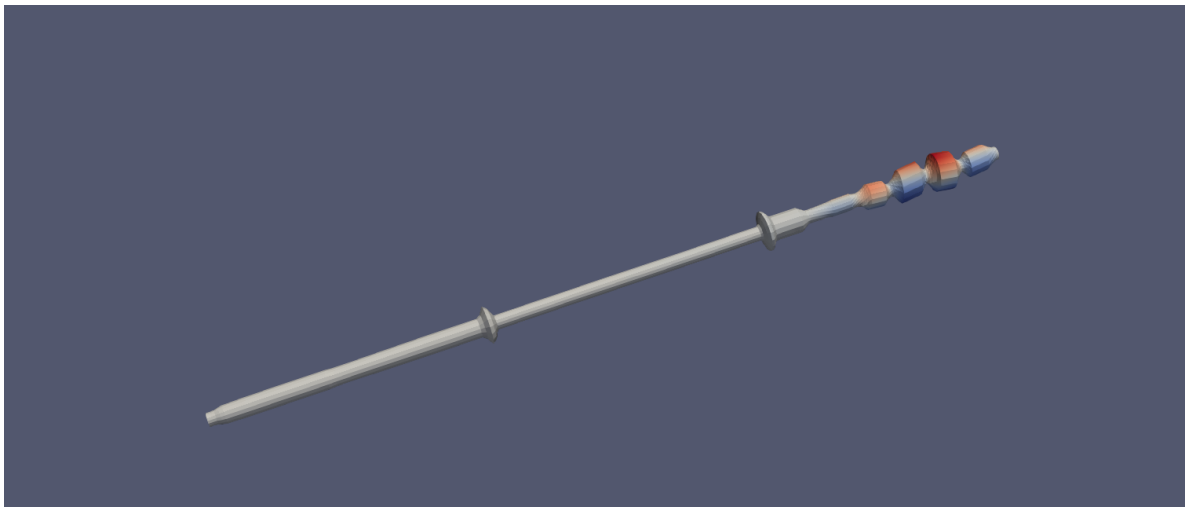

Figure 129: 15th Eigenmode

8 Conclusion

8.1 Results and Discussion

The goal of this diploma thesis is the development of software that can simulate any well-defined shafting system, taking into consideration the dynamic effects of rotation. Several algorithms were developed in the development cycle that gradually refined the software. The input file was also refined in order to facilitate direct input from standardized vibration manuals. The software was sufficiently validated against analytical models and used to simulate a typical two-stroke marine diesel engine of a Handysize Bulk Carrier. For the latter, an algorithm was developed to simulate the torque applied to each individual cylinder according to its crank angle. The conclusions from the aforementioned test cases are summarized below.

Initially, the validation cases will be discussed. The software demonstrated the ability to converge sufficiently to the analytical solutions, with the exception of the eigenvalues analysis, which presented an error of 10% for the Timoshenko's Beam. This is explained by the assumptions of constant area of sections and the boundary conditions being applied to surfaces, not points. The produced eigenmodes, while being close to the theoretical, support the aforementioned explanation, especially concerning the constant area assumption. These test cases were also executed in every software refinement cycle to ensure proper functionality. The results of the validation cases were encouraging and allowed the continuation to the simulation of the whole shafting system, which will be discussed below.

Starting with the comparison of the eigenvalues analysis for the reference shafting system, the model achieved a relative close result regarding the positioning of the eigenvalues, while producing eigenmodes resembling the reference ones. The divergence in the results is attributed to the added mass being handled differently in the reference manual. Specifically, the lateral vibration manual analysis does not consider as mass the weight of the cylinders, of the flywheel and of the propeller, while in the developed software the mass matrix is calculated for the equivalent cylinder that has the same radius and length with the reference but incorporates the mass moment of inertia as the parameter that dictates the density of the material.

Regarding the dynamic simulation for the MCR loading condition, the resulting stress is well in the linear region of the material, with the maximum being located at the bottom of the propeller shaft at the point where the propeller ends and the sterntube bearing starts. This is consistent with the trend observed in the maritime industry with the increasing number of sterntube failures. Furthermore, it is deduced that the movement of the propeller in both lateral and vertical axis is in the region of 0.75mm, with a variation from 0.75 to -0.75mm. Also, the functionality of the flywheel is observed, as the erratic input from the cylinders seems to be *flattened* after the end of the flywheel figs. 108 and 109. Finally, the maximum z in the variable torque test case is noted to be lower than in the consta torque test case in the intermediate shaft. The above are observed at fig. 88

Moreover, in the visualization of the results using ParaView, the hysteresis of the rotation of the propeller is visible, as is the different torque in each cylinder, which causes some stress concentrations between cylinders.

One weakness of the method of simulation that is evident in this software is the inability, currently, to apply kinematic constraints to the boundaries. This is the reason that the resulting mesh does not seem to rotate and the solution of the dynamic model is $\delta\ddot{u}$, although this does not affect the solution, requires the use of more vectors that can store this information, leading to higher memory usage.

Lastly, the development of the software will be discussed. The agile-iterative software development life cycle chosen provided the methodology that enabled rapid refinement with all the features mentioned

in this thesis. Moreover, the High Performance Computing elements used are measurable, affecting the overall simulation time and enabling the software to be deployed in scalable systems.

8.2 Future Work

This study aimed to develop the foundational framework so that a complete digital twin of the propulsion system can be based upon.

An important part of this study was the creation of the basic mathematical foundation required by FEM, so certain assumptions, like the bearings as springs with constant and predefined friction, the linear Constitutive Model for the material, and the gas torque applied to the cylinders. Having this in mind, the proposal for continuation of this project with concentrating on the shortcomings of the developed software and could include the following topics:

- Integration of preexisting Reynolds Solvers for the Bearings
- Validation of the software, using load cells[26]
- Combustion Model which will produce the Pressure-Crankshaft angle plot for both steady (as for the moment the AVL suite is used) and transient operation [15]
- Detail model of the shafting system with the full crankshaft geometry.
- Detailed propeller model, accounting for the Whirling Vibrations
- Creation of Elastoplastic Constitutive Model for the materials
- Coupling the shafting system with PTOs or PTIs
- Introduce misfiring into the model
- Creating monitoring framework that can detect faults
- and finally, batch running a sizable set of shafts in order to create a Physics Informed Neural Network

References

[1] *EEXI and CII - ship carbon intensity and rating system*. [Online]. Available: https://www.imo.org/en/MediaCentre/HotTopics/Pages/EEXI-CII-FAQ.aspx (visited on 10/18/2023).

[2] *IMO sustainable shipping amendments for EEDI, EEX, CII and BWM*, en. [Online]. Available: https://marine-offshore.bureauveritas.com/updated-imo-amendments-bring-sustainability-forefront (visited on 10/18/2023).

[3] *CII - Carbon Intensity Indicator*, en. [Online]. Available: https://www.dnv.com/Default (visited on 10/18/2023).

[4] *EEXI and CII requirements taking effect from 1 January 2023*, en, Jan. 2023. [Online]. Available: https://www.dnv.com/news/eexi-and-cii-requirements-taking-effect-from-1-january-2023--237817 (visited on 10/18/2023).

[5] *SEEMP III, EEXI & CII - 2023*, en-US. [Online]. Available: https://academy.marineinsight.com/courses/seemp-iii-eexi-cii-2023/ (visited on 10/18/2023).

[6] *Shaft alignment and propeller shaft aft bearing performance – recent trends call for action*, en, Feb. 2018. [Online]. Available: https://www.dnv.com/news/shaft-alignment-and-propeller-shaft-aft-bearing-performance-recent-trends-call-for-action--111385 (visited on 10/19/2023).

[7] *Ensuring satisfactory aft stern tube bearing lubrication performance - DNV*. [Online]. Available: https://www.dnv.com/expert-story/maritime-impact/Ensuring-satisfactory-aft-stern-tube-bearing-lubrication-performance.html (visited on 10/19/2023).

[8] *Environmentally acceptable lubricants show reduced capabilities under certain conditions*, en, Oct. 2019. [Online]. Available: https://www.dnv.com/news/environmentally-acceptable-lubricants-show-reduced-capabilities-under-certain-conditions-158982 (visited on 10/19/2023).

[9] W. Journal, *DNV GL Study Ties Stern Tube Bearing Failures To The Use Of Synthetic EALs*, en-US, Nov. 2019. [Online]. Available: https://www.waterwaysjournal.net/2019/11/18/dnv-gl-study-ties-stern-tube-bearing-failures-to-the-use-of-synthetic-eals/ (visited on 10/19/2023).

[10] *Lagersmit | The effect of Environmentally Acceptable Lubricants on stern tube bearings*, en-US. [Online]. Available: https://www.lagersmit.com/blog/the-effect-of-environmentally-acceptable-lubricants-eal-on-stern-tube-bearings/ (visited on 10/19/2023).

[11] *DNV GL completes study on the properties of EALs for stern tube applications*, en-US, Section: Fuels, Nov. 2019. [Online]. Available: https://safety4sea.com/dnv-gl-completes-study-on-the-properties-of-eals-for-stern-tube-applications/ (visited on 10/19/2023).

[12] "Basic principles of ship propulsion," en,

[13] D. Palomo Guerrero and F. J. Jiménez-Espadafor, "Torsional system dynamics of low speed diesel engines based on instantaneous torque: Application to engine diagnosis," en, *Mechanical Systems and Signal Processing*, vol. 116, pp. 858–878, Feb. 2019, ISSN: 08883270. DOI: 10.1016/j.ymssp.2018.06.051. [Online]. Available: https://linkinghub.elsevier.com/retrieve/pii/S0888327018303893 (visited on 04/28/2023).

[14] K.-M. Tsitsilonis, G. Theotokatos, N. Xiros, and M. Habens, "Systematic Investigation of a Large Two-Stroke Engine Crankshaft Dynamics Model," en, *Energies*, vol. 13, no. 10, p. 2486, May 2020, ISSN: 1996-1073. DOI: 10.3390/en13102486. [Online]. Available: https://www.mdpi.com/1996-1073/13/10/2486 (visited on 11/23/2023).

[15] ΚΩΝΣΤΑΝΤΙΝΟΣ ΚΑΤΗΜΕΡΤΖΗΣ, *ΜΕΤΑΒΑΤΙΚΗ αποκριση - λειτουργια διχρονου ναυτικου κινητηρα*, Greek.

[16] N. Izzuddin and P. Sunarsih Agoes, "Mathematical model of marine diesel engine simulator for a new methodology of self propulsion tests," vol. 1660, p. 070 018, May 2015, Conference Name: International Conference on Mathematics, Engineering and Industrial Applications 2014 (ICoMEIA 2014) ADS Bibcode: 2015AIPC.1660g0018I. DOI: 10.1063/1.4915736. [Online]. Available: https://ui.adsabs.harvard.edu/abs/2015AIPC.1660g0018I (visited on 11/23/2023).

[17] C. Georgios, "Investigation of tribological properties of mechanical systems of conventional merchant vessels," en,

[18] J. Liu and C. E. Dumitrescu, "Single and double Wiebe function combustion model for a heavy-duty diesel engine retrofitted to natural-gas spark-ignition," en, *Applied Energy*, vol. 248, pp. 95–103, Aug. 2019, ISSN: 03062619. DOI: 10.1016/j.apenergy.2019.04.098. [Online]. Available: https://linkinghub.elsevier.com/retrieve/pii/S0306261919307652 (visited on 11/24/2023).

[19] H. M. Hilber, T. J. R. Hughes, and R. L. Taylor, "Improved numerical dissipation for time integration algorithms in structural dynamics," en, *Earthquake Engineering & Structural Dynamics*, vol. 5, no. 3, pp. 283–292, Jul. 1977, ISSN: 00988847, 10969845. DOI: 10.1002/eqe.4290050306. [Online]. Available: https://onlinelibrary.wiley.com/doi/10.1002/eqe.4290050306 (visited on 10/12/2023).

[20] K.J. Bathe, *FEA Finite Element Procedures*.

[21] J. Yan, A. Nuertayi, Y. Yan, S. Liu, and Y. Liu, "Hybrid physical and data driven modeling for dynamic operation characteristic simulation of wind turbine," en, *Renewable Energy*, vol. 215, p. 118 958, Oct. 2023, ISSN: 09601481. DOI: 10.1016/j.renene.2023.118958. [Online]. Available: https://linkinghub.elsevier.com/retrieve/pii/S0960148123008649 (visited on 11/23/2023).

[22] *Damping in FEA Simulations | Materials*, en. [Online]. Available: https://www.simscale.com/docs/simulation-setup/materials/damping/ (visited on 06/14/2023).

[23] N. Mojsilovic, "Method of Finite Elements I," en,

[24] A. J. M. Ferreira, *MATLAB codes for finite element analysis: solids and structures*, en, ser. Solid mechanics and its applications 157. Dordrecht: Springer Science & Business Media, 2009, OCLC: ocn258090080, ISBN: 978-1-4020-9199-5 978-1-4020-9200-8.

[25] L. Freund, "Constitutive equations for elastic-plastic materials at finite strain," en, *International Journal of Solids and Structures*, vol. 6, no. 8, pp. 1193–1209, Aug. 1970, ISSN: 00207683. DOI: 10.1016/0020-7683(70)90056-9. [Online]. Available: https://linkinghub.elsevier.com/retrieve/pii/0020768370900569 (visited on 10/03/2023).

[26] D. E. Chatzi, "The Finite Element Method for the Analysis of Non-Linear and Dynamic Systems," en,

[27] M. K. Thompson and J. M. Thompson, *ANSYS mechanical APDL for finite element analysis*, en. Oxford, United Kingdom: Butterworth-Heinemann, an imprint of Elsevier, 2017, OCLC: ocn971048256, ISBN: 978-0-12-812981-4.

[28] J. F. Hall, "Problems encountered from the use (or misuse) of Rayleigh damping," en, *Earthquake Engineering & Structural Dynamics*, vol. 35, no. 5, pp. 525–545, Apr. 2006, ISSN: 0098-8847, 1096-9845. DOI: 10.1002/eqe.541. [Online]. Available: https://onlinelibrary.wiley.com/doi/10.1002/eqe.541 (visited on 10/31/2023).

[29] S. Mazumder, *Numerical methods for partial differential equations: finite difference and finite volume methods*, en. Amsterdam: Academic Press, 2016, OCLC: ocn913556966, ISBN: 978-0-12-849894-1.

[30] X. He, G. Li, P. Xing, *et al.*, "Experimental and numerical investigation on dynamic characteristics of ship propulsion shafting under uncertainty based on displacement response," en, *Ocean Engineering*, vol. 237, p. 109 637, Oct. 2021, ISSN: 00298018. DOI: 10.1016/j.oceaneng.2021.109637. [Online]. Available: https://linkinghub.elsevier.com/retrieve/pii/S0029801821010155 (visited on 11/23/2023).

[31] ABS, "Guide for Enhanced Shaft Alignment 2022," en, 2022.

[32] Vlachos O., *Elastohydrodynamic Lubrication (EHL): Theory and Definition - About Tribology*, en-US. [Online]. Available: https://www.tribonet.org/wiki/elastohydrodynamic-lubrication-ehl/ (visited on 07/23/2023).

[33] Χ. Γ. Προβατιδης, *Πεπερασμένα Στοιχεία στην Ανάλυση Κατασκευών*.

[34] M. Arghir, A. Alsayed, and D. Nicolas, "The ÿnite volume solution of the Reynolds equation of lubrication with ÿlm discontinuities," en, *International Journal of Mechanical Sciences*, 2002.

[35] T.G. Hughes and T. Hughes, *The Finite Element Method: Linear Static and Dynamic Finite Element Analysis*.

[36] J. T. Oden, "NONLINEAR CONTINUUM MECHANICS," en,

[37] Y.-L. Lee, M. E. Barkey, and H.-T. Kang, *Metal fatigue analysis handbook: practical problem-solving techniques for computer-aided engineering*. Waltham, MA: Butterworth-Heinemann, 2012, ISBN: 978-0-12-385204-5.

[38] S Sh Ghorashi, J Amani, A S Bagherzadeh, and And T Rabczuk, "Goal-oriented error estimation and mesh adaptivity in three-dimentional elasticity problems," en, 2014, Publisher: Unpublished. DOI: 10.13140/2.1.2884.9925. [Online]. Available: http://rgdoi.net/10.13140/2.1.2884.9925 (visited on 09/05/2023).

[39] *The deal.II Library: The step-44 tutorial program*. [Online]. Available: https://www.dealii.org/current/doxygen/deal.II/step_44.html#NeoHookeanmaterials (visited on 04/23/2023).

[40] G. Gurung, R. Shah, and D. P. Jaiswal, "Software Development Life Cycle Models-A Comparative Study," en, *International Journal of Scientific Research in Computer Science, Engineering and Information Technology*, pp. 30–37, Jul. 2020, ISSN: 2456-3307. DOI: 10.32628/CSEIT206410. [Online]. Available: http://ijsrcseit.com/paper/CSEIT206410.pdf (visited on 08/27/2023).

[41] W. Bangerth, C. Burstedde, T. Heister, and M. Kronbichler, "Algorithms and data structures for massively parallel generic adaptive finite element codes," en, *ACM Transactions on Mathematical Software*, vol. 38, no. 2, pp. 1–28, Dec. 2011, ISSN: 0098-3500, 1557-7295. DOI: 10.1145/2049673.2049678. [Online]. Available: https://dl.acm.org/doi/10.1145/2049673.2049678 (visited on 10/30/2023).

[42] S. Moore, *The Finite Element Method: Examples with a Timoshenko Beam and Poisson's Equation*, original-date: 2017-10-25T06:29:19Z, Mar. 2023. [Online]. Available: https://github.com/simoore/timoshenko-fem (visited on 11/22/2023).

Appendix

This Appendix presents the q stress applied on the right hand side vector to simulate a torque equally distributed over a boundary area.

Three distinct possibilities are considered and are modelled into the software:

- Torque Perpendicular to the surface (assumed circular section)
- Torque over the perimeter of a cylindrical body with constant radius over the length of the boundary and
- Torque over the perimeter of a cylindrical body with a linearly changing radius over the length of the boundary

Torque Perpendicular to circular section

The constant pressure q[N/m^2] required for the following loading condition is calculated by integrating a perimeter stripe of the face for dr and from r=0 to r=R.

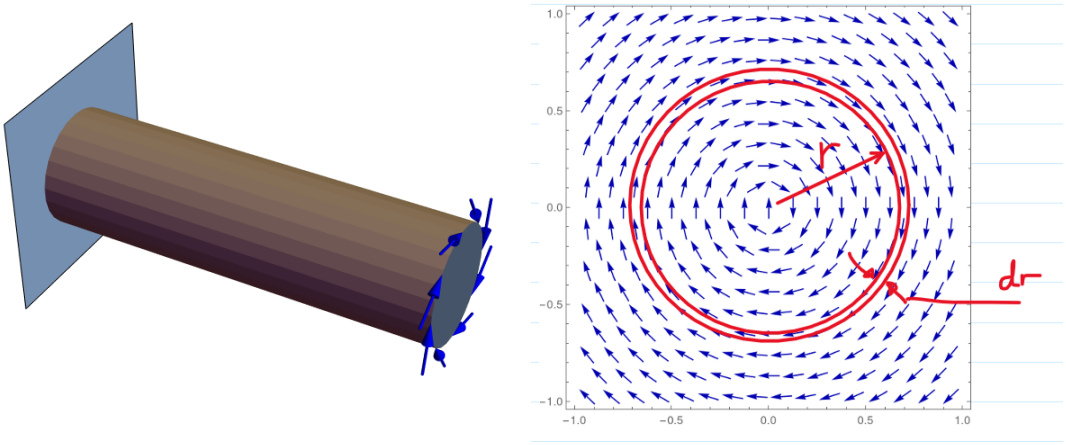

$\delta A = 2\pi\delta r$, and assuming a q with constant absolute value $\rightarrow \delta F = q\delta A = 2\pi\delta r$

$$\delta M = r\delta F = rq\delta A = 2\pi q r^2 \delta r$$

$$M = \int_0^R 2\pi q r^2 \delta r$$

$$M = 2\pi q[\frac{r^3}{3}]_0^R = \frac{2}{3}\pi q R^3$$

$$\text{So eventually, } q = \frac{3}{2}\frac{M}{\pi R^3}$$

Pressure of Perimeter with Constant Radius

To find the constant pressure q over the perimeter of a cylinder that produces a torque M over the whole length, we use the relationship between pressure, force, and torque.
The torque M is given by:

$$M = r \times F$$

where r is the radius of the cylinder, and F is the force applied.

The force F is related to pressure q by the equation:

$$F = q \times A$$

where A is the area over which the pressure is applied.
For a cylinder with height h, the lateral surface area A is:

$$A = 2\pi r h$$

Combining the above equations, we get:

$$M = r \times (q \times A) = r \times q \times (2\pi r h) = 2\pi r^2 h q$$

Solving for q, we find:

$$q = \frac{M}{2\pi r^2 h}$$

Torque over conical frustum

Similarly to the above, the radius is integrated over the length of the cylinder, with the radius: $R(x) = R_2 + \frac{x}{L}(R_1 - R_2)$, the pressure q equals to:

$$q = 3\frac{M}{2\pi L(7R_1^2 - 5R_2R_1 + R_2^2)} \tag{8.1}$$